Aspects of Gravitational and Cosmological Scattering Amplitudes

CONNOR WILLIAM ARMSTRONG

Aspects of Gravitational and Cosmological Scattering Amplitudes

Connor Armstrong

A Thesis presented for the degree of
Doctor of Philosophy

Department of Mathematical Sciences
Durham University
United Kingdom

May 2023

Aspects of Gravitational and Cosmological Scattering Amplitudes

Connor Armstrong

Submitted for the degree of Doctor of Philosophy

May 2023

Abstract: This thesis presents three distinct aspects of scattering amplitudes research along with background material on the concepts underpinning them. The first of these is the study of on-shell diagrams for $\mathcal{N} = 7$ supergravity and an associated recursion relation automatically encorporating the bonus relations. This is used to produce momentum twistor expressions which in the case of six-point NMHV use different 'coordinate patches' with different ordering of external legs to get compact results and see the cancellation of spurious poles through momentum twistors. The second is the study of colour/kinematics duality of Yang-Mills amplitudes in four-dimensional Anti-de Sitter (AdS) space. By applying a generalised gauge transformation the kinematic numerators can be made to obey a Jacobi relation and these shifted numerators also obey a deformed AdS version of the Bern-Carrasco-Johansson relations. Finally we study wavefunction coefficients of scalar effective field theories (EFTs) in de Sitter space using a representation involving boundary conformal generators acting on contact diagrams and the cosmological scattering equations. Through this representation, we show that four-point wavefunction coefficients of EFTs exhibit double copy relations analogous to those in flat space with additional curvature corrections with unfixed coefficients. Imposing enhanced soft limits analogous to the EFTs in flat space allows these to be unambiguously fixed and also recovers Lagrangians with hidden shift symmetries. This is explored at four- and six-point.

This thesis is based on work previously published in [1–4].

Declaration

The work in this thesis is based on research carried out in the Department of Mathematical Sciences at Durham University. No part of this thesis has been submitted elsewhere for any degree or qualification.

Acknowledgements

I'd firstly like to thank the Royal Society for funding this research through a PhD studentship, without the opportunity provided by them none of this would have been possible.

Then to my various collaborators over the course of this PhD. While we didn't always manage to meet in person, the discussions I had with Renann, Humberto and Jiajie were very fruitful and engaging. I'm particularly grateful to Joe Farrow for his friendship and words of wisdom throughout my PhD as well as the research we did together. Thanks to all the office mates and lunchtime friends over my years in Durham for their encouragement, friendship, and advice. Gabriel, Sophie, and Victor; John, Clare, Matthew, Rob, and the rest of the Zoom quiz group.

Thanks to Ustinov College and the GCR for the time I've spent there outside of research, meeting so many new people and helping each other. To Diana, Bryony, and especially Alastair for their support and innovation throughout the covid pandemic that let us not only get by but to create new and wonderful things.

Thank you to all those I've lived with throughout my PhD, through the strange and unpredictable time we've been through. I'll always remember fondly the times with Diane and Christoph. Then there's Jake, Scott, and Elly, some of the best friends I could have wished for.

To my parents for supporting me in every possible way throughout my PhD, even saving me from post-conference rail strikes and sending many care packages across the country. To all my other friends around the world for keeping each other sane throughout it all; those I've known for years and those whose voices are so familiar

despite us always being miles apart.

Finally to my supervisor Arthur Lipstein. When we first Skyped 5 years ago I don't think either of us ever imagined the things that would end up taking place. This has been an adventure I'm very happy I went on and research I'm proud of and your support and guidance has been invaluable throughout.

Contents

List of Figures

List of Tables

Chapter 1

Introduction

Scattering amplitudes have long been considered a nice set of objects to study in the context of quantum field theory. They arise when calculating the probability for interactions of fundamental particles and are one method for obtaining observables from quantum field theory. They are gauge-invariant, instead depending only on physical parameters (momentum, spin, flavour) and seem to exhibit a simplicity that is often obscured by the methods used to construct them. This is often exemplified by the famous Parke-Taylor amplitude for gluons, with the original six-point formula requiring hundreds of Feynman diagrams to compute but yielding a result that can be written in a single line for any number of particles [5, 6]. Furthermore, the formula perfectly encapsulates the symmetries and other properties required of it – factorisation channels, helicity assignments, colour structure. In the years since, this and other results have inspired the further study of amplitudes in their own right. On one side using known physical properties to find new methods of construction and increasingly compact and elegant way to express them. On the other, finding deeper mathematical insights contained within scattering amplitudes and forging connections into other areas of physics as well as pure mathematics. This thesis takes established mathematical and physical techniques that have been successfully applied to amplitudes in various theories and looks to see what they can teach us about other theories that are perhaps less well-understood. This often necessitates

developing new ideas to understand the results. It not only looks at frontiers in flat space, where the vast majority of amplitudes work has been carried out but also looks to appropriate generalisations in curved spacetimes – specifically de Sitter and Anti-de Sitter. These will be considered as fixed backgrounds on which particle interactions can occur, but where the Einstein equations for general relativity have a constant negative (AdS) or positive (dS) cosmological constant in constrast to flat space where the cosmological constant is zero. Particularly in curved spacetimes, the behavior of physics means that new insights are needed to manipulate expressions and deal with the increase in complexity. In the case of each chapter the fundamental aim is the same – to explore the suitability of taking amplitudes techniques and pushing them to an area where they may not apply in quite the same way, enabling us to study both amplitudes and potential generalisations of the techniques themselves.

This starts with work inspired by the geometry program for superamplitudes. Since the original discovery of the Parke-Taylor amplitude, much progress has been made using advances in notation and variable choices to find increasingly elegant ways of expressing Yang-Mills amplitudes. Much of this has used the maximally supersymmetric $\mathcal{N} = 4$ super Yang-Mills theory as a starting point. The high degree of supersymmetry and associated other symmetries mean that this can be used as an idealised toy theory where many calculations become analytically more tractable. There are now a variety of results for arbitrary numbers of particles being scattering (n-point) and including quantum corrections in the form of loops of unspecified degree (l-loop). These have been developed along with connections to algebraic geometry constructs such as cluster algebras and tropical Grassmannians [7, 8]. The state of the art now includes scattering amplitudes in other theories and many different combinatoric and geometric ways of understanding them [9–11]. The underlying philosophy has been summarised by Nima Arkani-Hamed as "What question can we ask to which scattering amplitudes are the answer?". The idea being that there may

be a way of constructing amplitudes directly from considerations on the external kinematics, with properties we expect from physical theories (locality, unitarity) appearing as emergent phenomena. This has already been partially realised with the amplituhedron, a geometrical way of producing planar $\mathcal{N} = 4$ Super Yang-Mills amplitudes from positive geometries [12, 13]. While work is still ongoing to understand all the aspects of the construction, the amplituhedron has nevertheless made it possible to find new results for planar $\mathcal{N} = 4$ amplitudes and loop integrands and lead to alternative formulations of known results [14]. One particularly nice aspect is the link between geometries and amplitude factorisation, an idea associated with the use of recursion relations. Recursion relations allow the construction of higher point amplitudes from lower point ones. Since three-point interactions can sometimes be constructed from symmetry arguments, this allows for amplitudes with any number of external legs to be obtained without reference to Feynman diagrams. For links to geometry, the focus is often on BCFW (Britto-Cachazo-Feng-Witten) recursion which uses complex momenta and residue theorems to calculate amplitudes [15–17]. Different ways of applying BCFW (different recursion schemes) can be understood as choices of triangulation in a geometric description. Similarly, poles from factorisation when an internal propagator goes on-shell can be associated with logarithmic singularities in differential forms which appear on specific boundaries of the geometry. That some of these cancel between regions with shared boundaries is the geometric avatar of spurious poles appearing in an expression for the amplitude – which must cancel in the final physical object. Indeed properties like this provided some of the original inspiration for attempts to find a geometric construction for amplitudes [18, 19]. Another important perspective came from on-shell diagrams [7], which provide a diagrammatic representation of BCFW recursion and give rise to Grassmannian integral formulas. Unlike Feynman diagrams, these do not make use of unphysical states (intermediate virtual particles) in the calculation of amplitudes. A crucial feature of this representation is that all tree-level amplitudes and loop integrands in planar $\mathcal{N} = 4$ SYM have a so-called dlog form, which was simultaneously discovered

using Wilson loops in momentum twistor space [20, 21]. On-shell diagrams for $\mathcal{N} < 4$ SYM and non-planar $\mathcal{N} = 4$ SYM were subsequently studied in [22, 23] and [24–26], respectively.

With this in mind, another natural frontier to consider is the other 4d maximally supersymmetric theory – that of $\mathcal{N} = 8$ supergravity. Here some progress has already been made in understanding how it might be approachable from a similar viewpoint. Progress has already been made in obtaining nice expressions for some tree-level amplitudes in terms of momentum twistors, a key stepping stone in the $\mathcal{N} = 4$ SYM story [27]. The use of BCFW for tree-level supergravity has been established [28, 29] and connected to a gravitational formulation of on-shell diagrams [30]. Nevertheless gravitational theories are more complex than gauge theories and the presence of full permutation symmetry as well as a more complicated pole structure means efforts to come up with a fully geometrical formulation of $\mathcal{N} = 8$ have so far not made much headway despite the discovery of elegant spinor formulae for the tree-level MHV amplitudes [31] and worldsheet expressions for general MHV degree [32, 33]. In the context of this thesis, a much narrower problem is considered although the ultimate goal is still that eventually it may be possible to construct a "gravituhedron" [34].

We start from the work done to recast supergravity in terms of on-shell diagrams [30, 35]. This is combined with a recursion for $\mathcal{N} = 7$ which uses the "bonus relations" to produce more compact formulae than can be found from the full $\mathcal{N} = 8$ theory allowing for established MHV results in terms of spinors and momentum twistors to be recovered diagrammatically [1]. This process involves work with a less-studied feature of on-shell diagrams, that of closed cycles encoding sums of geometric series and a new technique to avoid carrying explicit sums is introduced. The analysis then continues to the six-point NMHV case with the application of momentum twistors living on different coordinate patches, each defined for a different ordering of external legs. This clearly exposes the structure and cancellation of the spurious poles of the amplitude analogous to those seen in $\mathcal{N} = 4$ as well as producing expressions which generalise the $\mathcal{N} = 4$ notion of R-invariants. This suggests that there may be a

geometrical realisation of these properties and of supergravity amplitudes although more work is needed to fully realise these links. The $\mathcal{N} = 7$ recursion can also be applied to calculate leading singularities, quantities used for efficient computation of loop results and some demonstrations of this are included as an appendix. The work on this topic was first published in [1].

This is followed by a departure from flat space scattering amplitudes although the theme of using different notations to explore properties of scattering amplitudes and develop new formulations to describe them continues. It is natural to wonder which of the various techniques and relations established in flat space might apply to analogues of amplitudes on other fixed backgrounds. One spacetime of interest is Anti-de Sitter (AdS). This is perhaps a good place to start probing generalisations of amplitudes techniques as the quantities computed here can be related to those in flat space by taking a particular limit [36, 37]. So long as this limit does not conflict with the relations under study, then the original relation should hold up to some 'curvature corrections' that will need to be determined and understood. This spacetime also has the benefit of being very well studied due to interest in the AdS/CFT correspondence [38]. The correspondence is a series of maps between observables of a gravitational theory living in AdS and those of a conformal field theory (CFT) living at the boundary of the spacetime. It can be used to probe non-perturbative CFT properties via bulk AdS computations as well as using CFT constraints to explore the quantum theory of gravity living in AdS. This means that previous CFT results can be leveraged to aid in the study of amplitudes in AdS as well as raising the hope that any insights gained could potentially be extended to apply to conformal field theories.

The specific physics of interest here is the duality between colour and kinematics. This is the idea that gauge theory amplitudes can be written as a sum of terms whose numerators factorise into a colour piece (which comes from the gauge group) and a kinematic piece which contains all the momentum dependence. The colour factors

obey Jacobi relations from the Lie algebra of the gauge group and there exist ways of arranging the amplitude such that the kinematic numerators obey completely analogous Jacobi relations [39]. Furthermore, gravitational amplitudes can be obtained by replacing the colour factors with a second set of kinematic factors (which may be the same or different to the first) so long as those factors also obey Jacobi relations. This procedure is also related to the double copy, a general term for many different relations between gauge and gravity amplitudes. These include the KLT relations from string theory [40], relations between integrands for the scattering equations formalism [41] (which will be discussed in more detail below) and some extensions beyond tree level to loop integrands [42–44]. Colour-kinematics duality also implies relations among gauge theory amplitudes known as Bern-Carrasco-Johansson (BCJ) relations [45]. It is this that will be looked at in the context of AdS.

An AdS generalisation of amplitudes can be found using momentum space Witten diagrams, a natural extension of Feynman diagrams [37, 46–51]. An AdS object that can be studied with amplitudes techniques is thus given by the perturbative expansion of Witten diagrams with external states ending on the boundary. These encode the transverse parts of boundary conformal correlators and encode flat space amplitudes as a particular limit. A double copy between three-point correlators of currents and stress tensors has already been established [52, 53] but it is not clear how it should be extended to four points. The three-point correlators are all fixed by conformal Ward identities but this it not true for four points and beyond. Instead, the focus is on how BCJ can be modified for AdS and the new features that we see beyond flat space – a generalised gauge symmetry and richer space of kinematic variables. A spinor helicity formalism for AdS is used to calculate explicit results for four-point Yang-Mills amplitudes, including those with all-plus and single-minus configurations (which vanish in flat space). The relationship between these (which encode the transverse pieces of the boundary correlators) and the full correlators are also explored by recovering the missing longitudinal pieces using Ward identities. These new results first appeared in [2].

Finally we turn our attention to de Sitter. At tree-level, the quantities calculated here are closely related to those in AdS but have a different physical significance. We will be looking at wavefunction coefficients which can be computed by analytically continuing Witten diagrams from AdS, these represent correlators in the future boundary of dS. Objects living in the future boundary of dS are closely related to observables from the effective field theory describing the period of inflation in early cosmology [47, 54, 55]. Specifically the quantities of interest for experimental comparison are in-in correlators, which can be obtained from the squares of wavefunction coefficients integrated over boundary conditions [56, 57]. A study here of amplitude analogues therefore links closely to quantities of interest in experimental cosmology, connecting physics of fundamental particles on the smallest scales with that of the large-scale structure of our Universe. This interest has lead to lots of amplitudes-inspired calculations of correlators and their contributions to density fluctuations in the cosmic microwave background. For example, the ideas behind the geometry program in flat space have lead to the study of wavefunction coefficients through cosmological polytopes [58]. There is also work on bootstrapping wavefunction coefficients from consistency conditions, unitarity, and factorisation properties [58, 59]. In particular this allows for the construction of spinning correlators from those involving scalars using weight-shifting operators. A related puzzle is to determine what is the most suitable representation for studying properties of wavefunction coefficients. The increased complexity also means that dealing with expressions directly in momentum space is not always practical and can obscure interesting features. Alternatives such as working with momentum space differential operators [60] or the use of the Mellin-Barnes representation [61] each provide benefits over explicitly constructing and evaluating Witten diagrams. Another avenue being studied is the adaptation of the scattering equations and CHY formalism to calculate cosmological wavefunction coefficients in de Sitter – referred to as the cosmological scattering equations (CSE) [62, 63]. This opens new directions to explore amplitudes properties

beyond flat space.

The CHY (Cachazo, He & Yuan) formalism and the associated scattering equations [64, 65] provide a universal description of amplitudes in terms of worldsheet integrals [41, 66, 67]. The scattering equations are a set of equations linking particle momenta with a set of punctures on a Riemann sphere. Their solutions can be used to obtain a wide variety of amplitudes via an integral over the corresponding worldsheet, with the integrand containing a theory independent part (which includes enforcing the scattering equation solutions) and a theory-dependent integrand. The CHY formalism also leads to connections between a web of theories via relations applied to the integrands. These include a double copy between Yang-Mills and gravity but also generalised dimensional reductions leading to effective field theories of scalars with derivative interactions. These scalar field theories also have a double copy relation, here linking the non-linear sigma model (NLSM) with Dirac-Born-Infeld (DBI) theory and with the special galileon (sGal) [68–70]. The CSE allow for a straightforward uplift from flat space amplitudes to wavefunction coefficients and motivate expressions written as differential operator written in terms of boundary conformal generators acting on contact diagrams. This approach builds off of previous work on bi-adjoint scalar scalar theory in AdS position space [71, 72] as well as on wider uses of boundary conformal generators to express amplitudes [73–75]. The CSE provide a framework for encoding the double copy of scalar effective field theories (EFTs) in dS analogous to the one in flat space. The framework has the additional feature that one is free to add curvature corrections (which vanish in flat space) to obtain wavefunction coefficients for sGal, DBI and ϕ^4 theories as special cases of the same generalised double copy of the NLSM integrand [3].

A closely related phenomena is the study of soft theorems and hidden symmetries. Soft theorems describe the behavior of scattering amplitudes when one or more legs are taken soft and usually take the form of some universal factor independent of the starting number of legs. Hidden symmetries are those present in the Lagrangian and equations of motion for a theory but not present in its vacuum states. The study of

soft theorems for gravitons (and gluons) is well-established, with known factorisation properties motivated by the study of the cancellation of infrared divergences [76–78]. Graviton soft limits have been more recently linked to the study of asymptotic symmetries [79–81]. Of interest in this thesis are scalar EFTs such as the non-linear sigma model (NLSM), originally developed as a low-energy theory of nuclear interactions mediated by pions [82–84] and known to have an enhanced soft limit, one where the degree of soft behavior is greater than predicted by naive power-counting arguments [85]. The NLSM also encodes a spontaneously broken symmetry, a phenomena also observed in $\mathcal{N} = 8$ supergravity [86]. The soft behavior of the NLSM has now been extended to a whole family of theories with a classification of scalar amplitudes which can be constructed purely from consistency conditions (such as factorisation) along with a study of their soft behavior [87, 88]. This analysis leads to NLSM, DBI and sGal as the only three 'exceptional' scalar field theories with an enhanced behavior in the soft limit. Via S-matrix manipulations it can be shown that this is related to the shift symmetries displayed by the Lagrangians for these theories. Inspired by the CSE, writing wavefunction coefficients in terms of differential operators acting on contact diagrams provides a convenient way to study the constraints imposed by enhanced soft limits. Imposing enhanced soft behavior leads to the construction of wavefunction coefficients belonging to a series of Lagrangians which have shift symmetries in dS, despite there not being a clear S-matrix analogue to link these two properties [4, 89]. This can be applied to the CSE generalised double copy, implying a natural fixing of the coefficients which appear there.

This thesis starts with a review of some important basic concepts for scattering amplitudes in chapter 2: spinor helicity notation, the conformal group and supersymmetry generalisations as well as the analogues of amplitudes in AdS and dS. This introduction then looks in more detail at the amplitudes properties that we explore and generalise throughout the rest of the thesis – recursion relations, momentum twistors and on-shell diagrams then colour-kinematics and finally soft theorems and

EFTs. Chapter 3 then describes the construction of an on-shell diagrammatic recursion for $\mathcal{N} = 7$ supergravity, including MHV and NMHV examples up to six-points before analysing in detail the story of spurious poles for NMHV at six points. This requires the introduction of momentum twistors living on different coordinate patches and an appendix is provided on the transition functions to map between the different orderings of external legs. Other appendices explore how the $\mathcal{N} = 7$ formalism can be used to calculate leading singularities at one and two loops and to recover $\mathcal{N} = 8$ amplitudes from the $\mathcal{N} = 7$ case.

In chapter 4 we then turn to curved spacetime starting with Witten diagrams for Yang-Mills in AdS_4. An AdS generalisation of colour-kinematics duality via the BCJ relations is explored at four points followed by explicit calculations of the four different independent helicity amplitudes in spinor notation. The full boundary correlator (of which the Witten diagrams only compute the transverse piece) is then recovered via the use of Ward identities. There is also an appendix exploring the spinor helicity formalism in greater detail with a particular focus on the rich variety of identities which can be found.

This is followed by chapter 5 in dS_4, first introducing the flat space CHY formalism before uplifting to obtain cosmological scattering equations. This also covers the basics of working with dS wavefunction coefficients and the relevant aspects of the boundary conformal generators which will appear throughout. Four-point calculations of conformally and minimally coupled scalars are included for interactions with different numbers of derivatives, producing explicit results in momentum space.

Finally in chapter 6, these calculations are generalised to arbitrary dimension and conformal weight via the use of boundary generators acting on contact diagrams. This enables for a detailed study of their soft limits and the cases under which the wavefunction coefficients will have enhanced soft behavior. At four points this is done for NLSM, DBI and sGal whilst at six points only NLSM and DBI are analysed. In each case, the soft limits uniquely fix the masses and couplings including all the curvature coefficients. Appendices present the cases of sGal at four-points and DBI

at six-points in greater detail. This is followed by some brief comments on the thesis as a whole and some future directions of particular interest to the author in chapter 7.

Chapter 2

Basics of Scattering Amplitudes

As highlighted in the previous chapter, there are many different aspects to the study of scattering amplitudes and so there are also a variety of tools that can be used to manipulate and understand them. As the rest of this thesis covers a broad range of topics, this background chapter will introduce many different concepts. This will start with a review of scattering amplitude basics: definitions (2.1), spinor helicity notation (2.1.1) and the role of both the conformal group (2.1.2) and supersymmetry (2.1.3), particularly in relation to super Yang-Mills (SYM) and supergravity. It then introduces momentum twistor notation and supermomentum twistors in section 2.1.4. This is followed by more topics of relevence to the geometry program in amplitudes with a recap of BCFW recursion (2.2) and how it is linked to ideas about polytopes and spurious poles (2.2.1) as well as introducing on-shell diagrams (2.2.2). It then introduces analogues of scattering amplitudes in both Anti-de Sitter (2.3.1) and de Sitter (2.3.2), how these may be linked to flat space amplitudes and some of the basic features of each. Finally there is an introduction on some of the physics that will be explored in curved space times. This is divided into two areas: firstly colour-kinematics and the double copy linking gauge and gravitational theories (2.4); secondly the story of soft limits and hidden symmetries in 'exceptional' scalar field theories (2.5).

Further details on much of the background can be found in [90–92] as well as in the

other references.

2.1 Amplitude Definitions

Scattering amplitudes in flat space will generally be denoted as A_n with the number of spacetime dimensions given by d. These will be functions of n conserved momenta k_a^μ which are taken to all be incoming such that

$$\sum_{a=1}^{n} k_a^\mu = 0, \tag{2.1.1}$$

with $\mu = 0, 1, \ldots, d-1$. Metrics will use the mostly positive convention such that the (flat space) dot product of two momenta is given by contracting with $\eta_{\mu\nu} = \text{diag}(-1, 1, \ldots, 1)$

$$\eta_{\mu\nu} k_a^\mu k_b^\nu = -k_a^0 k_b^0 + \sum_{i=1}^{d-1} k_a^i k_b^i. \tag{2.1.2}$$

Massive on-shell particles therefore satisfy $k_a^2 = \eta_{\mu\nu} k_a^\mu k_a^\nu = -m_a^2$ although much of what follows will use null momenta satisfying $k_a^2 = 0$. For spinning particles, the A_n will also depend on some polarisation data associated to the external states. For spin-1 (gluons) these will be vectors ϵ_a^μ whilst for spin-2 (gravitons) they will be symmetric tensors $\epsilon_a^{\mu\nu}$. The exact form of these polarisations depends on the theory and will differ when deviating from flat space – more details are included in sections 2.1.1 and 2.3.1 where polarisations are introduced in the contexts of spinor helicity notation in 4d Minkowski and AdS_4 respectively. In the case of theories with supersymmetry, it is often convenient instead to work at the level of 'superamplitudes', where all the polarisation information is encoded within an on-shell superspace formalism. This will be elaborated on in section 2.1.3.

These scattering amplitudes characterise the interactions of fundamental particles. Physically the probability of a given interaction can be obtained from the differential cross-section $d\sigma/d\Omega \sim |A_n|^2$. This assumes that the initial and final states are independent (well-separated and non-interacting). They can be obtained via an LSZ

amputation procedure from Green's functions although the details of this will not be important for this thesis (except to note that the approach will need to be modified in curved spacetimes). Scattering amplitudes are perturbative objects computed as an expansion in some small coupling parameter (often denoted λ for scalar theories or g for Yang-Mills) corresponding to the strength of the interaction. The body of the thesis only considers tree-level quantities and so the coupling will often be set to 1 for simplicity.

One final key feature of amplitudes is the level of permutation symmetry they enjoy. This is related to both the spin of the particles and the gauge symmetry of the theory. As all the amplitudes in this thesis are bosonic, they should have full permutation symmetry. However for theories with colour (most notably Yang-Mills although this will also be relevent for the non-linear sigma model) dealing with the full colour structure is often unecessary and so the focus is instead on colour-ordered amplitudes which are only invariant under cyclic permutations. This is especially useful since for most of this thesis is primarily interested in the kinematic dependence of amplitudes. Colour factors are stripped off when defining the Feynman rules and such that colour assignments can be ignored throughout most of the calculation. Recovering the full amplitude at the end (if needed), can be done by summing over non-cyclic orderings

$$\mathbb{A}_n = \sum_{\sigma \in S_n/Z_n} \mathrm{Tr}(T^{a_{\sigma_1}} T^{a_{\sigma_2}} \dots T^{a_{\sigma_n}}) A_n(k_{\sigma_1}, k_{\sigma_2}, \dots, k_{\sigma_n}). \tag{2.1.3}$$

2.1.1 Spinor Helicity

When writing amplitudes involving massless particles with spin in 4 dimensions, it is often useful to use spinor helicity notation. They naturally encode information about the polarisations of the particles and in many cases can lead to dramatic simplifications in expressions (such as the famous Parke-Taylor result for gluons [6]). The formalism can also be modified to include supersymmetry data (required in chapter 3) or momenta in curved spacetimes (chapter 4).

The starting point can be given by contracting a massless 4-momentum $k \in \mathbb{C}^{1,3}$

with the Pauli matrices $(\mathbb{I}, \sigma_i)$ to get

$$k_{\alpha\dot{\alpha}} = k_\mu \sigma^\mu_{\alpha\dot{\alpha}} = \begin{pmatrix} -k_0 + k_3 & k_1 - ik_2 \\ k_1 + ik_2 & -k_0 - k_3 \end{pmatrix}, \tag{2.1.4}$$

where $\alpha, \dot{\alpha} = \{1, 2\}$ are $\mathrm{SL}(2, \mathbb{C})$ indices. Observing that $\det(k^{\alpha\,\dot{\alpha}}) = k_\mu k^\mu = 0$, the matrix has rank 1 and can be written as an outer product of a pair of spinors

$$k^{\alpha\dot{\alpha}} = \lambda^\alpha \widetilde{\lambda}^{\dot{\alpha}}. \tag{2.1.5}$$

Since a massless 4-momentum only has 3 independent components (with the 4th given by the on-shell constraint), the spinors must have some redundancy. This is given by the "little group" transformation which simultaneously scales both the λ and $\widetilde{\lambda}$ spinors

$$\lambda \to t\lambda, \quad \widetilde{\lambda} \to \frac{1}{t}\widetilde{\lambda}, \tag{2.1.6}$$

for some $t \in \mathbb{C}$. This little group scaling can be used to constrain three-point amplitudes.

The indices can be raised or lowered using the 2-index Levi-Civita symbol, allowing for the contraction of various spinors and the construction of kinematic invariants in the form of angle and square brackets.

$$\begin{aligned} \langle ab \rangle &= \epsilon^{\alpha\beta} \lambda_{a\alpha} \lambda_{b\beta} = \lambda_{a\alpha} \lambda_b^\alpha, \\ [ab] &= -\epsilon^{\dot{\alpha}\dot{\beta}} \widetilde{\lambda}_{a\dot{\alpha}} \widetilde{\lambda}_{b\dot{\beta}} = \widetilde{\lambda}_a^{\dot{\alpha}} \widetilde{\lambda}_{b\dot{\alpha}}, \end{aligned} \tag{2.1.7}$$

where $\epsilon^{12} = \epsilon^{\dot{1}\dot{2}} = -\epsilon_{12} = -\epsilon_{\dot{1}\dot{2}} = 1$. In the case of real momenta, these spinor brackets are complex conjugates of each other such that their product is real. This is required since the usual dot product between two 4-momenta is given by

$$\eta^{\mu\nu} k_{a\mu} k_{b\nu} = \frac{1}{2} \langle ab \rangle [ab]. \tag{2.1.8}$$

They can also be used to express gluon polarisation vectors. These contain unfixed degrees of freedom as a consequence of the gauge-symmetry of Yang-Mills theory, manifesting in the presence of arbitrary 'reference spinors' appearing in the

polarisations. Since these are unphysical, the final scattering amplitudes must be independent of any particular choice of reference spinor. This can sometimes be used to simplify calculations by choosing reference spinors which cause many spinor brackets to vanish. Using a refence spinor denoted μ, the polarisations can be expressed as

$$\epsilon^{+}_{\alpha\dot{\alpha}} = -\frac{\widetilde{\lambda}_{\dot{\alpha}}\mu_{\alpha}}{\langle\lambda\mu\rangle}, \qquad \epsilon^{-}_{\alpha\dot{\alpha}} = -\frac{\lambda_{\dot{\alpha}}\tilde{\mu}_{\alpha}}{[\lambda\mu]}. \tag{2.1.9}$$

Polarisation vectors will be revisited in section 2.3.1 for AdS.

Spinors satisfy a number of useful relations that can be used to manipulate and simplify expressions. The most straightforward of these is the Schouten identity, which is a consequence of the antisymmetry of the spinor brackets for a 2 component object. The Schouten identity for undotted spinors is given by

$$\langle ab\rangle\,\lambda_c + \mathrm{cyc}(abc) = 0, \tag{2.1.10}$$

where the α index has been suppressed; the case for dotted spinors is analogous. Outer products of spinors also inherit momentum conservation from the original 4-vectors

$$\sum_{a=1}^{n} \lambda_a^{\alpha}\widetilde{\lambda}_a^{\dot{\alpha}} = 0. \tag{2.1.11}$$

Schouten identities and momentum conservation can be contracted with additional spinors to produce a variety of specific relations. These are especially powerful for small n, for example at four point this implies

$$\langle 12\rangle[24] = -\langle 13\rangle[34]. \tag{2.1.12}$$

These relations will be used in flat space to work with $\mathcal{N} = 7$ supergravity whilst their AdS equivalents will be used for Yang-Mills.

2.1.2 The Conformal Group for Amplitudes

Symmetries underpin a lot of the study of scattering amplitudes. In most cases, amplitudes in flat space are invariant under translations and Lorentz transformations

(although there are some interesting physical systems where one or both of these is explicitly broken). This corresponds to the set of transformations that leaves a proper length (ie a difference of vectors contracted with the Minkowski metric) invariant. As such they will be functions only of the kinematic invariants given by the inner products of momenta and polarisations. This section looks at the extension of this group to include conformal symmetry since there are interesting amplitudes which exhibit this larger class of symmetries. One notable example is $\mathcal{N} = 4$ super Yang-Mills which also has additional symmetries including under dual conformal transformations and the larger class of Yangian symmetries [93]. The conformal group will also be important to work in AdS and dS, where the group is closely linked to the isometries of the spacetime.

The generators which make up the conformal group include the $\frac{d}{2}(d-1)$ rotations $L_{\mu\nu}$ and d translations P^μ from the Poincaré group. To these we add the dilatation (rescaling) operator $x^\mu \to Dx^\mu = \alpha x^\mu$ and the inversion $x^\mu \to \mathcal{I}x^\mu = \frac{x^\mu}{x^2}$. The inversion is typically treated using the special conformal transformation

$$K^\mu = \mathcal{I}P^\mu\mathcal{I}, \tag{2.1.13}$$

since it is easier to work with continuous transformations. Together these make up the $\frac{1}{2}(d+1)(d+2)$ generators of $\mathrm{SO}(d,2)$, the d-dimensional conformal group. The generators most commonly appear in position space where they take the form

$$\begin{aligned} P_\mu &= i\partial_\mu, \\ M_{\mu\nu} &= i\left(x_\mu\partial_\nu - x_\nu\partial_\mu\right), \\ D &= ix^\mu\partial_\mu, \\ K_\mu &= i(2x_\mu(x^\nu\partial_\nu) - x^2\partial_\mu), \end{aligned} \tag{2.1.14}$$

There also exist ways of encapsulating all the generators into a single set of objects with a universal commutator [94]. In the same way as momenta are conserved, the other generators also have corresponding conservation laws often referred to as conformal Ward identities. These will be discussed in more detail in section 2.3.2

where they will be applied to quantities in de Sitter.

The conformal generators can be rewritten in momentum space using the spinor helicity notation introduced in 2.1.1. These generators will not need to be explicitly used here, however their general form will help motivate the introduction of supersymmetry generators so they are included for completeness. They are given by [91]

$$\begin{aligned} P^{\mu} &\to P^{\alpha\dot{\alpha}} = \lambda^{\alpha}\widetilde{\lambda}^{\dot{\alpha}}, \\ K_{\mu} &\to K_{\alpha\dot{\alpha}} = \partial_{\alpha}\partial_{\dot{\alpha}}, \\ M_{\mu\nu} &\to M_{\alpha\beta} = \lambda_{(\alpha}\partial_{\beta)}, \\ &\to \bar{M}_{\dot{\alpha}\dot{\beta}} = \widetilde{\lambda}_{(\dot{\alpha}}\partial_{\dot{\beta})}, \\ D &\to \frac{1}{2}\lambda^{\alpha}\partial_{\alpha} + \frac{1}{2}\widetilde{\lambda}^{\dot{\alpha}}\partial_{\dot{\alpha}} + 1. \end{aligned} \tag{2.1.15}$$

In spinor notation, the action of the Lorentz group splits into the independent $\mathrm{SU}(2)_{\mathrm{L}}$ and $\mathrm{SU}(2)_{\mathrm{R}}$ actions. This is the reason that the λ and $\widetilde{\lambda}$ spinors carry different indices - they transform under different representations of the Lorentz group. These operators all commute with the helicity generator

$$h = -\frac{1}{2}\lambda^{\alpha}\partial_{\alpha} + \frac{1}{2}\widetilde{\lambda}^{\dot{\alpha}}\partial_{\dot{\alpha}}, \tag{2.1.16}$$

this will be relevant in section 2.2 when constructing amplitudes [91].

2.1.3 Superamplitudes

For the material in chapter 3 the above set of generators need to be extended to include supersymmetry. This extension will result in the 4d superconformal group. We start by introducing fermionic generators $Q^{\alpha A}$ and $\bar{Q}^{\dot{\alpha}}_{I}$, where I is an R-symmetry index running from 1 to $\mathcal{N}$ for a SUSY with $\mathcal{N}$ supersymmetric generators. These obey anticommutation relations

$$\{Q^{\alpha I}, \bar{Q}^{\dot{\alpha}}_{J}\} = \delta^{I}_{J} P^{\alpha\dot{\alpha}}. \tag{2.1.17}$$

The R-symmetry comes from the set of SU($\mathcal{N}$) transformations which map the Qs into each other. These operators generate the particle content of the theory. For example, one can start from the negative helicity gluon and $\mathcal{N} = 4$ and successively apply $Q^{\alpha I}$ to obtain the 4 anti-fermions, 6 scalars, 4 fermions and the positive helicity gluon that make up the rest of the content of $\mathcal{N} = 4$ SYM. Closure of the group also requires the addition of the superconformal generators $S_{\alpha I}$ and $\bar{S}^I_{\dot{\alpha}}$ but these will not be needed here (a full breakdown of the generators, their commutators and other properties may be found in [91] and [90]).

Analogous to the bispinor form of the momentum k, the supermomentum of a given particle can be represented using a fermionic variable η^A,

$$q_a^{\alpha I} = \lambda_a^\alpha \eta_a^I, \qquad \bar{q}_{aI}^{\dot{\alpha}} = \tilde{\lambda}_a^{\dot{\alpha}} \frac{\partial}{\partial \eta_a^I}. \tag{2.1.18}$$

It is these fermionic ηs that will enable us to work at the level of 'superamplitudes' rather than dealing with individual component amplitudes. This is especially useful in the case of maximally supersymmetric theories ($\mathcal{N} = 4$ for Yang-Mills and $\mathcal{N} = 8$ for gravity) since here the particle content of the theory can be collected into a single 'superfield'. For example in $\mathcal{N} = 4$ SYM, the superfield can be expanded as

$$\Phi(p, \eta) = g_+(k) + \eta^I \tilde{g}_I(k) + \cdots + \eta^4 g_-(k), \tag{2.1.19}$$

where we use the shorthand $\eta^4 = \frac{1}{4!}\eta^I\eta^J\eta^K\eta^L\epsilon_{IJKL}$. Superamplitudes are then constructed by considering scattering of superfields $\Phi(k_i, \eta_i)$ and the fermionic variables provide a natural bookkeeping mechanism to keep track of the component subamplitudes. For each superamplitude, momenta and supermomenta are conserved. This contributes a set of delta functions which form an overall factor and the rest can be expanded as a power series in η

$$\mathcal{A}_n(p, \eta) = \delta^{(4)}(P)\delta^{(2\mathcal{N})}(Q)\left(A_n^{(0)} + A_n^{(\mathcal{N})} + \cdots + A_n^{(\mathcal{N}(n-4))}\right), \tag{2.1.20}$$

where in the case of gluons and $\mathcal{N} = 4$ SYM we have that the A each have an η-scaling that is a multiple of 4. R-symmetry considerations ensure that all terms

in the series with fermionic powers other than $a\mathcal{N}$ for $a \in \mathbb{N}$ must vanish [91]. This leads us to recover the MHV classification of amplitudes from supersymmetry considerations – amplitudes with different numbers of positive and negative helicity gluons will appear in different A_n. Supersymmetry also provides an argument as to why all-plus and single-minus vanish. The η^8 dependence of the leading term requires that it come from scattering 2 negative helicity gluons with $n-2$ positive helicity. A hypothetical N^{-1}MHV amplitude would therefore not be invariant under SUSY transformations and so must vanish. The MHV superamplitude contains all the MHV gluon amplitudes along with other component amplitudes involving fermions and scalars.

Equation (2.1.19) and the superamplitude expansion also extend to higher $\mathcal{N}$ and supergravity in the obvious way. For maximal ($\mathcal{N} = 8$) supergravity we start with the positive helicity graviton and can generate the other 31 states in the theory using $Q^{\alpha A}$ with A running from 1 to 8. In each case, component amplitudes can be obtained by integrating out the fermionic degrees of freedom, taking advantage of the Grassman-odd nature of the ηs. For example in $\mathcal{N} = 8$, a graviton amplitude can be extracted by integrating

$$M_n = \int d^{8\times n}\eta \prod_{a\in+} \eta_a^8 \mathcal{M}_n(k,\eta), \tag{2.1.21}$$

where the product is over the legs associated to positive helicity gravitons. Equivalently, the same result can be obtained by integrating out only the η_i associated to the negative gravitons and setting the rest to zero.

This classification is discussed further in section 2.2 where symmetries are used to construct the three-point amplitudes and superamplitudes, required as an input to use recursion relations for generating higher point amplitudes.

2.1.4 Momentum Twistors

In our analysis of gravitational amplitudes in chapter 3, we will be interested in the pole structure and how it arises from recursion. This has been studied extensively for

gauge theory, often using momentum twistor variables [18] and so similar techniques shall be applied to supergravity.

Momentum twistors can be constructed as a variation on spinor helicity, motivated by looking for a set of variables under which all the generators of the conformal group are linear [90]. We start by defining new region momenta x based on a specific ordering of the external legs

$$(x_a - x_{a+1})^{\alpha\dot{\alpha}} = p_a^{\alpha\dot{\alpha}}. \tag{2.1.22}$$

These can be visualised as the vertices of a polygon with edges corresponding to the null momenta p_i as illustrated in figure 2.1. A new dotted spinor is then defined via the incidence relation

$$\mu^{\dot{\alpha}} = x^{\alpha\dot{\alpha}}\lambda_\alpha. \tag{2.1.23}$$

Unlike the $\widetilde{\lambda}$ spinors, this μ has the same little group scaling as λ so the pair (λ, μ) represents a point in projective spacetime $\mathbb{CP}^3$, known as twistor space. Momentum twistors are then defined as

$$Z_a^A = \left(\lambda_a^\alpha, \mu_a^{\dot{\alpha}}\right), \tag{2.1.24}$$

where $A \in \{1, .., 4\}$ are indices in the fundamental representation of the dual conformal group SU(4). These can mapped back into region momenta using

$$x_a^{\alpha\dot{\alpha}} = \frac{\lambda_a^\alpha \mu_{a-1}^{\dot{\alpha}} - \lambda_{a-1}^\alpha \mu_a^{\dot{\alpha}}}{\langle a{-}1\, a\rangle}, \tag{2.1.25}$$

implying that a point x_a corresponds to a line in momentum twistor space associated to a pair of twistors Z_{a-1} and Z_a. Using this correspondence, a null polygon in momentum space can be mapped into a polygon in momentum twistor space, as depicted in Figure 2.1. This mapping essentially swaps edges and vertices. From a practical standpoint, momentum twistors are very useful because they automatically encode momentum conservation, but they also have a number of other important properties. In the context of Yang-Mills amplitudes, they make the cancellation of spurious poles manifest and give rise to a geometric interpretation of NMHV

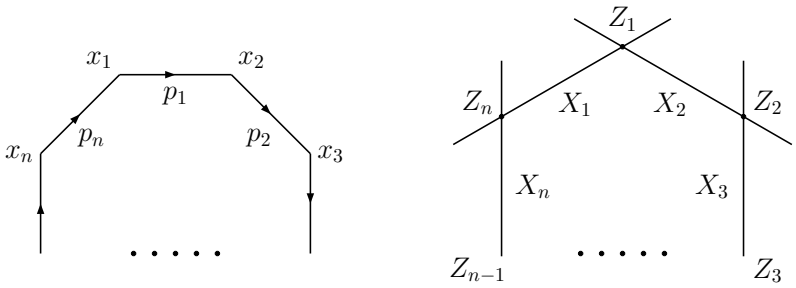

Figure 2.1: Diagrams indicating the relation between momenta p_i, dual variables x_i and momentum twistors Z_i.

amplitudes in terms of the volumes of polytopes [18, 19]. This will be discussed further in section 2.2.1 and chapter 3.

Using momentum twistors, one can define the following invariants of the dual conformal group:

$$\langle abcd\rangle = \epsilon_{ABCD} Z_a^A Z_b^B Z_C^A Z_D^A, \tag{2.1.26}$$

where ϵ is the 4d Levi-Cevita symbol. We can express the linear dependence of any 5 momentum twistors using this 4-bracket,

$$Z_a \langle bcde\rangle + \text{cyc}(abcde) = 0. \tag{2.1.27}$$

This can be thought of as a higher-dimensional analogue of the Schouten identity in equation (2.1.10). The angle-brackets in equation (2.1.7) can be obtained from momentum twistors using

$$\langle ab\rangle = I_{AB} Z_a^A Z_a^B, \;\; I_{AB} = \begin{pmatrix} \epsilon_{\alpha\beta} & 0 \\ 0 & 0 \end{pmatrix}, \tag{2.1.28}$$

where I_{AB} is called the infinity twistor and breaks dual conformal symmetry. It is also convenient to define the following 6-brackets [95]

$$\begin{aligned} \langle abc|I|ijk\rangle &= \langle ab\rangle \langle cijk\rangle + \text{cyclic}(a,b,c), \\ &= \langle abci\rangle \langle jk\rangle + \text{cyclic}(i,j,k), \end{aligned} \tag{2.1.29}$$

$$\langle a|I|bc|ijk\rangle = \langle ab\rangle \langle cijk\rangle - \langle ac\rangle \langle bijk\rangle ,$$

$$= -\left(\langle ai\rangle\,\langle jkbc\rangle + \text{cyclic}(i,j,k)\right), \tag{2.1.30}$$

where the second lines can be obtained using (2.1.27). These brackets have an elegant geometrical interpretation in terms of intersections of lines and planes in momentum twistor space (for more details see [95]). They can also be used to express the square brackets in (2.1.7) in terms of momentum twistors

$$[ab] = \frac{\langle a{-}1\, a\, a{+}1|I|b{-}1\, b\, b{+}1\rangle}{\langle a{-}1\, a\rangle\,\langle a\, a{+}1\rangle\,\langle b{-}b\, b\rangle\,\langle b\, b{+}1\rangle}. \tag{2.1.31}$$

In general, the numerator in (2.1.31) has three terms but there are two cases when it simplifies:

$$[a\, a{+}1] = \frac{\langle a{-}1\, a\, a{+}1\, a{+}2\rangle}{\langle a{-}1\, a\rangle\,\langle a\, a{+}1\rangle\,\langle a{+}1\, a{+}2\rangle}, \tag{2.1.32}$$

$$[a\, a{+}2] = \frac{\langle a{-}1\, a\, a{+}1\, a{+}2\rangle\,\langle a{+}3\, a{+}1\rangle + \langle a{-}1\, a\, a{+}1\, a{+}3\rangle\,\langle a{+}1\, a{+}2\rangle}{\langle a{-}1\, a\rangle\,\langle a\, a{+}1\rangle\,\langle a{+}1\, a{+}2\rangle\,\langle a{+}2\, a{+}3\rangle}. \tag{2.1.33}$$

Other kinematic invariants such as multi-particle factorisation poles $s_{a_1\ldots a_k}$ and spurious poles can also be written in terms of momentum twistor 4-brackets. They likewise take simpler forms when the momentum labels are adjacent.

2.1.5 Super Momentum Twistors

Now we will briefly review the extension to supersymmetric theories. By analogy to (2.1.22), we may define fermionic region momenta

$$(\theta_a - \theta_{a+1})^{\alpha I} = q_a^{\alpha I} = \lambda_a^\alpha \eta_a^I, \tag{2.1.34}$$

where the supermomentum q_a is defined in (3.1.2). Momentum supertwistors are then defined as $\left(Z_a^A, \chi_a^I\right)$, where $\chi_a = \theta_a \cdot \lambda_a$. The supersymmetric extension of (2.1.25) is then given by

$$\theta_a^{\alpha I} = \frac{\lambda_a^\alpha \chi_{a-1}^I - \lambda_{a-1}^\alpha \chi_a^I}{\langle a{-}1\, a\rangle}. \tag{2.1.35}$$

Combining equations 2.1.34 and 2.1.35 to eliminate the region variables θ allows us to convert directly between the η and χ fermionic variables with

$$\eta_a = \frac{\langle a\, a{+}1\rangle \chi_{a-1} + \langle a{+}1\, a{-}1\rangle \chi_i + \langle a{-}1\, a\rangle \chi_{a+1}}{\langle a{-}1\, a\rangle \langle a\, a{+}1\rangle}. \tag{2.1.36}$$

Fermionic delta functions can then be converted from the usual representation in terms of η into twistor notation via

$$\delta^{(0|\mathcal{N})}\left([a\, a{+}1]\, \eta_{a+2} + \text{cyc}\right) = \frac{\delta^{(0|\mathcal{N})}\left(\langle a{-}1\, a\, a{+}1\, a{+}2\rangle\, \chi_{a+3} + \text{cyc}\right)}{\left(\langle a{-}1\, a\rangle\, \langle a\, a{+}1\rangle\, \langle a{+}1\, a{+}2\rangle\, \langle a{+}2\, a{+}3\rangle\right)^{\mathcal{N}}}, \tag{2.1.37}$$

where $\mathcal{N}$ denotes the amount of supersymmetry. This formula is proved explicitly in [1].

2.2 BCFW Recursion

There are many different recursion relations that can be used to construct amplitudes but the one of interest to our analysis of supergravity is the on-shell BCFW recursion [15]. The original form of this will not be used to calculate amplitudes in this thesis, but the steps involved are nevertheless useful for understanding the construction of on-shell diagrams and how they are generalised to supergravity.

The starting point for this is an n-point amplitude with momenta taken to be complex. Obviously any physical process can only depend on real momenta but it is useful to consider the amplitude as a complex function in the intermediate stages. Two momenta are deformed such that they remain on-shell (massless) and that momentum conservation still holds. This can be done using the spinors defined in 2.1.1. For example, we can define shifted momenta $\hat{k}_1$ and $\hat{k}_n$ via

$$\begin{aligned} |\hat{1}\rangle &= |1\rangle + z|n\rangle, \qquad |1] = |1], \\ |\hat{n}] &= |n] - z|1], \qquad |n\rangle = |n\rangle, \end{aligned} \tag{2.2.1}$$

where $z \in \mathbb{C}$ then we still have that $\hat{k}_1^2 = \hat{k}_n^2 = 0$ and $\hat{k}_1 + \hat{k}_n = k_1 + k_n$ but now we can consider the amplitude as a function of the complex parameter z. The original

amplitude that we would like to calculate is given by $A_n(z=0)$. We then consider the poles of $A(z)$. At tree-level, it is a rational function of z and the kinematics. Any poles can thus only occur when some internal propagator goes on shell

$$\hat{P}^2 = P^2 + \langle n|P|1] = 0, \tag{2.2.2}$$

where $\langle n|P|1] = \lambda_{n\alpha} P^{\alpha\dot{\alpha}} \widetilde{\lambda}_{1\dot{\alpha}}$. These are the points where the amplitude factorises and we can write

$$\lim_{z\to z_P} A_n(z) = \frac{1}{z - z_P} \frac{1}{\langle n|P|1]} \sum_s \hat{A}_L(z_P) \hat{A}_R(z_P), \tag{2.2.3}$$

where z_P is the value where propagator $1/P^2$ is on-shell, A_L and A_R are the two subamplitudes and the sum is over the possible states which can be exchanged. Typically these will be gluons or gravitons and the sum is over the two helicity assignments. We can then use a contour integral to extract $A_n(0)$

$$A_n(0) = \oint_{z=0} \frac{dz}{2\pi i} \frac{A_n(z)}{z}, \tag{2.2.4}$$

where the integral is around a closed contour containing $z = 0$. If we have that $\lim_{z\to\infty} A_z(z) \to 0$ then the full amplitude can be recovered by a global residue theorem, wrapping the contour around all the other z_P poles. $A_n(0)$ can then be fully reconstructed from summing over the possible factorisation channels

$$A_n = \sum_P \sum_s \hat{A}_L(z_P) \frac{1}{P^2} \hat{A}_R(z_P). \tag{2.2.5}$$

Note that the propagators which appear in this final formula are unshifted, the BCFW shifts only enter via the two sub-amplitudes. Different choices of shift are possible, in particular with helicity amplitudes one can choose whether to shift legs of the same or differing helicities as well as which should have the λ or $\widetilde{\lambda}$ spinors shifted. The choices can lead to different z-scaling of the amplitude in the limit $z \to \infty$ as well as different terms contributing in the sum over residues [90]. The shift in equation (2.2.1) is the one that will be used in chapter 3 since it has nice features when it is used for $\mathcal{N} = 7$ sugra. There also exist other variants on BCFW,

for example some schemes choose to shift multiple legs in order to ensure the residue at infinity vanishes [96].

All that is needed to complete the recursion are the seed amplitudes that can appear as A_L and A_R. In the case of Yang-Mills and gravity these come from three-point and can be assembled entirely from symmetry considerations.

Kinematics for three massless particles is special since if we have three conserved momenta k_a with $a \in \{1, 2, 3\}$ then clearly

$$k_1 \cdot k_2 = k_3^2 = 0 \tag{2.2.6}$$

by momentum conservation. Applying this three times implies that all $k_a \cdot k_b = 0$ and the amplitude must be trivial. However, in the case of complex momenta this condition becomes

$$\langle 12\rangle[12] = 0, \tag{2.2.7}$$

where now each bracket is independent. We are now free to choose either bracket to be zero to satisfy the required constraint. Applying this three times and combining with the Schouten identity in equation (2.1.10) then implies that either all three $\langle ab\rangle = 0$ or all $[ab] = 0$. Choosing $[ab] = 0$ implies that all the $\widetilde{\lambda}_c$ spinors are proportional and vice versa for $\langle ab\rangle = 0$ and the λ_c spinors.

If we choose $[ab] = 0$ we can construct three-point amplitudes from the angle brackets. This is done by requiring that they transform correctly under the helicity operator in equation(2.1.16). Consistency conditions mean that for gluons (spin-1), the only valid amplitude is the MHV case whilst for non-zero square brackets we obtain the $\overline{\text{MHV}}$ amplitude. This gives the two three-point amplitudes

$$\begin{aligned} A_{3,2}(--+) &= \frac{\langle 12\rangle^4}{\langle 12\rangle\langle 23\rangle\langle 31\rangle}, \\ A_{3,1}(++-) &= \frac{[12]^4}{[12][23][31]}, \end{aligned} \tag{2.2.8}$$

where we have used the subscript $A_{n,k}$ for an amplitude with n points and MHV degree k (this counts the number of negative helicity gluons). The three-point $\overline{\text{MHV}}$ is unique in having MHV degree 1. Combining these with the recursion in equation

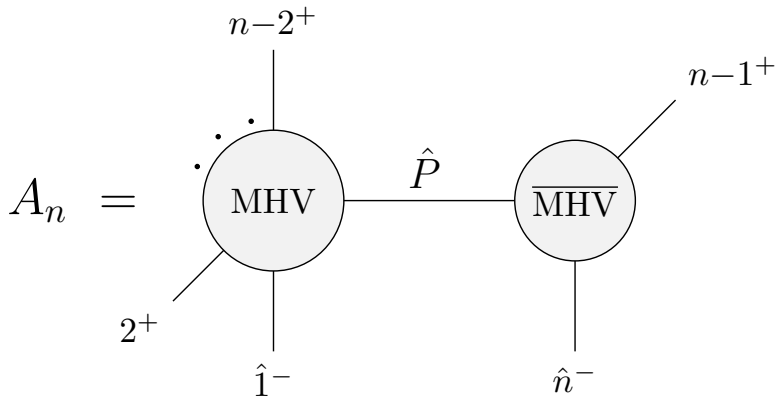

Figure 2.2: Diagram illustrating the single term BCFW recursion for MHV amplitudes with shifts on negative helicity gluons.

2.2.5 is sufficient to obtain all the tree-level amplitudes. The special three-point kinematics can lead to some useful simplifications when recursing MHV amplitudes. Since the only non-zero amplitude with a single negative gluon is the three-point one, if one chooses a BCFW shift on two negative helicty legs then an n-point MHV amplitude will only be consist of a single non-zero term in the recursion – the one containing the propagator $P^2 = (k_{n-1} + k_n)^2$. This is illustrated diagrammatically in figure 2.2.

Extending BCFW recursion to gravity requires no modifications to equation 2.2.5 although the sum will include all permutations of the unshifted legs rather than simply cyclic orderings, so that each term will generically be a sum of $(n-2)!$ terms. The seed amplitudes for gravity can be obtained analogously and are given by

$$\begin{aligned} M_{3,2}(--+) &= \frac{\langle 12\rangle^8}{\langle 12\rangle^2\langle 23\rangle^2\langle 31\rangle^2}, \\ M_{3,1}(++-) &= \frac{[12]^8}{[12]^2[23]^2[31]^2}. \end{aligned} \tag{2.2.9}$$

These are squares of the Yang-Mills cases, an example of double copy relations between Yang-Mills and gravity (discussed further in section 2.4). Including supersymmetry requires an additional shift to the supermomenta. This can be motivated in exactly the same way as the momentum shifts - defining a shifted $\hat{\lambda}_1$ will shift $\hat{Q}_1 = \hat{\lambda}_1\eta_1$ and so a corresponding shift is needed to preserve supermomentum

conservation. The obvious choice here is to shift

$$\hat{\eta}_n = \eta_n - z\eta_1, \tag{2.2.10}$$

such that $\hat{Q}_1 + \hat{Q}_n = Q_1 + Q_n$. This leaves the poles of the superamplitude unchanged, the only significant modification is that the sum over states present in each term is lifted to an integral over the η exchanged by the propagator. This uplift is important when constructing on-shell diagrams since it is more straightforward to implement than the non-SUSY sum over states.

The three-point amplitudes for super Yang-Mills and sugra are similarly constrained. In the case of $\mathcal{N} = 4$ and $\mathcal{N} = 8$ they take a very elegant form

$$\begin{aligned}
\mathcal{A}_{3,2} &= \frac{\delta^{(4|8)}(P|Q)}{\langle 12\rangle\langle 23\rangle\langle 31\rangle}, \\
\mathcal{A}_{3,1} &= \frac{\delta^{(4|4)}(P|[23]\eta_1 + [31]\eta_2 + [12]\eta_3)}{[12][23][31]}, \\
\mathcal{M}_{3,2} &= \frac{\delta^{(4|16)}(P|Q)}{\langle 12\rangle^2\langle 23\rangle^2\langle 31\rangle^2}, \\
\mathcal{M}_{3,1} &= \frac{\delta^{(4|8)}(P|[23]\eta_1 + [31]\eta_2 + [12]\eta_3)}{[12]^2[23]^2[31]^2}.
\end{aligned} \tag{2.2.11}$$

where we have included the bosonic as well as fermionic delta functions. The non-supersymmetric three-point amplitudes can be recovered by integrating out/ setting to zero the ηs as described in section 2.1.3.

One further detail of interest in chapter 3 are the so-called "bonus relations". This refers to a set of relations in supergravity that can be used to simplify the results from BCFW recursion [97, 98]. In supergravity, the scaling of $\lim_{z\to\infty} \mathcal{M}_n(z) \sim 1/z^2$. This means that a residue theorem involving the object $z\mathcal{M}_n(z)$ also has no contribution from infinity. This can be used to generate relations between BCFW terms and these bonus relations reduce the number of terms which appear from $(n-2)!$ to $(n-3)!$. In chapter 3 a recursion for $\mathcal{N} = 7$ is introduced which automatically encodes these relations.

2.2.1 Geometry and Spurious Poles

BCFW gives us a method for calculating amplitudes by recursing three-point quantities to generate amplitudes with any number of points. One important and interesting feature of the recursion is the appearance of spurious poles, and their relation to geometrical descriptions of the scattering amplitude. Amplitudes can only contain poles allowed by locality, these come either from when propagators go on-shell or when external momenta become soft or collinear. In the case of Yang-Mills, these can only be of the form $[a\,a{+}1] = 0$, $\langle a\,a{+}1\rangle = 0$, or $(k_1 + k_2 + \cdots + k_b)^2 = 0$; ie. the all involve adjacent or sequential momenta. In gravity, there is no external ordering so any poles of those types are allowed but there are other objects that can be constructed of spinor brackets that are excluded, the most simple of which is $[a|b+c|d\rangle$ (for other kinematic invariants to appear in spurious poles requires $n \geq 8$). If one of these appears in a term in BCFW, it must be cancelled by another corresponding pole from another term. This is one way of seeing a geometrical picture of amplitudes emerge. Applying BCFW in different schemes (eg. choosing to shift different external legs) leads to expressions with different spurious poles appearing yet they always cancel in the full amplitude. This can be seen as analogous to the different ways of triangulating a polytope [18]. In this picture, the association between amplitudes and geometry is such that poles an amplitude correspond to boundaries in corresponding geometry. Spurious poles are thus "spurious boundaries" ie. internal ones which do not appear as part of the full object.

For poles in super Yang-Mills amplitudes, the story is even more elegant. The NMHV amplitudes can be written as a sum of "R-invariants", given by

$$R^{(\mathcal{N})}_{abc} = \frac{\delta^{(0|\mathcal{N})}\left(\langle a\,b-1\,b\,c-1\rangle\,\chi_c + \text{cyc}\right)}{\langle a\,b-1\,b\,c-1\rangle\,\langle b-1\,b\,c-1\,c\rangle\,\langle b\,c-1\,c\,a\rangle\,\langle c-1\,c\,a\,b-1\rangle\,\langle c\,a\,b-1\,b\rangle}, \tag{2.2.12}$$

where we have used the twistor notation introduced in section 2.1.4. These are invariant under the dual superconformal group and are useful for exploring the properties of super Yang-Mills. Each R-invariant has 5 poles, those not of the form

$\langle a\, a{+}1\, b\, b{+}1\rangle$ are spurious. The use of R-invariants in supergravity and with $\mathcal{N}=7$ is explored in chapter 3. In the case $\mathcal{N}=4$, they are also projectively invariant and can be related to the volume of a polytope in $\mathbb{CP}^4$ [19]. The geometrical interpretation is less clear for $\mathcal{N}\neq 4$ however.

2.2.2 On Shell Diagrams

We conclude this discussion on recursion relations with a brief introduction to on-shell diagrams. These can be motivated as an elegant, graphical representation of super-BCFW recursion but the diagrams also encode many additional and surprising properties of SYM amplitudes with links to algebraic geometry and combinatorics [7]. They can also be used for loop level recursion. Here we will restrict to some of the more basic properties of on-shell diagrams including equivalence relations that can be used to map between them and how to use them to calculate the corresponding on-shell expressions in momentum space. This will be extended in chapter 3 with an extension to supergravity amplitudes.

The diagrams can be thought of as being similar to Feynman diagrams, each line carries a momentum and momentum conservation applies at each vertex. As the name implies, the momenta carried by all the internal lines obey an on-shell condition. Since we are dealing with superamplitudes, the internal lines carry all the states of the $\mathcal{N}=4$ supermultiplet which will be integrated over. The vertices can all be thought of as being either an MHV or $\overline{\text{MHV}}$ amplitude represented by black and white dots

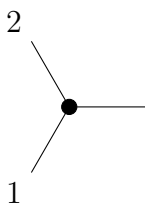

$$\equiv \mathcal{A}_{3,2}, \tag{2.2.13}$$

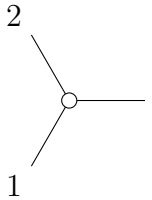

$$\equiv \mathcal{A}_{3,1}. \tag{2.2.14}$$

(2.2.15)

The special three-point kinematics mean that edges which meet at the vertices will either have all $\widetilde{\lambda}$ proportional (MHV) or all λ proportional ($\overline{\text{MHV}}$). The key insight for constructing and working with these on-shell diagrams is the use of Grassmannians, the space of k-planes in n-dimensions $\text{Gr}(k,n)$, to describe kinematics. $\text{Gr}(k,n)$ can also be thought of as the set of $k \times n$ matrices modulo $\text{GL}(k)$ transformations. The function associated to each on-shell diagram will then be given by an integral over an auxiliary Grassmannian $\text{Gr}(k,n)$ for an N^{k-2}MHV amplitude, with the integrand constructed from elements invariant under these transformations, namely products of minors with the appropriate weight. The use of Grassmannians gives a geometric picture of the on-shell constraints as well as linearising how they are enforced on the λ and $\widetilde{\lambda}$.

The simplest example of these is how the three-point amplitudes are expressed as Grassmannian integrals. Each of these is given by a single vertex. The three-point MHV kinematics are described by a 2-plane in the form

$$\mathcal{A}_{3,2} = \int \frac{d^{2\times 3}C}{\text{vol}(\text{GL}(2))} \frac{\delta^{2\times 4}(C\cdot\eta)}{(12)(23)(31)} \delta^{2\times 2}(C\cdot\widetilde{\lambda})\delta^{2\times 1}(\lambda\cdot C^{\perp}), \tag{2.2.16}$$

with $C \in \text{Gr}(2,3)$ and $C^{\perp}$ is the orthogonal complement of C such that $C^{\perp}\cdot C = 0$ as defined in [7]. (ab) are the minors of C obtained by taking the determinant of the 2×2 matrix formed from columns a and b. The dot products in this expression all represent sums over particle number. ie. $\delta^{2\times 2} \equiv \prod_{\substack{\alpha=1,2\\ a=1,2}} \left(\sum_{b=1}^{3} c_b^a \lambda_b^\alpha\right)$ with c_b^a the elements of C. The delta function constraints can be trivially satisfied by setting $C = \binom{\lambda_a^1}{\lambda_a^2}$. This sets $(ab) \to \langle ab\rangle$. The 2 degrees of freedom in the integration measure cancel with the final delta function and the expression reduces to the MHV amplitude in 2.2.11. All the on-shell diagrams considered in this thesis can be evaluated in similar ways – there will exist a clever choice of C-matrix that trivially satisfies the constraints and gives a momentum-space expression. In general this is only possible for MHV, $\overline{\text{MHV}}$ and the six-point NMHV amplitudes. The equivalent

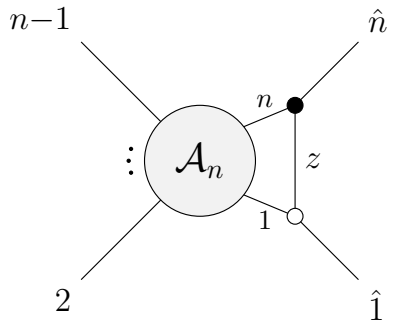

Figure 2.3: Example of a BCFW bridge deforming momenta for an n-point amplitude

expression for the $\overline{\text{MHV}}$ amplitude uses a 1-plane in $\text{Gr}(1,3)$.

A particularly nice feature of on-shell diagrams is how they naturally encode BCFW recursion. Adding a black and a white vertex to the external legs of a diagram as shown in figure 2.3 adds a single extra degree of freedom acting to shift the incoming momenta in precisely the BCFW shift discussed in section 2.2. Combining two amplitudes and joining them with this "BCFW bridge" thus allows for a pictorial representation of on-shell recursion. Each diagram can be directly evaluated using on-shell techniques rather than needing to be built up out of the composite sub-amplitudes. The process involves using the degrees of freedom attached to the edges in the diagram (a generalisation of the z shifts in BCFW) to construct an integrand which can be mapped into an integral over the associated auxiliary Grassmannian. The exact details of how this is carried out in the case of $\mathcal{N} = 4$ SYM are not needed for this thesis. The application of this recursion as specifically applied to $\mathcal{N} = 7$ supergravity is discussed in chapter 3 along with the modifications needed to the diagrams for supergravity.

Finally there are a number of equivalence relations between on-shell diagrams that do not affect the corresponding on-shell function. In the case of $\mathcal{N} = 4$ SYM these are linked to a classification of the diagrams as encoding a specific element of the permutation group [7]. There are two equivalence relations associated to merging and expanding vertices of the same colour, shown in figure 2.4. There is also the "square move", exchanging the colours of the vertices of a square as shown in figure

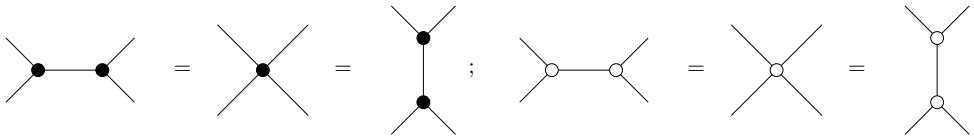

Figure 2.4: Merge and expand equivalence moves form on-shell diagrams

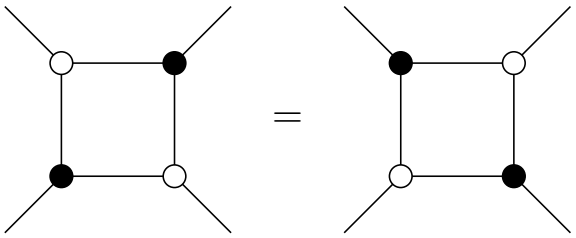

Figure 2.5: Square move equivalence for on-shell diagrams

2.5. There exist analogous moves in supergravity although the mergers require some modification whilst the square moves are modified for any OSD with non-maximal SUSY.

2.3 Amplitudes in Curved Space

2.3.1 Anti-de Sitter

In chapter 4 we will be exploring properties of objects analogous to scattering amplitudes that live in Anti-de Sitter space. We will be working in the Poincaré patch of AdS_4 with the metric given by

$$ds^2 = \frac{1}{z^2}(-dt^2 + dx^2 + dy^2 + dz^2), \tag{2.3.1}$$

where we have set the AdS radius to 1. We will be working with quantities which live on the flat 3d boundary of this space at $z \to 0$, calculated from momentum space Witten diagrams (the AdS analogue of Feynman diagrams). These have previously been used to study a variety of theories including Yang Mills and gravity as well as different types of scalar theories [50, 51, 99]. The quantities obtained from summing over Witten diagrams for a bulk Yang-Mills theory describe transitions between states on the past and future boundaries of the Poincaré patch and obeying Dirichlet

boundary conditions [46, 100]. They encode correlators of conserved currents in a 3d CFT living in the boundary. These will be referred to as AdS amplitudes and will be denoted by $\langle jjjj \rangle$. Specifically, they encode the transverse part of 3d conformal correlators, from which the full correlators can be reconstructed using Ward identities; the details of this are covered in section 4.3. As we will be working in momentum space, we will be writing the correlators as functions of the 3-momenta on the boundary $\boldsymbol{k} = (k^0, k^1, k^2)$. Boundary translational symmetry implies these are conserved. To take advantage of the spinor helicity formalism and relate to flat space helicity amplitudes it will be convenient to define a null 4-momentum

$$\begin{aligned} k^\mu &= (k^0, k^1, k^2, ik), \\ \text{where} \quad k &= |\boldsymbol{k}| = \sqrt{-(k^0)^2 + (k^1)^2 + (k^2)^2}, \end{aligned} \tag{2.3.2}$$

such that ik is the radial component of the momentum. If $\boldsymbol{k}$ is time-like, then k is imaginary but if $\boldsymbol{k}$ is space-like then k is real. We will work with space-like boundary momenta. The sum over radial momenta will not vanish in general and we define it as

$$E = \sum_{a=1}^{4} k_a, \tag{2.3.3}$$

where i is an external particle label. In the limit $E \to 0$, 3d correlators develop a pole whose residue is a 4d scattering amplitude in flat space [37]

$$\lim_{E \to 0} \langle jjjj \rangle = \frac{A_4}{E}. \tag{2.3.4}$$

This property will also appear in dS although we will see in the case of theories other than Yang Mills that the flat space limit is sometimes encoded as the residue of a higher order pole.

To make the relation to amplitudes more explicit, it is convenient to dress the correlators with polarisations of the form

$$\epsilon^\mu = (\boldsymbol{\epsilon}, 0)\,, \tag{2.3.5}$$

which satisfy

$$\boldsymbol{\epsilon}_a \cdot \boldsymbol{k}_a = 0, \;\; \boldsymbol{\epsilon}_a \cdot \boldsymbol{\epsilon}_a = 0. \tag{2.3.6}$$

These polarisations also arise when computing Witten diagrams in axial gauge. Since the polarisations are transverse to the momenta, they project out the longitudinal parts of correlators, giving AdS amplitudes.

AdS Spinor Helicity

As we will be interested in the properties of Yang-Mills amplitudes with specific helicity assignments, it will be useful to work with an AdS version of the spinor helicity formalism. To adapt the definitions in section 2.1.1 we start from the massless 4-momentum defined in equation (2.3.2)

$$k^\mu = (k^0, k^1, k^2, ik). \tag{2.3.7}$$

The AdS boundary breaks translations in the z-direction (leaving only the 3d Lorentz group in the boundary) so the dotted and undotted indices no longer live in different spaces. Instead, we can use the Pauli matrix associated with the broken symmetry to transform between them. Using the 4-vector $T^\mu = (0, 0, 0, 1)$ lets us define $T^{\alpha\dot{\alpha}} = T^\mu \sigma_\mu^{\alpha\dot{\alpha}}$ which can be used to map between the two types of indices

$$\overline{\lambda}_a^\alpha = T^{\alpha\dot{\alpha}} \widetilde{\lambda}_{a\dot{\alpha}}. \tag{2.3.8}$$

We can then convert any $\widetilde{\lambda}$ spinors into $\overline{\lambda}$ and work exclusively with objects in the undotted representation, with indices raised and lowered using $\epsilon_{\alpha\beta}$. Under this mapping, $[ab]$ brackets are replaced with $\langle \bar{a}\bar{b} \rangle$. We can additionally obtain a new type of bracket by contracting together dotted and undotted indices $\langle a\bar{b} \rangle$. This mixed bracket can be used to extract the magnitude of the 3-momenta

$$\langle a\bar{a} \rangle = -\langle \bar{a}a \rangle = -2ik_a, \tag{2.3.9}$$

illustrating its association with the broken symmetry. This corresponds to a decomposition of the form

$$k^{\alpha\beta} = \lambda^{\alpha}\overline{\lambda}^{\beta} = \lambda^{(\alpha}\overline{\lambda}^{\beta)} + ik\epsilon^{\alpha\beta}. \tag{2.3.10}$$

In general, for any vector with two undotted spinor indices, projecting out the symmetric components will leave only the data associated with the boundary direction. The dot product between 3-vectors is then given by

$$\boldsymbol{k}_a \cdot \boldsymbol{k}_b = \eta^{\mu\nu}k_{a\mu}k_{b\nu} + |\boldsymbol{k}_a||\boldsymbol{k}_b| = \frac{1}{2}\langle ab\rangle\langle\bar{a}\bar{b}\rangle - \frac{1}{4}\langle a\bar{a}\rangle\langle b\bar{b}\rangle, \tag{2.3.11}$$

where $\eta_{\mu\nu}$ is a 3d Minkowski metric.

The barred spinors inherit the same Schouten identities as the original $\widetilde{\lambda}$ however any relations involving momentum conservation are modified. We instead have

$$\sum_{a=1}^{n} \lambda_a^{\alpha}\overline{\lambda}_a^{\beta} = i\epsilon^{\alpha\beta}E, \tag{2.3.12}$$

where E is defined in equation (2.3.3). For the similar case of spinor formalism in dS, this has an interpretation as the total energy of the system. Here it instead represents an unconserved transverse momentum. We will again need polarisation vectors expressed in terms of spinors. As with the momenta, they now each have 2 undotted indices

$$\epsilon^{+}_{\alpha\beta} = \frac{\overline{\lambda}_{\alpha}\overline{\lambda}_{\beta}}{ik}, \qquad \epsilon^{-}_{\alpha\beta} = \frac{\lambda_{\alpha}\lambda_{\beta}}{ik}. \tag{2.3.13}$$

Since these are symmetric under $\alpha \leftrightarrow \beta$, we can see that the radial component of the corresponding 4-vector vanishes. It will be straightforward to take these expressions and substitute them into the results of Witten diagram computations, converting dot products between momenta and polarisations into spinor brackets. There are however a rich variety of identities that can be applied to simplify the expressions this gives and this is covered in more detail in appendix D.

2.3.2 de Sitter Wavefunction Coefficients

This section reviews the computation of field theory observables in de Sitter. Many of the mathematical steps here have parallels in AdS but the physics interpretation differs in places.

For convenience, we use the Poincaré patch in dS_{d+1} with radius set to one,

$$ds^2 = \frac{1}{\eta^2}(-d\eta^2 + d\boldsymbol{x}^2), \tag{2.3.14}$$

where $-\infty < \eta < 0$ is the conformal time, and $\boldsymbol{x}$ denotes the spatial coordinates on the boundary, with individual components x^i, $i = 1, .., d$. In chapter 5 we will usually take $d = 3$ whereas in chapter 6 it will be left general. Since the boundary is Euclidean, momenta here will be space-like (whereas in Anti-de Sitter they could also be time-like).

Unlike in flat space and AdS, there is no notion of time ordering as free states can only be defined for $\eta \to -\infty$. The quantities of interest are therefore in-in correlators [56], which can be computed from a cosmological wavefunction via a path integral formalism as

$$\langle \phi(\boldsymbol{k}_1) \dots \phi(\boldsymbol{k}_n) \rangle = \frac{\int \mathcal{D}\phi \, \phi(\boldsymbol{k}_1) ... \phi(\boldsymbol{k}_n) \left|\Psi[\phi]\right|^2}{\int \mathcal{D}\phi \left|\Psi[\phi]\right|^2}. \tag{2.3.15}$$

The scalars ϕ are taken to be in the future boundary (Fourier transformed to momentum space) and the functional $\Psi[\phi]$ is the cosmological wavefunction. The integral is over field configurations which reduce to the Bunch-Davies vacuum $\phi \sim (1 - ik\eta)e^{+ik\eta}$ in the limit $\eta \to -\infty$ and which reduce to momentum modes in the $\eta \to 0$ limit [57, 58]. The Bunch-Davies vacuum is the choice which recovers correlators of operators in the boundary CFT, however there are other choices which can still give valid physics in the bulk [101]. $\Psi[\phi]$ can be perturbatively expanded as

$$\ln \Psi[\phi] = -\sum_{n=2}^{\infty} \frac{1}{n!} \int \prod_{a=1}^{n} \frac{\mathrm{d}^d k_a}{(2\pi)^d} \Psi_n(\boldsymbol{k}_1, \dots, \boldsymbol{k}_n) \phi(\boldsymbol{k}_1) \dots \phi(\boldsymbol{k}_n). \tag{2.3.16}$$

The wavefunction coefficients Ψ_n can be treated as n-point CFT wavefunction coefficients in the future boundary and can also be computed by analytic continuation

of AdS Witten diagrams (this is a consequence of the choice of vacuum) [47, 48, 57, 102, 103]. In momentum space, they can be expressed as

$$\Psi_n = \delta^{(d)}(\boldsymbol{k}_T)\langle\langle \mathcal{O}(\boldsymbol{k}_1)...\mathcal{O}(\boldsymbol{k}_n)\rangle\rangle, \tag{2.3.17}$$

where $\boldsymbol{k}_T = \boldsymbol{k}_1 + \ldots + \boldsymbol{k}_n$, and the double brackets denote a CFT correlator on the boundary. The scalar operators $\mathcal{O}$ have scaling dimension Δ, and are dual to scalar fields ϕ in the bulk with mass

$$m^2 = \Delta(d - \Delta). \tag{2.3.18}$$

$\Delta = d$ describes minimally coupled scalars while $\Delta = (d+1)/2$ describes conformally coupled scalars.

The wavefunction coefficients Ψ_n satisfy conformal Ward identities (CWIs), which are a consequence of the de Sitter isometries. The conformal generators in position space were introduced in section 2.1.2. Here, their action on the wavefunction coefficients can be written as

$$\sum_{a=1}^{n} P_a^i \Psi_n = \sum_{a=1}^{n} D_a \Psi_n = \sum_{a=1}^{n} K_a^i \Psi_n = \sum_{a=1}^{n} M_a^{ij} \Psi_n = 0, \tag{2.3.19}$$

where $a, b, ...$ are particle labels and the momentum space generators are given by

$$\begin{aligned} P^i &= k^i, \\ D &= k^i \partial_i + (d - \Delta), \\ K_i &= k_i \partial^j \partial_j - 2k^j \partial_j \partial_i - 2(d - \Delta)\partial_i, \\ M_{ij} &= \left(k_i \partial_j - k_j \partial_i\right), \end{aligned} \tag{2.3.20}$$

with $\partial_i = \frac{\partial}{\partial k^i}$. In this representation, the conformal dimension of the scalars appear explicitly in generators. Boundary vector indices will be freely raised and lowered here using a flat metric.

2.4 Colour-Kinematics and the Double Copy

This subsection will present a review of colour-kinematics (CK) duality for tree-level 4-point scattering amplitudes [39, 104]. A 4-point colour-dressed gluon amplitude can be written as

$$\mathbb{A}_4 = \frac{n_s c_s}{s} + \frac{n_t c_t}{t} + \frac{n_u c_u}{u}, \tag{2.4.1}$$

where s, t, u are Mandelstam variables, c_i are colour factors, n_i are kinematic numerators, and we have set the YM coupling to one. The c_i can be written in terms of colour group structure constants

$$c_s = f^{a_1 a_2 b} f^{b a_3 a_4}, \;\; c_t = f^{a_1 a_4 b} f^{b a_2 a_3}, \;\; c_u = f^{a_3 a_1 b} f^{b a_2 a_4}, \tag{2.4.2}$$

which satisfy the Jacobi relation

$$c_s + c_u + c_t = 0. \tag{2.4.3}$$

Using this to express c_t in terms of c_s and c_u lets us rewrite the colour dressed amplitude (2.4.1) as

$$\mathbb{A}_4 = c_s A_{1234} - c_u A_{1342}, \tag{2.4.4}$$

where the colour-ordered amplitudes are given by

$$\begin{aligned} A_{1234} &= \frac{n_s}{s} - \frac{n_t}{t}, \\ A_{1324} &= \frac{n_t}{t} - \frac{n_u}{u}. \end{aligned} \tag{2.4.5}$$

The kinematic numerators can be represented using the cubic diagrams in Figure 2.6. These are not Feynman diagrams, but are derived by splitting the contact Feynman diagram into three pieces multiplied by s/s, t/t, and u/u, respectively, and combining them with exchange Feynman diagrams. When written in terms of polarisation vectors, the numerators are related by cyclic permutations on three particles:

$$n_t = n_s\Big|_{(234)\to(423)}, \qquad n_u = n_s\Big|_{(234)\to(342)}, \tag{2.4.6}$$

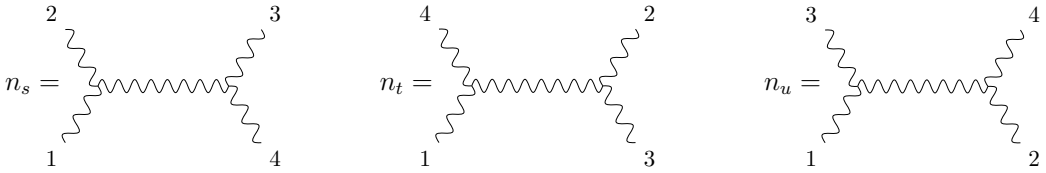

Figure 2.6: The three numerator structures for the colour-dressed amplitude. Two of these appear in each colour-ordered amplitude.

or equivalently using exchanges:

$$n_t = -n_s\Big|_{2\leftrightarrow 4}, \qquad n_u = -n_s\Big|_{2\leftrightarrow 3}. \tag{2.4.7}$$

These operations can be seen by permuting the labels on the diagrams in Figure 2.6. When we express the numerators using spinors, these relations continue to hold except when these mappings act on particles of different helicities. Note that exchanging the legs at a vertex gives rise to a minus sign, which can be seen from the antisymmetric structure of the three point vertex. This explains the minus signs in (2.4.6) and the relative signs in (2.4.5); we get a minus sign when we flip the legs at a vertex so that the ordering of the diagram matches the ordering of the partial amplitude.

The kinematic Jacobi relation states that

$$n_s + n_t + n_u = 0, \tag{2.4.8}$$

which is analogous to the colour Jacobi relation in (2.4.3) and encodes a remarkable duality between colour and kinematics. Given a set of numerators satisfying (2.4.8), one can then construct gravitational amplitudes from colour-dressed YM amplitudes by replacing the colour factors with kinematic numerators:

$$M_4 = \frac{n_s^2}{s} + \frac{n_t^2}{t} + \frac{n_u^2}{u}, \tag{2.4.9}$$

where we have set the gravitational coupling constant to 1. This relation is referred to as the double copy. The kinematic Jacobi relation can also be used to prove a

relation among colour-ordered amplitudes known as the BCJ relation:

$$uA_{1324} = sA_{1234}. \tag{2.4.10}$$

Substituting the colour ordered amplitudes (2.4.5) and the BCJ relation (2.4.10) into (2.4.9) then implies the famous KLT relation

$$M_4 = -sA_{1234}A_{1243}, \tag{2.4.11}$$

first discovered in the context of string theory [40]. Chapter 4 will extend CK duality to AdS amplitudes and chapter 5 will review the same physics from the CHY formalism as well as studying dS double copies between scalar field theories.

2.5 Soft Theorems and Effective Field Theories

Chapters 5 and 6 focus on certain scalar effective field theories (EFTs), namely the non-linear sigma model (NLSM), scalar Dirac-Born-Infeld theory (DBI), and special Galileon theory (sGal). In flat space these are all uniquely determined by their soft behavior and the corresponding shift symmetries of their Lagrangians [87, 88]. They are also theories which take on a simple form in the CHY approach [68].

These EFTs all have derivative interactions and so vanishing soft limits, when the momentum associated to a particular leg is taken soft we have

$$\lim_{p\to 0} A(p) = \mathcal{O}\left(p^{k+1}\right), \tag{2.5.1}$$

where k is a parameter characterising the degree of the soft limit. Beyond four points, this property is either trivial (if the degree of soft behavior is equal or less than the number of derivatives per field) or requires non-trivial cancellations between Feynman diagrams at all orders. This in turn constrains the interactions that can appear such that cancellations are allowed by dimensional considerations. This latter case is referred to as an 'enhanced' soft limit and there are only three cases for theories with a single scalar, they are the NLSM, DBI, and sGal theories which have

$k = 0, 1, 2$, respectively. These are also the theories with an order k shift symmetry in the Lagrangian (where k refers to the degree of dependence on spatial coordinates). In the case of the NLSM this is given by

$$\phi \to \phi + a, \tag{2.5.2}$$

for some constant a. The shift symmetries for DBI and sGal are more complex and have a spatial dependence [88]. The remainder of this section will briefly review the Lagrangians and some of the four- and sixpoint amplitudes for each EFT in preparation for exploring the corresponding behavior in dS.

2.5.1 EFT Lagrangians and Amplitudes

The NLSM Lagrangian is given by

$$\begin{aligned}\mathcal{L}_{\text{NLSM}} &= \frac{1}{8\lambda^2}\text{Tr}(\partial_\mu U^\dagger \partial^\mu U), \\ &= -\text{Tr}\left[\frac{1}{2}(\partial\Phi)^2 + \lambda^2\Phi^2(\partial\Phi)^2 + \lambda^4\left(\Phi^4(\partial\Phi)^2 + \frac{1}{2}\Phi^2\partial_\mu\Phi\Phi^2\partial^\mu\Phi\right) + \dots\right],\end{aligned} \tag{2.5.3}$$

where $U = (\mathbb{I}+\lambda\Phi)(\mathbb{I}-\lambda\Phi)^{-1}$ and $(\partial\Phi)^2 = \partial_\mu\Phi\partial^\mu\Phi$, Φ is in the adjoint representation of SU(N), and the ellipsis denotes higher-point interactions. This is the only one of the exceptional EFTs with a gauge symmetry and so we will work with colour-ordered amplitudes. The four-point amplitude is simply given by

$$A_4^{\text{NLSM}} = -2s_{13}, \tag{2.5.4}$$

using the shorthand $s_{ab} = k_a \cdot k_b$ and setting the coupling to one. Since the theory is massless it is clear that this scales as $\mathcal{O}(k_i)$ when any leg is taken soft. The six-point amplitude is more involved, consisting of an exchange diagram with two four-point vertices as well as a six-point contact diagram. These are shown in figure 2.7. The colour-ordered amplitude can be written as

$$A_6^{\text{NLSM}} = 4\frac{s_{13}s_{46}}{s_{123}} - 4s_{13} + \text{cyc}(a \to a{+}2), \tag{2.5.5}$$

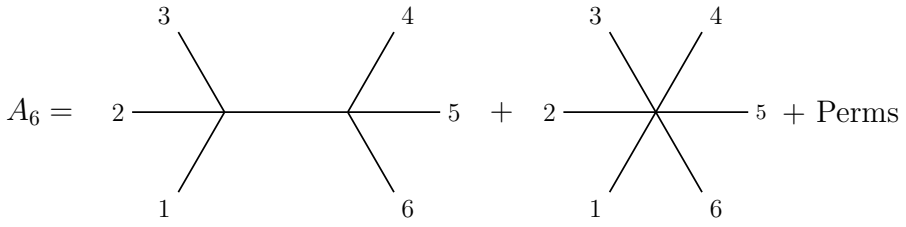

Figure 2.7: Feynman Diagrams for six-point NLSM and DBI amplitudes

where the pole is given by $s_{abc} = k_a \cdot k_b + k_b \cdot k_c + k_c \cdot k_a$. This is equivalent to the form found in [105]. Taking (for example) $k_1 \to 0$, four of the six terms scale as $\mathcal{O}(k_1)$ leaving

$$\lim_{k_1 \to 0} A_6^{\text{NLSM}} = 4\frac{s_{35}s_{62}}{s_{612}} - 4s_{35} + \mathcal{O}(k_1). \tag{2.5.6}$$

Since $\lim_{k_1 \to 0} s_{612} = s_{62}$ the pole cancels and the whole amplitude has the expected soft behavior. Alternatively, one could bootstrap the six-point amplitude by requiring that the soft limit vanish at this order, uniquely fixing the six-point coupling in terms of the four-point one. This process could then be repeated to reconstruct the entire shift-symmetric Lagrangian by imposing the enhanced soft behavior.

For the DBI theory we have

$$\begin{aligned} \mathcal{L}_{\text{DBI}} &= \frac{1}{\lambda}\left(\sqrt{1 - \lambda\left(\partial\phi\right)^2} - 1\right), \\ &= -\frac{1}{2}(\partial\phi)^2 - \frac{\lambda}{8}(\partial\phi)^4 - \frac{\lambda^2}{16}(\partial\phi)^6 + \ldots, \end{aligned} \tag{2.5.7}$$

where $(\partial\phi)^{2n} = (\partial_\mu\phi\partial^\mu\phi)^n$. The four-point amplitude is given by

$$A_4^{\text{DBI}} = s_{12}^2 + s_{13}^2 + s_{14}^2, \tag{2.5.8}$$

where the coupling has again been set to one. As in the NLSM case this trivially has the expected soft limit, in this case $\mathcal{O}(k_a^2)$. The six-point amplitude is more involved and is given by

$$\begin{aligned} A_6^{\text{DBI}} = 2\frac{\left(s_{12}s_{23} + s_{23}s_{31} + s_{31}s_{12}\right)\left(s_{45}s_{56} + s_{56}s_{64} + s_{64}s_{45}\right)}{s_{123}} + \text{Perms} \\ + 3s_{12}s_{34}s_{56} + \text{Perms}, \end{aligned} \tag{2.5.9}$$

where the exchange diagram is summed over the 10 possible factorisation channels and the contact term is summed over the 15 inequivalent permutations. Finding the soft limit of this expression by hand is tedious but if momentum conservation is used to eliminate one leg and the on-shell condition used to remove one extra s_{ab} (up to order k^2) then it can be shown that this indeed behaves as $\mathcal{O}(k_a^2)$ in the soft limit. Again this procedure could be bootstrapped to recover the expansion of the square root given in equation 2.5.7.

Finally, in $d = 4$ the special Galileon theory is given by [106]

$$\mathcal{L}_{\text{sGal}} = -\frac{1}{2}(\partial\phi)^2 - \frac{\lambda}{8}(\partial_\mu\partial_\nu\phi)^2(\partial\phi)^2 + \dots, \tag{2.5.10}$$

where the dots indicate higher order terms. This theory is special in that it can be reformulated such that it contains *only* a four-point interaction term and no higher valence interactions (this form has a more complicated four-point interaction term but this only affects exchange diagrams) [88]. The four-point amplitude is given by

$$A_4^{\text{sGal}} = s_{12}^3 + s_{13}^3 + s_{14}^3, \tag{2.5.11}$$

which clearly scales as $\mathcal{O}(k_a^3)$ in the soft limit. Higher point interactions contain only exchange diagrams but since these turn out to be very complex in dS they are not studied in detail in this thesis.

Note that the four-point interactions in the DBI and sGal theories contain four derivative and six-derivatives, respectively. They are unique up to integration by parts and equations of motion. Their lift to curved backgrounds, however, is not unique because covariant derivatives no longer commute and there are curvature corrections, as described in chapters 5 and 6.

Chapter 3

On-Shell Diagrams and Momentum Twistors for $\mathcal{N} = 7$ Supergravity

This chapter starts with a recap of on-shell diagrams for supergravity in section 3.1 and an introduction to $\mathcal{N} = 7$ supergravity. Section 3.1.2 then covers the details of the recursion with a focus on the new features which appear in contrast to the case of maximal supersymmetry. This is then applied to a number of examples starting with MHV up to six-point (3.2.1) then five-point $\overline{\text{MHV}}$ (3.2.2) and six-point NMHV (3.2.3). This is followed by a detailed look at how to rewrite the six-point NMHV amplitude in terms of momentum twistors using local coordinate patches in section 3.2.4. These expressions are then used to analyse the spurious poles and their cancellations in detail in section 3.2.5 before we conclude with some final remarks (3.3).

3.1 Supergravity On-shell diagrams

The work in the chapter will build off the use of OSDs to calculate $\mathcal{N} = 8$ tree-level amplitudes in [30] and [35] [1]. The first modification needed to describe supergravity with on-shell diagrams is apparent from considering how BCFW recursion differs between SYM and supergravity: supergravity on shell diagrams will need to incorporate permutation sums. At each stage in the recursion, diagrams will need to be summed over the $(n-2)!$ permutations of legs not attached to the BCFW bridge. In order to for the recursion via BCFW bridges to work it is also necessary to add 'decorations' to the bridge, modifying how it contributes to the corresponding Grassmannian integrand. These decorations affect some of the original properties of the diagrams; for example a decorated OSD can no longer be uniquely identified with an element of the permutation group. However the bridges do fit neatly with the properties of gravitational BCFW recursion, clearly denoting how the required permutation sums must be applied. i.e. We can write the recursion as

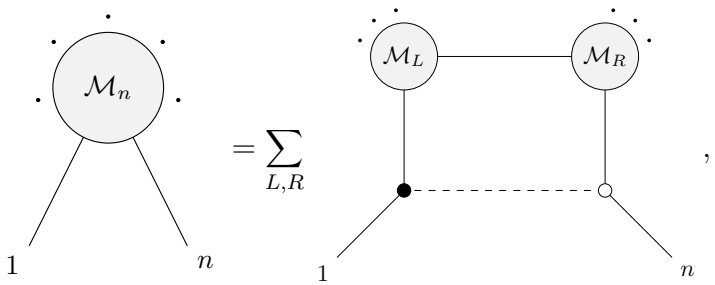

, (3.1.1)

where the sum is over all partitions of particles $\{2, \ldots, n-1\}$ into sets L and R. The recursion can also be applied in such a way that that it will generate non-planar diagrams. In $\mathcal{N} = 8$ this can be avoided with a careful choice of recursion scheme but when considering $\mathcal{N} = 7$ they turn out to be an essential feature [1].

[1] There exist other applications of OSDs to gravity, most notably [107] but their connection to direct amplitude calculations is less clear

3.1.1 $\mathcal{N} = 7$ Supergravity

As in equation 2.1.18, supermomentum is defined as

$$q_a^{\alpha A} = \lambda_a^\alpha \eta_a^A, \tag{3.1.2}$$

where now A runs from 1 to $\mathcal{N} = 7$. For all superamplitudes (except three-point $\overline{\text{MHV}}$), supermomentum conservation is imposed by the delta function $\delta^{(4|2\mathcal{N})}(P|Q)$, where $P = \sum_a p_a$ and $Q = \sum_a q_a$. It will be convenient to factor out the supermomentum delta function from scattering amplitudes, and we will denote the resulting quantity with a bar

$$\mathcal{M} = \delta^{(4|14)}(P|Q)\overline{\mathcal{M}}. \tag{3.1.3}$$

We will be scattering $\mathcal{N} = 7$ superfields. These have the same particle content as the $\mathcal{N} = 8$ superfield which is given by

$$\Phi = h^+ + ... + h^-\eta^8, \tag{3.1.4}$$

where $h^\pm$ are the two helicity states of the graviton, and the ellipsis denote the on-shell states of lower spin bosonic and fermionic fields. Analogous to the $\mathcal{N} = 4$ SYM superfield in equation 2.1.19 this is an expansion in the Grassmann variable η and so truncates at eighth order. For $\mathcal{N} = 7$, the particle content is split into two supermultiplets which contain the positive and negative helicity states of the graviton respectively

$$\Phi^+ = \Phi|_{\eta^8=0}\,, \;\; \Phi^- = \int d\eta^8 \Phi. \tag{3.1.5}$$

$\mathcal{N} = 7$ supergravity has the same field content as $\mathcal{N} = 8$ and they are perturbatively equivalent. From this, we also see that an N^{k-2}MHV amplitude (whose graviton component has k negative helicity gravitons) has fermionic degree $7k$. Using the relation between superfields, it is straightforward to extract $\mathcal{N} = 7$ superamplitudes

from $\mathcal{N}=8$. For example, at three points we have

$$\begin{aligned}\mathcal{M}_3^{\mathcal{N}=7}(--+) &= \int d\eta_1^8 d\eta_2^8\, \mathcal{M}_{3,2}^{\mathcal{N}=8}\Big|_{\eta_3^8=0}\,,\\ \mathcal{M}_3^{\mathcal{N}=7}(++-) &= \int d\eta_3^8\, \mathcal{M}_{3,1}^{\mathcal{N}=8}\Big|_{\eta_1^8=\eta_2^8=0}\end{aligned} \tag{3.1.6}$$

where $\mathcal{M}_{3,2}$ and $\mathcal{M}_{3,1}$ are the 3-point MHV and $\overline{\text{MHV}}$ amplitudes of $\mathcal{N}=8$ supergravity, respectively. An n-point $\overline{\text{MHV}}$ amplitude describes the scattering of two positive helicity gravitons and $n-2$ negative helicity gravitons.

3.1.2 $\mathcal{N}=7$ Recursion and Bonus Relations

When working with $\mathcal{N}=7$ supergravity on-shell diagrams we have to account for the two supermultiplets encoding the two graviton helicities. The edges will therefore be labelled with arrows to indicate helicity flow (which should not be confused with momentum flow). In particular, incoming arrows denote the negative helicity supermultiplet, and outgoing arrows denote the positive helicity supermultiplet. Hence, three-point MHV amplitudes will have two incoming arrows and one outgoing arrow, while three-point $\overline{\text{MHV}}$ amplitudes have two outgoing arrows and one incoming arrow. Three-point superamplitudes and edges are given by:

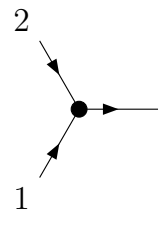

$$\equiv \langle 12\rangle \frac{\delta^{14}(\lambda_1\eta_1+\lambda_2\eta_2+\lambda_3\eta_3)}{\langle 12\rangle^2\langle 23\rangle^2\langle 31\rangle^2}, \tag{3.1.7}$$

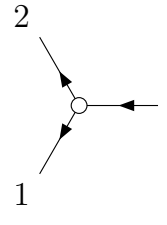

$$\equiv [12] \frac{\delta^{7}([12]\eta_3+[23]\eta_1+[31]\eta_2)}{[12]^2[23]^2[31]^2}, \tag{3.1.8}$$

$$\equiv \int \frac{d^2\lambda\, d^2\widetilde{\lambda}}{\text{GL}(1)} d^7\eta. \tag{3.1.9}$$

Momentum conservation implies that $\tilde{\lambda}_1 \propto \tilde{\lambda}_2 \propto \tilde{\lambda}_3$ for an MHV vertex and $\lambda_1 \propto \lambda_2 \propto \lambda_3$ for an $\overline{\text{MHV}}$ vertex.

The recursion in 3.1.1 therefore becomes

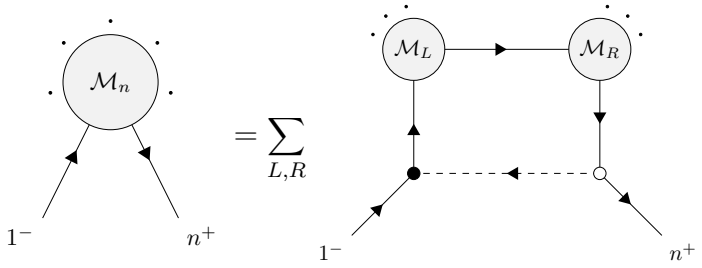

, (3.1.10)

where

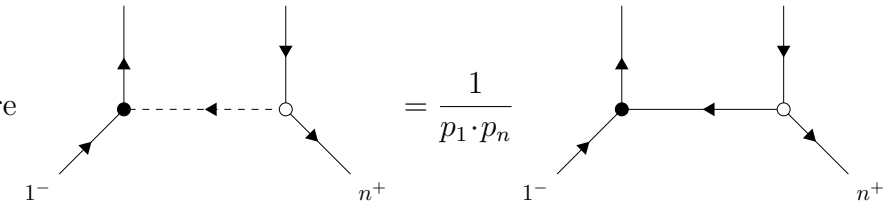

. (3.1.11)

The object connecting the lower-point amplitudes on the right-hand-side of (3.1.10 implements a BCFW shift of legs 1 and n and is known as a BCFW bridge. The external arrows of the bridge imply a $\langle 1^-, n^+]$ shift and the internal arrows are fixed by helicity flow. Choosing this BCFW bridge at every step of the recursion always produces on-shell diagrams with closed cycles and the choice also fixes their orientation. The sum in equation (3.1.10) is over all partitions of particles $\{2, \ldots, n-1\}$ into sets L and R. The recursion is carried out such that we always feed the fixed legs of the subamplitudes into the recursion. Using the BCFW bridge in (3.1.11), the $\mathcal{N} = 7$ recursion leads to fewer diagrams than the $\mathcal{N} = 8$ recursion[30]. For example, at MHV there are $(n-3)!$ instead of $(n-2)!$ terms so it appears that the $\mathcal{N} = 7$ recursion encodes bonus relations [86], as was previously observed in [108]. In [98], the bonus relations were used to write non-MHV amplitudes in $\mathcal{N} = 8$ supergravity as a sum over $(n-3)!$ terms. It would be interesting to investigate how this compares to the $\mathcal{N} = 7$ recursion.

Whereas $\mathcal{N} = 7$ supergravity amplitudes are well-behaved when the BCFW deformation is taken to infinity, this is not the case for $\mathcal{N} < 4$ SYM amplitudes [109, 110], so a different choice of BCFW bridge should be used in those theories. A $\langle 1^-, n^+]$ shift was considered in $\mathcal{N} = 3$ SYM using on-shell diagrams in [7], where it was shown that the correct result could be obtained at 4-points by summing over orientations of closed cycles, but we find that this prescription does not work at higher points.

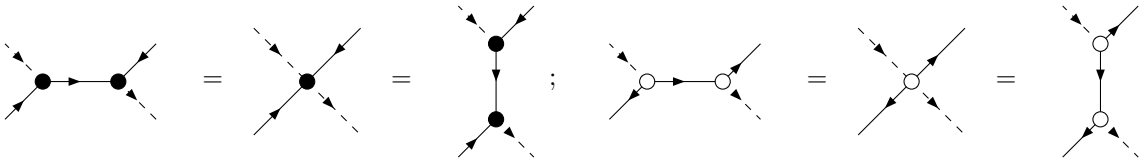

Figure 3.1: Merging rules for $\mathcal{N} = 7$ on-shell diagrams. The decorated edges must appear opposite.

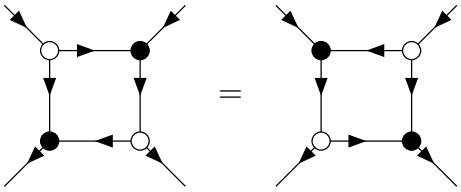

Figure 3.2: Square move for $\mathcal{N} = 7$ on-shell diagrams.

$\mathcal{N} = 7$ on-shell diagrams enjoy a number of equivalence relations similar to those of $\mathcal{N} = 8$ supergravity. In particular mergers appear with an orientation encoding helicity flow, as shown in Figure 3.1, and square moves are only valid for diagrams where the incoming arrows are adjacent, shown in Figure 3.2. We are also free to move decorations to the opposite edge of a box, which can be seen from the definition in (3.1.11).

$\mathcal{N} = 7$ OSD Algorithm

On-shell diagrams for n-point $\mathrm{N}^{k-2}\mathrm{MHV}$ amplitudes naturally give rise to integrals over the space of k planes in n dimensions, also known as the Grassmannian $\mathrm{Gr}(k, n)$. These integrals are represented as an integral over a $k \times n$ matrix C modulo a left action of $\mathrm{GL}(k)$. The rows of C are associated with the external legs with a Φ^- multiplet, or equivalently legs with incoming arrows, while the columns are associated will all external legs. As we describe below, the C matrix for a given on-shell diagram can be computed by assigning edge variables and summing over paths through the diagram taking the product of the edge variables encountered along each path. One then lifts the integral over edge variables to a covariant contour integral in the Grassmannian. A detailed algorithm for evaluating on-shell diagrams in $\mathcal{N} = 8$ supergravity can be found in [30] and Appendix A of [35]. The algorithm for $\mathcal{N} = 7$ is very similar, so it is described below more schematically

1. Label every half edge (including external edges) with an edge variable α. Set one of the two edge variables on each internal edge to unity and set one of the remaining edge variables associated with each vertex to unity, leaving $2n-4$ edge variables.

2. Include $d\alpha/\alpha^2$ for each edge entering a black vertex or leaving a white vertex and $d\alpha/\alpha^3$ for each edge leaving a black vertex or entering a white vertex.

3. Multiply by $\langle ab\rangle$ for each black vertex and $[ab]$ for each white vertex, where a, b are the two incoming or outgoing legs, respectively.

4. Include a kinematic factor to each decorated edge as shown in (3.1.11).

5. To relate internal and external spinors, sum over paths according to

$$\widetilde{\lambda}_a = \sum_{\text{paths } a\to b} \left(\prod_{\text{edges in path}} \alpha_e \right) \widetilde{\lambda}_b, \tag{3.1.12}$$

$$\lambda_a = \sum_{\text{paths } b\to a} \left(\prod_{\text{edges in path}} \alpha_e \right) \lambda_b. \tag{3.1.13}$$

   The matrix element C_{ab} can then be computed by summing over all paths from leg a to leg b, taking the product of all the edge variables encountered along each path as in (3.1.12).

6. If there is a closed cycle, one will need to sum an infinite series when computing the C-matrix in the previous step. Moreover, one will need to include the factor $\mathcal{J}_C^{\mathcal{N}-4} = \mathcal{J}_C^3$, where $\mathcal{J}_C$ comes from a sum over products of disjoint cycles [107]:

$$\mathcal{J}_C = 1 + \sum_i f_i + \sum_{\text{disjoint } i,j} f_i f_j + \sum_{\text{disjoint } i,j,k} f_i f_j f_k + ..., \tag{3.1.14}$$

   where f_i is minus the product of edge variables around the i^{th} cycle. In section 3.1.2 we will describe an alternative method which avoids summing over closed cycles when computing the C-matrix, and automatically computes $\mathcal{J}_C$.

7. Include $\delta^{k(2|7)}(C\cdot\widetilde{\lambda})\delta^{2\times(n-k)}(\lambda\cdot C^\perp)$ where $C^\perp$ is an $n\times(n-k)$ matrix satisfying $C\cdot C^\perp = 0$, whose matrix elements can be computed by summing over the

reverse paths in (3.1.13). The dot products appearing in the delta functions are with respect to particle number, so for example $C \cdot \tilde{\lambda}$ can be written more explicitly as $\sum_{a=1}^{n} C_{Ib}\tilde{\lambda}_b^{\alpha}$, where I labels the k rows. After taking into account momentum conservation, there are $2n-4$ bosonic delta functions, which precisely matches the number of edge variables. The argument of the fermionic delta functions is $C \cdot \eta$, which we suppress for brevity. The resulting integral over edge variables can be thought of as a gauge-fixed Grassmannian integral formula, where the gauge symmetry is $\mathrm{GL}(k)$.

8. Covariantise the integral over edge variables to an integral over $\mathrm{Gr}(k,n)$ by writing the edge variables in terms of minors of the C and $C^{\perp}$ matrices. Since $\mathrm{Gr}(k,n)$ has dimension $k(n-k)$ but there are only $2n-4$ edge variables, this will imply a contour in the Grassmannian of dimension $k(n-k)-(2n-4) = (k-2)(n-k-2)$.

Alternatively, to deal with the bridge decorations one may replace steps 3 and 4 with

3. For each BCFW bridge, look at the sub-diagram formed only by this bridge, its two vertices, and the four legs attached to it.

   - If there is only one path through the sub diagram which includes the bridge, assign a factor of the edge variable on the bridge, divided by the two edge variables on the legs which are not on that path.
   - If there are four possible paths through the sub diagram, divide through by a factor of each of the edge variables on the external legs, and the edge variable on the bridge squared. If there is no edge variable in any of the locations described above, then this edge variable was set to unity in step 2.

4. For each remaining black vertex not attached to a bridge, add a factor of $\langle ab\rangle$ where a, b are the two edges with ingoing arrows. For each remaining white

vertex not associated to a bridge, add a factor of $[ab]$ where a, b are the two edges with outgoing arrows.

This modification (first introduced in [35]) is used in appendix C to make evaluating the bridge decorations more straightforward. It is unaffected by the presence of closed cycles in the diagram.

Closed Cycles

The $\mathcal{N} = 7$ recursion has fewer diagrams compared to $\mathcal{N} = 8$, but the price to pay is that they generally contain more closed cycles, which can become very cumbersome to evaluate following step 5 of the algorithm in the previous subsection. This technical difficulty can be overcome as follows. Instead of expanding incoming $\widetilde{\lambda}_a$ in terms of only outgoing $\widetilde{\lambda}_b$, it is instead expanded in terms of all external $\widetilde{\lambda}_b$. In particular, when summing over paths originating from each incoming leg as described in step 5, the path can be truncated upon reaching another incoming leg and then writing the last internal spinor along the path in terms of the external spinor using the fact that all $\tilde{\lambda}$ spinors are proportional at a black vertex. For example, in Figure 3.3 suppose that A and B are internal edges while 2 is an external edge. Computing the C-matrix according to step 5 of the algorithm would give $\widetilde{\lambda}_A = \alpha_A \widetilde{\lambda}_B$ and before continuing to expand $\widetilde{\lambda}_B$. Instead the path is truncated by writing $\widetilde{\lambda}_A = \alpha_A \widetilde{\lambda}_2$. The resulting C matrix will have non-zero elements between incoming legs, but a GL(k) transformation can be found to set the columns of the incoming legs to a unit matrix. The C-matrix before this gauge-fixing will be referred to as $\tilde{C}$. This will yield the same result as step 5 of the algorithm without having to sum over closed cycles. Moreover the Jacobian in step 6 is given by the inverse of the determinant of the GL(k) transformation. This method can also be applied to on-shell diagrams in other theories.

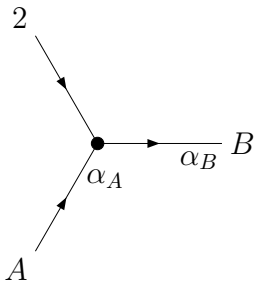

Figure 3.3: Vertex showing example of how to truncate geometric series. Here we take leg 2 to be external (with the corresponding edge variable set to 1) and legs A and B to be internal.

3.2 Applications of $\mathcal{N} = 7$ Recursion

In this section, we will use the on-shell diagram recursion in (3.1.10) to compute MHV amplitudes in $\mathcal{N} = 7$ supergravity up to six points, obtaining Grassmannian integral formulas and expressions in momentum twistor space in agreement with [27]. We will see that only $(n-3)!$ diagrams contribute, in contrast to $(n-2)!$ in the $\mathcal{N} = 8$ recursion, indicating that the $\mathcal{N} = 7$ recursion automatically incorporates the bonus relations. The same steps will then be carried out for the five-point $\overline{\text{MHV}}$ and six-point NMHV amplitudes and analyse the expressions obtained by writing them in terms of momentum twistors.

3.2.1 MHV Examples

Four-point

At four points, only a single on-shell diagram is needed, with no sum over permutations. For $\mathcal{M}_{4,2}(1^-, 2^+, 3^-, 4^+)$, this diagram is shown in Figure 3.4. If one requires a different helicity arrangement, this can be obtained simply by permuting the external legs. For example, the amplitude $\mathcal{M}_{4,2}(1^-, 2^-, 3^+, 4^+)$ can be obtained from the on-shell diagram in Figure 3.5. We shall denote individual on-shell diagrams contributing to an amplitude using the symbol $\mathcal{D}$. Following the algorithm in section

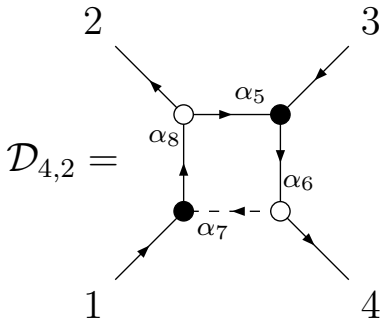

Figure 3.4: On-shell diagram for 4-point amplitude with alternating helicities.

3.1.2, this can be evaluated in terms of edge variables as

$$\mathcal{D}_{4,2} = \frac{1}{\langle 41\rangle[14]} \int \prod_{i=5}^{8} \left(\frac{d\alpha_i}{\alpha_i^2}\right) \frac{1}{\alpha_8\alpha_6} \langle 71\rangle[25]\langle 53\rangle[47]\, \mathcal{J}_C^3\, \delta^{(4|14)}(C\cdot\widetilde{\lambda})\delta^4(\lambda\cdot C^{\perp}), \quad (3.2.1)$$

where

$$C = \begin{pmatrix} 1 & -\Delta\alpha_8 & 0 & -\Delta\alpha_8\alpha_5\alpha_6 \\ 0 & -\Delta\alpha_6 & 1 & -\Delta\alpha_6\alpha_7\alpha_8 \end{pmatrix}, \quad (3.2.2)$$

$$\mathcal{J}_C = (1 - \alpha_5\alpha_6\alpha_7\alpha_8) = \Delta^{-1},$$

and the factor of Δ comes from a geometric series associated with the closed cycle. The rows of the C-matrix are associated with legs 1 and 3.

When uplifting to a Grassmannian integral there is a Jacobian to transform from an integral over edge variables into one over the entries of the C-matrix:

$$\frac{d^{2\times 4}C}{\mathrm{GL}(2)} = \Delta^4\alpha_6^2\alpha_8^2 \prod_{i=5}^{8} d\alpha_i. \quad (3.2.3)$$

The expression in (3.2.1) can then be written as follows:

$$\begin{aligned} \mathcal{D}_{4,2} &= \int \frac{d^{2\times 4}C}{\mathrm{GL}(2)} \frac{[23]\langle 32\rangle}{\Delta^7\alpha_5\alpha_6^5\alpha_7\alpha_8^5} \delta^{(4|14)}(C\cdot\widetilde{\lambda})\delta^4(\lambda\cdot C^{\perp}), \\ &= \int \frac{d^{2\times 4}C}{\mathrm{GL}(2)} \frac{[23]\langle 32\rangle}{(12)(23)(34)(41)(24)^2(31)} \frac{(24)(31)}{(23)(41)} \delta^{(4|14)}(C\cdot\widetilde{\lambda})\delta^4(\lambda\cdot C^{\perp}). \end{aligned} \quad (3.2.4)$$

This can be simplified by noting that $\langle ab\rangle/(ab)$ and $[ab]/(ab)^{\perp}$ are independent of a and b, where $(ab)^{\perp} = \varepsilon_{abcd}(cd)$ is a minor of $C^{\perp}$. The amplitude then simplifies to

$$\mathcal{M}_{4,2} = \mathcal{D}_{4,2} = \langle 13\rangle \int \frac{d^{2\times 4}C}{\mathrm{GL}(2)} \frac{[cd]}{(cd)^{\perp}} \prod_{a<b} \frac{1}{(ab)} \delta^{(4|14)}(C\cdot\widetilde{\lambda})\delta^4(\lambda\cdot C^{\perp}). \quad (3.2.5)$$

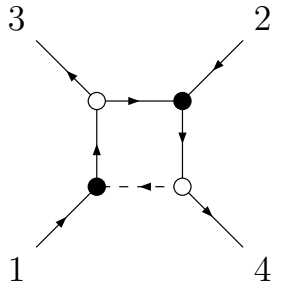

Figure 3.5: On-shell diagram for 4-point amplitude with a split helicity arrangement.

The Grassmannian integral can be evaluated by choosing

$$C = \begin{pmatrix} \lambda_1 & \lambda_2 & \lambda_3 & \lambda_4 \end{pmatrix}. \tag{3.2.6}$$

This sets $(ab) \to \langle ab \rangle$ and we obtain

$$\overline{\mathcal{M}}_{4,2}(1^-, 2^+, 3^-, 4^+) = \langle 13 \rangle \frac{[23]}{\langle 41 \rangle} \frac{1}{\prod_{a<b} \langle ab \rangle}, \tag{3.2.7}$$

where we have factored out the supermomentum delta function to give the quantity $\overline{\mathcal{M}}$, as defined in (3.1.3). This can be converted into a momentum twistor expression by substituting for the spinor bracket [23] in terms of a twistor 4-bracket according to (2.1.32):

$$\overline{\mathcal{M}}_{4,2}(1^-, 2^+, 3^-, 4^+) = \langle 13 \rangle \frac{\langle 1234 \rangle}{\prod_a \langle a\, a+1 \rangle \prod_{b<c} \langle bc \rangle}. \tag{3.2.8}$$

Five-Point

The 5-point MHV amplitude $\mathcal{M}_{5,2}(1^-, 2^+, 3^+, 4^-, 5^+)$ can be obtained from the on-shell diagram in Figure 3.6 after summing over $2 \leftrightarrow 3$. As we explained in the previous subsection, other helicity arrangements can be obtained by relabelling the diagrams. Because the diagram has two closed cycles, it is slightly tedious to evaluate the C-matrix following the algorithm in section 3.1.2, so we instead use the technique described in section 3.1.2. First we sum over paths originating from each incoming

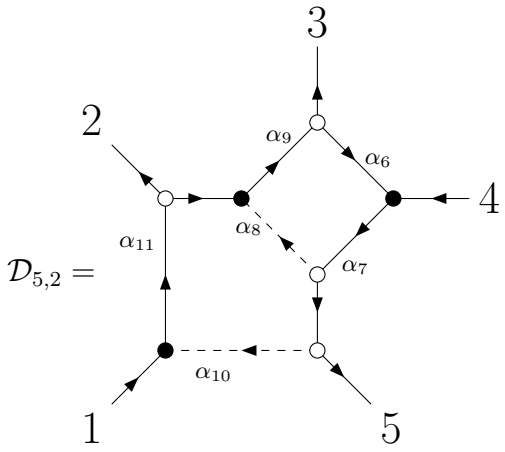

Figure 3.6: On-shell diagram for a 5-point MHV amplitude. To obtain the amplitude, sum over the exchange $2 \leftrightarrow 3$.

leg, truncating the path upon reaching another incoming leg

$$\begin{aligned}\widetilde{\lambda}_1 &= \alpha_{11}\widetilde{\lambda}_2 + \alpha_{11}\alpha_9(\widetilde{\lambda}_3 + \widetilde{\lambda}_6),\\ \widetilde{\lambda}_4 &= \alpha_7\alpha_8\alpha_9(\widetilde{\lambda}_3 + \widetilde{\lambda}_6) + \alpha_7\widetilde{\lambda}_5 + \alpha_7\widetilde{\lambda}_{10},\end{aligned} \tag{3.2.9}$$

where $\widetilde{\lambda}_6$ and $\widetilde{\lambda}_{10}$ are internal spinors adjacent to an incoming leg, which are associated with α_6 and α_{10} in Figure 3.6, respectively. We then we use the fact that all $\tilde{\lambda}$ spinors are proportional at a black vertex to write $\widetilde{\lambda}_6 = \alpha_6\widetilde{\lambda}_4$ and $\widetilde{\lambda}_{10} = \alpha_{10}\widetilde{\lambda}_1$. Combining these with equation (3.2.9) leads to the C-matrix

$$\tilde{C} = \begin{pmatrix} 1 & -\alpha_{11} & -\alpha_{11}\alpha_9 & -\alpha_{11}\alpha_9\alpha_6 & 0 \\ -\alpha_7\alpha_{10} & 0 & -\alpha_7\alpha_8\alpha_9 & 1-\alpha_7\alpha_8\alpha_9\alpha_6 & -\alpha_7 \end{pmatrix}, \tag{3.2.10}$$

where the rows are associated with legs 1 and 4. To bring the matrix to a canonical form, we apply a GL(2) transformation given by the inverse the submatrix constructed from columns 1 and 4. This gives

$$G_{\text{fix}} = \Delta_1\Delta_2 \begin{pmatrix} 1-\alpha_6\alpha_7\alpha_8\alpha_9 & \alpha_6\alpha_9\alpha_{11} \\ \alpha_{10}\alpha_7 & 1 \end{pmatrix}, \tag{3.2.11}$$

$$C = G_{\text{fix}}\tilde{C}$$
$$= \begin{pmatrix} 1 & -\Delta_2\alpha_{11} & -\Delta_1\Delta_2\alpha_9\alpha_{11} & 0 & -\Delta_1\Delta_2\alpha_9\alpha_{11}\alpha_6\alpha_7 \\ 0 & -\Delta_1\Delta_2\alpha_7\alpha_{10}\alpha_{11} & -\Delta_1\Delta_2\alpha_7\alpha_9(\alpha_8+\alpha_{10}\alpha_{11}) & 1 & -\Delta_1\Delta_2\alpha_7 \end{pmatrix}, \tag{3.2.12}$$

where $\Delta_1 = (1-\alpha_6\alpha_7\alpha_8\alpha_9)^{-1}$ and $\Delta_2 = (1-\Delta_1\alpha_9\alpha_{10}\alpha_{11}\alpha_6\alpha_7)^{-1}$. The Jacobian associated with the closed cycles is then given by

$$\mathcal{J}_C = \det\left(G_{\text{fix}}\right)^{-1} = \frac{1}{\Delta_1\Delta_2}. \tag{3.2.13}$$

The diagram can be written as the following integral over edge variables:

$$\begin{aligned} \mathcal{D}_{5,2} &= \int \prod_{i=6}^{11}\left(\frac{d\alpha_i}{\alpha_i^2}\right)\frac{1}{\alpha_7\alpha_9\alpha_{11}}\frac{\alpha_6\alpha_8\alpha_{10}\langle 34\rangle[34][21]}{\alpha_{11}}\mathcal{J}_C^3\,\delta^{(4|14)}(C\cdot\widetilde{\lambda})\delta^6(\lambda\cdot C^{\perp}), \\ &= \int \frac{d^{2\times 5}C}{\mathrm{GL}(2)}\frac{\langle 34\rangle[34][21]}{\Delta_1^8\Delta_2^8\alpha_6\alpha_7^6\alpha_8\alpha_9^5\alpha_{10}\alpha_{11}^7}\delta^{(4|14)}(C\cdot\widetilde{\lambda})\delta^6(\lambda\cdot C^{\perp}), \end{aligned}$$

where the spinor brackets from the decorations have been used to cancel those from the adjacent vertices, and we noted that

$$\frac{d^{2\times 5}C}{\mathrm{GL}(2)} = (\Delta_1\Delta_2)^5\alpha_7^3\alpha_9^2\alpha_{11}^3\prod_{i=6}^{11}d\alpha_i. \tag{3.2.14}$$

To uplift this to a covariant expression, note that

$$\begin{aligned} (12) &= -\Delta_1\Delta_2\alpha_7\alpha_{10}\alpha_{11}, & (14) &= 1, \\ (23) &= \Delta_1\Delta_2\alpha_7\alpha_8\alpha_9\alpha_{11}, & (25) &= \Delta_1\Delta_2\alpha_7\alpha_{11}, \\ (34) &= -\Delta_1\Delta_2\alpha_9\alpha_{11}, & (35) &= \Delta_1\Delta_2\alpha_7\alpha_9\alpha_{11}, \\ (45) &= \Delta_1\Delta_2\alpha_6\alpha_7\alpha_9\alpha_{11}, & (51) &= \Delta_1\Delta_2\alpha_7. \end{aligned} \tag{3.2.15}$$

Some products of these are especially useful:

$$\begin{aligned} (\Delta_1\Delta_2)^5\alpha_6\alpha_7^4\alpha_8\alpha_9^3\alpha_{10}\alpha_{11}^4 &= \prod_{i=1}^{5}(i\,i+1), \\ \Delta_1\Delta_2 &= \frac{(15)(34)}{(35)(14)}, \\ \alpha_{11} &= \frac{(25)}{(51)}, \\ (\Delta_1\Delta_2\alpha_7\alpha_9\alpha_{11})^2 &= \frac{(35)^2}{(14)}. \end{aligned} \tag{3.2.16}$$

Recalling that $\langle ab\rangle/(ab)$ is independent of a and b, we finally get

$$\mathcal{D}_{5,2} = \langle 14\rangle \int \frac{d^{2\times 5}C}{\mathrm{GL}(2)}[12][34](24)(13)\prod_{a<b}\frac{1}{(ab)}\delta^{(4|14)}(C\cdot\widetilde{\lambda})\delta^6(\lambda\cdot C^{\perp}). \tag{3.2.17}$$

The 5-point amplitude can then be recovered by summing the above formula over the permutation $2\leftrightarrow 3$:

$$\begin{aligned}\mathcal{M}_{5,2}(1^-,2^+,3^+,4^-,5^+) = \langle 14\rangle \int \frac{d^{2\times 5}C}{\mathrm{GL}(2)}&([12][34](24)(13)-[13][24](34)(12))\\ &\times\frac{\delta^{(4|14)}(C\cdot\widetilde{\lambda})\delta^6(\lambda\cdot C^{\perp})}{\prod_{a<b}(ab)}.\end{aligned} \tag{3.2.18}$$

The Grassmannian integral formula in (3.2.18) can be evaluated by setting the columns of C to λ_i giving

$$\overline{\mathcal{M}}_{5,2}(1^-,2^+,3^+,4^-,5^+) = \langle 14\rangle\frac{[12][34]\langle 24\rangle\langle 13\rangle - [13][24]\langle 12\rangle\langle 34\rangle}{\prod_{a<b}\langle ab\rangle}. \tag{3.2.19}$$

Note that $[12][34]\langle 24\rangle\langle 13\rangle - [13][24]\langle 12\rangle\langle 34\rangle = 4i\epsilon_{\mu\nu\rho\sigma}p_1^\mu p_2^\nu p_3^\rho p_4^\sigma$ is permutation-invariant on support of momentum conservation. Hence, we can equivalently write it as $[23][45]\langle 35\rangle\langle 24\rangle - [24][35]\langle 23\rangle\langle 45\rangle$. To convert the numerator to momentum twistor notation, let us consider the following quantity, first defined in [27]:

$$\begin{aligned}N_5 &= \Big([23][45]\langle 35\rangle\langle 24\rangle - [24][35]\langle 23\rangle\langle 45\rangle\Big)\langle 12\rangle\langle 23\rangle\langle 34\rangle\langle 45\rangle\langle 51\rangle,\\ &= \langle 1234\rangle\langle 2345\rangle\langle 51\rangle - \langle 1234\rangle\langle 3451\rangle\langle 25\rangle - \langle 5123\rangle\langle 2345\rangle\langle 14\rangle.\end{aligned} \tag{3.2.20}$$

This quantity will also play a role for non-MHV amplitudes. The second equality can be proved using (2.1.32), (2.1.33), and (2.1.27)

$$\begin{aligned}N_5 &= \frac{\langle 1234\rangle\langle 3451\rangle\langle 35\rangle\langle 24\rangle}{\langle 34\rangle} - \frac{(\langle 1234\rangle\langle 53\rangle + \langle 5123\rangle\langle 43\rangle)(\langle 4512\rangle\langle 43\rangle + \langle 3451\rangle\langle 42\rangle)}{\langle 34\rangle},\\ &= -(\langle 1234\rangle\langle 4512\rangle\langle 35\rangle + \langle 5123\rangle\langle 4512\rangle\langle 34\rangle + \langle 5123\rangle\langle 3451\rangle\langle 24\rangle).\end{aligned} \tag{3.2.21}$$

Equation (3.2.20) then follows from noting that N_5 is invariant under cyclic permutations. Hence, the five-point MHV amplitude has the following form in momentum

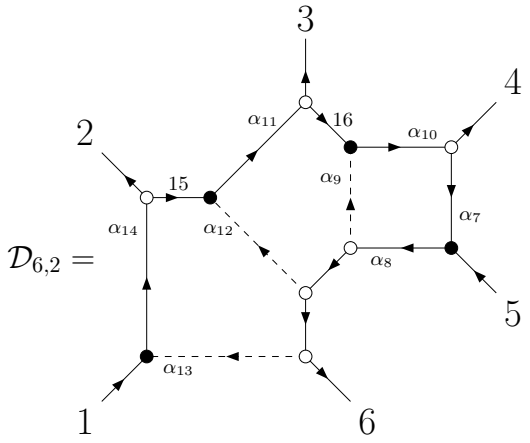

Figure 3.7: On-shell diagram for a six-point MHV amplitude. This diagram needs to be summed over all permutations of $\{2, 3, 4\}$.

twistor space:

$$\overline{\mathcal{M}}_{5,2}(1^-, 2^+, 3^+, 4^-, 5^+) = \frac{\langle 14\rangle}{\prod_a \langle a\, a{+}1\rangle \prod_{b<c}\langle bc\rangle} \times \left(\langle 1234\rangle\langle 2345\rangle\langle 51\rangle - \langle 1234\rangle\langle 3451\rangle\langle 25\rangle - \langle 2345\rangle\langle 5123\rangle\langle 14\rangle\right). \tag{3.2.22}$$

Six-point

The six-point MHV amplitude $\mathcal{M}_{6,2}(1^-, 2^+, 3^+, 4^+, 5^-, 6^+)$ can be obtained by summing the diagram shown in Figure 3.7 over permutations of legs $\{2, 3, 4\}$. As before, other helicity arrangements can be obtained by relabelling. Using the technique described in section 3.1.2, we obtain the C-matrix

$$\tilde{C} = \begin{pmatrix} 1 & -\alpha_{14} & -\alpha_{11}\alpha_{14} & -\alpha_{10}\alpha_{11}\alpha_{14} & \\ -\alpha_8\alpha_{13} & 0 & -\alpha_8\alpha_{11}\alpha_{12} & -\alpha_8\alpha_{10}(\alpha_9 + \alpha_{11}\alpha_{12}) & \\ & & & -\alpha_7\alpha_{10}\alpha_{11}\alpha_{14} & 0 \\ & & & 1 - \alpha_7\alpha_8\alpha_{10}(\alpha_9 + \alpha_{11}\alpha_{12}) & -\alpha_8 \end{pmatrix}. \tag{3.2.23}$$

We then gauge-fix using

$$G_{\text{fix}} = \Delta \begin{pmatrix} 1 - \alpha_7\alpha_8\alpha_{10}(\alpha_9 + \alpha_{11}\alpha_{12}) & \alpha_7\alpha_{10}\alpha_{11}\alpha_{14} \\ \alpha_8\alpha_{13} & 1 \end{pmatrix}, \tag{3.2.24}$$

and the Jacobian associated with closed cycles is

$$\mathcal{J}_C = \Delta^{-1} = (1 - \alpha_{10}\alpha_7\alpha_8\,(\alpha_9 + \alpha_{11}(\alpha_{12} + \alpha_{13}\alpha_{14}))\,. \tag{3.2.25}$$

This leads to the C-matrix

$$C = G_{\text{fix}}\tilde{C} = \begin{pmatrix} 1 & -\Delta\alpha_{14}\,(1 - \alpha_7\alpha_8\alpha_{10}(\alpha_9 + \alpha_{11}\alpha_{12})) & -\Delta\alpha_{11}\alpha_{14}(1 - \alpha_7\alpha_8\alpha_9\alpha_{10}) \\ 0 & -\Delta\alpha_8\alpha_{13}\alpha_{14} & -\Delta\alpha_8\alpha_{11}(\alpha_{12} + \alpha_{13}\alpha_{14}) \\ & -\Delta\alpha_{10}\alpha_{11}\alpha_{14} & 0 \quad -\Delta\alpha_7\alpha_8\alpha_{10}\alpha_{11}\alpha_{14} \\ & -\Delta\alpha_8\alpha_{10}\,(\alpha_9 + \alpha_{11}(\alpha_{12} + \alpha_{13}\alpha_{14})) & 1 \qquad -\Delta\alpha_8 \end{pmatrix}. \tag{3.2.26}$$

The bracket factors from the vertices are

$$\begin{aligned} [47] &= \alpha_7[45], \\ \langle 75\rangle &= \langle 45\rangle, \\ [2\,15] &= \frac{1}{\alpha_{14}}[21], \\ [3\,16] &= \frac{1}{\alpha_{11}\alpha_{14}}\left([31] - \alpha_{14}[32]\right), \\ &= -\frac{1}{(36)}\left([31](16) + [32](26)\right). \end{aligned} \tag{3.2.27}$$

To obtain a Grassmannian integral formula, some useful combinations of edge variables are given in terms of various minors as

$$\begin{aligned} \frac{d^{2\times 6}C}{\mathrm{GL}(2)} &= \Delta^6\alpha_8^4\alpha_{10}^2\alpha_{11}^3\alpha_{14}^4\prod_{i=7}^{14} d\alpha_i, \\ \prod_{i=1}^{6}(i\,i+1) &= \Delta^6\alpha_7\alpha_8^5\alpha_9\alpha_{10}^3\alpha_{11}^4\alpha_{12}\alpha_{13}\alpha_{14}^5, \\ (16) &= -\Delta\alpha_8, \\ (26) &= \Delta\alpha_8\alpha_{14}, \\ (36) &= \Delta\alpha_8\alpha_{11}\alpha_{14}, \\ (45) &= -\Delta\alpha_{10}\alpha_{11}\alpha_{14}, \\ (46) &= \Delta\alpha_8\alpha_{10}\alpha_{11}\alpha_{14}. \end{aligned} \tag{3.2.28}$$

After collecting all the terms, the on-shell diagram in Figure 3.7 evaluates to

$$\begin{aligned}\mathcal{D}_{6,2} &= \int \prod_{i=7}^{14}\left(\frac{d\alpha_i}{\alpha_i^2}\right)\frac{\alpha_9\alpha_{12}\alpha_{13}\alpha_7}{\alpha_8\alpha_{10}\alpha_{11}\alpha_{14}^2}\frac{[45]\langle 45\rangle[12]\left([31](16)+[32](26)\right)}{(36)} \\ &\qquad\qquad \times \mathcal{J}_C^3\delta^{(4|14)}(C\cdot\widetilde{\lambda})\delta^8(\lambda\cdot C^\perp), \\ &= \int \frac{d^{2\times 6}C}{\mathrm{GL}(2)}\frac{\delta^{(4|14)}(C\cdot\widetilde{\lambda})\delta^8(\lambda\cdot C^\perp)}{\Delta^9\alpha_7\alpha_8^7\alpha_9\alpha_{10}^5\alpha_{11}^6\alpha_{12}\alpha_{13}\alpha_{14}^8}\frac{[45]\langle 45\rangle[12]\left([31](16)+[32](26)\right)}{(36)}, \\ &= \int \frac{d^{2\times 6}C}{\mathrm{GL}(2)}\frac{\delta^{(4|14)}(C\cdot\widetilde{\lambda})\delta^8(\lambda\cdot C^\perp)}{\prod_{i=1}^6(i\,i+1)}\frac{[45]\langle 45\rangle[12]\left([31](16)+[32](26)\right)}{(36)(45)(64)(26)}.\end{aligned} \tag{3.2.29}$$

The Grassmannian integral can then be evaluated to give the spinorial expression

$$\overline{\mathcal{D}}_{6,2} = \langle 15\rangle\prod_{a<b}\frac{1}{\langle ab\rangle}[45][12][3|1+2|6\rangle\langle 25\rangle\langle 35\rangle\langle 24\rangle\langle 13\rangle\langle 14\rangle. \tag{3.2.30}$$

Finally, the six-point amplitude can be recovered by summing over the six permutations of legs 2, 3 and 4:

$$\overline{\mathcal{M}}_{6,2}(1^-,2^+,3^+,4^+,5^-,6^+) = \sum_{\mathcal{P}(2,3,4)}\overline{\mathcal{D}}_{6,2}, \tag{3.2.31}$$

which is the BGK form of the MHV gravity amplitude [111].

Equation (3.2.31) can be simplified by using momentum conservation to eliminate the square brackets $\{[23],[34],[42],[56],[61],[15]\}$, and then using the Schouten identity to eliminate the corresponding angle brackets. These are the brackets that transform into each other (or not at all) when we carry out the permutation sum. We are left with the following sum:

$$\overline{\mathcal{M}}_{6,2}(1^-,2^+,3^+,4^+,5^-,6^+) = \langle 15\rangle\sum_{\mathcal{P}(2,3,4)}\frac{[12][53][64]\langle 13\rangle\langle 14\rangle\langle 52\rangle\langle 54\rangle\langle 62\rangle\langle 63\rangle}{\prod_{a<b}\langle ab\rangle}. \tag{3.2.32}$$

Each of the six terms can be translated into a product of 6-brackets using (2.1.31). However, if we first exchange $3\leftrightarrow 6$ (using the permutation symmetry of the amplitude), this removes all square brackets of the form $[a\,a{+}2]$ and also ensures maximum cancellation of angle 2-brackets between numerator and denominator. This leads to the same compact twistor expression found in [27], which can be expressed

as

$$\overline{\mathcal{M}}_{6,2}(1^-,2^+,3^+,4^+,5^-,6^+) = \langle 15\rangle \frac{N_6}{\prod_a \langle a\, a{+}1\rangle \prod_{b<c}\langle bc\rangle}, \tag{3.2.33}$$

with

$$\begin{aligned} N_6 \;=\; & \langle 123|I|456\rangle\langle 234|I|561\rangle\langle 345|I|612\rangle \\ & + \langle 123|I|456\rangle\langle 5612\rangle\langle 2345\rangle\langle 14\rangle\langle 36\rangle \\ & + \langle 234|I|561\rangle\langle 6123\rangle\langle 3456\rangle\langle 25\rangle\langle 41\rangle \\ & + \langle 345|I|612\rangle\langle 1234\rangle\langle 4561\rangle\langle 36\rangle\langle 52\rangle \\ & + \langle 1234\rangle\langle 3456\rangle\langle 5612\rangle\langle 14\rangle\langle 25\rangle\langle 36\rangle \\ & + \langle 2345\rangle\langle 4561\rangle\langle 6123\rangle\langle 25\rangle\langle 36\rangle\langle 41\rangle. \end{aligned}$$

In [27], Hodges conjectured that the structure of (3.2.33) can be extended to all gravitational MHV amplitudes.

3.2.2 NMHV

In this section, we will use the on-shell diagram recursion to compute NMHV amplitudes in $\mathcal{N}=7$ supergravity. As a warm-up, we first consider the 5-point NMHV amplitude. Although this is just the parity conjugate of an MHV amplitude, converting it to momentum twistor space reveals interesting structure which extends to higher points, notably R-invariants analogous to the building blocks for non-MHV amplitudes in $\mathcal{N}=4$ SYM. We then go on to compute the 6-point NMHV amplitude. Unlike MHV amplitudes, the on-shell diagrams for non-MHV amplitudes correspond to residues of top-forms in the Grassmannian (this was previously observed in $\mathcal{N}=4$ SYM in [112–114] and $\mathcal{N}=8$ supergravity in [35]).

Another difference compared to MHV amplitudes is that we do not use globally defined momentum twistors to describe non-MHV amplitudes above 5-points. In particular, for the 6-point NMHV amplitude we split the on-shell diagrams into three sets and define momentum twistors with respect to a different ordering of external momenta in each set, analogous to defining local coordinates on different patches of

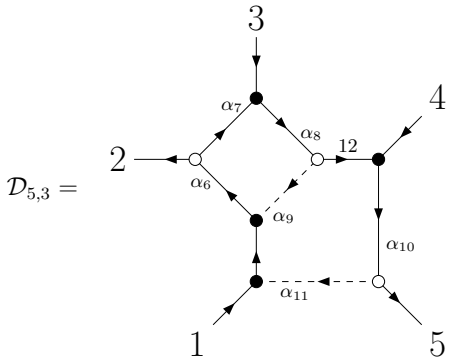

Figure 3.8: On-shell diagram for a 5-point NMHV amplitude. The full amplitude is recovered by summing over $3 \leftrightarrow 4$.

a manifold. Although this approach is unconventional, it has two important pay-offs. Firstly, the amplitudes can be expressed in terms of R-invariants similar to those found a 5-points. Secondly, the cancellation of spurious poles becomes completely transparent.

5pt $\overline{\text{MHV}}$

We will begin by computing the 5-point NMHV amplitude $\mathcal{M}_{5,3}(1^-, 2^+, 3^-, 4^-, 5^+)$, which can be obtained from the on-shell diagram in Figure 3.8 by summing over $3 \leftrightarrow 4$. Using the technique in section 3.1.2 we obtain the C-matrix

$$\tilde{C} = \begin{pmatrix} 1 & -\alpha_6 & -\alpha_6\alpha_7 & 0 & 0 \\ 0 & -\alpha_6\alpha_8\alpha_9 & 1-\alpha_6\alpha_7\alpha_8\alpha_9 & -\alpha_8 & 0 \\ -\alpha_{10}\alpha_{11} & 0 & 0 & 1 & -\alpha_{10} \end{pmatrix}. \tag{3.2.34}$$

This can be put in canonical form using the GL(3) transformation

$$G_{\text{fix}} = \Delta \begin{pmatrix} 1-\alpha_6\alpha_7\alpha_8\alpha_9 & \alpha_6\alpha_7 & \alpha_6\alpha_7\alpha_8 \\ \alpha_8\alpha_{10}\alpha_{11} & 1 & \alpha_8 \\ \alpha_{10}\alpha_{11}(1-\alpha_6\alpha_7\alpha_8\alpha_9) & \alpha_6\alpha_7\alpha_{10}\alpha_{11} & 1-\alpha_6\alpha_7\alpha_8\alpha_9 \end{pmatrix}, \tag{3.2.35}$$

where the Jacobian associated with closed cycles is

$$\mathcal{J}_C = \Delta^{-1} = \Big(1 - \alpha_6\alpha_7\alpha_8(\alpha_9 + \alpha_{10}\alpha_{11})\Big). \tag{3.2.36}$$

The gauge-fixed C-matrix is then given by

$$C = \begin{pmatrix} 1 & -\Delta\alpha_6 & 0 & 0 & -\Delta\alpha_6\alpha_7\alpha_8\alpha_{10} \\ 0 & -\Delta\alpha_6\alpha_8(\alpha_9+\alpha_{10}\alpha_{11}) & 1 & 0 & -\Delta\alpha_8\alpha_{10} \\ 0 & -\Delta\alpha_6\alpha_{10}\alpha_{11} & 0 & 1 & -\Delta\alpha_{10}(1-\alpha_6\alpha_7\alpha_8\alpha_9) \end{pmatrix}. \tag{3.2.37}$$

The bracket factors from the vertices are

$$\begin{aligned} \langle 13\,4\rangle &= \frac{1}{\alpha_{10}}\langle 54\rangle \\ [27] &= \alpha_7[23] \\ \langle 73\rangle &= \langle 23\rangle. \end{aligned} \tag{3.2.38}$$

To derive a Grassmannian integral formula the following relations are useful:

$$\begin{aligned} \frac{d^{3\times 5}C}{\mathrm{GL}(3)} &= \Delta^5\alpha_6^3\alpha_8^2\alpha_{10}^3\prod_{i=7}^{11}\alpha_i, \\ \prod_{i=1}^{5}(i\,i{+}1\,i{+}2) &= \Delta^5\alpha_6\alpha_7\alpha_8^2\alpha_{10}^3, \\ \frac{(145)(234)}{(245)} &= -\Delta, \\ \frac{(235)}{(234)} &= -\alpha_{10}, \\ (245) &= -\Delta\alpha_6\alpha_8\alpha_{10}. \end{aligned} \tag{3.2.39}$$

Using these relations, the diagram in Figure 3.8 evaluates to

$$\begin{aligned} \mathcal{D}_{5,3} &= \int\left(\prod_{i=6}^{11}\frac{d\alpha_i}{\alpha_i^2}\right)\frac{\delta^{(6|21)}(C\cdot\widetilde{\lambda})\delta^4(\lambda\cdot C^\perp)}{\alpha_6\alpha_8\alpha_{10}}\frac{\alpha_7\alpha_9\alpha_{11}}{\alpha_{10}}\langle 54\rangle[23]\langle 23\rangle\mathcal{J}_C^3, \\ &= \int\frac{d^{3\times 5}C}{\mathrm{GL}(3)}\frac{\langle 54\rangle[23]\langle 23\rangle}{\Delta^8\alpha_6^6\alpha_7^2\alpha_8^5\alpha_9\alpha_{10}^7\alpha_{11}}\delta^{(6|21)}(C\cdot\widetilde{\lambda})\delta^4(\lambda\cdot C^\perp), \\ &= \int\frac{d^{3\times 5}C}{\mathrm{GL}(3)}\delta^{(6|21)}(C\cdot\widetilde{\lambda})\delta^4(\lambda\cdot C^\perp)\frac{\langle 54\rangle[23]\langle 23\rangle}{\prod_{i=1}^{5}(i\,i+1\,i+2)(235)(145)(245)}, \\ &= [25]\int\frac{d^{3\times 5}C}{\mathrm{GL}(3)}\delta^{(6|21)}(C\cdot\widetilde{\lambda}|\eta)\delta^4(\lambda\cdot C^\perp)\frac{\langle 54\rangle\langle 23\rangle(124)(135)}{\prod_{a<b<c}(abc)}, \end{aligned} \tag{3.2.40}$$

where we have used that $[23]/[25] = (145)/(134)$. This relation can be derived by

noting that for the canonical choice

$$C = \begin{pmatrix} 1 & c_{12} & 0 & 0 & c_{15} \\ 0 & c_{32} & 1 & 0 & c_{35} \\ 0 & c_{42} & 0 & 1 & c_{45} \end{pmatrix}, \tag{3.2.41}$$

the bosonic delta functions $\delta^6\left(C\cdot\tilde{\lambda}\right)$ imply that $c_{a2} = [5a]\,/\,[25]$ and $c_{a5} = [a2]\,/\,[25]$, so $(abc) = \epsilon_{abcmn}[mn]/[25]$. Plugging this into (3.2.40) and summing over $3 \leftrightarrow 4$ finally gives

$$\overline{\mathcal{M}}_{5,3} = \frac{[25]}{\prod_{i<j}[ij]}\left([35][24]\langle 23\rangle\langle 54\rangle - [45][23]\langle 24\rangle\langle 53\rangle\right)\delta^{(0|7)}\left(\frac{[51]\eta_2 + \text{cyclic}}{\langle 34\rangle}\right). \tag{3.2.42}$$

If we pull out a helicity-dependent prefactor, (3.2.42) can alternatively be written as

$$\overline{\mathcal{M}}_{5,3}(1^-,2^+,3^-,4^-,5^+) = [25]\frac{1}{\langle 12\rangle\langle 23\rangle\langle 34\rangle\langle 45\rangle\langle 51\rangle}\,\hat{M}_5, \tag{3.2.43}$$

where $\hat{M}_5$ is little-group invariant which has the following form in momentum twistor space:

$$\hat{M}_5 = \frac{N_5 R^{(7)}_{135}}{D_5}, \tag{3.2.44}$$

where $R^{(7)}$ is an $\mathcal{N}=7$ R-invariant defined in (2.2.12), N_5 is defined in (3.2.20), and

$$D_5 = \prod_{a=1}^{5}\langle a{-}2\, a{-}1\, a|I|a\, a{+}1\, a{+}2\rangle. \tag{3.2.45}$$

Note that D_5 is proportional to the product of five spinor brackets $[a\, a{+}2]$ using (2.1.31) and (2.1.33). Neither $R^{(7)}$ nor D_5 are individually permutation invariant but their ratio should nevertheless have the S_5 symmetry since we pulled out the helicity-dependent part of the amplitude in (3.2.43). In $\mathcal{N}=4$ SYM, R-invariants form the building blocks for all tree-level non-MHV amplitudes, so it is interesting to see them appear in supergravity amplitudes. In [115], $\mathcal{N}=8$ supergravity amplitudes were constructed by squaring $\mathcal{N}=4$ R-invariants, but in this paper we define R-invariants which are more intrinsic to supergravity. Note that both $R^{(4)}$ and $R^{(7)}$ are invariant under the dual conformal group SU(4), but $R^{(4)}$ have additional GL(1) symmetry

which makes them projective and leads to an elegant geometric interpretation of NMHV amplitudes in $\mathcal{N}=4$ SYM as volumes of polytopes in $\mathbb{CP}^4$ [19]. Note that $\hat{M}_5$ in (3.2.44) is also GL(4) invariant, so it would be interesting explore its geometric interpretation.

Writing the remaining spinor bracket in (3.2.43) in terms of a twistor bracket using (2.1.31), we get

$$\overline{\mathcal{M}}_{5,3}(1^-,2^+,3^-,4^-,5^+) = \frac{R^{(7)}_{135}}{[\mathrm{PT}(5)]^2}\frac{\langle 123|I|451\rangle\langle 34\rangle N_5}{D_5}, \tag{3.2.46}$$

where

$$[\mathrm{PT}(n)] = \Pi_{a=1}^{n}\langle a\, a{+}1\rangle \tag{3.2.47}$$

and $n+1$ is identified with particle 1. We will find similar structure for 6-point NMHV amplitudes.

3.2.3 6pt NMHV

In this subsection, we will consider the amplitude with alternating helicities $\mathcal{M}_{6,3}(1^-,2^+,3^-,4^+,5^-,6^+)$. Any other can then be obtained by a relabelling. Using the recursion in (3.1.10), this amplitude can be obtained from four on-shell diagrams summed over permutations to give a total of 13 terms. It is then natural to combine them into 9 terms, each with a common pole of the form $s_{abc} = (p_a + p_b + p_c)^2$ [2]. In this way we obtain a superamplitude whose graviton component is equivalent to the spinorial expression obtained in [27] up to a relabelling. In the next subsection we obtain a new formula for the 6-point NMHV amplitude in terms of momentum twistors defined with respect to different orderings of the external momenta, which reveals surprising mathematical structure and provides a systematic understanding of spurious pole cancellation.

Since $\mathcal{N}=7$ on-shell diagrams are labelled with arrows encoding the helicities of the superfields, we will sometimes have to use non-cyclic labels for the external legs even

[2]This definition differs by a factor of 2 from that used in the other chapters of this thesis to follow previous conventions for spinor expressions for SYM and supergravity.

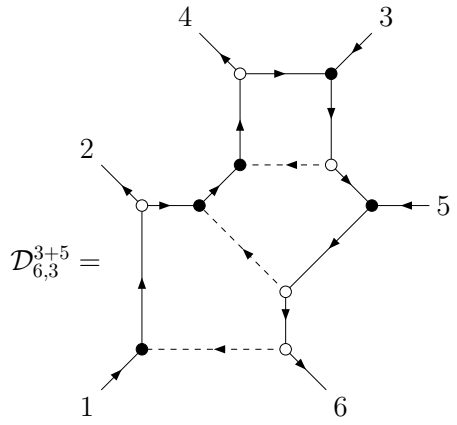

Figure 3.9: On-shell diagram combining a 3-point $\overline{\text{MHV}}$ amplitude with a 5-point $\overline{\text{MHV}}$ amplitude. This diagram needs to be summed over the permutations $2 \leftrightarrow 4$ and $3 \leftrightarrow 5$.

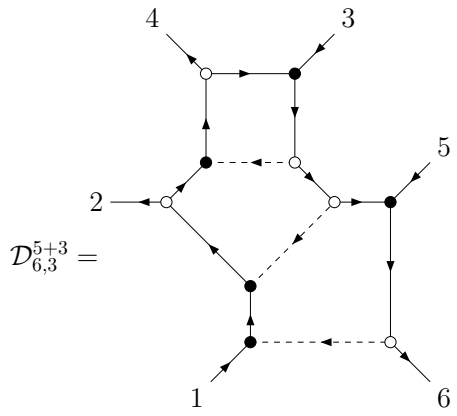

Figure 3.10: On-shell diagram combining a 5-point MHV amplitude with a 3-point MHV amplitude. This diagram needs to be summed over the permutations $2 \leftrightarrow 4$ and $3 \leftrightarrow 5$.

before we sum over permutations. Our description of how to evaluate the on-shell diagrams will be more schematic in this section. For more details, see Appendix A.

3+5 and 5+3 Diagrams

We begin with the diagrams in Figures 3.9 and 3.10, which encode factorisations into 3-point and 5-point subamplitudes. Using the methods described in section 3.1.2, they can be written compactly as

$$\begin{aligned}\mathcal{D}_{6,3}^{3+5} &= \operatorname*{Res}_{(612)=0} \int d^{3\times 6}\Omega_7 \frac{\langle 34\rangle[34]\langle 56\rangle[12]}{(346)(256)(356)} \frac{(123)}{(124)}, \\ \mathcal{D}_{6,3}^{5+3} &= \operatorname*{Res}_{(234)=0} \int d^{3\times 6}\Omega_7 \frac{\langle 34\rangle[34]\langle 56\rangle[12]}{(346)(256)(356)} \frac{(123)}{(124)},\end{aligned} \tag{3.2.48}$$

where

$$d^{3\times 6}\Omega_7 = \frac{d^{3\times 6}C}{\mathrm{GL}(3)}\frac{\delta^{(6|21)}(C\cdot\widetilde{\lambda}|\eta)\delta^{(6)}(\lambda\cdot C^{\perp})}{\prod_{a=1}^{6}(a\,a+1\,a+2)}. \tag{3.2.49}$$

These diagrams need to be summed over the permutations $2\leftrightarrow 4$ and $3\leftrightarrow 5$. In each case it can be seen that one of these permutations only affects the integrand whilst the other also changes which residue we take.

The Grassmannian integrals in (3.2.48) can be evaluated using a clever choice of gauge [7]. For example, to evaluate $\mathcal{D}_{6,3}^{3+5}$ we multiply by (612) and choose

$$C = \begin{pmatrix} \lambda_1 & \lambda_2 & \lambda_3 & \lambda_4 & \lambda_5 & \lambda_6 \\ 0 & 0 & [45] & [53] & [34] & 0 \end{pmatrix}. \tag{3.2.50}$$

Calculating the required minors and substituting into the first line of (3.2.48) then gives

$$\overline{\mathcal{D}}_{6,3}^{3+5} = \frac{\langle 34\rangle\langle 56\rangle[12]\,\delta^{(0|7)}\left([45]\eta_3+[53]\eta_4+[34]\eta_5\right)}{s_{345}\langle 12\rangle[35][34]\langle 61\rangle\langle 26\rangle[3|4+5|6\rangle[4|5+3|6\rangle[5|3+4|6\rangle[5|3+4|2\rangle}, \tag{3.2.51}$$

where $[a|b+c|d\rangle = [ab]\langle bf\rangle + [ac]\langle cd\rangle$. Terms of this form correspond to spurious poles which must cancel out in the amplitude. The full expression containing an s_{345} pole is obtained by summing over the exchange $3\leftrightarrow 5$:

$$\begin{aligned}\overline{\mathcal{D}}_{6,3}^{(345)} = &\frac{[12]\,\delta^{(0|7)}\left([45]\eta_3+[53]\eta_4+[34]\eta_5\right)}{s_{345}\langle 12\rangle\langle 26\rangle\langle 61\rangle[35][3|4+5|6\rangle[4|5+3|6\rangle[5|3+4|6\rangle} \\ &\times\left(\frac{\langle 34\rangle\langle 56\rangle}{[34][5|3+4|2\rangle}-\frac{\langle 54\rangle\langle 36\rangle}{[54][3|5+4|2\rangle}\right),\end{aligned} \tag{3.2.52}$$

where the sign which comes from exchanging of $3\leftrightarrow 5$ in the fermionic delta function is cancelled by the sign which comes from anticommuting the corresponding Φ^- superfields. The term with an s_{235} pole can be obtained by applying the permutation $2\leftrightarrow 4$ to (3.2.52).

Similarly, for $\mathcal{D}_{6,3}^{5+3}$, we choose

$$C = \begin{pmatrix} \lambda_1 & \lambda_2 & \lambda_3 & \lambda_4 & \lambda_5 & \lambda_6 \\ [56] & 0 & 0 & 0 & [61] & [15] \end{pmatrix}, \tag{3.2.53}$$

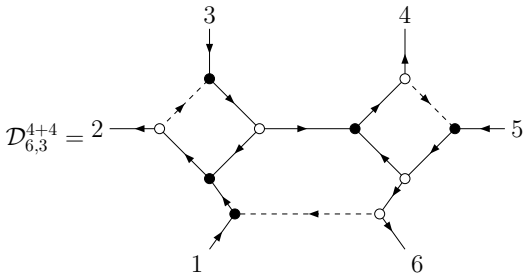

Figure 3.11: On-shell diagram combining two 4-point amplitudes with alternating helicities. This diagram needs to be summed over the permutations $2 \leftrightarrow 4$ and $3 \leftrightarrow 5$.

which gives

$$\overline{\mathcal{D}}_{6,3}^{(5+3)} = \frac{[34]\langle 56\rangle[12]\,\delta^{(0|7)}\left([56]\eta_1+[61]\eta_5+[15]\eta_6\right)}{s_{561}[61][15][56]\langle 43\rangle\langle 24\rangle[1|5+6|2\rangle[1|5+6|3\rangle[1|5+6|4\rangle[5|6+1|2\rangle}. \tag{3.2.54}$$

The full expression with an s_{561} pole is then obtained by summing over the permutation $2 \leftrightarrow 4$ and is given by

$$\begin{aligned}\overline{\mathcal{D}}_{6,3}^{(561)} = &\frac{\langle 56\rangle\,\delta^{(0|7)}\left([56]\eta_1+[61]\eta_5+[15]\eta_6\right)}{s_{561}[61][15][56]\langle 24\rangle[1|5+6|2\rangle[1|5+6|3\rangle[1|5+6|4\rangle} \\ &\times\left(\frac{[12][34]}{\langle 43\rangle[5|6+1|2\rangle}-\frac{[14][32]}{\langle 23\rangle[5|6+1|4\rangle}\right).\end{aligned} \tag{3.2.55}$$

The term with a pole in s_{361} is then obtained by applying the permutation $3 \leftrightarrow 5$.

4+4 Diagrams

These diagrams encode factorisations into 4-point subamplitudes. In the $\mathcal{N}=7$ formalism, there are two inequivalent types in which the 4-point amplitudes either have negative helicities opposite or adjacent to each other, as depicted in Figures 3.11 and 3.12, respectively. Using the methods described in section 3.1.2, the diagram in Figure 3.11 evaluates to

$$\mathcal{D}_{6,3}^{(4+4)} = \operatorname*{Res}_{(456)=0}\int d^{3\times 6}\Omega_7\frac{[13][45]\langle 23\rangle\langle 46\rangle}{(236)(246)^2}. \tag{3.2.56}$$

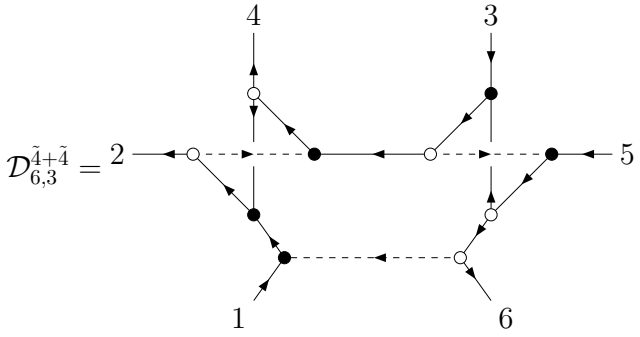

Figure 3.12: On-shell diagram combining two 4-point amplitudes with split helicities. This diagram does not require any permutation sums since it is invariant under $2 \leftrightarrow 4$ and $3 \leftrightarrow 5$.

To find a spinor expression for this diagram, we choose

$$C = \begin{pmatrix} \lambda_1 & \lambda_2 & \lambda_3 & \lambda_4 & \lambda_5 & \lambda_6 \\ [23] & [31] & [12] & 0 & 0 & 0 \end{pmatrix}, \tag{3.2.57}$$

which gives

$$\begin{aligned} \overline{\mathcal{D}}_{6,3}^{(4+4)} &\equiv \overline{\mathcal{D}}_{6,3}^{(123)}, \\ &= -\frac{[13][45]\langle 23\rangle\langle 46\rangle\, \delta^{(0|7)}\left([23]\eta_1 + [31]\eta_2 + [12]\eta_3\right)}{s_{123}[1|2+3|4\rangle[12][45]\langle 56\rangle[23][3|1+2|6\rangle[31]^2\langle 46\rangle^2[1|2+3|6\rangle}, \\ &= \frac{\langle 23\rangle[45]\, \delta^{(0|7)}\left([23]\eta_1 + [31]\eta_2 + [12]\eta_3\right)}{s_{123}[12][23][31]\langle 46\rangle\langle 45\rangle\langle 56\rangle[1|2+3|4\rangle[1|2+3|6\rangle[3|1+2|6\rangle}. \end{aligned} \tag{3.2.58}$$

The final diagram in Figure 3.12 is non-planar. This is a consequence of using the BCFW bridge in (3.1.11) with its fixed helicity assignments . The diagram is invariant under the permutations $2 \leftrightarrow 4$ and $3 \leftrightarrow 5$. Although this is not obvious from the Grassmannian integral formula, it will be manifest in the spinorial expression. The Grassmannian integral formula for this diagram is

$$\mathcal{D}_{6,3}^{(\tilde{4}+\tilde{4})} = \operatorname*{Res}_{(356)=0} \int d^{3\times 6}\Omega_7 \frac{[24]\langle 24\rangle[35]\langle 35\rangle(123)(456)}{(146)(245)(236)(124)(356)}. \tag{3.2.59}$$

To evaluate the Grassmannian integral, choose

$$C = \begin{pmatrix} \lambda_1 & \lambda_2 & \lambda_3 & \lambda_4 & \lambda_5 & \lambda_6 \\ [24] & [41] & 0 & [12] & 0 & 0 \end{pmatrix}, \tag{3.2.60}$$

which gives

$$\begin{aligned}\overline{\mathcal{D}}_{6,3}^{(\tilde{4}+\tilde{4})} &\equiv \overline{\mathcal{D}}_{6,3}^{(124)}, \\ &= \frac{[35]\langle 24\rangle\,\delta^{(0|7)}\left([24]\eta_1+[41]\eta_2+[12]\eta_4\right)}{s_{124}[12][14]\langle 56\rangle\langle 36\rangle[1|2+4|3\rangle[1|2+4|5\rangle[4|1+2|6\rangle[2|1+4|6\rangle}.\end{aligned} \tag{3.2.61}$$

From this spinor expression, it is clear that this term is invariant under the permutations $2\leftrightarrow 4$ and $3\leftrightarrow 5$.

The full amplitude is given by

$$\overline{\mathcal{M}}_{6,3}(1^-,2^+,3^-,4^+,5^-,6^+)=\sum_{\substack{2\leftrightarrow 4\\3\leftrightarrow 5}}\left(\overline{\mathcal{D}}_{6,3}^{3+5}+\overline{\mathcal{D}}_{6,3}^{4+4}+\overline{\mathcal{D}}_{6,3}^{5+3}\right)+\overline{\mathcal{D}}_{6,3}^{\tilde{4}+\tilde{4}}. \tag{3.2.62}$$

Combining terms with common s_{abc} poles gives a sum over nine terms, where we denote the term with a pole in s_{abc} as $\overline{\mathcal{D}}_{6,3}^{(abc)}$.

$$\begin{aligned}\sum_{\substack{2\leftrightarrow 4\\3\leftrightarrow 5}}\overline{\mathcal{D}}_{6,3}^{3+5}&=\overline{\mathcal{D}}_{6,3}^{(345)}+\overline{\mathcal{D}}_{6,3}^{(325)},\\ \sum_{\substack{2\leftrightarrow 4\\3\leftrightarrow 5}}\overline{\mathcal{D}}_{6,3}^{4+4}&=\overline{\mathcal{D}}_{6,3}^{(123)}+\overline{\mathcal{D}}_{6,3}^{(143)}+\overline{\mathcal{D}}_{6,3}^{(125)}+\overline{\mathcal{D}}_{6,3}^{(145)},\\ \sum_{\substack{2\leftrightarrow 4\\3\leftrightarrow 5}}\overline{\mathcal{D}}_{6,3}^{5+3}&=\overline{\mathcal{D}}_{6,3}^{(561)}+\overline{\mathcal{D}}_{6,3}^{(361)},\\ \overline{\mathcal{D}}_{6,3}^{\tilde{4}+\tilde{4}}&=\overline{\mathcal{D}}_{6,3}^{(124)}.\end{aligned} \tag{3.2.63}$$

3.2.4 Local Coordinates & Momentum Twistors

We will now rewrite the expressions obtained in the previous subsection in terms of momentum twistors. For concreteness, let us first consider the formula for the twisted on-shell diagram in (3.2.61). Using (2.1.31), (2.1.36), and (2.1.27), the fermionic delta function can be written as follows:

$$\delta^{(0|7)}\left([12]\eta_4+[41]\eta_2+[24]\eta_1\right)=\frac{\delta^{(0|7)}\Big(\langle 34\rangle\left(\langle 6123\rangle\chi_5+\text{cyc}\right)+\langle 53\rangle\left(\langle 6123\rangle\chi_4+\text{cyc}\right)\Big)}{\left(\langle 61\rangle\langle 12\rangle\langle 23\rangle\langle 34\rangle\langle 45\rangle\right)^7}. \tag{3.2.64}$$

Compared to the R-invariants which appear in non-MHV amplitudes of $\mathcal{N}=4$ SYM, this expression is complicated and difficult to interpret geometrically. A more

illuminating form can be obtained by defining momentum twistors with respect to permuted momenta. Note that we are not actually permuting momenta of the amplitude, so this should be thought of as a passive transformation as we will spell out below. In general, this transformation acts like a permutation of momentum labels, a linear transformation of region momenta, and a non-linear transformation of twistors

$$\begin{aligned} p_a|_{\mathcal{P}} &= p_{\mathcal{P}(a)}, \\ (x_a - x_{a+1})|_{\mathcal{P}} &= p_a|_{\mathcal{P}} = p_{\mathcal{P}(a)}, \\ Z_a|_{\mathcal{P}} = (\lambda_a, x_a \cdot \lambda_a)|_{\mathcal{P}} &= \left(\lambda_{\mathcal{P}(a)}, x_a|_{\mathcal{P}} \cdot \lambda_{\mathcal{P}(a)}\right), \end{aligned} \tag{3.2.65}$$

where the first line is used to express the right hand side of the other two lines. For concreteness, let $\mathcal{P}$ act on momentum labels as follows:

$$\mathcal{P} = \begin{pmatrix} 1 & 2 & 3 & 4 & 5 & 6 \\ 1 & 2 & 5 & 6 & 3 & 4 \end{pmatrix}. \tag{3.2.66}$$

Using (3.2.65), the fermionic delta function in (3.2.64) takes a much simpler form

$$\begin{aligned} \delta^{(0|7)}\left([12]\eta_4 + [41]\eta_2 + [24]\eta_1\right) &= \delta^{(0|7)}\left([61]\eta_2 + [12]\eta_6 + [26]\eta_1\right)\Big|_{\mathcal{P}}, \\ &= \frac{\delta^{(0|7)}(\langle 5612\rangle\chi_3 + \text{cyc.})}{(\langle 56\rangle\langle 61\rangle\langle 12\rangle\langle 23\rangle)^7}\Bigg|_{\mathcal{P}}, \end{aligned} \tag{3.2.67}$$

which can be written in terms of an R-invariant defined in (2.2.12).

Now let's consider a spurious pole in appearing in (3.2.61):

$$[1|2+4|5\rangle = -\frac{\langle 53\rangle(\langle 24\rangle\langle 6123\rangle + \langle 32\rangle\langle 6124\rangle) + \langle 23\rangle\langle 34\rangle\langle 5612\rangle}{\langle 61\rangle\langle 12\rangle\langle 23\rangle\langle 34\rangle}. \tag{3.2.68}$$

In terms of the momentum twistors defined with respect to the permutation $\mathcal{P}$ above, this also takes a much more compact and geometrical form:

$$[1|2+4|5\rangle = [1|2+6|3\rangle\Big|_{\mathcal{P}} = \frac{\langle 36\rangle\langle 5612\rangle + \langle 56\rangle\langle 6123\rangle}{\langle 56\rangle\langle 61\rangle\langle 12\rangle}\Big|_{\mathcal{P}} = \frac{\langle 612|I|356\rangle}{\langle 56\rangle\langle 61\rangle\langle 12\rangle}\Big|_{\mathcal{P}}, \tag{3.2.69}$$

Remarkably, this type of simplification occurs for all of the spurious poles we encounter in the six-point NMHV amplitude, which makes their cancellation much

more transparent, as we show in the next subsection. In Yang-Mills theory, such cancellations were explained by interpreting the amplitude as the volume of a polytope in momentum twistor space. We therefore expect a similar geometric picture for gravity, although it will be more complicated for reasons we will now explain.

The main complication is that we cannot simultaneously simplify all on-shell diagrams using a global choice of coordinates in momentum twistor space. In order to make progress, we will use different momentum twistor coordinates for different on-shell diagrams, analogous to assigning local coordinates on a manifold. In the present context, local coordinates refer to momentum twistors defined with respect to a certain permutation of external momenta which we will refer to as a *chart*, and the set of on-shell diagrams described by a given chart will be referred to as a *patch* [3]. The transition functions between different patches are complicated in general, but can deduced by decomposing the respective permutations into adjacent transpositions, as we explain in Appendix B. Finally, will refer to the set of all charts we use to describe a scattering amplitude as an *atlas*.

The set of all possible charts at $n = 6$ is the permutation group S_6, but we can quotient by cyclic permutations and the Z_2 transformation $\left(\begin{smallmatrix}1&2&3&4&5&6\\6&5&4&3&2&1\end{smallmatrix}\right)$, since these permute momentum twistors in a trivial way, leaving a total of 60 charts. Using a Python script, we found that at least three charts are needed to describe the 6-point NMHV amplitude in such a way that all fermionic delta functions can be described by R-invariants. This boils down to looking for the smallest atlases whose charts contain all nine 3-tuples (a, b, c) corresponding to the s_{abc} poles in the amplitude[4]. There are 32 such atlases. Further insisting that one chart corresponds to the identity permutation reduces this to four. We will choose one of these four atlases to demonstrate the relative compactness of the amplitude (the other three atlases lead to similar results). The charts it contains and the on-shell diagrams in each patch

[3] To make the analogy to a manifold more precise, we should distinguish between the amplitude and the underlying geometric object that it describes. Hence, a patch should really be thought of as a region of the underlying geometric object on which a set of on-shell diagrams is defined.

[4] Strictly speaking, the chart itself is the inverse of the permutation we need to apply.

Patch	Chart	Patch Content	Equations
1	123456	561, 345, 123	(3.2.55), (3.2.52), (3.2.58)
2	145236	361, 325, 145	(3.2.55), (3.2.52), (3.2.58)
3	125634	124, 134, 125	(3.2.61), (3.2.58), (3.2.58)

Table 3.1: An atlas for the 6-point NMHV amplitude in momentum twistor space. The permutation associated with each chart is listed in the second column. The on-shell diagrams in each patch are listed in the third column, and are labelled by three momenta appearing the corresponding factorisation channel. The final column lists where the expressions in the third column can be found (some after applying either $3 \leftrightarrow 5$ or $2 \leftrightarrow 4$ or both).

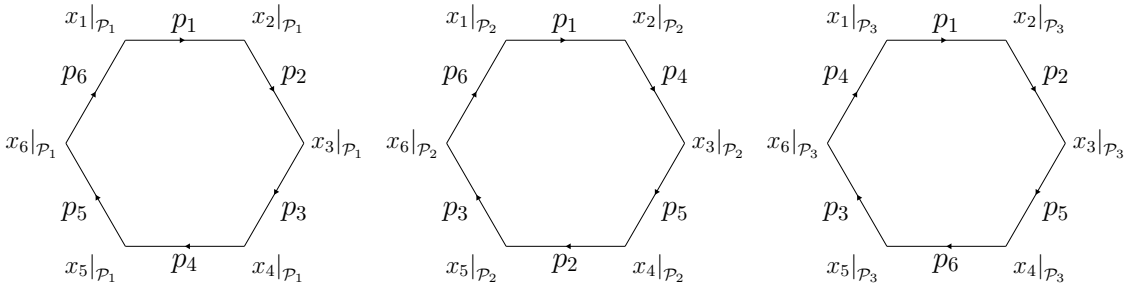

Figure 3.13: Three sets of region momentum variables for the atlas in Table 3.1.

are summarised in Table 3.1. We will denote the three charts by the permutations $\mathcal{P}_i$, $i \in \{1, 2, 3\}$. The region momentum coordinates in each patch are depicted in Figure 3.13, and the momentum twistors in a generic patch are depicted in Figure 3.14.

To start, let us look at the expressions obtained for the first patch in Table 3.1. In this case, the momentum twistors are defined with respect to unpermuted momenta and the three contributions from this patch are given by

$$\overline{\mathcal{D}}^{(561)}_{6,3} = \frac{R^{(7)}_{251}}{[\mathrm{PT}(6)]^2} \frac{\langle 456|I|124\rangle\langle 6123\rangle\langle 2345\rangle + \langle 612|I|345\rangle\langle 1234\rangle\langle 4562\rangle}{\langle 24\rangle\langle 612|I|456\rangle\langle 456|I|124\rangle\langle 245|I|612\rangle\langle 612|45|I|3\rangle}, \tag{3.2.70}$$

$$\overline{\mathcal{D}}^{(345)}_{6,3} = \frac{R^{(7)}_{246}}{[\mathrm{PT}(6)]^2} \frac{\langle 6123\rangle\left(\langle 234|I|256\rangle\langle 3456\rangle + \langle 36\rangle\langle 2345\rangle\langle 2456\rangle\right)}{\langle 26\rangle\langle 234|I|456\rangle\langle 345|I|236\rangle\langle 456|I|236\rangle\langle 234|I|256\rangle}, \tag{3.2.71}$$

$$\overline{\mathcal{D}}^{(123)}_{6,3} = \frac{R^{(7)}_{214}}{[\mathrm{PT}(6)]^2} \frac{\langle 3456\rangle}{\langle 34\rangle\langle 46\rangle\langle 234|I|612\rangle\langle 346|I|612\rangle}. \tag{3.2.72}$$

We can see that each term contains an R-invariant along with a squared Park-Taylor factor in the denominator, just as we found for the 5-point NMHV amplitude in

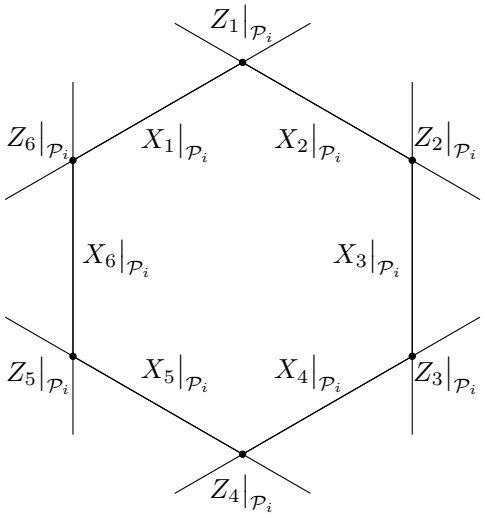

Figure 3.14: Definition of momentum twistors from dual variables on a given patch $\mathcal{P}_i$.

(3.2.46). Furthermore, the remaining terms are written in terms of 4-brackets and 6-brackets defined in (2.1.26), (2.1.29) and (2.1.30). Note that 4-bracket spurious poles are of the form $\langle a\, b{-}1\, b\, b{+}1\rangle$ for $a{+}1 \neq b{-}1$ and $a{-}1 \neq b{+}1$, while 6-bracket spurious poles are of the form $\langle a|I|bc|def\rangle$ or $\langle abc|I|def\rangle$ where (a, b, c) or (d, e, f) are non-adjacent. In the next subsection we will see that the structure of the terms dressing the R-invariants is required by spurious pole cancellation. It would be interesting to have a more systematic understanding of their structure in terms of some underlying geometric object.

The second patch in Table 3.1 does not require any additional work. The twistor expressions are identical to those in the first patch using twistors defined with respect to a different ordering:

$$\overline{\mathcal{D}}^{(361)}_{6,3} = \overline{\mathcal{D}}^{(561)}_{6,3}\Big|_{\mathcal{P}_2}, \tag{3.2.73}$$

$$\overline{\mathcal{D}}^{(325)}_{6,3} = \overline{\mathcal{D}}^{(345)}_{6,3}\Big|_{\mathcal{P}_2}, \tag{3.2.74}$$

$$\overline{\mathcal{D}}^{(145)}_{6,3} = \overline{\mathcal{D}}^{(123)}_{6,3}\Big|_{\mathcal{P}_2}. \tag{3.2.75}$$

Finally, the third patch in Table 3.1 has the following momentum twistor expressions:

$$\overline{\mathcal{D}}^{(124)}_{6,3} = \frac{R^{(7)}_{163}}{[\mathrm{PT}(6)]^2} \frac{\langle 26\rangle\langle 456|I|234\rangle\langle 5123\rangle\langle 5613\rangle}{\langle 23\rangle\langle 56\rangle\langle 612|I|325\rangle\langle 612|I|356\rangle\langle 4|I|23|561\rangle\langle 4|I|65|123\rangle}\Big|_{\mathcal{P}_3}, \tag{3.2.76}$$

$$\overline{\mathcal{D}}^{(134)}_{6,3} = \frac{R^{(7)}_{251}}{[\mathrm{PT}(6)]^2} \frac{\langle 1234\rangle\langle 4562\rangle}{\langle 24\rangle\langle 612|I|456\rangle\langle 612|I|452\rangle\langle 456|I|214\rangle}\Big|_{\mathcal{P}_3}, \tag{3.2.77}$$

$$\overline{\mathcal{D}}^{(125)}_{6,3} = \frac{R^{(7)}_{214}}{[\mathrm{PT}(6)]^2} \frac{\langle 4561\rangle\langle 6234\rangle}{\langle 46\rangle\langle 234|I|612\rangle\langle 234|I|614\rangle\langle 612|I|436\rangle}\Big|_{\mathcal{P}_3}. \tag{3.2.78}$$

In summary, it seems natural to describe supergravity amplitudes using momentum twistor coordinates which are defined with respect to different permutations of external momenta. This leads to compact expressions in terms of R-invariants dressed with rational functions of 4-brackets and 6-brackets which have geometric interpretations in terms of intersections of lines and planes in momentum twistor space. As we will demonstrate in the next subsection, this point of view will also make the cancellation of spurious poles in the 6-point NMHV amplitude much more transparent, suggesting a geometric interpretation analogous to the polytope picture discovered for Yang-Mills in [18]. Given that each pole of the 6-point NMHV amplitude can be written as either a 4-bracket or a 6-bracket, one may ask if this property holds for all possible poles one can write down at six points. In [1] an algorithm was developed to answer this question, finding the simplest possible form for all poles at six points. It was found that some poles must be written as a sum of terms, and cannot be written as a single 4-bracket or 6-bracket. Hence it is non-trivial that the pole structure of the 6-point NMHV amplitude can be written in a simple geometrical way, and we take this as further evidence that there is an underlying geometric object which encodes gravity amplitudes.

3.2.5 Spurious Pole Analysis & Cancellation

As first noted in [27], there are 18 different spurious poles in the 6-point NMHV amplitude. Each spurious pole appears twice, giving a total of 36 occurrences. Each

of the four diagram topologies has a different set of spurious poles associated with it. These cancel in pairs as shown in Figure 3.15. In principle, there are 18 cancellations to check, however the permutations used to simplify the twistor expressions can also be used to relate all the cancellations which appear on the same edge in Figure 3.15, leaving only six cases to check. We label a given cancellation using the notation $(j|j')$, where the cancellation takes place between two bubbles in Figure 3.15 labelled by $i \times j$ and $i' \times j'$. The integers i and i' indicate the number of times the j-type and j'-type poles occur, respectively. Note that j and j' are in 1-to-1 correspondence with the on-shell diagram topologies denoted $X + Y$ in Figure 3.15, so these two types of labels can be used interchageably when referring to spurious poles. The six cancellations can therefore be labelled $(5|\bar{5}), (5|3), (5|4), (3|3), (\bar{5}|3)$ and $(\bar{5}|4)$. The $(\bar{5}|3)$ and $(\bar{5}|4)$ cancellations can additionally be related to $(5|3)$ and $(5|4)$ by parity, so there are actually only four cases to check.

We have checked the four cases $(5|\bar{5}), (5|3), (5|4), (3|3)$ analytically using the local coordinates defined in the previous subsection, and in each case the calculation is manifestly supersymmetric and reduces to an application of the Schouten identity, as we illustrate for $(5|\bar{5})$ below. This represents major progress, since in previous work the cancellation of spurious poles was only checked numerically for the graviton component of the superamplitude due to the complexity of the spinorial expressions [27]. The cancellations we observe are also very reminiscent of those observed for Yang-Mills amplitudes in [18], which ultimately lead to a new geometric interpretation for NMHV amplitudes as volumes of polytopes. This suggests that a similar interpretation may hold for gravitational amplitudes. We will now demonstrate the $(5|\bar{5})$ spurious cancellation in Figure 3.15 using momentum twistors. To start with, consider the $[5|3+4|2\rangle$ pole shared by $\mathcal{D}^{(561)}$ and $\mathcal{D}^{(345)}$ given in (3.2.70) and (3.2.71), or equivalently (3.2.55) and (3.2.52). Recall that these expressions arise from $5+3$ and $3+5$ on-shell diagrams, so are associated with the corresponding bubbles in

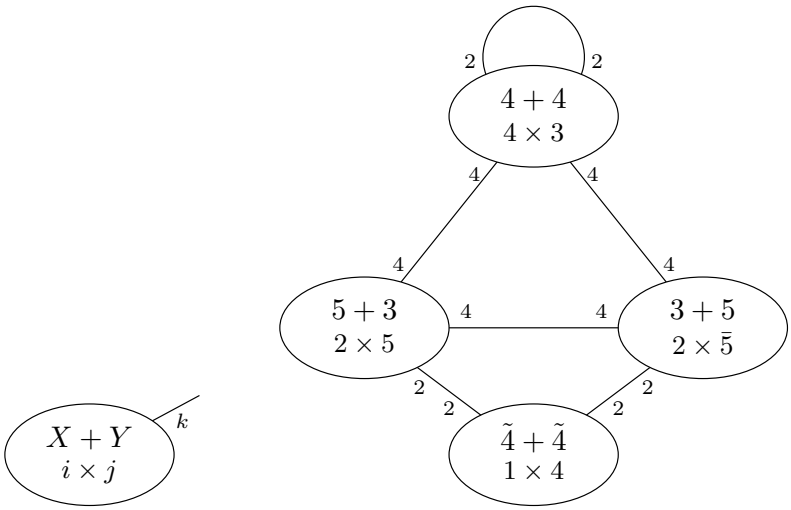

Figure 3.15: Spurious pole structure of the $\mathcal{N} = 7$ 6-point NMHV amplitude. The legend on the lower left represents an $X + Y$ diagram topology containing i terms in the permutation sum, each with j spurious poles. The edge represents k pairs of spurious poles which cancel against spurious poles appearing on the other end of the edge.

Figure 3.15. Using momentum twistors we can rewrite

$$[5|3+4|2\rangle = -\frac{\langle 4562\rangle}{\langle 45\rangle\langle 56\rangle}, \tag{3.2.79}$$

so it is clear that we are interested in the behaviour as $\langle 4562\rangle \to 0$. This can be viewed as the limit where Z_2 approaches the plane defined by $\{Z_4, Z_5, Z_6\}$, denoted (456). In this limit, the remaining twistors Z_1 and Z_3 become proportional. To see this, consider expanding in the basis $\{Z_4, Z_5, Z_6, Z_*\}$, where Z_* is an independent reference twistor:

$$\begin{aligned} Z_1 &= a_1 Z_4 + b_1 Z_5 + c_1 Z_6 + d_1 Z_*, \\ Z_2 &= a_2 Z_4 + b_2 Z_5 + c_2 Z_6 + d_2 Z_*, \\ Z_3 &= a_3 Z_4 + b_3 Z_5 + c_3 Z_6 + d_3 Z_*. \end{aligned} \tag{3.2.80}$$

The limit $\langle 4562\rangle \to 0$ corresponds to taking $d_2 \to 0$. In this limit, we can always write $d_3\langle ijk1\rangle = d_1\langle ijk3\rangle$ where $\{1,3\} \notin \{i,j,k\}$, since we can neglect any contribution from the (456) plane. Computing the residue of $\mathcal{D}^{(561)}$ and $\mathcal{D}^{(345)}$ of the pole $\langle 4562\rangle$

then gives

$$\begin{aligned}
\mathscr{P} &\equiv \operatorname*{Res}_{\langle 4562\rangle\to 0}\left(\overline{\mathcal{D}}^{(561)}_{6,3}+\overline{\mathcal{D}}^{(345)}_{6,3}\right),\\
&= \frac{\langle 6123\rangle}{[\mathrm{PT}(6)]^2\langle 24\rangle\langle 26\rangle^2}\left(\frac{\delta^{(0|7)}\left(\langle 4561\rangle\chi_2+\langle 5612\rangle\chi_4+\langle 6124\rangle\chi_5+\langle 1245\rangle\chi_6\right)\langle 2345\rangle}{\langle 5612\rangle\langle 4612\rangle\langle 4512\rangle^2\langle 4561\rangle^2\left(\langle 4612\rangle\langle 35\rangle+\langle 5612\rangle\langle 43\rangle\right)}\right.\\
&\quad\left.+\frac{\delta^{(0|7)}\left(\langle 3456\rangle\chi_2+\langle 5623\rangle\chi_4+\langle 6234\rangle\chi_5+\langle 2345\rangle\chi_6\right)}{\langle 2345\rangle\langle 2346\rangle\langle 2356\rangle\langle 3456\rangle^2\left(\langle 2345\rangle\langle 63\rangle+\langle 3456\rangle\langle 23\rangle\right)}\right),\\
&= \frac{\langle 6123\rangle}{[\mathrm{PT}(6)]^2\langle 24\rangle\langle 26\rangle^2}\left(\frac{\delta^{(0|7)}\left(\langle 4563\rangle\chi_2+\langle 5632\rangle\chi_4+\langle 6324\rangle\chi_5+\langle 3245\rangle\chi_6\right)\langle 2345\rangle}{\langle 5632\rangle\langle 4632\rangle\langle 4532\rangle^2\langle 4563\rangle^2\left(\langle 4632\rangle\langle 35\rangle+\langle 5632\rangle\langle 43\rangle\right)}\right.\\
&\quad\left.+\frac{\delta^{(0|7)}\left(\langle 3456\rangle\chi_2+\langle 5623\rangle\chi_4+\langle 6234\rangle\chi_5+\langle 2345\rangle\chi_6\right)}{\langle 2345\rangle\langle 2346\rangle\langle 2356\rangle\langle 3456\rangle^2\left(\langle 2345\rangle\langle 63\rangle+\langle 3456\rangle\langle 23\rangle\right)}\right),\\
&= -\frac{\langle 6123\rangle\delta^{(0|7)}\left(\langle 3456\rangle\chi_2+\langle 5623\rangle\chi_4+\langle 6234\rangle\chi_5+\langle 2345\rangle\chi_6\right)}{[\mathrm{PT}(6)]^2\langle 24\rangle\langle 26\rangle^2\langle 2345\rangle\langle 2346\rangle\langle 2356\rangle\langle 3456\rangle^2}\\
&\qquad\times\left(\frac{1}{\left(\langle 4632\rangle\langle 35\rangle+\langle 5632\rangle\langle 43\rangle\right)}-\frac{1}{\left(\langle 2345\rangle\langle 63\rangle+\langle 3456\rangle\langle 23\rangle\right)}\right),
\end{aligned}\tag{3.2.81}$$

. Hence we see that

$$\mathscr{P}\sim\langle 2345\rangle\langle 63\rangle+\langle 3456\rangle\langle 23\rangle+\langle 6234\rangle\langle 53\rangle+\langle 5623\rangle\langle 43\rangle=0,\tag{3.2.82}$$

where we used (2.1.27) in the last line. Conveniently, all factors of d_1 and d_3 cancel in the fraction. We can therefore see that there is no singularity as $\langle 4562\rangle\to 0$. The rest of the spurious poles cancel in a similar way. In summary, we find that using momentum twistors defined with respect to different orderings of external momenta provides a very simple and systematic way to prove spurious poles cancelleation in the 6-point NMHV amplitude of $\mathcal{N}=7$ supergravity.

3.3 Remarks

Motivated by the beautiful geometric description of scattering amplitudes in planar $\mathcal{N}=4$ SYM, we have tried to follow similar steps for supergravity amplitudes. In particular, we first developed an on-shell diagram recursion for $\mathcal{N}=7$ supergravity which gives rise to formulas for scattering amplitudes in terms of Grassmannian integrals. This is similar to the on-shell diagram formalism for $\mathcal{N}=8$ supergravity

developed in [30], but in $\mathcal{N} = 7$ there are two supermultiplets so the diagrams have arrows to indicate helicity flow. The $\mathcal{N} = 7$ recursion also appears to have fewer terms than $\mathcal{N} = 8$ and automatically incorporates bonus relations for MHV amplitudes. The price to pay for having fewer diagrams is that they contain more closed cycles which can become cumbersome to evaluate at high multiplicity, but we develop a technique to evaluate the diagrams without summing over closed cycles by using a non-canonical gauge-fixing of the Grassmannian integrals.

Next, we translated our results to momentum twistor space, reproducing Hodges' results for MHV amplitudes [27] and obtaining new momentum twistor formulas for non-MHV amplitudes. These formulas are manifestly supersymmetric and written in terms of $\mathcal{N} = 7$ R-invariants, analogous to the building blocks for non-MHV amplitudes in $\mathcal{N} = 4$ SYM. For the six-point NMHV superamplitude, this required defining momentum twistors with respect to three different permutations of the external momenta, which can be thought of local coordinates in three different patches. This way of defining momentum twistors was designed to give R-invariants in each patch, but an unexpected consequence of this definition is that the spurious poles greatly simplify and their cancellation becomes very simple to demonstrate. This strongly suggests a geometric interpretation for the cancellation of spurious poles analogous to $\mathcal{N} = 4$ SYM and is the main result of this chapter.

There are a number of future directions:

- Perhaps the most urgent task is to identify the underlying geometry responsible for cancellation of spurious poles in supergravity amplitudes. In the context of gluonic amplitudes, this cancellation was made manifest by interpreting 6-point NMHV amplitudes as polytopes in momentum twistor space [18]. For supergravity amplitudes, identifying the underlying geometry is more challenging because we are only able to describe it using local momentum twistor coordinates, which hide the permutation symmetry of the amplitude. Moreover, the Grassmannian integral formulae for supergravity amplitudes have a more

complicated form than planar $\mathcal{N} = 4$ SYM. It would be interesting to adapt recent work on the geometry of differential forms with non-logarithmic singularities [116] to supergravity. It would also be interesting to look for geometric structure in higher-point NMHV amplitudes. New n-point formulas recently obtained in [34] may be useful for this purpose.

- In $\mathcal{N} = 4$ SYM, planar amplitudes are dual to null polygonal Wilson loops [117–119]. In particular, R-invariants correspond to propagators connecting edges of the Wilson loop [120, 121]. Since R-invariants also appear to play a role in supergravity amplitudes, it would be interesting to look for some analogue of the amplitude/Wilson loop duality in supergravity. This was previously found to hold at four points in [122]. Our results suggest this should extend to five points, but at higher points one may need to consider multiple Wilson loops for non-MHV amplitudes, one associated with each momentum twistor coordinate patch (see Figure 3.13).

- Another interesting direction would be to extend the methods developed in this paper to loop amplitudes. When loop amplitudes of planar $\mathcal{N} = 4$ SYM are represented in momentum twistor space, they can be expressed in terms of chiral pentagon integrals [95], which were recently proposed to be building blocks for a dual Amplituhedron [123]. It would be interesting to see if such integrals can be used to describe supergravity amplitudes. While it is not yet clear how to compute loop-level supergravity amplitudes using on-shell diagrams, they can be used to compute leading singularities, such as those which were recently studied at 2-loops [124]. This is briefly explored in appendix C.

- The closed cycles in the $\mathcal{N} = 7$ on-shell diagrams may also have interesting properties in their own right, meriting further study. Recent work looking at the UV pole structure of $\mathcal{N} < 4$ SYM found that they were encoded within the closed cycle structure of on-shell diagrams for the associated leading

singularities [125]. It may be that a similar study of supergravity can offer insights into its own pole structure.

- Finally, it would be interesting to apply the approach we have developed to supergravity and conformal supergravity with $\mathcal{N} = 4$ supersymmetry. Although these theories have less supersymmetry and the latter is not unitary, their scattering amplitudes have interesting properties and have been studied from various points of view such as twistor string theory [126–130] and the double copy [131–133]. The amount of supersymmetry in these theories should make it possible to write their amplitudes in terms of the same R-invariants that appear in $\mathcal{N} = 4$ SYM.

In summary, the study of gravitational amplitudes has revealed many surprises and it seems likely that a more fundamental understanding of their structure remains to be found.

Chapter 4

Colour-Kinematics in AdS

This chapter focuses on Yang-Mills theory in AdS, exploring how colour-kinematics generalises away from flat space. We start with section 4.1 reviewing some basic properties of the AdS amplitudes we are calculating that will be relevent when adapting flat space colour-kinematics duality. We then explore how this changes the kinematic Jacobi relations and BCJ relations in section 4.1.1. We then provide an introduction to the use of Witten diagrams to calculate amplitudes, summarising the various building blocks and using them to build the 3 and 4pt Yang-Mills amplitudes 4.2. In section 4.2.3 these are specialised to helicity amplitudes using the spinors introduced in section 2.3.1. Finally we use Ward identities to reconstruct the full correlation functions from their transverse parts in 4.3 before concluding with an outlook in section 4.4.

4.1 Review of AdS Amplitudes

We start by defining the following AdS analogue of Mandelstam variables [59]

$$\begin{aligned} S &= (k_{12} + k_s)(k_{34} + k_s), \\ T &= (k_{14} + k_t)(k_{23} + k_t), \\ U &= (k_{13} + k_u)(k_{24} + k_u), \end{aligned} \tag{4.1.1}$$

where $k_s = |\boldsymbol{k}_1 + \boldsymbol{k}_2|$, $k_t = |\boldsymbol{k}_1 + \boldsymbol{k}_4|$, $k_u = |\boldsymbol{k}_1 + \boldsymbol{k}_3|$ and $k_{ab} = k_a + k_b$ with $k_a = |\boldsymbol{k}_a|$. Unlike in flat space, these variables do not add to zero for massless external states. Their sum is instead given by

$$\begin{gathered} S + T + U = \xi, \\ \text{where} \quad \xi = E\Big(E + k_s + k_t + k_u\Big), \end{gathered} \tag{4.1.2}$$

with $E = k_1 + k_2 + k_3 + k_4$. In the flat space limit discussed in section 2.3.1, $\xi \to 0$ and the Mandelstam variables reduce to their standard definitions after using 4-momentum conservation. Note that our treatment of the double copy in AdS will have some similarities to the double copy of massive amplitudes in flat space, where one also has $S + T + U \neq 0$ [134, 135].

4.1.1 Colour-Kinematics in AdS

The starting point for AdS colour-kinematics is analogous to the flat space case discussed in section 2.4. Using Witten diagrams, one finds that colour-ordered YM amplitudes in AdS_4 can be written in the form (2.4.5) using the generalised Mandelstam invariants in (4.1.1)

$$\begin{aligned} \langle j_1 j_2 j_3 j_4 \rangle &= \frac{n_s}{S} - \frac{n_t}{T}, \\ \langle j_1 j_3 j_2 j_4 \rangle &= \frac{n_t}{T} - \frac{n_u}{U}, \end{aligned} \tag{4.1.3}$$

where the kinematic numerators are again linked by the permutation operations in (2.4.6) and (2.4.7). Using these relations among kinematic numerators we can also show that colour-ordered AdS amplitudes obey a photon decoupling relation analogous to that of flat space amplitudes:

$$\langle j_1 j_2 j_3 j_4 \rangle + \langle j_1 j_3 j_4 j_2 \rangle + \langle j_1 j_4 j_2 j_3 \rangle = 0. \tag{4.1.4}$$

Unlike in flat space however, in AdS momentum space the kinematic numerators do not generically add to zero. Instead their sum will be denoted as

$$Q = n_s + n_t + n_u. \tag{4.1.5}$$

Using this equation, we can eliminate n_t in (4.1.3) to obtain the following relation between the colour-ordered AdS amplitudes and kinematic numerators

$$\begin{pmatrix} \langle j_1 j_2 j_3 j_4\rangle + Q/T \\ \langle j_1 j_3 j_2 j_4\rangle - Q/T \end{pmatrix} = \begin{pmatrix} 1/S + 1/T & 1/T \\ -1/T & -1/U - 1/T \end{pmatrix} \begin{pmatrix} n_s \\ n_u \end{pmatrix}. \tag{4.1.6}$$

In flat space, the matrix on the right is not invertible, which is expected since amplitudes on the left are gauge invariant while numerators on the right are not. In AdS however, we can invert the matrix to obtain

$$\begin{pmatrix} n_s \\ n_u \end{pmatrix} = \frac{1}{\xi} \begin{pmatrix} S(T+U) & SU \\ -SU & -U(S+T) \end{pmatrix} \begin{pmatrix} \langle j_1 j_2 j_3 j_4\rangle + Q/T \\ \langle j_1 j_3 j_2 j_4\rangle - Q/T \end{pmatrix}. \tag{4.1.7}$$

Note that the inverse becomes singular in the flat space limit as $\xi \to 0$. The solution for n_u implies

$$U\,\langle j_1 j_3 j_2 j_4\rangle - S\,\langle j_1 j_2 j_3 j_4\rangle = \xi\left(\langle j_1 j_3 j_2 j_4\rangle + \frac{n_u}{U}\right) - Q. \tag{4.1.8}$$

Plugging (4.1.3) into the right hand side finally gives the deformed BCJ relation:

$$U\,\langle j_1 j_3 j_2 j_4\rangle - S\,\langle j_1 j_2 j_3 j_4\rangle = \xi\frac{n_t}{T} - Q. \tag{4.1.9}$$

In the flat space limit, which is defined by multiplying by E and taking $E \to 0$, it is not difficult to see that this reduces to the standard BCJ relation in (2.4.10).

The AdS amplitudes in (2.4.5) are invariant under the following generalised gauge transformation of the kinematic numerators:

$$n_s \to n_s + S\Delta,\;\; n_t \to n_t + T\Delta,\;\; n_u \to n_u + U\Delta, \tag{4.1.10}$$

where Δ is an arbitrary function. Under this transformation, the parameter Q in (4.1.5) transforms as

$$Q \to Q + \xi\Delta. \tag{4.1.11}$$

Hence, by choosing $\Delta = -Q/\xi$, we can set Q to zero. We shall denote the kinematic numerators in this generalised gauge as $\tilde{n}_s$, $\tilde{n}_t$, $\tilde{n}_u$:

$$\tilde{n}_s = n_s - SQ/\xi, \;\; \tilde{n}_t = n_t - TQ/\xi, \;\; \tilde{n}_u = n_u - UQ/\xi. \tag{4.1.12}$$

In this generalised gauge, the numerators satisfy the kinematic Jacobi relation away from the flat space limit:

$$\tilde{n}_s + \tilde{n}_t + \tilde{n}_u = 0. \tag{4.1.13}$$

Hence, these numerators can also be obtained from (4.1.7) by setting $Q = 0$ on the right hand side. Moreover, the deformed BCJ relation in (4.1.9) reduces to

$$U \langle j_1 j_3 j_2 j_4 \rangle - S \langle j_1 j_2 j_3 j_4 \rangle = \xi \frac{\tilde{n}_t}{T}. \tag{4.1.14}$$

In flat space the generalised gauge transformations in (4.1.10) do not affect the sum of kinematic numerators and correspond to ordinary gauge transformations for a particular choice of Δ. In the next section, we will derive explicit formulas for 4-point AdS amplitudes and their kinematic numerators using Witten diagrams.

4.2 Yang-Mills in AdS_4

4.2.1 Witten Diagram Recap

In this section we will review four-point colour-ordered Witten diagrams for YM in AdS_4. We follow the approach developed in [48, 50, 136], and will review some basic formulas to make the discussion self-contained.

As introduced in section 2.3.1, we work with the AdS metric in equation 2.3.1 using the mostly positive metric convention. Additionally we will use axial gauge, where polarisation vectors do not have radial components. This means that gauge properties will be analogous to flat space, with the spacetime only affecting kinematics in the radial direction. We work in momentum space for the boundary directions whilst the radial components still depend on a position coordinate which will be integrated over

when calculating amplitudes. For space-like momenta along the boundary, the z-dependence of the bulk-to-boundary propagator is given by solving the Klein-Gordon equation in AdS

$$A_i(z,\boldsymbol{k}) = \epsilon_i \sqrt{\frac{2k}{\pi}} z^{\frac{1}{2}} K_{1/2}(kz), \tag{4.2.1}$$

where since the polarisation ϵ_m does not have a radial component m is a 3d Lorentz index, and K_ν is a modified Bessel function of the second kind. These will play the role of external wavefunctions in the Witten diagrams, propagating between the interaction itself and the boundary where the states are taken to live.

In axial gauge, the bulk-to-bulk propagator in momentum space is given by

$$\mathcal{G}_{ij}(z,z',\boldsymbol{k}) = -i\int_0^\infty \omega d\omega \frac{z^{\frac{1}{2}} J_{1/2}(\omega z) J_{1/2}(\omega z')(z')^{\frac{1}{2}}}{\boldsymbol{k}^2+\omega^2-i\varepsilon}\left(\eta_{ij}+\frac{\boldsymbol{k}_i\boldsymbol{k}_j}{\omega^2}\right), \tag{4.2.2}$$

where $\boldsymbol{k}$ is the momentum flowing through the propagator along the boundary directions, $\varepsilon > 0$ gives the pole prescription, and J_ν is a Bessel function of the first kind. This is a Green's function of the AdS Klein-Gordon operator.

The vertices have the same structure as those in flat space but the indices only run over the boundary directions since we are in axial gauge

$$\begin{aligned} V_{jkl}(\boldsymbol{k}_1,\boldsymbol{k}_2,\boldsymbol{k}_3) &= \frac{i}{\sqrt{2}}\left(\eta_{jk}(\boldsymbol{k}_1-\boldsymbol{k}_2)_l + \eta_{kl}(\boldsymbol{k}_2-\boldsymbol{k}_3)_j + \eta_{lj}(\boldsymbol{k}_3-\boldsymbol{k}_1)_k\right), \\ V^{jklm} &= i\eta^{jl}\eta^{km} - \frac{i}{2}\left(\eta^{jk}\eta^{lm}+\eta^{jm}\eta^{kl}\right), \end{aligned} \tag{4.2.3}$$

where we have set the YM coupling $g = 1$. When computing Witten diagrams, we must integrate over the radial coordinates z of each interaction vertex. In doing so, a factor of z^{-4} coming from $\sqrt{-g}$ will be cancelled by z^4 coming from two inverse metrics used to contract the Lorentz indices in each interaction vertex.

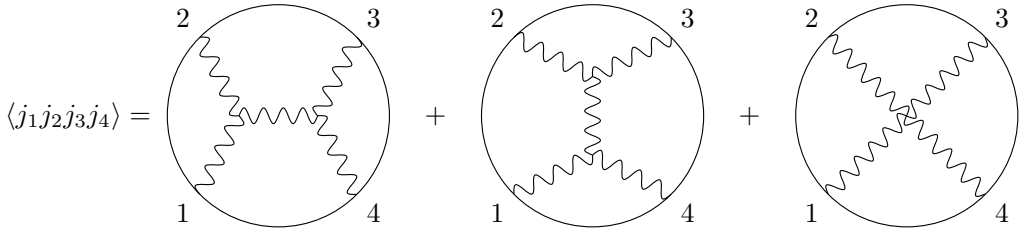

Figure 4.1: Witten diagrams for the colour-ordered 4-point AdS amplitude.

4.2.2 AdS_4 Amplitudes with General Polarizations

Using the rules given above, the three-point AdS_4 amplitude can be calculated as

$$\begin{aligned}\langle jjj \rangle &= V_{123}(\boldsymbol{k}_1, \boldsymbol{k}_2, \boldsymbol{k}_3) \int_0^\infty dz \prod_{i=1}^{3} \left(\sqrt{\frac{2k_i}{\pi}} z^{\frac{1}{2}} K_{1/2}(k_i z) \right), \\ &= \frac{1}{\sqrt{2}E} \left(\epsilon_1 \cdot \epsilon_2 \, (\boldsymbol{k}_1 - \boldsymbol{k}_2) \cdot \epsilon_3 + \text{Cyc}[123] \right).\end{aligned} \tag{4.2.4}$$

where $V_{123} = \epsilon_1^i \epsilon_2^i \epsilon_3^i V_{ijk}$.

The colour-ordered four-point AdS amplitude comes from three Witten diagrams, as shown in Figure 4.1. In particular, there are s- and t-channel exchanges, and a contact diagram:

$$\langle jjjj \rangle = W_s + W_t + W_c. \tag{4.2.5}$$

The quantity given by multiplying vertices and propagators together and summing diagrams is usually denoted as $i\mathcal{A}$. Since our final expressions will contain overall factors of i, these are dropped on both sides. The s-channel diagram is then given by

$$W_s = \int \omega d\omega \, dz dz' \, \text{KKJ}(k_1, k_2, \omega, z) \frac{M^{1234}(\boldsymbol{k}_1, \boldsymbol{k}_2, \boldsymbol{k}_3, \boldsymbol{k}_4)}{(k_s^2 + \omega^2)} \text{KKJ}(k_3, k_4, \omega, z'), \tag{4.2.6}$$

where

$$M^{ijkl}(\boldsymbol{k}_1, \boldsymbol{k}_2, \boldsymbol{k}_3, \boldsymbol{k}_4) = -V^{ijm}(\boldsymbol{k}_1, \boldsymbol{k}_2, -\boldsymbol{k}_{12}) \left(\eta_{mn} + \frac{\boldsymbol{k}_m \boldsymbol{k}_n}{\omega^2} \right) V^{kln}(\boldsymbol{k}_3, \boldsymbol{k}_4, \boldsymbol{k}_{12}), \tag{4.2.7}$$

and

$$\mathrm{KKJ}(p,r,s,z)=\sqrt{\frac{4pr}{\pi^2}}z^{3/2}K_{1/2}(pz)K_{1/2}(rz)J_{1/2}(sz). \tag{4.2.8}$$

The integrals in (4.2.6) were performed in [50] with the final result

$$W_s=-\frac{V^{12m}(\boldsymbol{k}_1,\boldsymbol{k}_2,-\boldsymbol{k}_{12})V^{34n}(\boldsymbol{k}_3,\boldsymbol{k}_4,\boldsymbol{k}_{12})}{ES}\left(\eta_{mn}+\frac{(E+k_s)(\boldsymbol{k}_{12})_m(\boldsymbol{k}_{12})_n}{k_{12}k_{34}k_s}\right), \tag{4.2.9}$$

where $V^{12m}=\epsilon_1^i\epsilon_2^jV_{ijm}$ and $E=k_1+k_2+k_3+k_4$. In the flat-space limit, this reduces to the usual Feynman diagram expression in axial gauge:

$$\lim_{E\to0}EW_s=V^{12m}V_{34m}\frac{1}{(k_{1\mu}+k_{2\mu})^2}\left(-\eta_{mn}+\frac{\boldsymbol{k}_{12m}\boldsymbol{k}_{12n}}{k_{12}^2}\right). \tag{4.2.10}$$

We can simplify (4.2.9) by applying momentum conservation and other identities at each vertex:

$$\begin{aligned}V^{12m}\cdot(\boldsymbol{k}_{12})_m&=\frac{i}{\sqrt{2}}(\epsilon_1{\cdot}\epsilon_2\,(k_1^2-k_2^2)+2\boldsymbol{k}_2{\cdot}\epsilon_1\,\epsilon_2{\cdot}\boldsymbol{k}_{12}-2\boldsymbol{k}_1{\cdot}\epsilon_2\,\epsilon_1{\cdot}\boldsymbol{k}_{12})\\&=\frac{i}{\sqrt{2}}\epsilon_1{\cdot}\epsilon_2\,(k_1^2-k_2^2),\end{aligned} \tag{4.2.11}$$

since $\boldsymbol{k}_i{\cdot}\epsilon_i=0$. Using momentum conservation the contraction of two Vs is given by

$$\begin{aligned}V^{12m}\cdot V_m^{34}=&-\frac{1}{2}(\epsilon_1\cdot\epsilon_2\epsilon_3\cdot\epsilon_4)(\boldsymbol{k}_1-\boldsymbol{k}_2){\cdot}(\boldsymbol{k}_3-\boldsymbol{k}_4)\\&-\epsilon_1{\cdot}\epsilon_2\,\boldsymbol{k}_4{\cdot}\epsilon_3(\boldsymbol{k}_1-\boldsymbol{k}_2){\cdot}\epsilon_4+\epsilon_1{\cdot}\epsilon_2\,\boldsymbol{k}_3{\cdot}\epsilon_4(\boldsymbol{k}_1-\boldsymbol{k}_2){\cdot}\epsilon_3\\&-\epsilon_3{\cdot}\epsilon_4\,\boldsymbol{k}_2{\cdot}\epsilon_1(\boldsymbol{k}_3-\boldsymbol{k}_4){\cdot}\epsilon_2+\epsilon_3{\cdot}\epsilon_4\,\boldsymbol{k}_1{\cdot}\epsilon_2(\boldsymbol{k}_3-\boldsymbol{k}_4){\cdot}\epsilon_1\\&-2\epsilon_2{\cdot}\epsilon_4\,\boldsymbol{k}_2{\cdot}\epsilon_1\,\boldsymbol{k}_4{\cdot}\epsilon_3+2\epsilon_2{\cdot}\epsilon_3\,\boldsymbol{k}_2{\cdot}\epsilon_1\,\boldsymbol{k}_3{\cdot}\epsilon_4\\&+2\epsilon_1{\cdot}\epsilon_4\,\boldsymbol{k}_1{\cdot}\epsilon_2\,\boldsymbol{k}_4{\cdot}\epsilon_3-2\epsilon_1{\cdot}\epsilon_3\,\boldsymbol{k}_1{\cdot}\epsilon_2\,\boldsymbol{k}_3{\cdot}\epsilon_4.\end{aligned} \tag{4.2.12}$$

The terms containing $\boldsymbol{k}_i{\cdot}\epsilon_j$ will be collected into a single term W_s^B, which is given in (4.2.14). In section D.1, we will show how this term can be greatly simplified after converting to spinor notation. The s-channel diagram is then given by

$$W_s=\frac{1}{2}\frac{\epsilon_1{\cdot}\epsilon_2\,\epsilon_3{\cdot}\epsilon_4}{ES}[(k_{1\mu}-k_{2\mu})(k_3^\mu-k_4^\mu)-\frac{E}{k_{\underline{12}}}(k_1-k_2)(k_3-k_4)]+W_s^B, \tag{4.2.13}$$

with

$$W_s^B = \frac{1}{E}\frac{1}{S}\Big[\epsilon_1\cdot\epsilon_2\boldsymbol{k}_4\cdot\epsilon_3(\boldsymbol{k}_1-\boldsymbol{k}_2)\cdot\epsilon_4-\epsilon_1\cdot\epsilon_2\boldsymbol{k}_3\cdot\epsilon_4(\boldsymbol{k}_1-\boldsymbol{k}_2)\cdot\epsilon_3 + \epsilon_3\cdot\epsilon_4\boldsymbol{k}_2\cdot\epsilon_1(\boldsymbol{k}_3-\boldsymbol{k}_4)\cdot\epsilon_2-\epsilon_3\cdot\epsilon_4\boldsymbol{k}_1\cdot\epsilon_2(\boldsymbol{k}_3-\boldsymbol{k}_4)\cdot\epsilon_1 + 2\epsilon_2\cdot\epsilon_4\boldsymbol{k}_2\cdot\epsilon_1\boldsymbol{k}_4\cdot\epsilon_3-2\epsilon_2\cdot\epsilon_3\boldsymbol{k}_2\cdot\epsilon_1\boldsymbol{k}_3\cdot\epsilon_4 - 2\epsilon_1\cdot\epsilon_4\boldsymbol{k}_1\cdot\epsilon_2\boldsymbol{k}_4\cdot\epsilon_3+2\epsilon_1\cdot\epsilon_3\boldsymbol{k}_1\cdot\epsilon_2\boldsymbol{k}_3\cdot\epsilon_4\Big]. \tag{4.2.14}$$

The t-channel diagram can be obtained by taking the s-channel diagram and swapping $2\leftrightarrow 4$:

$$W_t = W_s|_{2\leftrightarrow 4}\,. \tag{4.2.15}$$

Finally, the contact diagram is given by

$$W_c = -iV^{1234}\int_0^\infty dz\,\mathrm{KKKK}(k_1,k_2,k_3,k_4,z), \tag{4.2.16}$$

where $V^{1234}=\epsilon_1^i\epsilon_2^j\epsilon_3^k\epsilon_4^l V_{ijkl}$ and

$$\mathrm{KKKK}(p,r,s,t,z)=\sqrt{\frac{16prst}{\pi^4}}z^2K_{1/2}(pz)K_{1/2}(rz)K_{1/2}(sz)K_{1/2}(tz). \tag{4.2.17}$$

After integrating over z, one gets

$$W_c=\frac{1}{E}\left(\epsilon_1\cdot\epsilon_3\,\epsilon_2\cdot\epsilon_4-\frac{1}{2}(\epsilon_1\cdot\epsilon_2\,\epsilon_3\cdot\epsilon_4+\epsilon_1\cdot\epsilon_4\,\epsilon_2\cdot\epsilon_3)\right). \tag{4.2.18}$$

Summing the three diagrams gives the full colour-ordered AdS_4 amplitude

$$\begin{aligned}\langle j_1j_2j_3j_4\rangle =&\frac{1}{2E}\frac{\epsilon_1\cdot\epsilon_2\,\epsilon_3\cdot\epsilon_4}{S}[(k_{1\mu}-k_{2\mu})(k_3^\mu-k_4^\mu)-\frac{E}{k_s}(k_1-k_2)(k_3-k_4)]+W_s^B\\ &+\frac{1}{2E}\frac{\epsilon_1\cdot\epsilon_4\,\epsilon_2\cdot\epsilon_3}{T}[(k_{1\mu}-k_{4\mu})(k_3^\mu-k_2^\mu)-\frac{E}{k_t}(k_1-k_4)(k_3-k_2)]+W_t^B\\ &+\frac{1}{E}(\epsilon_1\cdot\epsilon_3\,\epsilon_2\cdot\epsilon_4-\frac{1}{2}(\epsilon_1\cdot\epsilon_2\,\epsilon_3\cdot\epsilon_4+\epsilon_1\cdot\epsilon_4\,\epsilon_2\cdot\epsilon_3)).\end{aligned} \tag{4.2.19}$$

Let us now derive kinematic numerators by writing (4.2.19) in the form (2.4.5). In doing so, we must split the contact term into two pieces multiplied by S/S and T/T, respectively, such that the resulting numerators obey (2.4.6) or equivalently (2.4.7).

A natural choice for the s-channel numerator is

$$n_s = \frac{1}{2}\frac{\epsilon_1{\cdot}\epsilon_2\,\epsilon_3{\cdot}\epsilon_4}{E}\left[(k_{1\mu}-k_{2\mu})(k_3^\mu-k_4^\mu)-\frac{E}{k_s}(k_1-k_2)(k_3-k_4)\right] + SW_s^B + S\frac{1}{2E}\left[\epsilon_1{\cdot}\epsilon_3\,\epsilon_2{\cdot}\epsilon_4-\epsilon_1{\cdot}\epsilon_4\,\epsilon_2{\cdot}\epsilon_3\right]. \tag{4.2.20}$$

In the flat space limit, this expression reduces to the one obtained in [104]. The kinematic numerators n_t and n_u can be deduced from (4.2.20) using the relations in (2.4.6) or (2.4.7). After some algebra, the sum of kinematic numerators is given by

$$Q = \frac{\epsilon_1{\cdot}\epsilon_2\,\epsilon_3{\cdot}\epsilon_4}{2}[(k_t-k_u)-\frac{1}{k_s}(k_1-k_2)(k_3-k_4)]+\text{Cyc}[234]. \tag{4.2.21}$$

We therefore see that for this choice of numerators, the kinematic Jacobi relation is only satisfied in the flat space limit (recall that taking the flat space limit involves multiplying by E and taking $E\to 0$). However in AdS$_4$ we can use the generalised gauge symmetry in (4.1.10) to obtain numerators that obey the kinematic Jacobi relation even away from the flat space limit. The preferred numerators $\{\tilde{n}_s,\tilde{n}_t,\tilde{n}_u\}$ are obtained by plugging (4.2.20) and (4.2.21) into (4.1.12) and using (2.4.7).

We can prove (4.2.21) by summing the kinematic numerators and first considering the terms containing four polarisation vectors contracted together. For example, we get the following terms proportional to $\epsilon_1{\cdot}\epsilon_2\,\epsilon_3{\cdot}\epsilon_4$:

$$\epsilon_1{\cdot}\epsilon_2\,\epsilon_3{\cdot}\epsilon_4[(k_{1\mu}-k_{2\mu})(k_{3\mu}-k_{4\mu})+t-u]=\epsilon_1{\cdot}\epsilon_2\,\epsilon_3{\cdot}\epsilon_4[E(k_t-k_u)], \tag{4.2.22}$$

where we have dropped for now the terms with a pole in $k_{\underline{ij}}$. From the W^B terms appearing in the kinematic numerators, let us consider the term proportional to $\epsilon_2\cdot\epsilon_3$:

$$2\epsilon_2{\cdot}\epsilon_3\,\boldsymbol{k}_2{\cdot}\epsilon_1\,\boldsymbol{k}_3{\cdot}\epsilon_4+2\epsilon_2{\cdot}\epsilon_3\,(\boldsymbol{k}_1{\cdot}\epsilon_4\,\boldsymbol{k}_2{\cdot}\epsilon_1-\boldsymbol{k}_4{\cdot}\epsilon_1\,\boldsymbol{k}_2\cdot\epsilon_4)-2\epsilon_2{\cdot}\epsilon_3\,\boldsymbol{k}_3{\cdot}\epsilon_1\,\boldsymbol{k}_2\cdot\epsilon_4=0, \tag{4.2.23}$$

where the first term comes from n_s, the second term from n_t, and the third term from n_u. All the contributions from W_B drop out in an analogous manner. We are therefore only left with the terms in equation (4.2.22) and the $|\boldsymbol{k}_a+\boldsymbol{k}_b|$ poles, which

sum to (4.2.21).

4.2.3 AdS_4 Helicity Amplitudes

In this section, we will specialise the results obtained in the previous section to particular helicities of the external gluons and write them in terms of spinors adapted to AdS_4. The AdS_4 amplitudes will then be labelled by the helicities of the external gluons $\langle h_1 h_2 h_3 h_4\rangle$, where $h_i = \pm$. An amplitude with k negative helicity gluons is referred to as an $N^{k-2}MHV$ amplitude. In the flat space limit, only the $k = 2$ (or MHV) amplitude is non-zero at tree-level but in AdS_4, the amplitude is non-zero for $k = 0, 1$ as well. Amplitudes with $k = 3, 4$ are related to $k = 1, 0$ via parity. A spinorial expression for the MHV amplitude was previously obtained in [49] using a recursive approach. Using numerous identities derived in Appendix D, we obtain a new expression which appears to be much simpler. We also obtain compact new expressions for non-MHV amplitudes, first computed in [2].

$N^{-2}MHV$

We will start with the case $++++$. Writing the kinematic numerator in (4.2.20) in terms of the AdS spinors introduced in section 2.3.1 and using the Schouten identity to rewrite the contact diagram as

$$\begin{aligned}\frac{1}{2E}\left[\epsilon_1\cdot\epsilon_3\,\epsilon_2\cdot\epsilon_4 - \epsilon_1\cdot\epsilon_4\,\epsilon_2\cdot\epsilon_3\right] =& \frac{1}{8Ek_1k_2k_3k_4}\left(\langle\bar{1}\bar{3}\rangle^2\langle\bar{2}\bar{4}\rangle^2 - \langle\bar{1}\bar{4}\rangle^2\langle\bar{2}\bar{3}\rangle^2\right)\\ =& \frac{1}{8Ek_1k_2k_3k_4}\left(2\langle\bar{1}\bar{3}\rangle\langle\bar{2}\bar{4}\rangle\langle\bar{1}\bar{2}\rangle\langle\bar{3}\bar{4}\rangle - \langle\bar{1}\bar{2}\rangle^2\langle\bar{3}\bar{4}\rangle^2\right),\end{aligned} \tag{4.2.24}$$

we obtain

$$\begin{aligned}n_s^{++++} =& \frac{\langle\bar{1}\bar{2}\rangle\langle\bar{3}\bar{4}\rangle}{8k_1k_2k_3k_4}\frac{1}{E}\Big[\langle\bar{1}\bar{2}\rangle\langle\bar{3}\bar{4}\rangle\left(\langle 13\rangle\langle\bar{1}\bar{3}\rangle + \langle 24\rangle\langle\bar{2}\bar{4}\rangle - \frac{E}{k_s}(k_1-k_2)(k_3-k_4) - Ek_s\right)\\ &+ 2S\langle\bar{1}\bar{3}\rangle\langle\bar{2}\bar{4}\rangle\Big] + sW_s^{B,++++}.\end{aligned} \tag{4.2.25}$$

where $W_s^{B,++++}$ has a very compact form given by

$$W_s^{B,++++} = \frac{i}{8k_1k_2k_3k_4}\frac{2}{S}\langle\bar{1}\bar{2}\rangle\langle\bar{3}\bar{4}\rangle(\langle 1\bar{2}\rangle\langle\bar{4}\bar{1}\rangle\langle\bar{1}\bar{3}\rangle + \langle 2\bar{1}\rangle\langle\bar{3}\bar{2}\rangle\langle\bar{2}\bar{4}\rangle). \tag{4.2.26}$$

We explain how (4.2.26) was derived in Appendix D.1 using the $--++$ case as an example.

To achieve further cancellations, it is convenient to keep the maximum amount of symmetry in our expressions. We therefore write the generalised Mandelstam variable S as

$$S = \frac{1}{2}(\langle 12\rangle\langle\bar{1}\bar{2}\rangle + \langle 34\rangle\langle\bar{3}\bar{4}\rangle + E(E+k_s)). \tag{4.2.27}$$

We then apply various spinor identities in Appendix D to terms with a (spurious) $1/E$ pole to get

$$\begin{aligned} n_s^{++++} =& \frac{1}{8k_1k_2k_3k_4}\frac{\langle\bar{1}\bar{2}\rangle\langle\bar{3}\bar{4}\rangle}{E}\Big[iE(\langle 1\bar{4}\rangle\langle\bar{1}\bar{2}\rangle\langle\bar{1}\bar{3}\rangle + \langle 4\bar{1}\rangle\langle\bar{3}\bar{4}\rangle\langle\bar{2}\bar{4}\rangle) \\ &+ \langle\bar{1}\bar{2}\rangle\langle\bar{3}\bar{4}\rangle\left(-\frac{E}{k_s}(k_1-k_2)(k_3-k_4) - Ek_s\right) + (E^2+2Ek_s)\langle\bar{1}\bar{3}\rangle\langle\bar{2}\bar{4}\rangle\Big] \\ &+ SW_s^{B,++++}, \end{aligned} \tag{4.2.28}$$

and then use (D.0.9) to combine the first line with $W_s^{B,++++}$ to obtain the final form

$$\begin{aligned} n_s^{++++} = \frac{1}{8k_1k_2k_3k_4}\langle\bar{1}\bar{2}\rangle\langle\bar{3}\bar{4}\rangle\Big[i\Big(\langle 1\bar{2}\rangle\langle\bar{4}\bar{1}\rangle\langle\bar{1}\bar{3}\rangle + \langle 2\bar{1}\rangle\langle\bar{3}\bar{2}\rangle\langle\bar{2}\bar{4}\rangle\Big) \\ - k_s\left(\langle\bar{2}\bar{3}\rangle\langle\bar{4}\bar{1}\rangle - \langle\bar{1}\bar{3}\rangle\langle\bar{2}\bar{4}\rangle\right) - \frac{1}{k_s}\langle\bar{1}\bar{2}\rangle\langle\bar{3}\bar{4}\rangle(k_1-k_2)(k_3-k_4)\Big]. \end{aligned} \tag{4.2.29}$$

The other kinematic numerators can then be obtained using (2.4.7). Summing the three numerators and applying the Schouten identity gives

$$\begin{aligned} Q^{++++} = \frac{1}{8k_1k_2k_3k_4}\Big(k_s\left(\langle\bar{1}\bar{3}\rangle^2\langle\bar{2}\bar{4}\rangle^2 - \langle\bar{2}\bar{3}\rangle^2\langle\bar{4}\bar{1}\rangle^2\right) \\ - \frac{1}{k_s}\langle\bar{1}\bar{2}\rangle^2\langle\bar{3}\bar{4}\rangle^2(k_1-k_2)(k_3-k_4)\Big) + \text{cyc}(234), \end{aligned} \tag{4.2.30}$$

matching the general structure in equation (4.2.21). The numerators satisfying kinematic Jacobi relations are then obtained by plugging (4.2.29) (and the analogous formulas for n_t and n_u) and (4.2.30) into (4.1.12).

Finally, plugging the kinematic numerators into the first line of (4.1.3) gives a very compact formula for the all-plus AdS_4 amplitude:

$$\langle++++\rangle = \frac{1}{8k_1k_2k_3k_4}\frac{1}{S}\langle\bar{1}\bar{2}\rangle\langle\bar{3}\bar{4}\rangle\Big[i(\langle1\bar{2}\rangle\langle\bar{4}\bar{1}\rangle\langle\bar{1}\bar{3}\rangle + \langle2\bar{1}\rangle\langle\bar{3}\bar{2}\rangle\langle\bar{2}\bar{4}\rangle) \\ - k_s\Big(\langle\bar{2}\bar{3}\rangle\langle\bar{4}\bar{1}\rangle - \langle\bar{1}\bar{3}\rangle\langle\bar{2}\bar{4}\rangle\Big) - \frac{1}{k_s}\langle\bar{1}\bar{2}\rangle\langle\bar{3}\bar{4}\rangle(k_1-k_2)(k_3-k_4)\Big] + 2\leftrightarrow 4. \tag{4.2.31}$$

Using (2.3.4), we see that it manifestly vanishes in the flat space limit, as expected.

$\mathbf{N^{-1}MHV}$

Next, let us consider the $-+++$ case. Converting equation (4.2.20) to spinor notation for the case where particle 1 has negative helicity and the rest positive gives

$$n_s^{-+++} = \frac{\langle1\bar{2}\rangle\langle\bar{3}\bar{4}\rangle}{8k_1k_2k_3k_4}\frac{1}{E}\Big[\langle1\bar{2}\rangle\langle\bar{3}\bar{4}\rangle\Big(\langle13\rangle\langle\bar{1}\bar{3}\rangle + \langle24\rangle\langle\bar{2}\bar{4}\rangle - \frac{E}{k_s}(k_1-k_2)(k_3-k_4) - Ek_s\Big) \\ + 2S\langle1\bar{3}\rangle\langle\bar{2}\bar{4}\rangle\Big] + sW_s^{B,-+++}, \tag{4.2.32}$$

where

$$W_s^{B,-+++} = \frac{i}{8k_1k_2k_3k_4E}\frac{2(E-2k_1)}{S}\langle1\bar{2}\rangle\langle\bar{3}\bar{4}\rangle\Big(\langle12\rangle\langle\bar{2}\bar{3}\rangle\langle\bar{2}\bar{4}\rangle + \langle\bar{2}\bar{1}\rangle\langle1\bar{4}\rangle\langle1\bar{3}\rangle\Big), \tag{4.2.33}$$

as shown in Appendix D.1. As in the all-plus case, we use 4-point spinor and Schouten identities to combine the terms with a $1/E$ pole. In the end, the kinematic numerator can be written as

$$n_s^{-+++} = = \frac{1}{8k_1k_2k_3k_4}\langle1\bar{2}\rangle\langle\bar{3}\bar{4}\rangle\Big[\frac{4ik_1}{E}\langle\bar{1}\bar{2}\rangle\langle1\bar{4}\rangle\langle1\bar{3}\rangle + i\Big(\langle12\rangle\langle\bar{2}\bar{3}\rangle\langle\bar{2}\bar{4}\rangle + \langle\bar{2}\bar{1}\rangle\langle1\bar{4}\rangle\langle1\bar{3}\rangle\Big) \\ + (k_s+2k_1)\Big(\langle1\bar{4}\rangle\langle\bar{2}\bar{3}\rangle - \langle1\bar{3}\rangle\langle\bar{4}\bar{2}\rangle\Big) - \frac{1}{k_s}\langle1\bar{2}\rangle\langle\bar{3}\bar{4}\rangle(k_1-k_2)(k_3-k_4)\Big]. \tag{4.2.34}$$

Using this result and (2.4.7), we find that the sum over kinematic numerators is

$$Q^{-+++} = \frac{1}{8k_1k_2k_3k_4}\Big(k_s\left(\langle 1\bar{3}\rangle^2\langle\bar{2}\bar{4}\rangle^2 - \langle 1\bar{4}\rangle^2\langle\bar{2}\bar{3}\rangle^2\right) - \frac{1}{k_s}\langle 1\bar{2}\rangle^2\langle\bar{3}\bar{4}\rangle^2(k_1-k_2)(k_3-k_4)\Big) + \text{cyc}(234). \tag{4.2.35}$$

Plugging the above equation along with (4.2.34) (and the analogous numerators in the the t- and u-channels) into (4.1.12) then gives numerators satisfying kinematic Jacobi relations.

Unlike the all-plus case, the kinematic numerators do not vanish in the flat-space limit, although this will hold for the full AdS_4 amplitude. The flat space numerators in this case can be derived from the self-dual sector of Yang-Mills theory [137]. Plugging the kinematic numerators into the first line of (4.1.3), the amplitude can be reduced to the following concise expression:

$$\begin{aligned}\langle -+++\rangle = \frac{1}{8k_1k_2k_3k_4}\frac{1}{ES}\langle 1\bar{2}\rangle\langle\bar{3}\bar{4}\rangle\Big[&4ik_1\langle\bar{1}\bar{2}\rangle\langle 1\bar{4}\rangle\langle 1\bar{3}\rangle \\ &+ iE\left(\langle 12\rangle\langle\bar{2}\bar{3}\rangle\langle\bar{2}\bar{4}\rangle + \langle\bar{2}\bar{1}\rangle\langle 1\bar{4}\rangle\langle 1\bar{3}\rangle\right) \\ &+ E(k_s+2k_1)\left(\langle 1\bar{4}\rangle\langle\bar{2}\bar{3}\rangle - \langle 1\bar{3}\rangle\langle\bar{4}\bar{2}\rangle\right) \\ &- \frac{1}{k_s}E\langle 1\bar{2}\rangle\langle\bar{3}\bar{4}\rangle(k_1-k_2)(k_3-k_4)\Big] + 2\leftrightarrow 4.\end{aligned} \tag{4.2.36}$$

To see that the pole in E is in fact spurious, we combine the two terms over a single denominator. Collecting the terms that go as k_1/E, we get a numerator proportional to

$$\begin{aligned}-4k_1\langle 1\bar{2}\rangle\langle 1\bar{3}\rangle\langle 1\bar{4}\rangle&\left(\langle\bar{1}\bar{2}\rangle\langle\bar{3}\bar{4}\rangle T + \langle\bar{2}\bar{3}\rangle\langle\bar{4}\bar{1}\rangle S\right) \\ &= -2k_1\langle 1\bar{2}\rangle\langle 1\bar{3}\rangle\langle 1\bar{4}\rangle E\Big(E\left(\langle\bar{1}\bar{2}\rangle\langle\bar{3}\bar{4}\rangle + \langle\bar{2}\bar{3}\rangle\langle\bar{4}\bar{1}\rangle\right) + 2k_t\langle\bar{1}\bar{2}\rangle\langle\bar{3}\bar{4}\rangle \\ &\quad + 2k_s\langle\bar{2}\bar{3}\rangle\langle\bar{4}\bar{1}\rangle + i(\langle 3\bar{1}\rangle\langle\bar{2}\bar{3}\rangle\langle\bar{3}\bar{4}\rangle + \langle 1\bar{3}\rangle\langle\bar{4}\bar{1}\rangle\langle\bar{1}\bar{2}\rangle)\Big),\end{aligned} \tag{4.2.37}$$

so there is no pole in E and the flat space limit vanishes. We can write the amplitude in a way that manifestly has the correct flat space limit as follows:

$$\begin{aligned}\langle -+++\rangle = \frac{1}{8k_1k_2k_3k_4}\frac{1}{S}\langle 1\bar{2}\rangle\langle\bar{3}\bar{4}\rangle\Big[&i(\langle 12\rangle\langle\bar{2}\bar{4}\rangle\langle\bar{2}\bar{3}\rangle + \langle\bar{2}\bar{1}\rangle\langle 1\bar{3}\rangle\langle 1\bar{4}\rangle)\\ &+(k_s+2k_1)(\langle 1\bar{4}\rangle\langle\bar{2}\bar{3}\rangle - \langle 1\bar{3}\rangle\langle\bar{4}\bar{2}\rangle)\\ &-\frac{1}{k_s}\langle 1\bar{2}\rangle\langle\bar{3}\bar{4}\rangle(k_1-k_2)(k_3-k_4)\\ &+\frac{2ik_1\langle 1\bar{3}\rangle\langle 1\bar{4}\rangle}{T}\left(\langle\bar{1}\bar{2}\rangle(E+2k_t)+i\langle 4\bar{2}\rangle\langle\bar{4}\bar{1}\rangle\right)\Big] + 2\leftrightarrow 4,\end{aligned} \tag{4.2.38}$$

where we have used Schouten identities and collected the terms proportional to $\langle 1\bar{2}\rangle\langle\bar{3}\bar{4}\rangle$ to identify a symmetry under $2\leftrightarrow 4$.

MHV

Let us now consider the $-+-+$ case. By substituting spinors into equation (4.2.20), we get (after some manipulations and identities)

$$\begin{aligned} n_s^{-+-+} = \frac{1}{8k_1k_2k_3k_4}\Big[&\frac{4}{E}(k_1k_4+k_2k_3)\langle 1\bar{2}\rangle\langle 3\bar{4}\rangle\langle 13\rangle\langle\bar{2}\bar{4}\rangle\\ &+i\frac{(E-2k_1-2k_3)}{E}\langle 1\bar{2}\rangle\langle 3\bar{4}\rangle(\langle 21\rangle\langle\bar{2}\bar{4}\rangle\langle 3\bar{2}\rangle+\langle\bar{1}\bar{2}\rangle\langle 31\rangle\langle 1\bar{4}\rangle)\\ &+k_s\left(\langle 13\rangle^2\langle\bar{4}\bar{2}\rangle^2-\langle 1\bar{4}\rangle^2\langle 3\bar{2}\rangle^2\right)\\ &-\frac{1}{k_s}\langle 1\bar{2}\rangle^2\langle 3\bar{4}\rangle^2(k_1-k_2)(k_3-k_4)\Big],\\ n_t^{-+-+} = -n_s^{-+-+}&\Big|_{2\leftrightarrow 4}.\end{aligned} \tag{4.2.39}$$

The final two lines of this can be seen directly from equation (4.2.20) after substituting for polarisation vectors and using equation (4.2.27) to combine over a common denominator. The second line comes from the W_s^B term, specialised to the $-+-+$ case. This is covered in more detail in Appendix D.1. This just leaves the first line, which is analogous to the all-plus and single minus cases, but with a few extra Schouten identities needed to rewrite the pole in E. The 'extra' pieces we see compared to equation (4.2.29) are what will give the non-zero MHV flat space amplitude.

The u-channel numerator cannot simply be obtained by applying (2.4.7) to (4.2.39)

as this would involve exchanging particles of different helicity. Instead, we must first apply (2.4.7) to (4.2.20) in terms of general polarisation vectors, and then convert the resulting expression for n_u to spinor notation using methods similar to those used to obtain (4.2.39). In the end, we find

$$\begin{aligned} n_u^{-+-+} = \frac{1}{8k_1k_2k_3k_4}\langle 13\rangle\langle\bar{4}\bar{2}\rangle\Big[&\frac{4}{E}\Big((k_1k_2+k_3k_4)\langle 1\bar{4}\rangle\langle 3\bar{2}\rangle + (k_1k_4+k_2k_3)\langle 3\bar{4}\rangle\langle 1\bar{2}\rangle\Big) \\ &+ i\frac{(E-2k_1-2k_3)}{E}\Big(\langle 1\bar{3}\rangle\langle 3\bar{2}\rangle\langle 3\bar{4}\rangle + \langle 3\bar{1}\rangle\langle 1\bar{4}\rangle\langle 1\bar{2}\rangle\Big) \\ &+ k_u\Big(\langle 1\bar{4}\rangle\langle 3\bar{2}\rangle + \langle 1\bar{2}\rangle\langle 3\bar{4}\rangle\Big) \\ &- \frac{1}{k_u}\langle 13\rangle\langle\bar{4}\bar{2}\rangle(k_1-k_3)(k_4-k_2)\Big]. \end{aligned} \tag{4.2.40}$$

Adding up the kinematic numerators or directly converting (4.2.21) to spinor notation, we find that

$$\begin{aligned} Q^{-+-+} = \frac{1}{8k_1k_2k_3k_4}\Big(&k_s\Big(\langle 13\rangle^2\langle\bar{4}\bar{2}\rangle^2 - \langle 1\bar{4}\rangle^2\langle 3\bar{2}\rangle^2\Big) \\ &- \frac{1}{k_s}\langle 1\bar{2}\rangle^2\langle 3\bar{4}\rangle^2(k_1-k_2)(k_3-k_4)\Big) + \text{cyc}(234), \end{aligned} \tag{4.2.41}$$

where the permutations act on the bars as well as the particle labels. Plugging (4.2.39)-(4.2.41) into (4.1.12) then gives the numerators which satisfy the kinematic Jacobi relation.

Moreover, plugging the above kinematic numerators into the first line of (2.4.5), we obtain the following remarkably compact formula for the MHV amplitude in AdS_4:

$$\begin{aligned} \langle -+-+\rangle &= \frac{n_s^{-+-+}}{S} - \frac{n_t^{-+-+}}{T} \\ &= \frac{1}{8k_1k_2k_3k_4}\frac{1}{ES}\langle 1\bar{2}\rangle\langle 3\bar{4}\rangle\Big[4(k_1k_4+k_2k_3)\langle 13\rangle\langle\bar{2}\bar{4}\rangle \\ &\qquad + i(E-2k_2-2k_4)(\langle 12\rangle\langle\bar{2}\bar{4}\rangle\langle 3\bar{2}\rangle + \langle\bar{2}\bar{1}\rangle\langle 31\rangle\langle 1\bar{4}\rangle) \\ &\qquad + Ek_s(\langle 13\rangle\langle\bar{2}\bar{4}\rangle - \langle 1\bar{4}\rangle\langle 3\bar{2}\rangle) \\ &\qquad - \frac{1}{k_s}E\langle 1\bar{2}\rangle\langle 3\bar{4}\rangle(k_1-k_2)(k_3-k_4)\Big] + 2\leftrightarrow 4. \end{aligned} \tag{4.2.42}$$

This formula represents substantial progress beyond the formula first obtained in the pioneering work [49] which contained many more terms and several functions of

spinor brackets in the denominators, whereas the denominators of (4.2.42) contain only k_a and $|\boldsymbol{k}_a + \boldsymbol{k}_b|$. The key to obtaining such a simple expression was to focus on simplifying the kinematic numerators and make use of numerous spinor identities derived in Appendix D. It would be interesting to see if this simplicity extends to higher-point amplitudes, and in particular if there is some analogue of the Parke-Taylor formula [6] for MHV amplitudes in AdS_4.

As in the single-minus case, this does not have the flat space limit manifest until we combine parts from the two numerators. If consider only the terms with a pole in E, we get

$$\begin{aligned}\lim_{E\to 0}\langle - + -+\rangle = \lim_{E\to 0}\frac{1}{8k_1k_2k_3k_4}\frac{1}{EST}\Big[&\\ &4\langle 13\rangle\langle\bar{2}\bar{4}\rangle\Big(T\langle 1\bar{2}\rangle\langle 3\bar{4}\rangle(k_1k_4+k_2k_3)\\ &\quad - S\langle 1\bar{4}\rangle\langle 3\bar{2}\rangle(k_1k_2+k_3k_4)\Big)\\ &+2(k_2+k_4)\Big(T\langle 1\bar{2}\rangle\langle 3\bar{4}\rangle(\langle\bar{1}\bar{2}\rangle\langle 13\rangle\langle 1\bar{4}\rangle+\langle 12\rangle\langle 3\bar{2}\rangle\langle\bar{2}\bar{4}\rangle)\\ &\quad + S\langle 1\bar{4}\rangle\langle 3\bar{2}\rangle(\langle\bar{1}\bar{4}\rangle\langle 13\rangle\langle 1\bar{2}\rangle+\langle 14\rangle\langle 3\bar{4}\rangle\langle\bar{4}\bar{2}\rangle)\Big)\Big],\\ =-\frac{2}{E}\frac{\langle 13\rangle^2\langle\bar{2}\bar{4}\rangle^2}{\langle 12\rangle\langle\bar{1}\bar{2}\rangle\langle 23\rangle\langle\bar{2}\bar{3}\rangle},&\end{aligned} \tag{4.2.43}$$

where we recognise the final line as the familiar four point flat space amplitude. The intermediate steps involve many spinor and Schouten identities but the general idea is to start with the lowest order terms in k_i and apply identities that generate higher powers (avoiding any k_i^2) along with corrections of order E, which are discarded. Eventually the only remaining contribution is a numerator proportional to $k_1k_2k_3k_4$ (which cancels the factors from the polarisation vectors) and corrections subleading in E, which we have omitted here.

Amplitudes with a u-channel contribution are less compact. For example the $\langle - - ++\rangle$ amplitude can be obtained from

$$\langle - - ++\rangle = \frac{n_s^{--++}}{S} - \frac{n_t^{--++}}{T}, \tag{4.2.44}$$

$$\text{where}\quad n_s^{--++} = -n_u^{-+-+}\Big|_{2\leftrightarrow 3},\quad n_t^{--++} = -n_t^{-+-+}\Big|_{2\leftrightarrow 3}, \tag{4.2.45}$$

where we exchange particle label but not helicity labels (i.e. bars on spinors), and the numerators are as defined in (4.2.39) and (4.2.40). This operation should be thought of as a relabelling (rather than a permutation) and can easily be seen by taking the diagrams in Figure 2.6, dressing with helicities and applying the relabellings. For completeness, we also note that

$$n_u^{--++} = -n_s^{-+-+}\Big|_{2\leftrightarrow 3}. \tag{4.2.46}$$

We can then see that the sum over kinematic numerators for $--++$ is given by

$$Q^{--++} = -Q^{-+-+}\Big|_{2\leftrightarrow 3}. \tag{4.2.47}$$

4.3 Relation to 3d Conformal Correlators

The AdS amplitudes we computed in previous sections are closely related to 3d CFT correlators in momentum space. In particular, they encode the transverse parts of the correlators from which the full correlators can be reconstructed using Ward identities, as we will explain in this section. The transverse part of a correlator can be recovered from an AdS amplitude by stripping off the polarisation vectors and replacing them with projection tensors:

$$\begin{aligned} \langle j_1 \dots j_n \rangle_\pi &= \langle j_1 \dots j_n \rangle\Big|_{\epsilon_i \to \pi_i}, \\ \text{where,} \quad \pi_i^{jk} &= \eta^{jk} - \frac{k_i^j k_i^k}{k_i^2}. \end{aligned} \tag{4.3.1}$$

In the above formula for transverse projection tensors, upper indices are 3d Lorentz indices while lower indices are particle labels.

The full correlator, which will be denoted as $\langle J_1 \dots J_n \rangle$, can then be reconstructed using the transverse Ward identity. For spin-1 currents with colour indices, this is

well known [1]:

$$k_{1i_1}\langle J^{a_1 i_1}(k_1)J^{a_2 i_2}(k_2)\dots J^{a_n i_n}(k_n)\rangle = -if^{a_1 a_2 b}\langle J^{b i_2}(k_2+k_1)\dots J^{a_n i_n}(k_n)\rangle \\ \cdots - if^{a_1 a_n b}\langle J^{a_2 i_2}(k_2)\dots J^{b i_n}(k_n+k_1)\rangle, \tag{4.3.2}$$

where we have defined the structure constants such that $[T^a, T^b] = -if^{abc}T^c$ and $\mathrm{tr}\left(T^a T^b\right) = \delta^{ab}$. The right hand side of this equation corresponds to the standard sum over contact terms in position space. In the flat space limit, the contact terms don't contribute because they are constructed from lower-point correlators and therefore do not contain a pole in $E = \sum_{a=1}^{n} k_a$. Hence, the Ward identity for conformal correlators reduces to a Ward identity for flat space scattering amplitudes in one higher dimension. For colour-ordered correlators, there are only two contact terms

$$k_{1i_1}\langle J^{i_1}(k_1)J^{i_2}(k_2)\dots J^{i_n}(k_n)\rangle = (-1)^n\Big(\left\langle J^{i_2}(k_2)\dots J^{i_n}(k_n+k_1)\right\rangle \\ - \left\langle J^{i_2}(k_2+k_1)\dots J^{i_n}(k_n)\right\rangle\Big). \tag{4.3.3}$$

The full correlator can then be obtained from the transverse part by adding terms proportional to lower-point correlators which give the required contact terms when contracted with the momentum k_1^i.

The reconstruction of 3-point correlators was spelled out in [138], and we will review it here for completeness. We will then present a new formula for 4-point correlators, which is the main focus of this paper. At three points the Ward identity can be written as

$$k_{1i}\langle J^i(\boldsymbol{k}_1)J^j(\boldsymbol{k}_2)J^k(\boldsymbol{k}_3)\rangle = \langle J^j(-\boldsymbol{k}_3)J^k(\boldsymbol{k}_3)\rangle - \langle J^j(\boldsymbol{k}_2)J^k(-\boldsymbol{k}_2)\rangle, \tag{4.3.4}$$

where the 2-point function is fixed by conformal Ward identities to be [138]:

$$\langle J^i(\boldsymbol{k})J^j(-\boldsymbol{k})\rangle = c_J k\,\pi^{ij}, \tag{4.3.5}$$

[1] This Ward identity can be found in many text books. For a discussion in the context of cosmology see [47, 59].

where c_J is a normalisation. The full correlator can be recovered by adding terms to the transverse piece such that (4.3.4) is satisfied, symmetrising (recalling that colour-ordered correlators are cyclically symmetric), and adding further terms to cancel the new terms which arise after symmetrising and contracting with k_1. In the end this gives

$$\begin{aligned}\langle J^i(\boldsymbol{k}_1)J^j(\boldsymbol{k}_2)J^k(\boldsymbol{k}_3)\rangle &= \langle j^i(\boldsymbol{k}_1)j^j(\boldsymbol{k}_2)j^k(\boldsymbol{k}_3)\rangle_\pi \\ &+ \left[\frac{k_1^i}{k_1^2}\Big(\langle J^j(-\boldsymbol{k}_3)J^k(\boldsymbol{k}_3)\rangle - \langle J^j(\boldsymbol{k}_2)J^k(-\boldsymbol{k}_2)\rangle\Big) + \frac{k_1^i k_2^j}{k_1^2 k_2^2}\, k_{1a}\langle J^a(\boldsymbol{k}_3)J^k(-\boldsymbol{k}_3)\rangle\right] \\ &\qquad + \text{Cyc}[123],\end{aligned} \tag{4.3.6}$$

where $\langle jjj\rangle_\pi$ is obtained from the 3-point AdS amplitude in (4.2.4). The cyclic sum includes permutations of i, j, k along with the particle labels.

At higher points, the procedure for reconstructing the full correlator from the transverse piece by adding terms to solve the Ward identity, symmetrising, and adding new terms to cancel unwanted contributions must be iterated. At four-points, this will involve adding numerous terms with both 2-point and 3-point correlators. Using

(4.3.4) to tidy up, we are left with

$$\begin{aligned}\langle J_1^i J_2^j J_3^k J_4^l\rangle = \langle j_1^i j_2^j j_3^k j_4^l\rangle_\pi \\ + \Bigg[\frac{k_1^i}{k_1^2}\Big(\langle J^j(k_2)J^k(k_3)J^l(k_4+k_1)\rangle - \langle J^j(k_1+k_2)J^k(k_3)J^l(k_4)\rangle\Big) \\ + \frac{k_1^i k_2^j}{k_1^2 k_2^2}\Big(\langle J^k(\boldsymbol{k}_3)J^l(-\boldsymbol{k}_3)\rangle - \langle J^k(\boldsymbol{k}_2+\boldsymbol{k}_3)J^l(-\boldsymbol{k}_2-\boldsymbol{k}_3)\rangle \\ + k_{2a}\langle J^a(k_1+k_2)J^k(k_3)J^l(k_4)\rangle\Big) \\ + \frac{k_1^i k_3^k}{2k_1^2 k_3^2}\Big(\langle J^j(\boldsymbol{k}_2+\boldsymbol{k}_3)J^l(-\boldsymbol{k}_2-\boldsymbol{k}_3)\rangle + \langle J^j(\boldsymbol{k}_3+\boldsymbol{k}_4)J^l(-\boldsymbol{k}_3-\boldsymbol{k}_4)\rangle \\ - \langle J^j(\boldsymbol{k}_2)J^l(-\boldsymbol{k}_2)\rangle - \langle J^j(\boldsymbol{k}_4)J^l(-\boldsymbol{k}_4)\rangle\Big) \\ + \frac{k_2^j k_3^k k_4^l}{k_2^2 k_3^3 k_4^4}k_{3a}\Big(\langle J^a(\boldsymbol{k}_1)J^i(-\boldsymbol{k}_1)\rangle - \langle J^a(\boldsymbol{k}_2+\boldsymbol{k}_3)J^i(-\boldsymbol{k}_2-\boldsymbol{k}_3)\rangle \\ - \langle J^a(\boldsymbol{k}_3+\boldsymbol{k}_4)J^i(-\boldsymbol{k}_3-\boldsymbol{k}_4)\rangle\Big) \\ + \frac{k_1^i k_2^j j_3^k k_4^l}{4k_1^2 k_2^2 k_3^2 k_4^2}k_{1a}k_{3b}\Big(\langle J^a(\boldsymbol{k}_2+\boldsymbol{k}_3)J^b(-\boldsymbol{k}_2-\boldsymbol{k}_3)\rangle \\ + \langle J^a(\boldsymbol{k}_3+\boldsymbol{k}_4)J^b(-\boldsymbol{k}_3-\boldsymbol{k}_4)\rangle\Big)\Bigg] \\ + \text{cyc}(1234),\end{aligned} \tag{4.3.7}$$

where the first term is obtained from the 4-point AdS amplitudes computed in the previous sections.

4.4 Remarks

In this chapter we explored how CK duality is realised for tree-level 4-point YM amplitudes in AdS_4. In particular, we found a decomposition of these amplitudes into kinematic numerators analogous to those of flat space amplitudes. In contrast to flat space, we find that numerators in AdS_4 do not generically satisfy kinematic Jacobi identities. We also find that colour-ordered amplitudes obey a deformed BCJ relation which reduces to the usual one in the flat space limit (see (4.1.9)). On the other hand, the numerators can be shifted in such a way that the amplitudes

are preserved. Using this generalised gauge symmetry, there is a unique choice of numerators which do obey the kinematic Jacobi identity, given in (4.1.12). We then recast these results in spinor notation to obtain concise new formulae for all helicity configurations using numerous spinor identities derived in Appendix D, and explain how to reconstruct 3d conformal correlators of conserved currents from AdS_4 amplitudes using Ward identities.

The numerators which obey kinematic Jacobi relations may play a role in obtaining gravitational amplitudes in AdS_4 via a double copy procedure. In more detail, we can construct an object analogous to the flat space gravitational amplitude in (2.4.9) by squaring these numerators

$$\begin{aligned}\langle t_1 t_2 t_3 t_4\rangle &= \frac{k_1k_2k_3k_4}{E}\left(\frac{\tilde{n}_s^2}{S}+\frac{\tilde{n}_t^2}{T}+\frac{\tilde{n}_u^2}{U}\right),\\ &= \frac{k_1k_2k_3k_4}{E}\left(\frac{n_s^2}{S}+\frac{n_t^2}{T}+\frac{n_u^2}{U}-\frac{1}{\xi}Q^2\right),\end{aligned} \tag{4.4.1}$$

where S, T and U are generalised Mandelstam variables as given in (4.1.1). We label this object $\langle t_1 t_2 t_3 t_4\rangle$ to denote the transverse traceless part of a stress tensor correlator, dual to a gravitational amplitude in the bulk. We have also included a prefactor with an additional pole in E since in the flat space limit, 3d stress tensor correlators behave as follows [37]:

$$\lim_{E\to 0}\langle t_1 t_2 t_3 t_4\rangle = \frac{k_1k_2k_3k_4}{E^3}M_4, \tag{4.4.2}$$

where M_4 is the 4d graviton amplitude in flat space. This result can be compared more conveniently by dimensionally reducing to obtain 4 minimally coupled scalars exchanging a graviton, which may be compared more readily to Witten diagram calculations and cross-checked with other results such as [59, 139]. Preliminary finding suggest that a double copy at the level of integrated Witten diagrams misses some important physics. Instead, an integrand-level double copy may be more appropriate although this alone is still incapable of capturing the entire graviton amplitude in AdS [140]. It is also not yet clear in this approach how to define a set of shifted numerators that obey the kinematic Jacobi identity.

In addition to comparing (4.4.1) and variations to explicit Witten diagram calculations, there are several other directions for future work. Perhaps the most obvious is to see if CK duality in AdS_4 can be extended to higher points. At first sight, the five-point expressions obtained in [50] look somewhat formidable, but it may be possible to simplify them by converting to spinor notation and generalising the spinor identities in Appendix D to higher points. As was noted in section 4.1, the CK duality in AdS has some similarities to that of massive amplitudes in flat space. On the other hand, it has recently been shown that the massive double copy generally introduces unphysical singularities above 4-points [135], so it would also be interesting to see if this can be avoided in AdS. In flat space, many aspects of the double copy become manifest by expressing amplitudes in terms of scattering equations [41, 67]. Chapter 5 explores a dS version of this for scalars but such a description of Yang-Mills and gravity beyond flat space is still elusive.

It would also be interesting to explore to what extent CK duality and double copy hold for generic theories in AdS_4, or equivalently correlators in generic 3d CFTs. Perhaps the best way to approach this question would be to find general solutions to the conformal Ward identities in momentum space for n-point correlators of currents and stress tensors analogous to the general solution for scalar correlators recently obtained in terms of Feynman integrals in [141]. It may then be possible to look for double copy structure by studying their leading singularities, as was shown at three points in [53]. There are also alternative formulations of AdS amplitudes such as the Mellin representation used to construct kinematic numerators in [142]. Finally, it would be very interesting to adapt this story to dS_4 with the goal of seeing new mathematical structure in cosmological observables. Some work on the double copy in dS_4 has been carried out in [143, 144].

Chapter 5

Generalised Double Copy in de Sitter

The aim of this chapter is to introduce the CHY formalism and how it can be applied to de Sitter wavefunction coefficients in the form of the Cosmological Scattering Equations (CSE). By uplifting CHY integrands from flat space we can compute wavefunction coefficients from a worldsheet integral and also construct a double copy between scalar EFTs analogous to the flat space one introduced in [68]. The CSE will also let us motivate the construction of wavefunction coefficients directly from the action of Casimir operators acting on a contact diagram, rather than using Witten diagrams as an intermediate step. This not only provides compact expressions (since the Casimir operators appear analogous to flat space Mandelstam variables) but it will also allow us to study properties for arbitrary dimension d and conformal weight Δ. In this chapter we will provide some concrete examples for EFT wavefunction coefficients in $d = 3$ for the minimal ($\Delta = 3$) and conformal ($\Delta = 2$) scalars and comment on their properties and soft limits. The operator approach will then be taken further in chapter 6 where we analyse the soft behavior of general scalar EFTs and use it to reconstruct theories with 'exceptional' soft behavior.

We start with an introduction to the boundary conformal generators which underpin the CSE and later treatment of soft limits (section 5.1). This is followed by a review

of the CHY formalism in flat space (5.2) and its uplift to dS (5.2.1). In section 5.2.1 we look at the computation of scalar EFTs in dS using Witten diagrams and these are then compared to the corresponding CSE calculations in 5.3.1. This is used to motivate the generalised double copy in section 5.3.2. Finally section 5.3.3 deals with explicit results for minimal and conformally coupled scalars before some remarks in section 5.4.

5.1 Boundary Conformal Generators

The mathematics describing the calculation of dS wavefunction coefficients is very similar to the AdS Witten diagrams in the last chapter. From the perspective of the physics at the boundary, the main difference is that the space is Euclidean rather than Lorentzian. The role of the radial coordinate in AdS is now played by the conformal time η and at tree-level, many of the same quantities can be reused after a Wick rotation to account for the time-like transverse direction

The solutions to the classical equations of motion in this background are formed from products of plane waves $e^{i\boldsymbol{k}\cdot\boldsymbol{x}}$ multiplied by an η-dependent piece described by the free equations of motion $(\mathcal{D}_k^2 + m^2)\phi^\nu = 0$, where

$$\mathcal{D}_k^2 = \eta^2\partial_\eta^2 + (1-d)\eta\partial_\eta + \eta^2 k^2, \tag{5.1.1}$$

with $k = |\boldsymbol{k}|$. The solutions are given by

$$\phi^\nu(k,\eta) = (-1)^{\nu-\frac{1}{2}}\sqrt{\frac{\pi}{2}}k^\nu\eta^{d/2}H_\nu(-k\eta), \tag{5.1.2}$$

where $\nu = \Delta - d/2$, H_ν is a Hankel function of the second kind, and the normalisation is chosen for convenience. These ϕ^ν will be used as bulk-to-boundary propagators. We then define an n-point contact diagram as follows:

$$\mathcal{C}_n^\Delta = \int \frac{d\eta}{\eta^{d+1}}U_{1,n}(\eta),\ \ U_{m,n}(\eta) = \prod_{a=m}^{n}\phi_a, \tag{5.1.3}$$

where a labels an external leg, k_a is the magnitude of the boundary momentum of that leg, and $\phi_a = \phi^\nu(k_a, \eta)$. When acting on these ϕ^ν, the conformal generators introduced in section 2.3.20 take a simple form which can be expressed in terms of boundary momenta and conformal time derivatives

$$\begin{aligned} D\phi^\nu &= \eta\tfrac{\partial}{\partial\eta}\phi^\nu, \qquad & P^i\phi^\nu &= k^i\phi^\nu, \\ K_i\phi^\nu &= \eta^2 k_i\phi^\nu, \qquad & M_{ij}\phi^\nu &= 0. \end{aligned} \tag{5.1.4}$$

We will collectively denote the generators by $\mathcal{D}^A \in \{P^i, M_{ij}, D, K_i\}$, where A is an adjoint index. In this notation, the conformal Ward identities in (2.3.19) are all encapsulated in a single expression

$$\sum_{a=1}^{n} \mathcal{D}_a^A \Psi_n = 0. \tag{5.1.5}$$

The inner product of these gives a Casimir operator that will play an important role throughout our analysis of de Sitter wavefunction coefficients here and in chapter 6

$$\mathcal{D}_a \cdot \mathcal{D}_b = \frac{1}{2}\left(P_a^i K_{bi} + K_{ai} P_b^i - M_{a,ij} M_b^{ij}\right) + D_a D_b, \tag{5.1.6}$$

where $\mathcal{D}_a$ is a boundary conformal generator defined in terms of the boundary momentum associated with leg a. Acting on a pair of bulk-to-boundary propagators associated with legs a and b, the operator in (5.1.6) satisfies

$$(\mathcal{D}_a \cdot \mathcal{D}_b)\,(\phi_a\phi_b) = \eta^2[\partial_\eta\phi_a\partial_\eta\phi_b + (\boldsymbol{k}_a \cdot \boldsymbol{k}_b)\phi_a\phi_b]., \tag{5.1.7}$$

and it will be shown below that this is equivalent to the vertex given by a scalar interaction with 2 derivatives. It will therefore be useful to use the shorthand $\mathcal{D}_a \cdot \mathcal{D}_b = \hat{s}_{ab}$. A useful identity that these satisfy is

$$\begin{aligned} [(\mathcal{D}_a \cdot \mathcal{D}_b), (\mathcal{D}_b \cdot \mathcal{D}_c)]\mathcal{C}_n^\Delta &= \Big(2(K_a \cdot P_c - P_a \cdot K_c)D_b + \text{cyc}(abc)\Big)\mathcal{C}_n^\Delta, \\ &= 0. \end{aligned} \tag{5.1.8}$$

The commutator is not zero but vanishes when acting on a contact diagram. This was first derived in the embedding space formalism [73], and its generalization to

momentum space is straightforward. Using (5.1.4) we can easily show that the right hand side vanishes.

We will also need bulk-to-bulk propagators, $G_\nu(k,\eta,\tilde{\eta})$ to consider interactions that exchange particles in the bulk. For our purposes, we will only need to use the following property:

$$[(\mathcal{D}_1+\ldots+\mathcal{D}_p)^2+m^2]^{-1}\mathcal{C}_n^\Delta=\int\frac{d\eta}{\eta^{d+1}}\frac{d\tilde{\eta}}{\tilde{\eta}^{d+1}}U_{p+1,n}(\eta)G_\nu(k_{1\ldots p},\eta,\tilde{\eta})U_{1,p}(\tilde{\eta}). \quad (5.1.9)$$

This follows from the equation of motion

$$(\mathcal{D}_k^2+m^2)G_\nu=\eta^{d+1}\delta(\eta-\tilde{\eta}), \quad (5.1.10)$$

and the following identity:

$$(\mathcal{D}_{1\ldots p}^2U_{1,p})U_{p+1,n}=(\mathcal{D}_1+\ldots+\mathcal{D}_p)^2U_{1,n}, \quad (5.1.11)$$

where in the left-hand side $\mathcal{D}_{1\ldots p}^2$ is defined in (5.1.1) with $k=|\boldsymbol{k}_1+\ldots+\boldsymbol{k}_p|$ and $p<n$. For more details, see for example section 2.2 of [63]. This will let us express tree-level exchange diagrams in terms of differential operators which will be useful in chapter 6.

5.2 CHY Formalism

Here we briefly review flat space CHY and how it may be used to calculate EFT amplitudes in preparation for introducing the dS cosmological scattering equations. The CHY formalism (sometimes referred to as 'the scattering equations') is a method for calculating scattering amplitudes from an integral over the moduli space of punctures on a Riemann sphere [41]. The original proposal was for pure Yang-Mills and pure gravity amplitudes at tree level and this has since been extended to a variety of other particle theories and to loops [68, 145, 146]. The key is that the kinematics are described in a theory-independent way, as the solution to the scattering equations

given by

$$S_a = \sum_{a \neq b} \frac{2\, k_a \cdot k_b}{\sigma_{ab}} = 0, \qquad \sigma_{ab} \equiv \sigma_a - \sigma_b, \tag{5.2.1}$$

where σ_a is the holomorphic coordinate of the a-th puncture on a Riemann sphere. A sphere with n punctures thus corresponds to an n-point scattering amplitude. These are invariant under $\mathrm{SL}(2,\mathbb{C})$ transformations acting on the σ_a (provided the vectors satisfy momentum conservation). This means that only $n-3$ of the n equations are independent and so the position of up to three punctures can be fixed much like choosing a gauge.

The theory information is then contained within the 'CHY-integrand', which may be assembled from various building blocks. These contain dependence on the momenta and punctures as well as polarisation data (if present in the theory). For example, the Yang-Mills integrand can be constructed from the antisymmetric block matrix

$$\Upsilon(k,\epsilon,\sigma) = \begin{pmatrix} A & -C^T \\ C & B \end{pmatrix}, \tag{5.2.2}$$

where

$$\begin{aligned} A_{ab} &= \begin{cases} \dfrac{k_a \cdot k_b}{\sigma_a - \sigma_b} & a \neq b, \\ 0 & a = b, \end{cases} \qquad B_{ab} = \begin{cases} \dfrac{\epsilon_a \cdot \epsilon_b}{\sigma_a - \sigma_b} & a \neq b, \\ 0 & a = b, \end{cases} \\ C_{ab} &= \begin{cases} \dfrac{\epsilon_a \cdot k_b}{\sigma_a - \sigma_b} & a \neq b, \\ -\displaystyle\sum_{c \neq a} \dfrac{\epsilon_a \cdot k_c}{\sigma_a - \sigma_c} & a = b, \end{cases} \end{aligned} \tag{5.2.3}$$

along with the Parke-Taylor factor

$$\mathrm{PT} = \frac{1}{\sigma_{12}\sigma_{23}\cdots\sigma_{n1}}. \tag{5.2.4}$$

The colour-ordered tree-level amplitudes are then given by

$$A_n = \int \frac{d^n\sigma}{\mathrm{vol}\,\mathrm{SL}(2,\mathbb{C})} \prod_a{}' \delta(S_a)\, \mathrm{PT}\, \mathrm{Pf}'\Upsilon(k,\epsilon,\sigma), \tag{5.2.5}$$

where the $\prod_a{}'$ and $\mathrm{vol}\,\mathrm{SL}(2,\mathbb{C})$ redundancy in the scattering equations and $\mathrm{Pf}'\Upsilon = \frac{(-1)^{a+b}}{\sigma_{ab}}\mathrm{Pf}|\Upsilon|^{ab}_{ab}$ is the reduced Pfaffian where rows and columns a and b have been removed [41]. This reduction is necessary as the rows/ columns are not all independent and the Pfaffian will otherwise give zero. The Pfaffian can be computed as

$$\mathrm{Pf}\Upsilon^{ab}_{ab} = \frac{\epsilon^{r_1 s_1 \dots r_{p-1} s_{p-1}} (\Upsilon^{ab}_{ab})_{r_1 s_1} \cdots (\Upsilon^{ab}_{ab})_{r_{p-1} s_{p-1}}}{2^{p-1}(p-1)!}, \tag{5.2.6}$$

or alternatively as the square root of the determinant of Υ^{ab}_{ab}. There also exist recursive definitions to compute the Pfaffian just as with determinants.

This formula is of particular interest as gravitational amplitudes can be obtained by replacing the Parke-Taylor factor with a second copy of Υ (possibly with different polarisation vectors) to get

$$M_n = \int \frac{d^n\sigma}{\mathrm{vol}\,\mathrm{SL}(2,\mathbb{C})} \prod_a{}' \delta(S_a)\,\mathrm{PT}\,\mathrm{Pf}'\Upsilon(k,\epsilon,\sigma)\,\mathrm{Pf}'\Upsilon(k,\tilde{\epsilon},\sigma). \tag{5.2.7}$$

This is another example of a double copy relation like those discussed in 2.4. In each case, the integral can be evaluated by gauge-fixing, solving the remaining scattering equations and then summing over the solutions using the delta function.

In this chapter, we will not be calculating gauge or gravity integrands but instead those of the scalar EFTs from 2.5. The integrands for these theories can all be obtained from the Υ matrix from various dimensional reduction procedures. For example, if we start in $d+d$ dimensions and set $\epsilon_a = (\mathbf{0}|k_a)$ whilst constraining the momenta to only have d non-zero entries, the Pfaffian reduces to

$$\mathrm{Pf}'\Upsilon \to \mathrm{Pf}'A\mathrm{Pf}'A. \tag{5.2.8}$$

Similarly if we start from $d+1$ and set $\epsilon_a = (\mathbf{0}|1)$, we get

$$\mathrm{Pf}'\Upsilon \to \mathrm{Pf}X\mathrm{Pf}'A, \tag{5.2.9}$$

where

$$X_{rs} = \begin{cases} \dfrac{1}{\sigma_{rs}}, & r \neq s, \\ 0, & r = s. \end{cases} \tag{5.2.10}$$

Theory	Integrand
NLSM	$\mathrm{PT}(\mathrm{Pf}'A)^2$
DBI	$\mathrm{Pf}X(\mathrm{Pf}'A)^3$
sGal	$(\mathrm{Pf}'A)^4$

Table 5.1: A summary of CHY integrands for a selection of scalar EFTs.

From these building blocks we can assemble the three EFTs of interest as summarised in table 5.1. As in the Yang-Mills case, the corresponding NLSM amplitudes will be colour-ordered. The full amplitude can be recovered by dressing with colour factors and summing over permutations of legs in the PT factor. These integrands show that there are also double copy relations between the EFTs, for example replacing the colour PT piece in the NLSM integrand with either $\mathrm{Pf}X\mathrm{Pf}'A$ or $(\mathrm{Pf}'A)^2$ will yield the DBI or sGal cases. The EFT double copy can thus be summarised as

$$\mathrm{PT} \quad \to \quad \mathrm{Pf}X(\mathrm{Pf}'A), \tag{5.2.11}$$

$$\mathrm{PT} \quad \to \quad (\mathrm{Pf}'A)^2, \tag{5.2.12}$$

for DBI and sGal respectively. Roughly speaking, sGal = NLSM^2 and DBI = NLSM $\times$ YM, where YM corresponds to the dimensional reduction of Yang-Mills theory as discussed prior to equation (5.2.10).

Finally it should also be noted that the amplitudes from CHY can also be computed using residue theorems to map them to a sum over Feynman diagrams [147]. This will become useful in de Sitter where the operatorial nature of the scattering equations means that solving the system is not a well-understood problem. We therefore recast a general amplitude in the form of a contour integral

$$\mathcal{A}_n = \int_\gamma \prod_{\substack{a=1 \\ a\neq b,c,d}}^{n} d\sigma_a \frac{1}{S_a} (\sigma_{bc}\sigma_{cd}\sigma_{db})^2 \mathcal{I}_n, \tag{5.2.13}$$

where $\mathcal{I}_n$ is a generic n point integrand and γ is contour enclosing the solutions of $n-3$ scattering equations. This is defined as the intersection $\gamma = \bigcap_{a\neq b,c,d} \gamma_{S_a}$, where γ_{S_a} encircles the poles of S_a [3]. The other factors in the integrand come from the gauge fixing process. To evaluate, we choose a specific theory integrand and n

and use a global residue theorem to wrap the contour around the other poles in the integrand and compute the integral as a sum of those residues. We will demonstrate this below for some simple (four-point) examples. More detailed calculations can be found in [3, 71, 147].

5.2.1 Cosmological Scattering Equations

The cosmological scattering equations were introduced in [62] and used to compute wavefunction coefficients for ϕ^4 in de Sitter. Here we will present the uplift from flat space and how it can be extended to the EFT integrands discussed above. The key point is that kinematic invariants appearing in the scattering equations and integrand will be replaced with the Casimir operators introduced in section 5.1. These will then act on a contact diagram made from a product of bulk-to-boundary propagators. Since these operators do not commute in general, there is an ordering ambiguity. We will always place the integrand to the right, acting directly on the contact diagram and then arrange expressions such that the final results are free from such ambiguities as was done in [3].

We first uplift the scattering equations, replacing $k_a \cdot k_b$ in (5.2.1) with mass-deformed differential operators acting in the future boundary

$$S_a = \sum_{\substack{b=1 \\ b\neq a}}^{n} \frac{2\left(\mathcal{D}_a \cdot \mathcal{D}_b\right) + \mu_{ab}}{\sigma_{ab}} \equiv \sum_{\substack{b=1 \\ b\neq a}}^{n} \frac{\alpha_{ab}}{\sigma_{ab}} \,, \tag{5.2.14}$$

where $\mu_{a\,a\pm1} = -m^2$ modulo n and zero otherwise. This mass deformation is analogous to the flat space one in [147] and assumes canonical ordering of the external legs $\mathbb{I}_n = (1, 2, \ldots, n)$. These are referred to as cosmological scattering equations (CSE). The conformal Ward identities (CWIs) can be expressed in terms of these mass-deformed operators as

$$\sum_{b\neq a} \alpha_{ab} \Psi_n = 0, \tag{5.2.15}$$

where a is any external leg and we sum over b. This implies an underlying $\mathrm{SL}(2,\mathbb{C})$ symmetry in the scattering equations, just like in flat space and again this symmetry

can be used to fix the location of three punctures. More details on this can be found it [63].

The worldsheet formula in (5.2.13) can then be lifted to de Sitter space such that a generic tree-level wavefunction coefficient is given by

$$\Psi_n = \delta^{(d)}(\boldsymbol{k}_T) \int_\gamma \prod_{a\neq b,c,d}^{n} \mathrm{d}\sigma_a \, S_a^{-1} (\sigma_{bc}\sigma_{cd}\sigma_{db})^2 \, \mathcal{I}_n \mathcal{C}_n^{\Delta}, \tag{5.2.16}$$

where both the CSE and integrand can contain boundary conformal generators. For theories with ϕ^n interactions, we are free to shuffle the CSE with other terms in the integrand $\mathcal{I}_n$ [63]. This may not be the case in general (eg for a theory with derivative interactions) and so we will keep the ordering fixed. So far it is only understood how to use this formula to calculate scalar wavefunction coefficients but it is hoped that in the future it can be extended to include propagators with spin.

Of the matrices discussed in flat space, only the A-matrix in equation (5.2.3) needs uplifting (the B and C matrices are not needed for EFTs while the X matrix requires no adjustments). The obvious uplift to de Sitter is by making the same replacement as was used to obtain the CSE. We therefore now define the elements of the matrix A as

$$A_{rs} = \begin{cases} \dfrac{\alpha_{rs}}{\sigma_{rs}}, & r \neq s, \\ 0, & r = s, \end{cases} \tag{5.2.17}$$

with the operator α_{ab} as defined in (5.2.14). As discussed previously, theories with higher-derivative interactions can have curvature corrections that are absent in flat space. Therefore, we cannot simply lift the flat space integrands in section 2.5.1 to dS by replacing kinematic invariants with differential operators. This procedure has to be supplemented by curvature corrections and mass deformations, which we will describe in the following subsections.

5.3 EFTs in de Sitter

Our strategy in this section will be to lift the effective actions in section 2.5.1 to de Sitter space for four-point interactions, use them to compute the four-point wavefunction coefficients using Witten diagrams, and express the result in terms of boundary conformal generators acting on a contact term. We will see that the conformal generators $\hat{s}_{ab}$ introduced below equation (5.1.7) will play the role of Mandelstam variables. For example they satisfy

$$\hat{s}_{12} + \hat{s}_{14} + \hat{s}_{13} = m^2, \tag{5.3.1}$$

when acting on contact diagrams. This can be seen using the CWIs in (2.3.19).
In de Sitter space, the expansion of the NLSM Lagrangian up to four points can be written as

$$\frac{\mathcal{L}_4^{\text{NLSM}}}{\sqrt{|g|}} = -\text{Tr}\{\frac{1}{2}(\nabla\Phi)^2 + \frac{1}{2}m^2\Phi^2 + \lambda^2\Phi^2(\nabla\Phi)^2 + \tfrac{1}{4}C\Phi^4\}, \tag{5.3.2}$$

where we have included a mass term and a possible quartic interaction coming from a curvature correction (recall we have set the dS radius to one). We use $(\nabla\Phi)^{2n} = (\nabla_\mu\Phi\nabla^\mu\Phi)^n$ analogous to the shorthand in section 2.5.1. The mass is also proportional to the curvature and vanishes in the flat space limit. Using the identity (5.1.7), it is straightforward to show that the four-point wavefunction coefficient obtained from Witten diagrams is given by

$$\Psi_4^{\text{NLSM}} = \left[2\lambda^2\left(\hat{s}_{12} + \hat{s}_{14}\right) - C\right]\mathcal{C}_4^\Delta = -\left(2\lambda^2\hat{s}_{13} + C - m^2\right)\mathcal{C}_4^\Delta, \tag{5.3.3}$$

where we have suppressed the delta function conserving boundary momentum $\delta^3(\boldsymbol{k}_T)$. The DBI and sGal 4pt wavefunction coefficients can both be obtained as special cases of the same Lagrangian. Up to quartic vertices and six-derivative interactions, the most general effective action for a scalar field in (A)dS is given by [148]

$$\begin{aligned} S_4^{(6)} = -\int d^4x\sqrt{|g|}\Big\{&\frac{1}{2}(\nabla\phi)^2 + \frac{1}{2}m^2\phi^2 \\ &+ \frac{1}{8}A(\nabla_\mu\nabla_\nu\phi)^2(\nabla\phi)^2 + \frac{1}{8}B(\nabla\phi)^4 + \tfrac{1}{4!}C\phi^4\Big\}, \end{aligned} \tag{5.3.4}$$

where A, B, and C are undetermined numerical coefficients. Other possible interactions are related by integration by parts or the free equation of motion $\nabla^2\phi = -m^2\phi$. For the sGal theory, the 6-derivative interaction is the naive uplift of the one in (2.5.10) while the lower-derivative interactions correspond to curvature corrections and a mass term. In the flat space limit, these are subleading and the action reduces to (2.5.10) for $A = \lambda$. Hence, (5.3.4) represents the uplift of the special Galileon theory to a curved background, with unfixed coefficients corresponding to curvature corrections. Additional data must be specified in order to fix them, such as soft limits, and we will explore this chapter 6. For the DBI theory, we set $A = 0, B = \lambda$, and there is a single curvature correction with unfixed coefficient C. In the flat space limit, the action reduces to (2.5.7) up to quartic interactions.

The four-point wavefunction coefficient obtained from (5.3.4) is

$$\Psi_4^{(6)} = [A(\hat{s}_{12}^3 + \hat{s}_{14}^3 + \hat{s}_{13}^3) + (dA - B)(\hat{s}_{12}^2 + \hat{s}_{14}^2 + \hat{s}_{13}^2) - C]\mathcal{C}_4^{\Delta}. \tag{5.3.5}$$

The four-derivative interaction can be evaluated using partial derivatives so its Witten diagram can be evaluated analogously to the NLSM. The six-derivative term is more complicated as it has covariant derivatives acting on $\partial_\mu\phi$. We therefore need to expand in terms of the de Sitter Christoffel symbols. This gives

$$\begin{aligned}(\nabla\phi)^2\,(\nabla_\mu\nabla_\nu\phi)^2 &= \eta^6\eta^{\mu\nu}\eta^{\rho\sigma}\eta^{\kappa\lambda}(\nabla_\mu\phi)(\nabla_\nu\phi)(\nabla_\rho\nabla_\kappa\phi)(\nabla_\sigma\nabla_\lambda\phi),\\ &= \eta^6(\partial_\mu\phi\partial^\mu\phi)\eta^{\rho\sigma}\eta^{\kappa\lambda}(\partial_\rho\partial_\kappa - \Gamma^\alpha_{\rho\kappa}\partial_\alpha\phi)(\partial_\sigma\partial_\lambda\phi - \Gamma^\beta_{\sigma\lambda}\partial_\beta\phi).\end{aligned} \tag{5.3.6}$$

This produces the Witten diagram expression

$$\begin{aligned}\int_{-\infty}^0 \frac{d\eta}{\eta^4}\eta^6\Big[&(\boldsymbol{k}_1\cdot\boldsymbol{k}_2)^2\phi_1\phi_2 + 2\boldsymbol{k}_1\cdot\boldsymbol{k}_2\dot{\phi}_1\dot{\phi}_2 + \ddot{\phi}_1\ddot{\phi}_2\\ &+ \frac{1}{\eta}\left(2\boldsymbol{k}_1\cdot\boldsymbol{k}_2(\phi_1\dot{\phi}_2 + \dot{\phi}_1\phi_2) - k_1^2\phi_1\dot{\phi}_2 - k_2^2\dot{\phi}_1\phi_2 + \dot{\phi}_1\ddot{\phi}_2 + \ddot{\phi}_1\dot{\phi}_2\right)\\ &+ \frac{2}{\eta^2}\left(\boldsymbol{k}_1\cdot\boldsymbol{k}_2\phi_1\phi_2 + 2\dot{\phi}_1\dot{\phi}_2\right)\Big]\Big[\boldsymbol{k}_3\cdot\boldsymbol{k}_4\phi_3\phi_4 + \dot{\phi}_3\dot{\phi}_4\Big] + \text{Perms},\end{aligned} \tag{5.3.7}$$

where we have used the shorthand $\partial_\eta \phi = \dot{\phi}$. This is to be compared to the cubic action of operators

$$\begin{aligned}\hat{s}_{12}^2 \hat{s}_{34} \phi_1 \phi_2 = \eta^4 \Big[& (\boldsymbol{k}_1 \cdot \boldsymbol{k}_2)^2 \phi_1 \phi_2 + 2 \boldsymbol{k}_1 \cdot \boldsymbol{k}_2 \dot{\phi}_1 \dot{\phi}_2 + \ddot{\phi}_1 \ddot{\phi}_2, \\ & + \frac{1}{\eta} \left(2 \boldsymbol{k}_1 \cdot \boldsymbol{k}_2 \left(\phi_1 \dot{\phi}_2 + \dot{\phi}_1 \phi_2 \right) - k_1^2 \phi_1 \dot{\phi}_2 - k_2^2 \dot{\phi}_1 \phi_2 + \dot{\phi}_1 \ddot{\phi}_2 + \ddot{\phi}_1 \dot{\phi}_2 \right) \\ & + \frac{1}{\eta^2} \left((2-d) \boldsymbol{k}_1 \cdot \boldsymbol{k}_2 \phi_1 \phi_2 + \dot{\phi}_1 \dot{\phi}_2 \right) \Big] \left[\boldsymbol{k}_3 \cdot \boldsymbol{k}_4 \phi_3 \phi_4 + \dot{\phi}_3 \dot{\phi}_4 \right],\end{aligned} \tag{5.3.8}$$

which makes it apparent that the only difference is in the 3rd line. In general dimensions, these are related by

$$-\frac{1}{8} \left(\nabla_\mu \nabla_\nu \phi \right)^2 \left(\nabla \phi \right)^2 \to \left[\hat{s}_{12}^3 + \hat{s}_{13}^3 + \hat{s}_{14}^3 + d \left(\hat{s}_{12}^2 + \hat{s}_{13}^2 + \hat{s}_{14}^2 \right) \right] \mathcal{C}_4^\Delta, \tag{5.3.9}$$

where we restored the symmetry factor on the left-hand side and used the 4pt conformal Ward identity $\hat{s}_{12} = \hat{s}_{34}$. This recovers the full wavefunction coefficient in equation 5.3.5.

5.3.1 Four-point CSE Examples

To explore the four-point EFT wavefunction coefficients we will focus on the four basic building blocks for the four-point integrands as summarised in table 5.1. Here we will describe each of them, explaining how to evaluate the corresponding worldsheet integrals.

The simplest building block is

$$\mathcal{I}^{\phi^4} = \mathrm{PT}\ \mathrm{Pf} X|_{\mathrm{conn}}\, \mathrm{Pf}' A, \tag{5.3.10}$$

where the matrix X is defined in (5.2.10) and

$$\mathrm{Pf}\, X = \frac{1}{\sigma_{12}\sigma_{34}} - \frac{1}{\sigma_{13}\sigma_{24}} + \frac{1}{\sigma_{23}\sigma_{14}}, \tag{5.3.11}$$

$$\mathrm{Pf}\, X|_{\mathrm{conn}} = -\frac{1}{\sigma_{13}\sigma_{24}}. \tag{5.3.12}$$

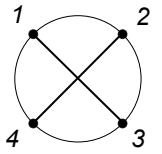

Figure 5.1: Graphic representation of $\mathrm{PT}\,\mathrm{Pf}X|_{\mathrm{conn}}$. The circle refers to the PT factor while the intersecting lines correspond to $\mathrm{Pf}X|_{\mathrm{conn}}$.

The integrand (5.3.10) describes a contact diagram for a ϕ^4 interaction [62, 68]. Note that at four-points, Pf X can be written as a sum of three terms which correspond to perfect matchings and $\mathrm{Pf}X|_{\mathrm{conn}}$ refers to the connected perfect matching with respect to the ordering of the Parke-Taylor factor (see Figure 5.1). Fixing legs $\{1,2,4\}$ and deleting legs $\{2,4\}$ from the A-matrix in the Pfaffian leads to the wavefunction coefficient

$$\Psi_4^{\phi^4} = -\int_{\gamma_3} d\sigma_3 \left(\sigma_{41}\sigma_{12}\sigma_{24}\right)^2 \left[\frac{1}{\sigma_{12}\sigma_{23}\sigma_{34}\sigma_{41}} \frac{\sigma_{13}\sigma_{23}\sigma_{43}}{\hat{S}_3} \frac{\alpha_{13}}{\left(\sigma_{13}\sigma_{24}\right)^2}\right] \mathcal{C}_4^{\Delta}, \tag{5.3.13}$$

where the contour γ_3 encircles the pole arising from S_3. The first term in the integrand is the standard Jacobian associated with the $\mathrm{SL}(2,\mathbb{C})$ fixing, and we have rescaled the third scattering equation to

$$\hat{S}_3 = \alpha_{13}\sigma_{23}\sigma_{43} + \alpha_{23}\sigma_{13}\sigma_{43} + \alpha_{43}\sigma_{13}\sigma_{23}. \tag{5.3.14}$$

After some cancellations we see there is only a simple pole at $\sigma_{13} = 0$ so we wrap the contour around this pole to obtain

$$\Psi_4^{\phi^4} = \int_{\gamma_3} d\sigma_3 \left[\frac{\sigma_{41}\sigma_{12}}{\sigma_{13}} \frac{1}{\hat{S}_3}\alpha_{13}\right] \mathcal{C}_4 = -\int_{\sigma_{13}} d\sigma_3 \left[\frac{\sigma_{41}\sigma_{12}}{\sigma_{13}} \frac{1}{\hat{S}_3}\alpha_{13}\right] \mathcal{C}_4^{\Delta}. \tag{5.3.15}$$

Computing the residue then gives

$$\Psi_4^{\phi^4} = -\left[\left.\frac{\sigma_{12}\sigma_{41}}{\hat{S}_3}\right|_{\sigma_{13}=0} \alpha_{13}\right] \mathcal{C}_4^{\Delta} = \mathcal{C}_4^{\Delta}. \tag{5.3.16}$$

Next we consider the naive uplifts of the flat space integrands of section 2.5.1. Note

that these uplifts will not describe the full four-point wavefunction coefficients in dS because they will be missing mass deformations and curvature corrections. We will explain how to encode these additional terms in the worldsheet integrands in the next chapter. The naive uplift of the NLSM integrand in 5.1 is given by

$$\mathcal{I}^{\text{NLSM}} = \text{PT}\left(\text{Pf}'A\right)^2. \tag{5.3.17}$$

As before, we will fix legs $\{1,2,4\}$ and delete legs $\{2,4\}$ from the A-matrix to obtain

$$\Psi_4^{\text{NLSM}} = \int_{\gamma_3} d\sigma_3 \left(\sigma_{41}\sigma_{12}\sigma_{24}\right)^2 \left[\frac{1}{\sigma_{12}\sigma_{23}\sigma_{34}\sigma_{41}} \frac{\sigma_{13}\sigma_{23}\sigma_{43}}{\hat{S}_3} \left(\frac{\alpha_{13}}{\sigma_{13}\sigma_{24}}\right)^2\right] \mathcal{C}_4^{\Delta}. \tag{5.3.18}$$

After simplifying the integrand there is once again a simple pole at $\sigma_{13} = 0$, so we wrap the contour around this pole:

$$\Psi_4^{\text{NLSM}} = -\int_{\gamma_3} d\sigma_3 \left[\frac{\sigma_{12}\sigma_{41}}{\sigma_{13}} \frac{1}{\hat{S}_3} \alpha_{13}^2\right] \mathcal{C}_4^{\Delta} = \int_{\sigma_{13}=0} d\sigma_3 \left[\frac{\sigma_{12}\sigma_{41}}{\sigma_{13}} \frac{1}{\hat{S}_3} \alpha_{13}^2\right] \mathcal{C}_4^{\Delta}. \tag{5.3.19}$$

Evaluating the residue of this pole finally gives

$$\Psi_4^{\text{NLSM}} = \left[\frac{\sigma_{12}\sigma_{41}}{\hat{S}_3}\bigg|_{\sigma_{13}=0} \alpha_{13}^2\right] \mathcal{C}_4^{\Delta} = -\alpha_{13}\, \mathcal{C}_4^{\Delta}. \tag{5.3.20}$$

Extending this calculation to six points involves dealing with a number of subtleties that can arise for worldsheet descriptions of theories with derivative interactions, such as the presence of higher-order poles and potential ordering ambiguities. These are considered in detail in [3]. In chapter 6 these will be side-stepped by instead lifting the flat space calculation directly to an operator form before checking it behaves as expected in the soft limit.

Now we analyse the naive uplift of the DBI integrand,

$$\mathcal{I}^{\text{DBI}} = \text{Pf}X \left(\text{Pf}'A\right)^3. \tag{5.3.21}$$

Fixing legs $\{1,2,4\}$ as above, we find

$$\Psi_4^{\text{DBI}} = \int_{\gamma_3} d\sigma_3 (\sigma_{14}\sigma_{12}\sigma_{24})^2 \left[\text{Pf}X \frac{1}{S_3} \left(\text{Pf}'A\right)^3\right] \mathcal{C}_4^{\Delta}. \tag{5.3.22}$$

Recall from (5.3.11) that PfX has three terms. To evaluate the worldsheet integral containing the first term, it is convenient to choose $(\mathrm{Pf}'A)^3 = (\mathrm{Pf}A^{23}_{23})^2(\mathrm{Pf}A^{24}_{24})$ such that

$$\Psi_4^{12,34} = \int_{\gamma_3} d\sigma_3 \frac{(\sigma_{14}\sigma_{12}\sigma_{24})^2}{\sigma_{12}\sigma_{34}} \left[\frac{\sigma_{13}\sigma_{23}\sigma_{43}}{\hat{S}_3}\left(\frac{\alpha_{14}}{\sigma_{14}\sigma_{23}}\right)^2 \frac{\alpha_{13}}{\sigma_{13}\sigma_{24}}\right] \mathcal{C}_4^{\Delta}, \tag{5.3.23}$$

where the superscript on Ψ_4 denotes the contribution from the first term in (5.3.11). The contour integral can be evaluated as above to obtain

$$\Psi_4^{12,34} = \left[\frac{\sigma_{12}\sigma_{24}}{\hat{S}_3}\bigg|_{\sigma_{23}=0} \alpha_{14}^2\alpha_{13}\right] \mathcal{C}_4^{\Delta} = -\alpha_{14}\alpha_{13}\mathcal{C}_4^{\Delta}, \tag{5.3.24}$$

where we wrapped the contour around the pole $\sigma_{23} = 0$, evaluated the residue, and used the CWI to cancel α_{23} in the denominator with α_{14} in the numerator. Note that the ordering of α_{14} and α_{13} in the final result is not important since the two operators commute when acting on a contact diagram as demonstrated in (5.1.8). For the remaining two terms in (5.3.22) we choose $(\mathrm{Pf}'A)^3$ to be $(\mathrm{Pf}A^{14}_{14})^2(\mathrm{Pf}A^{12}_{12})$ and $(\mathrm{Pf}A^{13}_{13})^2(\mathrm{Pf}A^{12}_{12})$, respectively. Using similar manipulations, we finally obtain

$$\Psi_4^{\mathrm{DBI}} = -\left(\alpha_{12}\alpha_{14} + \alpha_{14}\alpha_{13} + \alpha_{13}\alpha_{12}\right)\mathcal{C}_4^{\Delta}. \tag{5.3.25}$$

This choice of Pfaffians avoids higher-order poles in the worldsheet coordinates which are more subtle to evaluate. Examples with such poles are discussed in more detail in [3].

In the next subsection it will also be useful to consider the following integrand, whose corresponding wavefunction coefficient follows trivially from the above calculation:

$$(\mathrm{Pf}'A)^3\ \mathrm{Pf}X|_{\mathrm{conn}} \to -\alpha_{12}\alpha_{14}\mathcal{C}_4^{\Delta}. \tag{5.3.26}$$

Finally, let us consider the naive uplift of the special Galileon integrand

$$\mathcal{I}^{\mathrm{sGal}} = \left(\mathrm{Pf}'A\right)^4. \tag{5.3.27}$$

In this case, the four-point wavefunction coefficient is given by

$$\Psi_4^{\text{sGal}} = \int_{\gamma_3} d\sigma_3 \, (\sigma_{14}\sigma_{12}\sigma_{24})^2 \left[\frac{1}{S_3}\left(\text{Pf}'A\right)^4\right] \mathcal{C}_4^{\Delta}. \tag{5.3.28}$$

As in the DBI case, there are Pfaffian choices exclusively leading to simple poles. The following choice leads to a permutation invariant result:

$$(\text{Pf}'A)^4 = \frac{1}{3}\left\{\frac{1}{\sigma_{34}^2}(\text{Pf}A_{34}^{34})^2 \, \frac{(-1)}{\sigma_{23}}(\text{Pf}A_{23}^{23})\frac{1}{\sigma_{24}}\,(\text{Pf}A_{24}^{24}) + \text{cyclic}(2,3,4)\right\}. \tag{5.3.29}$$

Note that other choices can give different results due to non-trivial commutators which only vanish in the flat space limit. Hence we must specify a choice of Pfaffian. Following closely the computations above, we obtain

$$\Psi_4^{\text{sGal}} = \frac{1}{3}\left(\alpha_{12}\alpha_{14}\alpha_{13} + \alpha_{14}\alpha_{13}\alpha_{12} + \alpha_{13}\alpha_{14}\alpha_{12}\right)\mathcal{C}_4^{\Delta}. \tag{5.3.30}$$

Using the commutation properties in (5.1.8) it is not difficult to see that the above expression is permutation invariant.

5.3.2 Generalised Double Copy

Using the building blocks in the previous subsection (in particular (5.3.16) and (5.3.20)), we see that the four-point NLSM wavefunction coefficient (including a curvature correction) in (5.3.3) follows from the following integrand:

$$\mathcal{I}_4^{\text{NLSM}} = \lambda^2 \text{PT}\left(\text{Pf}'A\right)^2 + c\text{PT}\;\text{Pf}X|_{\text{conn}}\,\text{Pf}'A, \tag{5.3.31}$$

if we identify the unfixed parameter c with $-C$. Now consider the following shift of the first term in (5.3.31):

$$\lambda^2\text{PT} \to a\text{Pf}'A\left(\text{Pf}'A + m^2\;\text{Pf}X|_{\text{conn}}\right) + b\left(\text{Pf}'A\text{Pf}X + m^2\text{PT}\right), \tag{5.3.32}$$

where a and b are also free coefficients. We then obtain the following integrand:

$$\begin{aligned}\mathcal{I}_4^{(6)} = {} & a(\text{Pf}'A)^3(\text{Pf}'A + m^2\;\text{Pf}X|_{\text{conn}}) \\ & + b(\text{Pf}'A)^2(\text{Pf}'A\text{Pf}X + m^2\text{PT}) + c\text{PT}\;\text{Pf}X|_{\text{conn}}\,\text{Pf}'A.\end{aligned} \tag{5.3.33}$$

Using the prescription for evaluating worldsheet integrals described the previous subsection (in particular (5.3.16), (5.3.20), (5.3.25), (5.3.26), and (5.3.30)), we see that the corresponding wavefunction coefficient is

$$\Psi_4^{(6)} = \left[\frac{8}{3}a(\tilde{s}_{12}\tilde{s}_{14}\tilde{s}_{13} + \tilde{s}_{14}\tilde{s}_{13}\tilde{s}_{12} + \tilde{s}_{13}\tilde{s}_{12}\tilde{s}_{14}) - 4b(\tilde{s}_{12}\tilde{s}_{14} + \tilde{s}_{14}\tilde{s}_{13} + \tilde{s}_{13}\tilde{s}_{12}) + c\right]\mathcal{C}_4^{\Delta}, \tag{5.3.34}$$

where $\tilde{s}_{ab}$ is related to $\hat{s}_{ab}$ (5.1.6) by

$$\tilde{s}_{ab} = \hat{s}_{ab} - \tfrac{1}{2}m^2. \tag{5.3.35}$$

It is then straightforward to match (5.3.34) with (5.3.5) via the following identification of unfixed coefficients:

$$A = \tfrac{8}{3}a, \;\; B = 2a\left(m^2 + \tfrac{4}{3}d\right) - 2b, \;\; C = -\tfrac{1}{3}am^6 + bm^4 - c. \tag{5.3.36}$$

Hence, the worldsheet integrand (5.3.33) encodes the effective action in (5.3.4). Moreover, (5.3.32) can be thought of as a double copy procedure encoding mass deformations and curvature corrections. In particular, it reduces to (5.2.12) and (5.2.11) in the flat space limit for $a \neq 0$ and $a = 0$, respectively (recalling that the mass is measured in units of the inverse dS radius). We therefore refer to this as a generalised double copy. Note that this prescription leaves the curvature corrections and mass deformations unfixed. To fix these coefficients, we must specify additional data beyond the flat space limit, this is explored in chapter 6.

5.3.3 Explicit Results for Conformal & Minimal Scalars

In the previous section, we found the building blocks of four-point wavefunction coefficients of scalar EFTs in dS to be

$$\mathcal{C}_4^{\Delta}, \;\; \hat{s}_{13}\mathcal{C}_4^{\Delta}, \;\; \left(\hat{s}_{12}^2 + \hat{s}_{14}^2 + \hat{s}_{13}^2\right)\mathcal{C}_4^{\Delta}, \;\; \left(\hat{s}_{12}^3 + \hat{s}_{14}^3 + \hat{s}_{13}^3\right)\mathcal{C}_4^{\Delta}, \tag{5.3.37}$$

for notational simplicity, we will continue to leave out the delta function imposing momentum conservation along the boundary. The first one is a ϕ^4 contact diagram,

while the remaining building blocks arise from the action on this contact diagram with the differential operators defined in (5.1.6). The first two terms contribute when lifting NLSM to dS, while the last two arise when lifting the DBI and sGal theories. In this section, we will compute these objects explicitly in the cases $\Delta = 2, 3$ and analyse their soft limits. In practice, all the integrals we encounter will be of the form $\int_{-\infty}^{0} \eta^{\alpha} e^{-iE\eta} d\eta$. To evaluate them, we rotate the contour clockwise onto the complex plane so that the integrand is exponentially damped as $\eta \to -\infty$ [47]. To simplify our expressions we will set the normalisation of the bulk-to-boundary propagators in (5.1.2) to be $\mathcal{N} = (-1)^{\nu-\frac{1}{2}} \sqrt{2/\pi}$.

We will show that the soft limits of the building blocks in (5.3.37) are given in terms of boundary conformal generators acting on certain three-point contact diagrams. Soft limits play an important role in cosmology where they appear in constraints relating higher-point functions to symmetry transformations of lower-point functions [57, 149–151] and allow one to deduce 3-point inflationary correlators from four-point dS correlators [55, 152–155]. Soft limits of DBI and sGal wavefunction coefficients in flat space were recently analysed in [156]. Note that the soft limit of the four-point wavefunction coefficients in (5.3.3) and (5.3.5) can be obtained from linear combinations of soft limits we derive in this section. This analysis will be generalised in chapter 6 to arbitrary d and Δ and it will be demonstrated that soft limits of wavefunction coefficients are in fact linked to symmetries of the Lagrangian allowing us to fix the mass and curvature corrections in the naive uplifts in section 5.3.2.

Contact diagram

Let us first consider the four-point contact diagram. For conformally coupled scalars, we find

$$\mathcal{C}_4^{\Delta=2} = \int \frac{d\eta}{\eta^4} \left(\prod_{a=1}^{4} \phi_a^{1/2} \right) = \frac{1}{E}. \tag{5.3.38}$$

It is trivial to see that the soft limit of this quantity corresponds to a three-point contact diagram for conformally coupled scalars with a time-dependent interaction

$$\lim_{\boldsymbol{k}_1\to 0} C_4^{\Delta=2} = \mathcal{C}_{3,\eta}^{\Delta=2}, \tag{5.3.39}$$

where

$$\mathcal{C}_{3,\eta}^{\Delta=2} = \int \frac{d\eta}{\eta^4}\left(\eta \prod_{a=2}^{4}\phi_a^{1/2}\right) = \frac{1}{E}. \tag{5.3.40}$$

This three-point contact diagram will also arise in the soft limit of more complicated four-point wavefunction coefficients of conformally coupled scalars. In particular, we will obtain conformal generators acting on (5.3.40).

For minimally coupled scalars, the integrals need to be regulated. We will use the prescription $d \to d+2\epsilon$, $\Delta \to \Delta+\epsilon$, which leaves the spectral parameter $\nu = \Delta - d/2$ unchanged [157–160], such that

$$\begin{aligned}\mathcal{C}_4^{\Delta=3+\epsilon} &= \int \frac{d\eta}{\eta^{4+2\epsilon}}\prod_{a=1}^{4}\phi_a^{3/2},\\ &= \frac{1}{E^{2\epsilon}}\Big\{E^3[\Gamma(-2+2\epsilon)+\Gamma(-3+2\epsilon)] + \Gamma(2\epsilon)(k_1k_2k_3+\ldots)\\ &+ \Gamma(-1+2\epsilon)E\,(k_1k_2+\ldots) + \frac{k_1k_2k_3k_4}{E}\Gamma(1+2\epsilon)\Big\},\end{aligned} \tag{5.3.41}$$

where the ellipsis inside each parenthesis denotes a sum over permutations of all four legs. We then find the following soft limit:

$$\begin{aligned}\lim_{\boldsymbol{k}_1\to 0}\mathcal{C}_4^{\Delta=3+\epsilon} = \frac{1}{E^{2\epsilon}}\{&E^3[\Gamma(-2+2\epsilon)+\Gamma(-3+2\epsilon)] + \Gamma(2\epsilon)k_2k_3k_4\\ &+\Gamma(-1+2\epsilon)E(k_2k_3+k_2k_4+k_3k_4)\}.\end{aligned} \tag{5.3.42}$$

We can now compare this with the three-point contact diagram of minimally coupled scalars:

$$\mathcal{C}_3^{\Delta=3+\epsilon} = \int \frac{d\eta}{\eta^{4+2\epsilon}}\prod_{a=2}^{4}\phi_a^{3/2}. \tag{5.3.43}$$

Unlike the contact diagram in (5.3.40), this contact diagram does not contain a time-dependent interaction. After performing the integral in (5.3.43) and changing

$\epsilon \to 2\epsilon$, we finally obtain (5.3.42):

$$\lim_{\boldsymbol{k}_1 \to 0} C_4^{\Delta=3+\epsilon} = \mathcal{C}_3^{\Delta=3+2\epsilon}, \tag{5.3.44}$$

which, for clarity, can be easily expanded in ϵ:

$$\mathcal{C}_3^{\Delta=3+\epsilon} = \frac{k_2^3 + k_3^3 + k_4^3}{3}\left(\frac{1}{\epsilon} - \gamma_E - \ln E + 1\right) + \frac{1}{9}E^3 - k_2 k_3 k_4 + \mathcal{O}(\epsilon), \tag{5.3.45}$$

where γ_E is the Euler-Mascheroni constant. As we will see, (5.3.43) will continue to play a role in the soft limit of more complicated four-point wavefunction coefficients of minimally coupled scalars.

Two Derivatives

Next, we will analyse the soft limit of $\hat{s}_{13}\mathcal{C}_4^{\Delta}$. In the conformally coupled case, the conformal time integral can be evaluated to get

$$\hat{s}_{13}\mathcal{C}_4^{\Delta=2} = -\frac{2}{E^3}[\boldsymbol{k}_1 \cdot \boldsymbol{k}_3 - k_1 k_3 - \frac{E}{2}(k_2 + k_4)], \tag{5.3.46}$$

with soft limit

$$\lim_{\boldsymbol{k}_1 \to 0} \hat{s}_{13}\mathcal{C}_4^{\Delta=2} = \frac{1}{E} - \frac{k_3}{E^2}. \tag{5.3.47}$$

We recognise this expression as the dilatation operation:

$$D_3\left(\frac{1}{E}\right) = \frac{1}{E} - \frac{k_3}{E^2}. \tag{5.3.48}$$

Hence, we find that the soft limit of (5.3.46) can be obtained by acting with a dilatation on the three-point contact diagram of (5.3.40):

$$\lim_{\boldsymbol{k}_1 \to 0} \hat{s}_{13}\mathcal{C}_4^{\Delta=2} = D_3\, \mathcal{C}_{3,\eta}^{\Delta=2}. \tag{5.3.49}$$

In the minimally coupled case, we find

$$\hat{s}_{13}\mathcal{C}_4^{\Delta=3} = \frac{\boldsymbol{k}_1\cdot\boldsymbol{k}_3}{E}\left[-E^2+\sum_{a<b}k_ak_b+\frac{k_1k_2k_3k_4}{E}\left(\frac{1}{k_1}+\frac{1}{k_2}+\frac{1}{k_3}+\frac{1}{k_4}+\frac{2}{E}\right)\right] - \frac{k_1^2k_3^2}{E}\left(1+\frac{k_2+k_4}{E}+\frac{2k_2k_4}{E^2}\right), \tag{5.3.50}$$

which requires dimensional regularisation in intermediate steps but has a finite output. Taking the soft limit then gives

$$\lim_{\boldsymbol{k}_1\to 0}\hat{s}_{13}\mathcal{C}_4^{\Delta=3} = \frac{\boldsymbol{k}_1\cdot\boldsymbol{k}_3}{E}\left(k_2^2+k_3^2+k_4^2+k_2k_3+k_3k_4+k_4k_2-\frac{k_2k_3k_4}{E}\right), \tag{5.3.51}$$

which can be obtained by acting with a conformal boost on the three-point contact diagram in (5.3.43):

$$\lim_{\boldsymbol{k}_1\to 0}\hat{s}_{13}\mathcal{C}_4^{\Delta=3} = (\boldsymbol{k}_1\cdot K_3)\,\mathcal{C}_3^{\Delta=3}. \tag{5.3.52}$$

Note that the divergences in (5.3.45) are removed by the action of conformal generators so we set $\epsilon = 0$. This will continue to hold for higher-derivative wavefunction coefficients so we will set $\epsilon = 0$ in those cases as well.

Four Derivatives

We now consider the term $(\hat{s}_{12}^2+\hat{s}_{14}^2+\hat{s}_{13}^2)\mathcal{C}_4^{\Delta}$. For conformally coupled scalars, we obtain

$$(\hat{s}_{12}^2+\hat{s}_{14}^2+\hat{s}_{13}^2)\mathcal{C}_4^{\Delta=2} = \frac{24}{E^5}[(\boldsymbol{k}_1\cdot\boldsymbol{k}_2-k_1k_2)(\boldsymbol{k}_3\cdot\boldsymbol{k}_4-k_3k_4)+\text{cyc}(234)]-\frac{8}{E^3}\sum_{a<b}k_ak_b+\frac{4}{E}. \tag{5.3.53}$$

In this case the soft limit is simply

$$\lim_{\boldsymbol{k}_1\to 0}(\hat{s}_{12}^2+\hat{s}_{14}^2+\hat{s}_{13}^2)\mathcal{C}_4^{\Delta=2} = \frac{4}{E^3}(k_2^2+k_3^2+k_4^2), \tag{5.3.54}$$

which can be recast as a second order combination of dilatation operators acting on the three-point contact diagram of (5.3.40):

$$\lim_{\boldsymbol{k}_1\to 0}(\hat{s}_{12}^2+\hat{s}_{14}^2+\hat{s}_{13}^2)\mathcal{C}_4^{\Delta=2} = 2(D_2^2+D_3^2+D_4^2)\mathcal{C}_{3,\eta}^{\Delta=2}. \tag{5.3.55}$$

In the minimally coupled case, we obtain

$$\begin{aligned}(\hat{s}_{12}^2+\hat{s}_{14}^2+\hat{s}_{13}^2)\mathcal{C}_4^{\Delta=3} &= \frac{24k_1k_2k_3k_4}{E^5}(\boldsymbol{k}_1\cdot\boldsymbol{k}_2-k_1k_2)(\boldsymbol{k}_3\cdot\boldsymbol{k}_4-k_3k_4)\\ &\quad+\frac{2}{E^3}(\boldsymbol{k}_1\cdot\boldsymbol{k}_2)(\boldsymbol{k}_3\cdot\boldsymbol{k}_4)\Big(E^2+E\sum_{a<b}k_ak_b+\sum_{a<b<c}k_ak_bk_c\Big)\\ &\quad-\frac{2}{E^4}[(\boldsymbol{k}_1\cdot\boldsymbol{k}_2)k_3^2k_4^2(E+2(k_1+k_2)+(\boldsymbol{k}_3\cdot\boldsymbol{k}_4)k_1^2k_2^2(E+2(k_3+k_4))+\text{cyc}(234)].\end{aligned} \tag{5.3.56}$$

We then find that the soft limit is given by

$$\begin{aligned}\lim_{\boldsymbol{k}_1\to 0}(\hat{s}_{12}^2+\hat{s}_{14}^2+\hat{s}_{13}^2)\mathcal{C}_4^{\Delta=3} &= \frac{\boldsymbol{k}_1\cdot\boldsymbol{k}_2}{E^3}\Big[4k_2^2k_3k_4+k_2E(k_3k_4+2k_2(k_3+k_4))\\ &\qquad+E^2(2k_2^2+k_2k_3+k_3k_4+k_4k_2)-E^4)\Big]\\ &\quad+\text{cyc}(234),\end{aligned} \tag{5.3.57}$$

which corresponds to applying the following quadratic combination of conformal generators to a three-point contact diagram:

$$\lim_{\boldsymbol{k}_1\to 0}(\hat{s}_{12}^2+\hat{s}_{14}^2+\hat{s}_{13}^2)\mathcal{C}_4^{\Delta=3} = -2\Big[D_2(\boldsymbol{k}_1\cdot K_2)+\text{cyc}(234)\Big]\mathcal{C}_3^{\Delta=3}. \tag{5.3.58}$$

In practice, the soft limits in (5.3.55) and (5.3.58) are most easily derived at the level of the integrand. In particular, this requires taking the soft limit of bulk-to-boundary propagators and their derivatives, and then using equations of motion to remove derivatives acting on the bulk-to-boundary propagator for the soft leg as well as factors of k_a^2. For example, in the conformally coupled case we have

$$\begin{aligned}\lim_{\boldsymbol{k}_1\to 0}(\hat{s}_{12}^2+\hat{s}_{14}^2+\hat{s}_{13}^2)\mathcal{C}_4^{\Delta=2} &= \int d\eta\left(\frac{1}{\eta}(-k_2^2\dot{\phi}_1\phi_2+\dot{\phi}_1\ddot{\phi}_2)-\frac{1}{\eta^2}\dot{\phi}_1\dot{\phi}_2\right)\phi_3\phi_4+\text{cyc}(234),\\ &= \int\frac{d\eta}{\eta^3}[2\eta^2\ddot{\phi}_2-\eta\dot{\phi}_2-2\phi_2]\phi_3\phi_4+\text{cyc}(234),\\ &= 2\left(D_2^2+D_3^2+D_4^2\right)\int\frac{d\eta}{\eta^3}\phi_2\phi_3\phi_4.\end{aligned} \tag{5.3.59}$$

The analogous construction in the minimally coupled case is given by

$$\lim_{\boldsymbol{k}_1\to 0}\left(\hat{s}_{12}^2+\hat{s}_{14}^2+\hat{s}_{13}^2\right)\mathcal{C}_4^{\Delta=3}=(\boldsymbol{k}_1\cdot\boldsymbol{k}_2)\int d\eta\left(\frac{2}{\eta}\phi_1\dot{\phi}_2+\frac{1}{\eta^2}\phi_1\phi_2\right)\phi_3\phi_4+\text{cyc}(234),$$
$$=-2[D_2(\boldsymbol{k}_1\cdot K_2)+\text{cyc}(234)]\int\frac{d\eta}{\eta^4}\phi_2\phi_3\phi_4. \tag{5.3.60}$$

Using this method, one can also derive the soft limits in (5.3.49) and (5.3.52).

Six Derivatives

Finally we consider the six derivative interaction $(\hat{s}_{12}^3+\hat{s}_{14}^3+\hat{s}_{13}^3)\mathcal{C}_4^{\Delta}$. In the conformally coupled case we obtain

$$\begin{aligned}(\hat{s}_{12}^3+\hat{s}_{14}^3+\hat{s}_{13}^3)\mathcal{C}_4^{\Delta=2}=\Big(&\frac{90}{E^7}[\boldsymbol{k}_1\cdot\boldsymbol{k}_2+\boldsymbol{k}_3\cdot\boldsymbol{k}_4-k_1k_2-k_3k_4]^3\\&+\frac{156}{E^5}[\boldsymbol{k}_1\cdot\boldsymbol{k}_2-k_1k_2][\boldsymbol{k}_3\cdot\boldsymbol{k}_4-k_3k_4]\\&-\frac{54}{E^5}(k_1k_2+k_3k_4)[\boldsymbol{k}_1\cdot\boldsymbol{k}_2+\boldsymbol{k}_3\cdot\boldsymbol{k}_4-k_1k_2-k_3k_4]\\&-\frac{79}{E^3}(k_1k_2+k_3k_4)+\text{cyc}(234)\Big)+\frac{93}{4E},\end{aligned} \tag{5.3.61}$$

with soft limit

$$\lim_{\boldsymbol{k}_1\to 0}(\hat{s}_{12}^3+\hat{s}_{14}^3+\hat{s}_{13}^3)\mathcal{C}_4^{\Delta=2}=-\frac{108}{E^4}k_2k_3k_4+\frac{52}{E^3}(k_2k_3+k_3k_4+k_4k_2)-\frac{12}{E}. \tag{5.3.62}$$

Using the methods described above, we can obtain this by acting with the following combination of conformal generators on a three-point contact diagram:

$$\lim_{\boldsymbol{k}_1\to 0}(\hat{s}_{12}^3+\hat{s}_{14}^3+\hat{s}_{13}^3)\mathcal{C}_4^{\Delta=2}=\Big(6(D_2^3+D_3^3+D_4^3)-22(D_2^2+D_3^2+D_4^2)+20\Big)\mathcal{C}_{3,\eta}^{\Delta=2}. \tag{5.3.63}$$

In the minimally coupled case, the expression for the integrated wavefunction coefficient can be found in appendix E.1. The soft limit is given by

$$\lim_{\boldsymbol{k}_1\to 0}(\hat{s}_{12}^3+\hat{s}_{14}^3+\hat{s}_{13}^3)\mathcal{C}_4^{\Delta=3}=\frac{(\boldsymbol{k}_1\cdot\boldsymbol{k}_2)}{E^4}\big[3k_2^5+12k_2^4(k_3+k_4)+k_2^3(k_3^2+36k_3k_4+k_4^2)$$
$$-k_2^2(k_3+k_4)(11k_3^2+21k_3k_4+11k_4^2)-4k_2(k_3+k_4)^2(k_3^2+k_3k_4+k_4^2)$$

$$- (k_3 + k_4)^3(k_3^2 + k_3k_4 + k_4^2)\Big] + \text{cyc}(234). \quad (5.3.64)$$

This expression can also be recast in terms of conformal generators acting on a three-point contact diagram. For example, we can write

$$\lim_{\boldsymbol{k}_1 \to 0} (\hat{s}_{12}^3 + \hat{s}_{14}^3 + \hat{s}_{13}^3)\mathcal{C}_4^{\Delta=3} = [2(3D_2^2 - 11D_2)(\boldsymbol{k}_1 \cdot K_2) + \text{cyc}(234)]\mathcal{C}_3^{\Delta=3}. \quad (5.3.65)$$

Observe that these expressions are not unique. For example, the operators K_2 and D_2 do not commute and so we could choose to order them differently and pick up different coefficients. Note also that unlike (5.3.63), the term in brackets in (5.3.65) contains no constant term. This comes from the different behavior of the soft limits for different values of Δ. The constant term in (5.3.63) arises from $D_2 + D_3 + D_4$ and the equivalent term in the case of massless scalars would be a sum over $\boldsymbol{k}_1 \cdot K_i$. We can rewrite this using CWI to get a contribution of order k_1^2 which we then drop as it is subleading.

That all these soft limits can be written in terms of the action of conformal generators is an interesting feature. Considering $d = 3$ with $\Delta = 2, 3$ are special cases however.

The soft limits for the minimal scalar are all of order $\mathcal{O}(k)$ (except the ϕ^4 contact) whilst the conformal scalar limits are all non-vanishing. Intuitively this suggests that the mass term is important – this is indeed the case and is explored for general d in chapter 6 which also links these soft limits to Lagrangian symmetries. There is perhaps still interesting physics to be explored in the case of small Δ such as the conformal scalar. The four-point soft limits here can be written in terms of three-point wavefunction coefficients with a time-dependent interaction. It may be that a more general study of the soft limits of conformally coupled scalars could link them to the wavefunction coefficients of another theory. These are the types of interactions explored through cosmological polytopes and it would be interesting to see if some connection could be made between the two approaches [58, 161].

5.4 Remarks

The study of correlation functions in (Anti) de Sitter space using curved-space analogues of the scattering equations is still an ongoing endeavour. Prior to [3], they had only been formulated for scalar theories with polynomial interactions, notably ϕ^3 [71, 72] and ϕ^4 [62, 63]. Now, this has been extended to scalar theories with derivative interactions. In particular, we study the wave function coefficients of the NLSM, DBI, and sGal theories in dS using the cosmological scattering equations. These effective scalar theories are of particular interest in flat space since their scattering amplitudes have a very elegant description and are related to each other in a simple way in terms of CHY formulae [68].

In this chapter we have proposed new formulae for four-point wavefunction coefficients of different scalar EFTs in the form of worldsheet integrals which encode both curvature corrections and mass deformations. We showed that the DBI and sGal integrands can be obtained from the NLSM integrand by replacing a Parke-Taylor factor with a linear combination of simple building blocks involving Pfaffians of certain operatorial matrices. Because the integrands are constructed from differential operators which do not generally commute, this leads to potential ordering ambiguities that are absent in theories with polynomial interactions. Such ambiguities can occur in the DBI and sGal theories at four points and the NLSM at six points. At four points we introduced a simple prescription for defining the worldsheet integrals such that the final results are permutation-invariant. We have also studied the soft limits of the resulting four-point wavefunction coefficients and derived formulae in the form of differential operators acting on three-point contact diagrams. For conformally coupled scalars, the three-point contact diagrams involve a time-dependent interaction, while for minimally coupled scalars the contact diagram is divergent and needs to be regulated. However, all divergences cancel out after acting with the appropriate combinations of boundary conformal generators.

There are a number of directions for future investigation. For example, it would

be of interest to generalise our formulae to any number of points. In order to do so, there are several technical questions that need to be addressed. First of all, we need to develop a systematic classification of higher-derivative corrections to scalar EFTs analogous to the one in [148] beyond four-points, which to our knowledge has not been carried out yet. It would then be interesting to see if there is a simple generalisation of the double copy prescription in (5.3.32) which encodes such corrections at higher points. Secondly, we need a systematic understanding of ordering ambiguities that could arise in the corresponding worldsheet integrals and a prescription for removing them. A natural starting point along these lines would be to analyse potential ordering ambiguities in the six-point NLSM calculation dealt with in [3].

Chapter 6

Soft Limits of Cosmological Wavefunctions

We now move to analysing the soft limits of scalar wavefunction coefficients for general d and Δ. The method presented lets us consider their behavior without needing to explicitly carry out the conformal time integrals. We start by presenting dS Lagrangians with shift symmetries. We will then demonstrate that by demanding wavefunction coefficients display enhanced soft behavior analogous to what is observed in flat space (see section 2.5) we can reconstruct these Lagrangians directly. This can be done for all three 'exceptional' scalar field theories and in the case of NLSM and DBI we also demonstrate how it can be bootstrapped beyond 4pt via cancellations between contact and exchange diagrams. Finally we revisit the generalised double copy introduced in chapter 5 and show that this enhanced soft behavior can be used as a physical input to fix the coefficients in 5.3.33.

6.1 Lagrangians with Enhanced Shift Symmetry

Here we introduce the Lagrangians of interest in de Sitter. Unlike the previous chapter, we are interested in fixing specific values for the masses and coefficients of curvature corrections as well as considering interaction terms beyond four points.

These Lagragians are therefore specifically constructed to exhibit shift symmetries analogous to those in flat space (as discussed in section 2.5). We will then demonstrate in section 6.2 that these Lagrangians correspond to wavefunction coefficients with enhanced soft limits just as in flat space.

The Lagrangian for NLSM in dS_{d+1} is given by

$$\frac{\mathcal{L}^{\mathrm{NLSM}}}{\sqrt{|g|}} = \mathrm{Tr}\left(\partial_\mu U^\dagger \partial^\mu U\right), \;\; U = \exp\left(i\phi\right), \tag{6.1.1}$$

where ϕ is in the adjoint of an $\mathrm{SU}(N)$ flavour symmetry, the same as in flat space. No masses or curvature corrections are allowed because they would spoil the $\phi \to \phi + c$ shift symmetry. This can also be deduced from enhanced soft limits of the wavefunction coefficients as will be demonstrated below. In practice, it is also convenient to use the parametrisation $U = (\mathbb{I} + \Phi)(\mathbb{I} - \Phi)^{-1}$ (where the coupling has been set to one). Expanding the Lagrangian in Φ then gives

$$\frac{\mathcal{L}^{\mathrm{NLSM}}}{\sqrt{|g|}} = -\mathrm{Tr}\left[\frac{1}{2}(\partial\Phi)^2 + \Phi^2(\partial\Phi)^2 + \left(\Phi^4(\partial\Phi)^2 + \frac{1}{2}\Phi^2\partial_\mu\Phi\Phi^2\partial^\mu\Phi\right) + \mathcal{O}(\Phi^8)\right], \tag{6.1.2}$$

using the shorthand $(\partial\Phi)^2 = \partial_\mu\Phi\partial^\mu\Phi$. Note that we do not need covariant derivatives here since $\nabla \sim \partial$ when acting on a scalar.

The Lagrangians for the DBI and sGal theory do not trivially lift to dS and were recently derived from the following shift symmetry [89]

$$\delta\phi = \theta_{A_1\ldots A_k} X^{A_1}\ldots X^{A_k} + \ldots, \tag{6.1.3}$$

where X^A are embedding coordinates satisfying $-\left(X^1\right)^2 + \sum_{A=2}^{d+2}\left(X^A\right)^2 = 1$ and the ellipsis denotes field-dependent terms. This symmetry fixes the mass to be $m^2 = -k(k+d)$. In the DBI case ($k = 1$), the resulting action is quite simple and given by

$$\frac{\mathcal{L}^{\mathrm{DBI}}}{\sqrt{|g|}} = \frac{1}{(1-\phi^2)^{\frac{d+1}{2}}}\sqrt{1 - \frac{(\partial\phi)^2}{1-\phi^2}}, \tag{6.1.4}$$

where $(\partial\phi)^2 = \partial_\mu\phi\partial^\mu\phi$. In the sGal case ($k = 2$) the Lagrangian is very nontrivial

$$\begin{aligned}\frac{\mathcal{L}^{\text{sGal}}}{\sqrt{|g|}} = \sum_{j=0}^{d} &\frac{(1+\phi)^{d+1-j} + (-1)^j(1-\phi)^{d+1-j}}{2^{j+1}(1-\phi^2)^{\frac{d+4}{2}}\Gamma(j+3)} \\ &\times \left((j+1)f_{j+1}(\phi) - (j+2)f_j(\phi)\right)\partial^\mu\phi\partial^\nu\phi X^{(j)}_{\mu\nu}(\phi) \\ &- \frac{2}{d+2}\left(1 - \frac{(1+\phi)^{d+2} + (1-\phi)^{d+2}}{2(1-\phi^2)^{\frac{d+2}{2}}}\right),\end{aligned} \tag{6.1.5}$$

where $X^{(j)}_{\mu\nu}$ is defined recursively as $X^{(n)}_{\mu\nu} = -n\nabla_\mu\nabla^\alpha\phi X^{(n-1)}_{\alpha\nu} + g_{\mu\nu}\nabla^\alpha\nabla^\beta\phi X^{(n-1)}_{\alpha\beta}$ with $X^0_{\mu\nu} = g_{\mu\nu}$, and

$$f_j(\phi) = {}_2F_1\left(\frac{d+4}{2}, \frac{j+1}{2}; \frac{j+3}{2}; \frac{(\partial\phi)^2}{4(1-\phi^2)}\right). \tag{6.1.6}$$

In the remainder of this chapter, we will demonstrate that the masses and couplings of these theories can be treated as unknown coefficients and fixed by demanding that the wavefunction coefficients have vanishing soft limits analogous to (2.5.1). It is worth noting that the conformal weight of the fields Δ (or equivalently the symmetry parameter k) will play an important role in what follows. In flat space, the cancellations required to obtain the expected enhanced limits are non-trivial. For example with DBI, requiring that the soft limit scales as $\mathcal{O}(k^2)$ is an additional constraint that is needed to fully fix the form of the interactions beyond 4pt. In dS however, once Δ has been fixed using the 4pt soft behavior we will see that the subleading soft limits are no longer necessary to fix the curvature corrections. Unlike in flat space, they provide no additional constraints beyond those already imposed by the leading order soft behavior. To phrase this another way, once Δ has been specified, requiring that a wavefunction coefficient exhibit enhanced soft behavior is equivalent to demanding it vanish at all in the soft limit.

6.2 Soft limits for arbitrary d and Δ

In this section we will develop the methods necessary to take soft limits for general d and Δ. The starting point for this is the wavefunction coefficients expressed

as differential operators acting on a contact diagram. We use the action of these operators to express the wavefunction coefficient as an η integrand for general d and Δ and then take the soft limit of one of the momenta. This will then be used to fix the masses and 4-point couplings of the NLSM, DBI, and sGal theories in de Sitter space from enhanced soft limits of their wavefunction coefficients. We then use these results to fix the unknown coefficients in the generalised double copy introduced in section 5.3.2. In the next section we will then use the same procedures at six points for the NLSM and DBI theories, bootstrapping the 6pt interaction Lagrangian from the four-point case and enhanced soft limits.

When expanding the conformal time integrands in terms of the soft momentum we need the soft limit of the corresponding bulk-to-boundary propagator in the contact diagram. This soft limit can be read off from the series expansion of (5.1.2) which is schematically given by

$$\phi^{\nu}(k,\eta) \sim \sum_{m=0}^{\infty} \left(a_{2m} + b_{2m} k^{2\Delta-d}\right) k^{2m}. \tag{6.2.1}$$

We can see that the second series has $k^{2(\nu+m)}$ terms which are subleading for positive ν (in the case of negative ν, the series diverges as k goes soft). In each case of interest, the enhanced soft limits will fix $\Delta = d + k$ where k is the order of the shift symmetry in the Lagrangian. This sets $\nu = d/2 + k$ and ensures that the second series does not contribute to the soft limit. We therefore take the soft limit of the wavefunction to be

$$\begin{aligned} \phi^{\nu}(k,\eta) &= \frac{\mathcal{N}}{\eta^{\Delta-d}} \left(1 + \frac{\eta^2 k^2}{2(2\Delta - d - 2)}\right) + \mathcal{O}(k^4), \\ \text{where } \mathcal{N} &= \frac{\Gamma\left(\Delta - d/2\right) 2^{\Delta - d/2 - 1/2}}{\sqrt{\pi}}, \end{aligned} \tag{6.2.2}$$

this can be used to study the soft limit of wavefunction coefficients [1].

[1] The apparent divergence where $\Delta = \frac{d}{2} + 1$ only appears when the $k^{2\Delta-d}$ terms should not be neglected but this will not occur in any of the cases studied here.

6.2.1 Four-point Soft Limits

NLSM

At four points, the tree-level flavour-ordered 4-point wavefunction coefficient can be obtained from two Witten diagrams. This was given in section 5.3 as

$$\begin{aligned}\Psi_4^{\rm NLSM} &= -\left(2\hat{s}_{13}+C-m^2\right)\mathcal{C}_4^{\Delta},\\ &= (-1)^d\int\frac{d\eta}{\eta^{d+1}}\left[2\eta^2\left(\boldsymbol{k}_1\cdot\boldsymbol{k}_3\phi_1\phi_3+\dot{\phi}_1\dot{\phi}_3\right)\phi_2\phi_4+(C+\Delta(\Delta-d))\phi_1\phi_2\phi_3\phi_4\right],\end{aligned} \tag{6.2.3}$$

where C is a curvature correction from a Φ^4 interaction and have set the coupling λ to 1. The $(-1)^d$ sign comes from the $|\eta|^{-(d+1)}$ factor in the volume element. If we take a soft limit on $\boldsymbol{k}_1$, we find

$$\begin{aligned}\lim_{\boldsymbol{k}_1\to 0}\Psi_4^{\rm NLSM} &= \tilde{\mathcal{N}}\int\frac{d\eta}{\eta^{d+1}}\left[\eta^2\frac{2(\Delta-d)}{\eta^{\Delta-d+1}}\phi_2\dot{\phi}_3\phi_4+\frac{C+\Delta(\Delta-d)}{\eta^{\Delta-d}}\phi_2\phi_3\phi_4\right]+\mathcal{O}(k_1),\\ &= \tilde{\mathcal{N}}\int\frac{d\eta}{\eta^{\Delta+1}}\left[2(\Delta-d)\eta\phi_2\dot{\phi}_3\phi_4+\left(C+\Delta(\Delta-d)\right)\phi_2\phi_3\phi_4\right]+\mathcal{O}(k_1),\end{aligned} \tag{6.2.4}$$

where we have used $\tilde{\mathcal{N}}=(-1)^d\mathcal{N}$. We see from (6.2.4) that the soft limit will vanish to $\mathcal{O}(k_1)$ if $\Delta=d$ and $C=0$, i.e. if we have a massless scalar and no curvature corrections in agreement with (6.1.2). We can also see from (5.3.3) that it is not possible to for the soft limit to vanish at higher order since there is no way to cancel the $\boldsymbol{k}_1\cdot\boldsymbol{k}_3$ term as the bulk-to-boundary propagators only depend on magnitudes of momenta. Hence, the wavefunction coefficient with enhanced soft behavior is simply

$$\Psi_4^{\rm NLSM}=-2\hat{s}_{13}\mathcal{C}_4^{\Delta=d}. \tag{6.2.5}$$

DBI

At four points, DBI theory can be described by the following general effective Lagrangian (modulo integration by parts and free equations of motion)

$$\frac{\mathcal{L}_4^{\rm DBI}}{\sqrt{|g|}} = -\left(\frac{1}{2}(\partial\phi)^2 + \frac{1}{2}m^2\phi^2 + \frac{1}{8}(\partial\phi)^4 + \frac{1}{4!}C\phi^4\right), \tag{6.2.6}$$

where the 4-derivative interaction (whose coupling we have normalised to one) arises from the naive uplift from flat space and we leave the mass and curvature correction C unfixed. This is a special case of the Lagrangian in equation (5.3.4). The tree-level 4-point wavefunction coefficient can be computed from Witten diagrams and is given by

$$\Psi_4^{\rm DBI} = -\left(\hat{s}_{12}^2 + \hat{s}_{13}^2 + \hat{s}_{14}^2 + C\right)\mathcal{C}_4^{\Delta}. \tag{6.2.7}$$

To obtain the conformal time integrand, we use the action of $\hat{s}_{12}^2$ on bulk-to-boundary propagators which appeared in section 5.3 and is given by

$$\begin{aligned}\hat{s}_{12}^2\phi_1\phi_2 = \eta^4\Big[&(\boldsymbol{k}_1\cdot\boldsymbol{k}_2)^2\phi_1\phi_2 + 2\boldsymbol{k}_1\cdot\boldsymbol{k}_2\dot{\phi}_1\dot{\phi}_2 + \ddot{\phi}_1\ddot{\phi}_2,\\ &+\frac{1}{\eta}\left(2\boldsymbol{k}_1\cdot\boldsymbol{k}_2\left(\phi_1\dot{\phi}_2 + \dot{\phi}_1\phi_2\right) - k_1^2\phi_1\dot{\phi}_2 - k_2^2\dot{\phi}_1\phi_2 + \dot{\phi}_1\ddot{\phi}_2 + \ddot{\phi}_1\dot{\phi}_2\right)\\ &+\frac{1}{\eta^2}\left((2-d)\boldsymbol{k}_1\cdot\boldsymbol{k}_2\phi_1\phi_2 + \dot{\phi}_1\dot{\phi}_2\right)\Big].\end{aligned} \tag{6.2.8}$$

Here we use $\hat{s}_{12}^2$ rather than $\hat{s}_{12}\hat{s}_{34}$ as it makes the soft limit on $\boldsymbol{k}_1$ more transparent. We then insert the soft limit for ϕ_1 from equation (6.2.2) and expand to $\mathcal{O}(k_1^2)$ in order to fix Δ and C. Since this is more complex than the NLSM case, we need to use the equations of motion and integration by parts to eliminate terms which are not independent. One option is to use the equations of motion of the bulk-to-boundary propagators to remove any explicit dependence on k_2^2 in (5.3.8) (k_2 will still enter in the arguments of ϕ_2). Alternatively, we can apply the equations of motion to leave only terms containing ϕ_2 and $\dot{\phi}_2$ along with factors of k_2^2 [2]. Removing the explicit

[2]This second approach is equivalent to using the identity $H_{\nu-1}(x) = -H_{\nu+1}(x) + \frac{2\nu}{x}H_\nu(x)$ on the Hankel functions which appear in the derivatives of propagators to leave only two independent functions.

dependence on k_2^2 in the first term of (6.2.7) and summing over cyclic permutations then gives

$$\lim_{\boldsymbol{k}_1\to 0}\Psi_4^{\rm DBI}=\tilde{\mathcal{N}}\int\frac{d\eta}{\eta^{\Delta+1}}\Big[(\Delta-d-1)\left((\Delta-d)\eta^2\ddot{\phi}_2-2\eta^3\boldsymbol{k}_1\cdot\boldsymbol{k}_2\dot{\phi}_2\right)\phi_3\phi_4 \\ +\text{Cyc.}[234]+(\Delta(\Delta-d)(4\Delta-3d-1)+C)\,\phi_2\phi_3\phi_4+\mathcal{O}(k_1^2)\Big], \tag{6.2.9}$$

where we used the following identity to remove the $\dot{\phi}_a$ terms ($a\in\{2,3,4\}$) at $\mathcal{O}(k_1^0)$:

$$\int\frac{d\eta}{\eta^{\Delta+1}}\eta\partial_\eta\left(\prod_{i=2}^n\phi_i\right)\sim\Delta\int\frac{d\eta}{\eta^{\Delta+1}}\left(\prod_{i=2}^n\phi_i\right). \tag{6.2.10}$$

In deriving the above formula, we discarded a total derivative term. This term actually gives divergent contributions at $\eta=0$ and therefore needs to be regulated, however these contributions are analytic in at least two momenta and therefore correspond to contact terms which have delta function support when Fourier transformed to position space [47].

From (6.2.9), we see that the soft limit vanishes to $\mathcal{O}(k_1^2)$ if $\Delta=d+1$ and $C=-(d+1)(d+3)$. Plugging these values into (6.2.7) gives

$$\Psi_4^{\rm DBI}=-\delta^{(d)}\left(\boldsymbol{k}_T\right)\left(\hat{s}_{12}^2+\hat{s}_{13}^2+\hat{s}_{14}^2-(d+1)(d+3)\right)\mathcal{C}_4^{\Delta=d+1}. \tag{6.2.11}$$

Moreover, (6.2.6) becomes

$$\frac{\mathcal{L}_4^{\rm DBI}}{\sqrt{|g|}}=-\left(\frac{1}{2}(\partial\phi)^2-\frac{d+1}{2}\phi^2+\frac{1}{8}(\partial\phi)^4-\frac{(d+1)(d+3)}{4!}\phi^4\right). \tag{6.2.12}$$

From (5.3.8) we can see that it is not possible for the soft limit to vanish beyond $\mathcal{O}(k_1^2)$ since this term contains a piece proportional to $(\boldsymbol{k}_1\cdot\boldsymbol{k}_2)^2$ but the soft limit of Witten diagrams coming from the ϕ^4 interaction will only depend on the magnitude k_1. We also note that while the $\mathcal{O}(k_1)$ contribution to the wavefunction coefficient is needed to fix Δ, once this is fixed only the leading soft limit is needed to fix C. This is appears to be a general feature in de Sitter space, in contrast to flat space where all the subleading data is needed to fix coefficients.

Let us now compare to the Lagrangian in (6.1.4) which was derived from shift symmetries. Expanding it to quartic order gives

$$\begin{aligned}\frac{\mathcal{L}^{\rm DBI}}{\sqrt{|g|}} &= \frac{1}{(1-\phi^2)^{(d+1)/2}}\sqrt{1-\frac{(\partial\phi)^2}{1-\phi^2}},\\ &= -\left(\frac{1}{2}(\partial\phi)^2-\frac{d+1}{2}\phi^2+\frac{1}{8}(\partial\phi)^4-\frac{(d+1)(d+3)}{4!}\phi^4+\mathcal{O}(\phi^6)\right),\end{aligned} \tag{6.2.13}$$

where we have used integration by parts and the free equation of motion $\nabla^2\phi = m^2\phi$ to remove a $(\nabla\phi)^2\phi^2 = (\partial\phi)^2\phi^2$ term. This precisely matches (6.2.12), which was derived from enhanced soft limits.

sGal

At 4-points, the sGal wavefunction coefficient can also be obtained from the Lagrangian in equation (5.3.4). The corresponding wavefunction coefficient is given by

$$\Psi_4^{\rm sGal} = [(\hat{s}_{12}^3+\hat{s}_{13}^3+\hat{s}_{14}^3)+(d-B)(\hat{s}_{12}^2+\hat{s}_{13}^2+\hat{s}_{14}^2)-C]\mathcal{C}_4^{\Delta}, \tag{6.2.14}$$

where we have taken equation (5.3.5) and set the unknown A to 1, corresponding to a rescaling of the fields. The $\hat{s}_{ab}^3$ terms are quite lengthy and can be found in Appendix E.2. The $\hat{s}_{ab}^2$ terms were already considered in the previous subsection (and in section 5.3).

We will now expand the integrand up to $\mathcal{O}(k_1^2)$ and present the soft limit in parts. After substituting (6.2.2) we apply equations of motion to eliminate any explicit dependence on k_2^2 in the $\hat{s}_{12}^3$ term and sum over permutations to obtain

$$\begin{aligned}\lim_{\boldsymbol{k}_1\to 0}\Psi_4^{\rm sGal} = \tilde{\mathcal{N}}(\Delta-d-2)\int\frac{d\eta}{\eta^{\Delta+1}}\Bigg[\eta\Bigg((\Delta-d-1)(\Delta-d)\eta^2\\ +\frac{k_1^2}{2\Delta-d-2}(\Delta-d-3)(\Delta-d-4)\Bigg)\dddot{\phi}_2\\ -3\boldsymbol{k}_1\cdot\boldsymbol{k}_2\eta^4\ddot{\phi}_2+3(\boldsymbol{k}_1\cdot\boldsymbol{k}_2)^2\eta^5\dot{\phi}_2\Bigg]\phi_3\phi_4+\text{Cyc.}[234]+\mathcal{O}(k_1^3)+\ldots,\end{aligned} \tag{6.2.15}$$

where the ellipsis represent terms that can also arise from 4-derivative and ϕ^4 interactions. Equation (6.2.15) therefore represents terms which must scale as $\mathcal{O}(k_1^3)$ in the soft limit since they cannot cancel against any other terms in the wavefunction coefficient. We must therefore set $\Delta = d + 2$. When this is substituted into the remaining terms they simplify significantly and we obtain

$$\lim_{\boldsymbol{k}_1\to 0}\Psi_4^{\text{sGal}} = \tilde{\mathcal{N}}(B+2d+2)\int\frac{d\eta}{\eta^{\Delta+1}}\eta^2\left(2\ddot{\phi}_2 - 2\eta(\boldsymbol{k}_1\cdot\boldsymbol{k}_2)\dot{\phi}_2 + \eta^2(\boldsymbol{k}_1\cdot\boldsymbol{k}_2)^2\phi_2\right)\phi_3\phi_4 + \text{Cyc.}[234] + \mathcal{O}(k_1^3) + \ldots, \tag{6.2.16}$$

where the ellipsis denote terms that can also arise from ϕ^4 interactions. After setting $B = -2(d+1)$ the above terms vanish and the soft limit of the wavefunction coefficient reduces to

$$\lim_{\boldsymbol{k}_1\to 0}\Psi_4^{\text{sGal}} = -\tilde{\mathcal{N}}(4(d+2)^2 - C)\int\frac{d\eta}{\eta^{\Delta+1}}\frac{4+2d+\eta^2k_1^2}{2(d+2)}\phi_2\phi_3\phi_4 + \mathcal{O}(k_1^3), \tag{6.2.17}$$

which fixes $C = 4(d+2)^3$. The wavefunction coefficient with $\mathcal{O}(k_1^3)$ soft behavior is therefore

$$\Psi_4^{\text{sGal}} = \left(\hat{s}_{12}^3 + \hat{s}_{13}^3 + \hat{s}_{14}^3 + (3d+2)\left(\hat{s}_{12}^2 + \hat{s}_{13}^2 + \hat{s}_{14}^2\right) - 4(d+2)^3\right)\mathcal{C}_4^{\Delta=d+2}. \tag{6.2.18}$$

We can see from equations (6.2.16) and (6.2.17) that once Δ is fixed, we can fix B and C using only the leading order soft limit.

Moreover, we find that the Lagrangian in (5.3.4) is given by

$$\frac{\mathcal{L}_4^{\text{sGal}}}{\sqrt{|g|}} = -\{\frac{1}{2}\nabla\phi\cdot\nabla\phi - (d+2)\phi^2 + \frac{1}{8}(\nabla_\mu\nabla_\nu\phi)^2(\nabla\phi)^2 - \frac{d+1}{4}(\nabla\phi)^4 + \frac{(d+2)^3}{6}\phi^4\}. \tag{6.2.19}$$

Let us compare the above Lagrangian to the one derived from hidden symmetry. Expanding (6.1.5) to quartic order gives

$$\begin{aligned}\frac{\mathcal{L}^{\text{sGal}}}{\sqrt{|g|}} = -\Bigg(&\frac{1}{2}(\nabla\phi)^2 - (d+2)\phi^2 - \frac{1}{4!}2(d+2)(d(d+4)+12)\phi^4 \\ &+ \frac{1}{4!}(d(3d+8)+28)\phi^2(\nabla\phi)^2 + \frac{d+4}{96}(\nabla\phi)^4 \\ &+ \frac{2-d}{24}\phi\nabla^\mu\phi\nabla^\nu\phi\nabla_\mu\nabla_\nu\phi - \frac{1}{96}(\nabla\phi)^2\left(\nabla_\mu\nabla_\nu\phi\right)^2 \\ &+ \frac{1}{48}\nabla^\mu\phi\nabla^\nu\phi\nabla_\sigma\nabla_\mu\phi\nabla^\sigma\nabla_\nu\phi\Bigg) + \mathcal{O}(\phi^6),\end{aligned} \tag{6.2.20}$$

where we have used the free equation of motion $\nabla^2\phi = m^2\phi = -2(d+2)\phi$. We can then use integration by parts and free equations of motion to bring this to the form in (5.3.4). The final term in (6.2.20) can be written as

$$\partial^\mu\phi\partial^\nu\phi\nabla^\sigma\nabla_\mu\phi\nabla_\sigma\nabla_\nu\phi \sim -\frac{1}{2}\left((\nabla\phi)^2\nabla^\sigma\nabla^\mu\phi\nabla_\sigma\nabla_\mu\phi + (\nabla\phi)^2\partial^\nu\phi\nabla^2\nabla_\nu\phi\right), \tag{6.2.21}$$

by applying integration by parts on ∇^σ. The second term on the right-hand side can then be reduced to lower-derivative terms via a commutator of covariant derivatives

$$\begin{aligned}\nabla_\sigma\nabla^\sigma\partial_\nu\sigma\phi &= \nabla_\sigma\nabla_\nu\partial^\sigma\phi, \\ &= \nabla_\nu\nabla^2\phi + [\nabla_\nu\nabla_\sigma]\partial^\sigma\phi, \\ &= m^2\partial_\nu\phi + R_{\mu\nu}\partial^\mu\phi, \\ &= -(d+4)\partial_\nu\phi.\end{aligned} \tag{6.2.22}$$

Similarly, using integration by parts and free equations of motion, the two-derivative term in the first line of (6.2.20) can be reduced to a ϕ^4 term, and the second four-derivative term in the second line of (6.2.20) can be written in the form $(\nabla\phi\cdot\nabla\phi)^2$ plus a ϕ^4 term. In the end, we are left with three interaction terms:

$$\frac{\mathcal{L}^{\text{sGal}}_{\text{int}}}{\sqrt{|g|}} = -\frac{1}{48}(\nabla\phi)^2\nabla^\alpha\nabla^\beta\phi\nabla_\alpha\nabla_\beta\phi + \frac{d+1}{24}(\nabla\phi)^4 - \frac{1}{36}(d+2)^3\phi^4 + \mathcal{O}(\phi^6). \tag{6.2.23}$$

After multiplying by 6 (equivalent to rescaling the six-derivative coupling) this indeed matches the interaction terms in (6.2.19), which were deduced from enhanced soft limits.

6.2.2 Fixing Double Copy coefficients

We can now apply these enhanced soft limits to fix the general curvature coefficients in the CSE integrands introduced in section 5.3.2. For the NLSM at 4-points, the general integrand was given in equation (5.3.31) by

$$\mathcal{I}_4^{\text{NLSM}} = \lambda^2 \text{PT}\left(\text{Pf}'A\right)^2 + c\text{PT Pf}X|_{\text{conn}}\,\text{Pf}'A, \tag{6.2.24}$$

Evaluating the contour integral as discussed in section 5.3.1 then gives

$$\Psi_4^{\text{NLSM}} = -\delta^3(\boldsymbol{k}_T)\left(2\lambda^2\hat{s}_{13} - c - m^2\right)\mathcal{C}_4^{\Delta}. \tag{6.2.25}$$

Comparing this to the wavefunction coefficient with enhanced soft limits in (6.2.5) then fixes the mass and coefficients as follows:

$$\lambda = 1, \;\; c = m = 0. \tag{6.2.26}$$

For the DBI and sGal theories at four-points the generalised double copy integrand in equation (5.3.33) was given as

$$\begin{aligned}\mathcal{I}_4^{(6)} = a(\text{Pf}'A)^3(\text{Pf}'A + m^2\,\text{Pf}X|_{\text{conn}}) \\ + b(\text{Pf}'A)^2(\text{Pf}'A\text{Pf}X + m^2\text{PT}) + c\text{PT Pf}X|_{\text{conn}}\,\text{Pf}'A,\end{aligned} \tag{6.2.27}$$

As in section 5.3.2 this gives the wavefunction coefficient

$$\Psi_4^{(6)} = \left[\frac{8a}{3}(\hat{s}_{12}^3 + \hat{s}_{13}^3 + \hat{s}_{14}^3) + 2(b - am^2)(\hat{s}_{12}^2 + \hat{s}_{13}^2 + \hat{s}_{14}^2) + \frac{1}{3}am^6 - bm^4 + c\right]\mathcal{C}_4^{\Delta}, \tag{6.2.28}$$

where we have expanded all the $\tilde{s}_{ij}$ in terms of $\hat{s}_{ij}$ and the mass. Comparing this to the wavefunction coefficient for the DBI theory derived from enhanced soft limits in (6.2.11) then fixes the parameters as follows:

$$a = 0, \;\; b = -\frac{1}{2}, \;\; c = \frac{1}{2}\left(d^2 + 6d + 5\right), \;\; m^2 = -(d+1). \tag{6.2.29}$$

Furthermore, comparing (6.2.28) to the wavefunction coefficient for the sGal theory in (6.2.18) implies that

$$a = \frac{3}{8}, \;\; b = \frac{1}{4}\left(3d-2\right), \;\; c = -8(d+2)^2, \;\; m^2 = -2(d+2). \tag{6.2.30}$$

In summary, the parameters of the generalised double copy for four-point wavefunction coefficients can be fully fixed by enhanced soft limits. In the next section we will show that enhanced soft limits also fix higher-point wavefunction coefficients, so it would be interesting to see if the double copy prescription can be extended to higher points as well.

6.3 Soft limits with Exchange Diagrams

In this section, we will show that all 6-point couplings of the NLSM and DBI theory in dS can also be fixed from enhanced soft limits of wavefunction coefficients. The method we develop can also be applied to the sGal theory, but at six points its Lagrangian has 13 interaction terms going up to ten derivatives so Witten diagram calculations become very tedious. We will therefore leave that case for future work.

6.3.1 NLSM

We start with the NLSM, which is very simple but nicely illustrates the procedure for fixing higher-point couplings. At six points, the most general Lagrangian is given by

$$\begin{aligned}\frac{\mathcal{L}_6^{\text{NLSM}}}{\sqrt{|g|}} = \text{Tr}\Big[&-\frac{1}{2}(\partial\Phi)^2 - \frac{1}{2}m^2\Phi^2 - \Phi^2(\partial\Phi)^2 - \frac{1}{4}C\Phi^4 \\ &-A\left(\Phi^4(\partial\Phi)^2 + \frac{1}{2}\Phi^2\partial_\mu\Phi\Phi^2\partial^\mu\Phi\right) - \frac{1}{6}F\Phi^6\Big],\end{aligned} \tag{6.3.1}$$

where the Φ^4 and Φ^6 terms are curvature corrections. We have already fixed $m = 0$ and $C = 0$ from the enhanced soft limit at four points. The coefficient A can be fixed by the flat space limit but we will deduce it along with F from enhanced soft

limits at six points.

The wavefunction coefficient is given by a sum of exchange and contact diagrams shown in Figure 6.1. To obtain the desired form, we must write the four-point vertices in the exchange diagrams in such a way that derivatives only act on bulk-to-boundary propagators. Let us consider the four-point vertex appearing on the left-hand-side of an exchange diagram, illustrated in Figure 6.2. Using the Feynman rules derived from (6.3.1) and the identity in (5.1.7) we find

$$\mathcal{A}_L = -(-1)^d \int \frac{d\eta}{\eta^{d+1}} \eta^2 \Big\{ \phi_1\phi_2\phi_3\phi_L[(\boldsymbol{k}_1\cdot\boldsymbol{k}_2)+(\boldsymbol{k}_2\cdot\boldsymbol{k}_3)+(\boldsymbol{k}_3\cdot\boldsymbol{k}_L)+(\boldsymbol{k}_L\cdot\boldsymbol{k}_1)] + \dot{\phi}_1\dot{\phi}_2\phi_3\phi_L + \phi_1\dot{\phi}_2\dot{\phi}_3\phi_L + \phi_1\phi_2\dot{\phi}_3\dot{\phi}_L + \dot{\phi}_1\phi_2\phi_3\dot{\phi}_L \Big\}, \tag{6.3.2}$$

where ϕ_L is associated to the bulk-to-bulk propagator and $\dot{\phi} = \partial_\eta \phi$. Using integration by parts to remove the derivatives acting on ϕ_L gives

$$\mathcal{A}_L = -(-1)^d \int \frac{d\eta}{\eta^{d-1}} \phi_L \Big[(-2\boldsymbol{k}_1\cdot\boldsymbol{k}_3\phi_1\phi_2\phi_3 - 2\dot{\phi}_1\phi_2\dot{\phi}_3 - k_1^2\phi_1\phi_2\phi_3 - k_3^2\phi_1\phi_2\phi_3 - \phi_1\phi_2\ddot{\phi}_3 - \ddot{\phi}_1\phi_2\phi_3 + \frac{1-d}{\eta}\left(\dot{\phi}_1\phi_2\phi_3 + \phi_1\phi_2\dot{\phi}_3\right) \Big], \tag{6.3.3}$$

where we have also used momentum conservation at the vertex, such that $\boldsymbol{k}_L = -(\boldsymbol{k}_1+\boldsymbol{k}_2+\boldsymbol{k}_3)$. Using the equations of motion for ϕ_1 and ϕ_3, we are left with

$$\mathcal{A}_L = -2 \int \frac{d\eta}{|\eta|^{d+1}} \left[\phi_2\phi_L\eta^2 \left(\boldsymbol{k}_1\cdot\boldsymbol{k}_3\phi_1\phi_2\phi_3 + \dot{\phi}_1\phi_2\dot{\phi}_3 \right) \right], \tag{6.3.4}$$

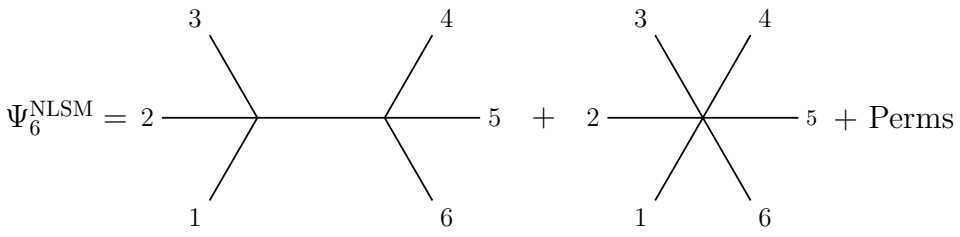

Figure 6.1: Witten diagrams for the six-point NLSM and DBI wavefunction coefficients. The exchange diagram is summed over the three inequivalent cyclic permutations (NLSM) or over the 10 inequivalent factorisation channels (DBI).

which is equivalent to the action of $\hat{s}_{13}$. Performing the same steps at the other 4pt vertex and adding in the other diagrams gives

$$\Psi_6^{\text{NLSM}} = \left[\left(\frac{\hat{s}_{13}\hat{s}_{46}}{\hat{s}_{123}} + A\,\hat{s}_{13} + \text{Cyc.}[i \to i{+}2]\right) + F\right]\mathcal{C}_6^{\Delta=d}, \tag{6.3.5}$$

where we've used the shorthand and $\hat{s}_{abc} = \mathcal{D}_a \cdot \mathcal{D}_b + \mathcal{D}_b \cdot \mathcal{D}_c + \mathcal{D}_c \cdot \mathcal{D}_a$. Note that the first term comes from the exchange diagrams and the second term is from the contact diagram. These can be seen from the Witten diagrams in Figure 6.1. In this form, the expression is free of ordering ambiguities since $[\hat{s}_{abc}, \hat{s}_{ab}]\mathcal{C}^{\Delta} = 0$. It can also be obtained by uplifting flat space Feynman diagrams simp,y by replacing $k_a \cdot k_b$ with $\hat{s}_{ab}$. A similar formula was also previously derived in [73] using AdS embedding coordinates.

If we take $\boldsymbol{k}_1$ soft, all operators of the form $\mathcal{D}_1 \cdot \mathcal{D}_a$ will vanish up to $\mathcal{O}(k_1)$ when acting on the contact diagram $\mathcal{C}_6^{\Delta}$ as in (6.2.4) since $\Delta = d$. Hence two of the channels in (6.3.5) drop out immediately and it reduces to

$$\lim_{\boldsymbol{k}_1 \to 0} \Psi_6^{\text{NLSM}} = \left[\left(\frac{\hat{s}_{35}\hat{s}_{62}}{\hat{s}_{612}} + A\,\hat{s}_{35}\right) + F\right]\mathcal{C}_6^{\Delta=d}. \tag{6.3.6}$$

Noting that $\lim_{\boldsymbol{k}_1 \to 0} \hat{s}_{612} \sim \hat{s}_{62}$ when $\Delta = d$, we then can see the soft limit vanishes if $A = -1$ and $F = 0$, in agreement with (6.1.2). The flat space limit is then also equivalent to the result given in [105].

In summary, we see that the enhanced soft limit arises via cancellations between exchange and contact diagrams, fixing higher-point couplings in terms of lower-point couplings. In this way, we can in principle bootstrap all tree-level wavefunction

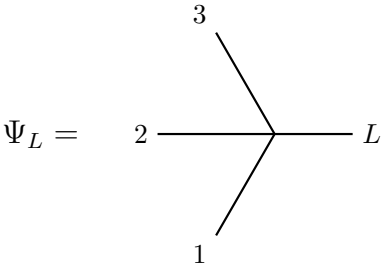

Figure 6.2: Four-point vertex appearing on the left-hand-side of a 6-point NLSM exchange diagram.

coefficients and reconstruct the Lagrangian.

6.3.2 DBI

We now consider the following 6-point effective Lagrangian:

$$\frac{\mathcal{L}_6^{\rm DBI}}{\sqrt{|g|}} = \frac{\mathcal{L}_4^{\rm DBI}}{\sqrt{|g|}} + \frac{A}{48}(\partial\phi)^6 + \frac{B}{16}(\partial\phi)^4\phi^2 + \frac{C}{6!}\phi^6, \tag{6.3.7}$$

where the 4-point Lagrangian was fixed by enhanced soft limits in (6.2.12). The coefficient A can be determined by the flat space limit but we will fix it along with the other coefficients from enhanced soft limits. First we compute the 6-point wavefunction coefficient from Witten diagrams, which are depicted in Figure 6.1. To compute the exchange diagrams, first consider the 4-point vertex on the left of the exchange diagram in Figure 6.1 which is illustrated in Figure 6.2:

$$\Psi_L = \left(\hat{s}_{12}\hat{s}_{3L} + \hat{s}_{23}\hat{s}_{1L} + \hat{s}_{31}\hat{s}_{2L} - (d+1)(d+3)\right), \tag{6.3.8}$$

which is understood to act on a 6-point contact diagram in combination with a bulk-to-bulk propagator and another 4-point vertex.

We can then use the conformal Ward identities at the vertex $\mathcal{D}_1 + \mathcal{D}_2 + \mathcal{D}_3 = -\mathcal{D}_L$ to get

$$\Psi_L = \Big(-2\left(\hat{s}_{12}\hat{s}_{23} + \hat{s}_{23}\hat{s}_{31} + \hat{s}_{31}\hat{s}_{12}\right) + m^2(\hat{s}_{12} + \hat{s}_{23} + \hat{s}_{31}) - (d+1)(d+3)\Big), \tag{6.3.9}$$

where $-m^2 = \Delta(\Delta - d) = d+1$. Combining this with the rest of the Witten diagram and summing over permutations then gives

$$\begin{aligned}\Psi^{DBI}_{6,\,\rm exch} = \frac{1}{\left(\mathcal{D}_1 + \mathcal{D}_2 + \mathcal{D}_3\right)^2 + m^2}\Big(&2\left(\hat{s}_{12}\hat{s}_{23} + \hat{s}_{23}\hat{s}_{31} + \hat{s}_{31}\hat{s}_{12}\right) \\ &+ (d+1)(\hat{s}_{12} + \hat{s}_{23} + \hat{s}_{31} + (d+3))\Big) \times (123) \to (456))\mathcal{C}_6^{\Delta=d+1} \\ &+ \text{perms},\end{aligned} \tag{6.3.10}$$

where the permutation sum is over 10 inequivalent factorisation channels. Note that this expression is free of ordering ambiguities. Moreover, it is straightforward to read off the contact Witten diagrams from (6.3.7):

$$\Psi^{\rm DBI}_{6,\,\rm cont} = \delta^3(\boldsymbol{k}_T)\left[A\left(\hat{s}_{12}\hat{s}_{34}\hat{s}_{56}+\text{perms}\right)+B\left(\hat{s}_{12}\hat{s}_{34}+\text{perms}\right)+C\right]\mathcal{C}_6^{\Delta=d+1}, \quad (6.3.11)$$

where we sum over inequivalent permutations giving 61 terms.

Let us now expand the wavefunction coefficient to $\mathcal{O}(k_1^2)$. To this order, the 4-point vertex in (6.3.9) is given by

$$\Psi_L = -((\mathcal{D}_1+\mathcal{D}_2+\mathcal{D}_3)^2+m^2)\left(\hat{s}_{12}+\hat{s}_{31}+\frac{1}{2}(d-1)\right)+\mathcal{O}(k_1^2), \quad (6.3.12)$$

As a result, the numerator of the exchange diagram in Figure 6.1 can be written as

$$\begin{aligned}&\left(2\left(\hat{s}_{12}\hat{s}_{23}+\hat{s}_{23}\hat{s}_{31}+\hat{s}_{31}\hat{s}_{12}\right)+(d+1)(\hat{s}_{12}+\hat{s}_{23}+\hat{s}_{31}+(d+3))\right)\\ &\qquad=((\mathcal{D}_1+\mathcal{D}_2+\mathcal{D}_3)^2+m^2)\left(\hat{s}_{12}+\hat{s}_{31}+\frac{1}{2}(d-1)\right)+\mathcal{O}(k_1^2).\end{aligned} \quad (6.3.13)$$

Hence, in the soft limit we can cancel all the propagators and are left with a cubic polynomial in $\hat{s}_{ij}$. We then we apply conformal Ward identities to cancel exchange and contact contributions, mimicking the analogous cancellation of terms that arises in the flat space limit using momentum conservation.

We then use integration by parts and equations of motion to write the conformal time integrand in terms of linearly independent terms, as before. In the present case, the procedure is somewhat complicated so further details can be found in in Appendix F. In the end, we find that the soft limit of the 6-point wavefunction coefficient vanishes to $\mathcal{O}(k_1^2)$ if and only if $A=3, B=d+1, C=2(d+1)(9-d^2)$. Since Δ was already fixed from the 4-point soft limit, these values can be deduced by considering only the leading order soft limit at six points. We therefore find that the 6-point effective Lagrangian can be written as

$$\begin{aligned}\frac{\mathcal{L}_6^{\rm DBI}}{\sqrt{|g|}} = &-\frac{1}{2}(\partial\phi)^2+\frac{d+1}{2}\phi^2-\frac{1}{8}(\partial\phi)^4+\frac{(d+1)(d+3)}{4!}\phi^4-\frac{1}{16}(\partial\phi)^3\\ &+\frac{d+1}{16}(\partial\phi)^4\phi^2+\frac{2(d+1)(9-d^2)}{6!}\phi^6.\end{aligned} \quad (6.3.14)$$

On the other hand, expanding the Lagrangian in (6.1.5) to sixth order (without applying equations of motion) gives

$$\begin{aligned}\frac{\mathcal{L}_6^{\rm DBI}}{\sqrt{|g|}} = &-\frac{1}{2}(\partial\phi)^2 + \frac{d+1}{2}\phi^2 - \frac{1}{8}(\partial\phi)^4 - \frac{1}{4}(d+3)(\partial\phi)^2\phi^2 \\ &+ \frac{3(d+1)(d+3)}{4!}\phi^4 - \frac{1}{16}(\partial\phi)^6 - \frac{3(d+5)}{16}(\partial\phi)^4\phi^2 \\ &- \frac{3(d+3)(d+5)}{48}(\partial\phi)^2\phi^4 + \frac{15(d+1)(d+3)(d+5)}{6!}\phi^6.\end{aligned} \tag{6.3.15}$$

Matching the two Lagrangians using integration by parts and equations of motion is very tedious, so we instead verify that they give the same 6-point wavefunction coefficient in Appendix F.1.

6.4 Remarks

In this paper, we have found evidence that the link between hidden symmetries and enhanced soft limits for scattering amplitudes in flat space extends to wavefunction coefficients in de Sitter space. In more detail, we have shown that enhanced soft limits fix the masses and couplings (including curvature corrections) of scalar effective field theories in agreement with the Lagrangians recently derived for the DBI and sGal theories from hidden symmetries in [89]. Moreover, we have shown that enhanced soft limits imply that the NLSM in dS must be massless and cannot receive curvature corrections, which would spoil its shift symmetry. We have carried out these calculations up to six points in the NLSM and DBI theory and four points in the sGal theory. At six points, the enhanced soft limits arise from cancellations between exchange and contact Witten diagrams, allowing us to fix all 6-point couplings in terms 4-point couplings. In principle, this procedure can be extended to any number of points allowing us to reconstruct the entire tree-level wavefunction coefficient, or equivalently the entire Lagrangian.

There are a number of future directions. First of all, it would be interesting to extend these calculations to any number of points. This would involve writing

down the most general effective action that reduces to the known one in the flat space limit, computing the tree-level wavefunction coefficients up to a given number of points using Witten diagrams, fixing the couplings from enhanced soft limits, and showing that the result agrees with the Lagrangians recently derived from hidden shift symmetries. If this were possible, it would be very significant because it would allow us to prove the relation between enhanced soft limits and hidden symmetries in dS. The difficulty with this approach is that the number of Witten diagrams quickly becomes very large at higher points. A more efficient method for fixing higher-point couplings from enhanced soft limits would therefore be very welcome. In flat space, enhanced soft limits allow one to define recursion relations for scattering amplitudes [96, 162]. It seems likely that similar progress can be made for wavefunction coefficients in dS by combining enhanced soft limits with knowledge of their singularity structure. This direction was recently explored in the context of flat space wavefunction coefficients, which do not exhibit enhanced soft limits but do obey soft theorems [156]. The Mellin-Barnes representation also allows for the study of soft limits for arbitrary d and Δ as well as for spinning particles and potentially offers an easier path to higher-point wavefunction coefficients [163].

This leads us to the next question: how do we prove that higher shift symmetries in dS imply enhanced soft limits of the wavefunction coefficients without using Lagrangians? The analogous proof in flat space, which was sketched in [4], relied heavily on the definition of the S-matrix, and does not immediately lift to wavefunction coefficients or CFT correlators. A useful strategy for addressing this question may be the one developed in [164, 165] which studied soft limits of cosmological correlators from a boundary perspective. On the other hand, the shift symmetries underlying the NLSM, DBI, and sGal theories in dS are generated by diffeomorphisms which change the asymptotic behaviour of bulk fields so it is not immediately clear how to interpret them from the CFT perspective. We hope to gain a deeper understanding of this issue in the future.

Finally, it would be interesting to adapt these methods to other models. In flat space,

[70, 166] showed that soft limits of the NLSM, DBI, and sGal theories are actually controlled by larger theories which become visible when one expands beyond the order at which the soft limits vanish. It would therefore be interesting to extend our calculations to higher orders in the soft limit and investigate the emergence of extended theories in dS. Moreover the flat space Lagrangian for Born-Infeld theory (which is a vector effective field theory) can be uniquely fixed by the vanishing of multiple chiral soft limits [167], so it would natural to look for an analogue of this in dS. It would also be interesting to consider soft limits of more realistic inflationary models where Lorentz boosts are spontaneously broken [168–170]. In the flat space limit, the scattering amplitudes of such effective field theories do not generally exhibit enhanced soft limits, except in the case of the spontaneously broken DBI theory which exhibits an emergent Lorentz invariance with respect to the speed of sound [171, 172]. It would be fascinating if this phenomenon also occurs in de Sitter background.

Chapter 7

Conclusion

This thesis has explored several different frontiers of scattering amplitudes. In each chapter it has seemed as though there are tantalising hints of deeper structures to be uncovered, needing further study and perhaps clever insights about how to re-express current results in a novel way.

In chapter 3 the idea of defining momentum twistors on different 'coordinate patches' was introduced, each with a different ordering of external legs. It was then shown how that these patches exposed the cancellation of spurious poles in supergravity amplitudes. Serendipitously the representation that lead to the simplest form of the fermionic delta functions in the 6pt NMHV amplitude also gave simple expressions for all the spurious poles as well. As was discussed in section 3.3, this is a hint that there may exist a geometrical realisation of supergravity amplitudes like the $\mathcal{N} = 4$ SYM amplituhedron. Work on higher point amplitudes such as those in [34] is perhaps a natural place to start as MHV amplitudes may be too trivial to understand from a geometrical point of view. It may also be that $\mathcal{N} = 4$ conformal supergravity would be a better starting point since the presence of conformal symmetry means it would be more straightforward to adapt results from the amplituhedron, despite having less supersymmetry. It would also be interesting to explore in detail the on-shell diagrams associated with leading singularities constructed in appendix C. While these were constructed to specifically avoid the presence of closed cycles

running through the loops, it may be that introducing such closed cycles produces on-shell diagrams encoding some intersting new physics as was studied for $\mathcal{N} < 4$ SYM in [125].

The rest of the material in this thesis dealt with scattering in curved space times. Recent advances mean that physics in (A)dS is of phenomenological interest as well as theoretical and so this seems a good place to push our understanding of amplitudes and amplitude-like objects. The Yang-Mills and gravitational functions discussed in chapter 4 are perhaps the closest topic to having some new advances in understanding. Already the gravitational 4pt function is far better understood than it was a few years ago [139] making it more straightforward to manipulate and understand double-copy conjectures from Yang-Mills and to deduce how they should be modified compared to the flat space double copy. Alternatively, the spinor expressions in chapter 4 may a good place to look for new physics. It seems plausible that there may exist n-point expressions for Yang-Mills amplitudes in AdS just as in flat space although whether they should be expected for MHV or the simpler all-plus amplitudes remains to be seen. As well as the spinor techniques used in this thesis there are also operatorial approaches being developed for spinning particles and it may be that this is a better analogue of momentum-space amplitudes in flat space [173]. The soft behavior of gluons and gravitons in AdS has also not yet been studied closely and it would be interesting to see if there is a curved space analogue of the Weinberg soft theorems and perhaps even the associated asymptotic symmetries.

This idea was explored throughout chapters 5 and 6, using both the cosmological scattering equations and Witten diagrams to produce wavefunction coefficients expressed in terms of boundary conformal generators acting on contact diagrams. This appears to be a natural way of generalising expressions from flat space which are independent of dimension since the conformal time integrals needed to get momentum-space results in dS depend explicitly on d. This approach leads to interesting technical problems such as the ordering of operators (both in CSE integrands and the operator polynomials obtained after integration). Once these are better understood, it would

be interesting to push the double copy calculation to six-point (at least for NLSM and DBI), seeing if there is a natural extension to the integrand building blocks examined in this thesis. The soft limits of these theories were already studied in chapter 6 and these could be used to determine unfixed coefficients in the worldsheet integrand for a hypothetical six-point double copy. This would also require a more systematic study of higher derivative curvature corrections like the 4pt analysis in [148]. It should also be possible to calculate the 6pt sGal wavefunction coefficient from Witten diagrams. The larger polynomials which will appear here may be tedious to manipulate but shouldn't pose any specific obstruction and so can be dealt with analagously to the 6pt DBI case. The complexity of the curvature corrections and larger number of integration-by-parts identities in the Lagrangian will be harder to deal with though. The hope is that success may lead to a much simplified form of the Lagrangian (in comparison to those found in [89]) since in flat space the sGal Lagrangian can be written such that it only has a 4pt interaction term. While it seems unlikely that this will also hold in dS, it would still be interesting to find a Lagrangian that manifestly has this feature in the flat space limit. There may also be interesting physics encoded within the non-vanishing soft limits of conformal scalar wavefunction coefficients that appeared in chapter 5. These bear some similarities to the types of interactions explored through the use of cosmological polytopes in [58, 161] and it would be interesting to see if they could be used to further explore EFTs or soft limits.

It may also be the case that the use of momentum space to work with wavefunction coefficients leads to intractably complex expressions at higher points or in attempts to find n-point results. Finding ways to explore physics of interest in alternative formulations may lead to new insights. For example, the integrals appearing in section can also be expressed compactly using the differential representation explored in [60] and this may offer a better avenue to manipulate wavefunction coefficients (ie one which scales better with increasing numbers of external particles). Similarly the Mellin-Barnes representation also offers a way to study more general cosmological

and inflationary correlators without needing to deal with the complexity associated with the conformal time integrals which appear in Witten diagrams [163]. Recent work in linking this to celestial correlators [174, 175] also points to potential connections with techniques used to study the links between soft theorems and symmetries in flat space [81].

Appendix A

Details of 6pt NMHV

In this Appendix, we provide additional details about the 6-point NMHV calculation in section 3.2.3. We continue to denote $\Delta = \mathcal{J}_C^{-1}$ and $\delta = \delta^{(6|21)}\left(C \cdot \tilde{\lambda}\right)\delta^6\left(\lambda \cdot C^{\perp}\right)$, where $\mathcal{J}_C$ is the Jacobian associated with closed cycles defined in section 3.1.2.

3+5

First we consider the $3+5$ diagram in Figure A.1. This diagram gives the C-matrix and Jacobian

$$C = \begin{pmatrix} 1 & -\alpha_{14} & -\alpha_7\alpha_{10}\alpha_{14} & -\alpha_{10}\alpha_{14} & 0 & 0 \\ 0 & \tilde{\alpha} & 1-\alpha_7\alpha_8\alpha_9\alpha_{10} & -\alpha_8\alpha_9\alpha_{10} & -\alpha_8 & 0 \\ -\alpha_{11}\alpha_{13} & 0 & -\alpha_7\alpha_{10}\alpha_{11}\alpha_{12} & \alpha_{10}\alpha_{11}\alpha_{12} & 1 & -\alpha_{11} \end{pmatrix}, \tag{A.0.1}$$

$$\mathcal{J}_C = (1-\alpha_7\alpha_8\alpha_9\alpha_{10}-\alpha_7\alpha_8\alpha_{10}\alpha_{11}\alpha_{12}-\alpha_7\alpha_8\alpha_{10}\alpha_{11}\alpha\_13\alpha_{14}),$$

where we have inserted an extra $\tilde{\alpha}$ to ensure that $(612) \neq 0$. The brackets from the vertex factors are

$$\begin{aligned} [2\,15] &= \frac{1}{\alpha_{14}}[21], \\ [47] &= \alpha_7[43], \\ \langle 73\rangle &= \langle 43\rangle, \\ \langle 16\,5\rangle &= \frac{1}{\alpha_{11}}\langle 65\rangle. \end{aligned} \tag{A.0.2}$$

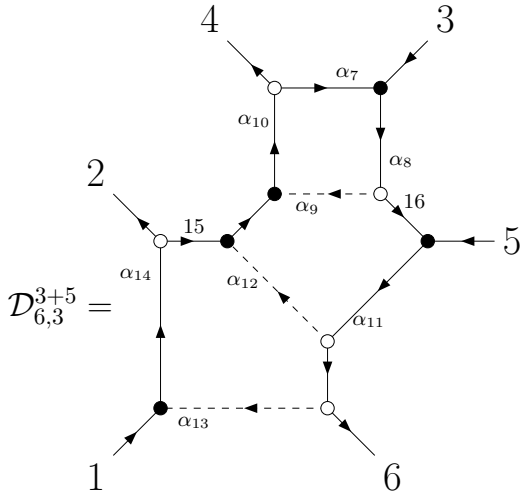

Figure A.1: '3+5' on-shell diagram to be summed over $2 \leftrightarrow 4$ and $3 \leftrightarrow 5$. Edge variables are indicated.

As an integral over edge variables, the diagram is then

$$\begin{aligned}
\mathcal{D}_{6,3}^{3+5} &= \operatorname*{Res}_{(612)=0} \int \prod_{i=7}^{14} \frac{d\alpha_i}{\alpha_i^2} \frac{d\tilde{\alpha}}{\tilde{\alpha}} \frac{\delta}{\alpha_8\alpha_{10}\alpha_{11}\alpha_{14}} \frac{\mathcal{J}_C^3 \mathcal{J}}{\mathcal{J}} \frac{\alpha_7\alpha_9\alpha_{12}\alpha_{13}}{\alpha_{11}\alpha_{14}} \langle 34\rangle[34]\langle 56\rangle[12], \\
&= \operatorname*{Res}_{(612)=0} \int \frac{d^{3\times 6}C}{\mathrm{GL}(3)} \frac{\delta\,\langle 34\rangle[34]\langle 56\rangle[12]}{\Delta^9 \alpha_7\alpha_8^5\alpha_9\alpha_{10}^6\alpha_{11}^8\alpha_{12}\alpha_{13}\alpha_{14}^7\tilde{\alpha}}, \\
&= \operatorname*{Res}_{(612)=0} \int \frac{d^{3\times 6}C}{\mathrm{GL}(3)} \frac{\delta\,\langle 34\rangle[34]\langle 56\rangle[12]}{(124)(234)(345)(356)(561)(612)(456)(346)(256)}, \\
&= \operatorname*{Res}_{(612)=0} \int d\Omega_7^{3\times 6} \frac{\langle 34\rangle[34]\langle 56\rangle[12]}{(256)(346)(356)} \frac{(123)}{(124)}.
\end{aligned} \tag{A.0.3}$$

5+3

We can obtain the result from (A.0.3) using the fact that the 3+5 and 5+3 diagrams are parity conjugates. In particular, we need to exchange square and angle brackets, substitute $(ijk) \to \epsilon_{ijklmn}(lmn)$ and apply the permutation $\mathcal{P} = \begin{pmatrix} 1 & 2 & 4 & 3 & 5 & 6 \\ 6 & 5 & 3 & 4 & 2 & 1 \end{pmatrix}$. This gives

$$\begin{aligned}
\mathcal{D}_{6,3}^{5+3} &= \operatorname*{Res}_{(345)\to 0} \int \frac{d^{3\times 6}C}{\mathrm{GL}(3)} \frac{\delta\,[34]\langle 34\rangle[56]\langle 12\rangle}{(356)(561)(612)(124)(234)(345)(123)(125)(134)}\bigg|_{\mathcal{P}}, \\
&= \operatorname*{Res}_{(432)\to 0} \int \frac{d^{3\times 6}C}{\mathrm{GL}(3)} (-1) \frac{\delta\,\langle 34\rangle[34]\langle 56\rangle[12]}{(421)(216)(165)(653)(543)(432)(654)(652)(643)}, \\
&= \operatorname*{Res}_{(432)\to 0} \int d\Omega_7^{3\times 6} \frac{\langle 34\rangle[34]\langle 56\rangle[12]}{(256)(346)(356)} \frac{(123)}{(124)}.
\end{aligned} \tag{A.0.4}$$

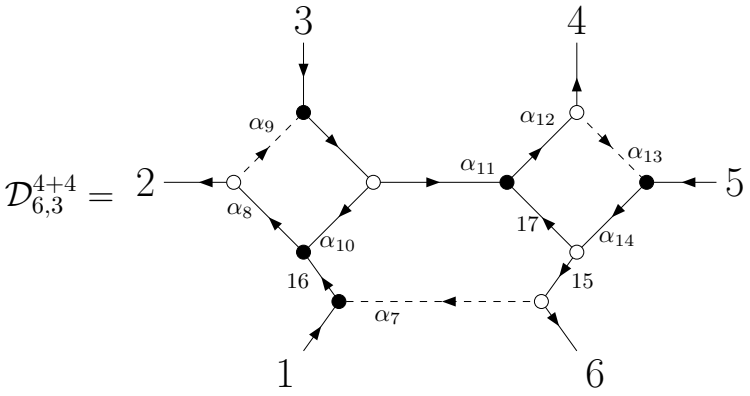

Figure A.2: '4+4' on-shell diagram to be summed over $2 \leftrightarrow 4$ and $3 \leftrightarrow 5$. Edge variables are indicated.

4+4

Next, we consider the $4+4$ diagram in Figure A.2. This gives the C-matrix and Jacobian

$$C = \begin{pmatrix} 1 & -\alpha_8 & -\alpha_8\alpha_9 & 0 & 0 & \tilde{\alpha} \\ -\alpha_{10} & 0 & 1 & -\alpha_{11}\alpha_{12} & -\alpha_{11}\alpha_{12}\alpha_{13} & 0 \\ -\alpha_7\alpha_{14} & 0 & 0 & -\alpha_{12}\alpha_{14} & 1-\alpha_{12}\alpha_{13}\alpha_{14} & \alpha_{14} \end{pmatrix},$$

$$\mathcal{J}_C = (1 - \alpha_8\alpha_9\alpha_{10} - \alpha_{12}\alpha_{13}\alpha_{14} - \alpha_7\alpha_8\alpha_9\alpha_{11}\alpha_{12}\alpha_{13}\alpha_{14} + \alpha_8\alpha_9\alpha_{10}\alpha_{12}\alpha_{13}\alpha_{14}). \tag{A.0.5}$$

This diagram corresponds to a residue around the pole $(456) = 0$. The bracket factors for the diagram are

$$\begin{aligned} \langle 10\,16\rangle &= \frac{1}{\alpha_8}\langle 10\,2\rangle = \frac{1}{\alpha_8}\langle 32\rangle, \\ [11\,10] &= \alpha_{10}[31], \\ \langle 17\,11\rangle &= \langle 6\,11\rangle = \frac{1}{\alpha_{11}\alpha_{12}}\langle 64\rangle, \\ [15\,17] &= \frac{1}{\alpha_{14}}[5\,17] = \frac{\alpha_{12}}{\alpha_{14}}[54]. \end{aligned} \tag{A.0.6}$$

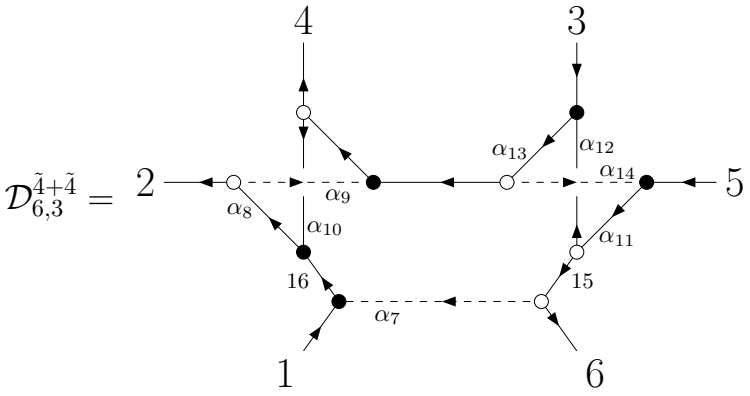

Figure A.3: '$\tilde{4}$+$\tilde{4}$' on-shell diagram with edge variables indicated.

The diagram then evaluates to

$$\begin{aligned}\mathcal{D}_{6,3}^{(4+4)} &= \operatorname*{Res}_{(456)=0}\int\prod_{i=7}^{14}\frac{d\alpha_i}{\alpha_i^2}\frac{d\tilde{\alpha}}{\tilde{\alpha}}\frac{\delta}{\alpha_8\alpha_{12}\alpha_{14}}\frac{\mathcal{J}_C^3\mathcal{J}}{\mathcal{J}}\frac{\alpha_7\alpha_9\alpha_{10}\alpha_{13}}{\alpha_8\alpha_{11}\alpha_{14}}[13][45]\langle 23\rangle\langle 46\rangle,\\ &= \operatorname*{Res}_{(456)=0}\int\frac{d^{3\times 6}C}{\mathrm{GL}(3)}\frac{\delta\,[13][45]\langle 23\rangle\langle 46\rangle}{\Delta^9\alpha_7\alpha_8^7\alpha_9\alpha_{10}\alpha_{11}^5\alpha_{12}^6\alpha_{13}\alpha_{14}^7\tilde{\alpha}},\\ &= \int d^{3\times 6}\Omega_7\frac{[13][45]\langle 23\rangle\langle 46\rangle}{(236)(246)^2}.\end{aligned} \tag{A.0.7}$$

$\tilde{\mathbf{4}}+\tilde{\mathbf{4}}$

Finally, we compute the non-planar $\tilde{4}+\tilde{4}$ diagram in Figure A.3. The C-matrix and Jacobian are given by

$$C = \begin{pmatrix} 1-\alpha_8\alpha_9\alpha_{10} & -\alpha_8 & 0 & -\alpha_8\alpha_9 & \tilde{\alpha} & \\ -\alpha_{10}\alpha_{13} & 0 & 1-\alpha_{13} & -\alpha_{13}\alpha_{14} & 0 & \\ -\alpha_7\alpha_{11} & 0 & -\alpha_{11}\alpha_{12} & 0 & 1 & -\alpha_1 1 \end{pmatrix}, \tag{A.0.8}$$

$$\mathcal{J}_C = (\Delta_1\Delta_2)^{-1} \equiv (1-\alpha_8\alpha_9\alpha_{10})(1-\alpha_{11}\alpha_{12}\alpha_{13}\alpha_{14}).$$

Moreover, the bracket factors are

$$\begin{aligned}\langle 10\,16\rangle &= \frac{1}{\alpha_8}\langle 2\,16\rangle = \frac{1}{\alpha_8}\langle 24\rangle,\\ [10\,4] &= \Delta_1\alpha_8\alpha_{10}[24],\\ \langle 3\,12\rangle &= \Delta_2\alpha_{11}\langle 35\rangle,\\ [15\,12] &= \alpha_{12}[15\,3] = \frac{\alpha_{12}}{\alpha_{11}}[53].\end{aligned} \tag{A.0.9}$$

Putting it all together, we obtain

$$\begin{aligned}
\mathcal{D}_{6,3}^{(\tilde{4}+\tilde{4})} &= \operatorname*{Res}_{(356)=0}\int\prod_{i=7}^{14}\frac{d\alpha_i}{\alpha_i^2}\frac{d\tilde{\alpha}}{\tilde{\alpha}}\frac{\mathcal{J}_C^3\mathcal{J}}{\mathcal{J}}\frac{\delta}{\alpha_8\alpha_{11}\alpha_{13}}\Delta_1\Delta_2\alpha_7\alpha_9\alpha_{10}\alpha_{12}\alpha_{14}\langle 24\rangle[24]\langle 35\rangle[53],\\
&= \operatorname*{Res}_{(356)=0}\int\frac{d^{3\times 6}C}{\mathrm{GL}(3)}\frac{\delta\,\langle 24\rangle[24]\langle 35\rangle[53]}{\Delta_1^8\Delta_2^7\alpha_7\alpha_8^6\alpha_9\alpha_{10}\alpha_{11}^6\alpha_{12}\alpha_{13}^6\alpha_{14}\tilde{\alpha}},\\
&= \operatorname*{Res}_{(356)=0}\int\frac{d^{3\times 6}C}{\mathrm{GL}(3)}\frac{\delta\,\langle 24\rangle[24]\langle 35\rangle[35]}{(124)(234)(345)(356)(561)(612)(146)(236)(245)},\\
&= \mathcal{D}_{6,3}^{(\tilde{4}+\tilde{4})} = \operatorname*{Res}_{(356)=0}\int d^{3\times 6}\Omega_7\frac{[24]\langle 24\rangle[35]\langle 35\rangle(123)(456)}{(146)(245)(236)(124)(356)}.
\end{aligned}\tag{A.0.10}$$

Appendix B

Momentum Twistor Transition Functions

In this Appendix, we will explain how to relate momentum twistors which are defined with respect to different permutations of momenta, which arise in section 3.2.4. First note that cyclic permutations ($a \to a+1$) and reflections ($a \to n-a$) simply permute the momentum twistors in a trivial way. The first non-trivial case is a permutation which exchanges two legs. For concreteness, let us consider the case

$$\mathcal{P} = \begin{pmatrix} 1 & 2 & \dots & n-1 & n \\ 1 & 2 & \dots & n & n-1 \end{pmatrix}, \tag{B.0.1}$$

where we have swapped the final two momenta. We will denote the transformed momenta as $p_n\big|_{\mathcal{P}} = p_{n-1}$ and vice versa. We can then consider new region momentum and momentum twistor coordinates defined via (3.2.65). In particular, this permutation only changes a single x_a so we can write

$$x_a\big|_{\mathcal{P}} = \begin{cases} x_a & , a \neq n, \\ x_{n-1} - p_n & , a = n. \end{cases} \tag{B.0.2}$$

This means only two twistor variables transform:

$$\begin{aligned} Z_a\Big|_{\mathcal{P}} &= Z_a, \qquad a < n{-}1 \\ Z_{n-1}\Big|_{\mathcal{P}} &= \begin{pmatrix} \lambda_n \\ \lambda_n x_{n-1} \end{pmatrix}, \\ Z_n\Big|_{\mathcal{P}} &= \begin{pmatrix} \lambda_{n-1} \\ \lambda_{n-1}(x_{n-1} - p_n) \end{pmatrix}, \end{aligned} \tag{B.0.3}$$

which we can rewrite to put both new twistors on an equal footing:

$$\begin{aligned} Z_{n-1}\Big|_{\mathcal{P}} &= Z_n - \langle n{-}1\, n\rangle \begin{pmatrix} 0 \\ \widetilde{\lambda}_{n-1} \end{pmatrix} = Z_n - \langle n{-}1\, n\rangle I Z_{n-1} \\ Z_n\Big|_{\mathcal{P}} &= Z_{n-1} - \langle n{-}1\, n\rangle \begin{pmatrix} 0 \\ \widetilde{\lambda}_{n} \end{pmatrix} = Z_{n-1} - \langle n{-}1\, n\rangle I Z_{n}, \end{aligned} \tag{B.0.4}$$

where IZ_i is the infinity twistor contracted with Z_i.

Now let's consider how twistor brackets transform. Using the rules derived above, we find that

$$\begin{aligned} \langle a\, b\, c\, n{-}1\rangle\Big|_{\mathcal{P}} &= \epsilon_{ABCD} Z_a^A Z_b^B Z_c^C\ Z_{n-1}^D\Big|_{\mathcal{P}}\,, \\ &= \langle abcn\rangle + \langle n{-}1\, n\rangle \left(-\epsilon_{ABCD} Z_a^A Z_b^B Z_c^C \begin{pmatrix} 0 \\ \widetilde{\lambda}_{n-1} \end{pmatrix}^D \right), \\ &= \langle abcn\rangle + \langle n{-}1\, n\rangle \left(-\epsilon_{ABCD} Z_a^A Z_b^B Z_c^C I^{DE} \frac{Z_{n-2}^F Z_{n-1}^G Z_n^H \epsilon_{EFGH}}{\langle n{-}2\, n{-}1\rangle\langle n{-}1\, n\rangle} \right), \\ &= \langle abcn\rangle - \frac{1}{\langle n{-}2\, n{-}1\rangle} \langle abc|I|n{-}2\, n{-}1\, n\rangle. \end{aligned} \tag{B.0.5}$$

Using analogous methods, we also find that

$$\langle a\, b\, c\, n\rangle\Big|_{\mathcal{P}} = \langle a\, b\, c\, n{-}1\rangle - \frac{1}{\langle n1\rangle} \langle abc|I|n{-}1\, n\, 1\rangle, \tag{B.0.6}$$

and

$$\begin{aligned}\langle a\, b\, n{-}1\, n\rangle\big|_{\mathcal{P}} = -\Bigg(&\langle a\, b\, n{-}1\, n\rangle + \frac{\langle abn|I|n{-}2\, n{-}1\, n\rangle}{\langle n{-}2\, n{-}1\rangle} \\ &- \frac{\langle ab\, n{-}1|I|n{-}1\, n\, 1\rangle}{\langle n1\rangle} + \frac{\langle ab\rangle\langle n{-}1\, n\rangle\langle n{-}2\, n{-}1\, n\, 1\rangle}{\langle n{-}2\, n{-}1\rangle\langle n1\rangle}\Bigg).\end{aligned} \tag{B.0.7}$$

The transformation rules for 6-brackets can then be deduced from the above rules using (2.1.29) and (2.1.30). Transition functions for more general permutations can be deduced from repeated composition of the above rules.

The extension to supertwistors is straightforward. Note that the fermionic components

$$\chi_a = \langle a\, \theta_a\rangle = \langle a\, \theta_{a+1}\rangle, \tag{B.0.8}$$

transform analogously to the $\tilde{\mu}$ components of the momentum twistors since the fermionic dual variables θ_a transform analogously to the x_a in (B.0.2). We therefore obtain

$$\theta_a\big|_{\mathcal{P}} = \begin{cases} \theta_a & , a \neq n, \\ \theta_{n-1} - q_n & , a = n. \end{cases} \tag{B.0.9}$$

so that

$$\chi_a\big|_{\mathcal{P}} = \begin{cases} \chi_a & , a < n-1, \\ \chi_n - \langle n{-}1\, n\rangle\, \eta_{n-1} & , a = n{-}1, \\ \chi_{n-1} - \langle n{-}1\, n\rangle\, \eta_n & , a = n. \end{cases} \tag{B.0.10}$$

Appendix C

Supergravity Leading Singularities from On-Shell Diagrams

On-shell diagrams for $\mathcal{N} = 4$ SYM have been used to obtain a number of loop-level results. While using the construction to get results for arbitrary loop order and MHV degree is not well-understood, there nevertheless exists a good understanding of 1-loop MHV along with a number of 2-loop results. It is therefore natural to ask if any of this can be carried over to supergravity? At the moment there exists only one loop integrand that can be obtained from an on-shell diagram, that of the 1-loop, four-point, MHV integrand for $\mathcal{N} = 8$. It is not clear how to extend this to higher points without introducing spurious poles into the loop integrand (poles that do not cancel). Instead we will consider here the calculation of leading singularities, rational functions of the external kinematics that are used to obtain loop amplitudes via generalised unitarity. This appendix will present a few 1- and 2-loop examples of six-point MHV leading singularities that may be calculated with on-shell diagrams, and where the $\mathcal{N} = 7$ formalism can be exploited to reduce the number of permutation sums required.

A detailed study of 1-loop supergravity leading singularities was carried out in [176] with n-point results for both MHV and NMHV, on-shell diagrams can be used to recover their results. 2-loop six-point supergravity leading singularities were

presented in [124] using diagrams suggestive of OSDs however the authors state that they did not use an OSD formalism to calculate their results. This appendix will demonstrate how OSDs may be used to obtain the same expressions.

Leading singularities come from putting the maximum possible number if propagators in loop diagrams on-shell without constraining the external kinematics. This leaves a set of tree-level amplitudes connected by on-shell propagators. To calculate the LS, the amplitudes are combined as a product and the states exchanged along the cuts are summed over (as with BCFW, this becomes a fermionic integral in the SUSY case). Since OSDs can already be used to calculate tree-amplitudes and automatically sum over the exchanged states it is natural to use them to calculate leading singularities. In the case of supergravity, we must be careful to ensure that any sums over permutations of external legs are included – ideally as permutations of external legs for the LS, so that sums over different diagram topologies are not needed. Since we will be working in $\mathcal{N} = 7$, we also need to be careful about the presence of closed cycles. Those appearing as part of the sub-amplitudes are necessary but care must be taked when assigning orientations to the full LS diagram to avoid introducing further cycles (thus reducing the number of permutations of external legs required). In each case, we shall proceed as follows:

1. Draw diagram for leading singularity as sub-amplitudes connected by on-shell propagators.

2. Decorate diagram with arrows indicating helicity flow so as to avoid closed cycles in the diagram.

3. Replace any sub-amplitudes with $n \geq 4$ with their corresponding on-shell diagrams as introduced in chapter 3.

4. Calculate corresponding spinor expression using algorithm in 3.

For all 1-loop and MHV diagrams these steps should always be possible.

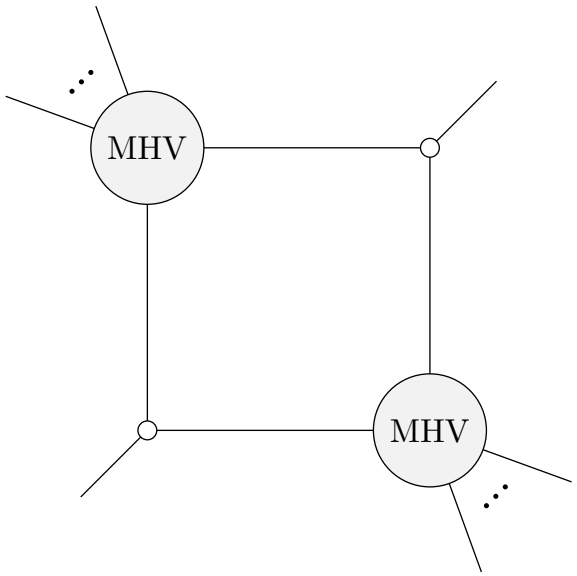

Figure C.1: Diagram for 1-loop n-pt MHV leading singularity

C.1 1 Loop Leading Singularities

We start at 1-loop. For MHV leading singularities there is one non-vanishing type known as the two-mass easy diagram, shown in figure C.1. This consists of two three-point $\overline{\text{MHV}}$ amplitudes positioned alternately with two MHV amplitudes with arbitrary points (the one mass LS is a special case where one MHV amplitude has three legs). In both cases, a helicity assignment avoiding a closed cycle around the cut propagators can be found by taking the legs attached to the $\overline{\text{MHV}}$ vertices to be the negative helicity ones (arrows incoming in the correspondbeing permutated will not attach to the internal propagators). All that remains is to attach the MHV amplitudes explored in chapter 3. For the six-point case, there are two ways to do this, shown in figure C.2. For illustrative purposes we will explicitly show how to evaluate the 2-mass easy case. This is the example where the use of $\mathcal{N} = 7$ removes the need for any permutation sums. Using the algorithm in section 3.1.2 we find

$$\mathcal{C}_6^{2me} = \int \prod_{i=7}^{14} \left(\frac{d\alpha_i}{\alpha_i^2}\right) \frac{1}{\alpha_8\alpha_{10}\alpha_{12}\alpha_{14}} \Delta_1^2\Delta_2^2\alpha_7\alpha_8\alpha_9\alpha_{10}\alpha_{11}\alpha_{12}\alpha_{13}\alpha_{14}\langle 26\rangle\langle 53\rangle[12][45]$$
$$\times \left([32] + \alpha_9\alpha_{10}[31]\right)\left([65] + \alpha_{13}\alpha_{14}[64]\right) \mathcal{J}_C^3 \delta^{(4|14)}(C\cdot\widetilde{\lambda})\delta^{(8)}(\lambda\cdot C^{\perp}) \tag{C.1.1}$$

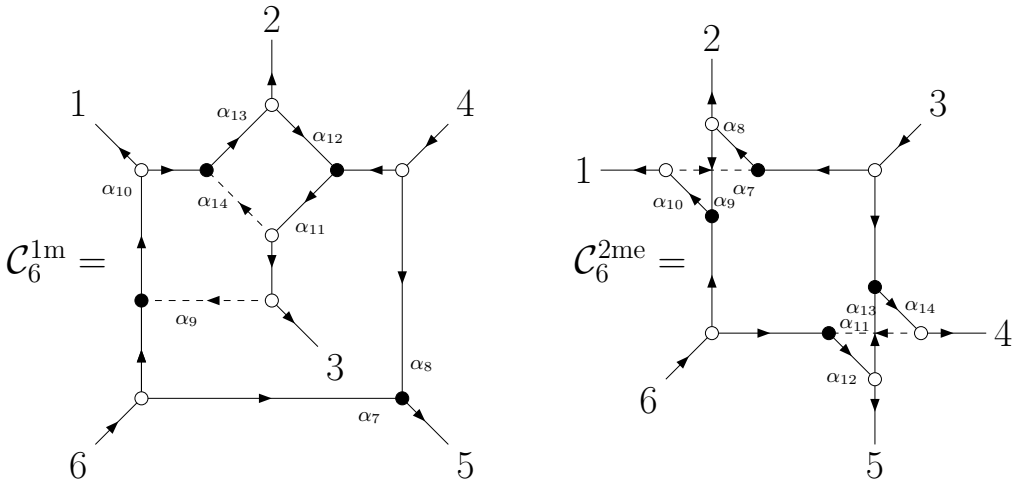

Figure C.2: On-shell diagrams for both six-point 1-loop MHV leading singularities, decorated with a possible helicity assignment

with

$$C = \begin{pmatrix} -\Delta_1\alpha_8\alpha_9\alpha_{10} & \Delta_1\alpha_8 & 1 & \Delta_2\alpha_{14} & -\Delta_2\alpha_{11}\alpha_{12}\alpha_{14} & 0 \\ -\Delta_1\alpha_{10} & -\Delta_1\alpha_7\alpha_8\alpha_{10} & 0 & -\Delta_2\alpha_{12}\alpha_{13}\alpha_{14} & -\Delta_2\alpha_{12} & 1 \end{pmatrix}, \tag{C.1.2}$$

where we have used $\mathcal{J}_C = (\Delta_1\Delta_2)^{-1}$, $\Delta_1 = (1 - \alpha_7\alpha_8\alpha_9\alpha_{10})^{-1}$, and $\Delta_2 = (1 - \alpha_{11}\alpha_{11}\alpha_{12}\alpha_{13}\alpha_{14})^{-1}$. The bridge decorations are simplest to work out using the algorithm originally worked out in [35]. The layout of the helicity flows means it is more straightforward to manually sum over the closed cycles rather than fixing them using a GL(2) transformation. To convert to a Grassmannian integral, we need the Jacobian

$$\frac{d^{2\times 6}C}{\text{GL}(2)} = \Delta_1^4\Delta_2^4\alpha_8\alpha_{10}^2\alpha_{12}^2\alpha_{14}^2. \tag{C.1.3}$$

It is also useful to use

$$\begin{aligned} \alpha_9\alpha_{10} &= \frac{(16)}{(26)}, \\ \alpha_{13}\alpha_{14} &= \frac{(34)}{(35)}. \end{aligned} \tag{C.1.4}$$

We therefore find $\langle 26\rangle([32]+\alpha_9\alpha_{10}[31]) \to [3|1+2|6\rangle$ and $\langle 53\rangle(65]+\alpha_{13}\alpha_{14}[64]) \to [6|5+4|3\rangle$. The remaining α_i in the integrand can be rewritten using

$$\Delta_1^5\Delta_2^5\alpha_7\alpha_8^4\alpha_9\alpha_{10}^4\alpha_{11}\alpha_{12}^4\alpha_{13}\alpha_{14}^4 = \frac{\mathrm{PT}(6)(13)(35)(46)(62)}{(36)}. \tag{C.1.5}$$

Making these substitutions and evaluation the Grassmannian integral gives

$$\mathcal{C}_6^{2me} = \delta^{(4|14)}(P|Q)\langle 36\rangle\frac{[3|1+2|6\rangle[6|5+4|3\rangle[12][45]}{\mathrm{PT}(6)\langle 13\rangle\langle 35\rangle\langle 46\rangle\langle 62\rangle}. \tag{C.1.6}$$

C.2 2 Loop Leading Singularities

For the two-loop case, the analysis here is more cursory. We take one of the examples from [124], present the helicity assignment necessary to uplift to $\mathcal{N}=7$ on-shell diagrams and then show that this produces the same results. When working with these 2-loop quantities we find a richer variety of on-shell diagram topologies including many non-planar diagrams. These give a greater variety of spinor bracket combinations than are seen in the amplitudes.

The calculations are intended as a proof of concept. There seems no obvious obstruction to extending to NMHV (although then translating between $\mathcal{N}=7$ and $\mathcal{N}=8$ becomes non-trivial) or to higher point cases (especially for one-loop). There also exist other on-shell diagram formulations for supergravity and it would be interesting to see if there is a systematic way to recover leading singularities without the use of bridge decorations. It would also be interesting to undertake a more detailed analysis of what happens if additional closed cycles are incorporated and if it is possible to associate any physical interpretation to (for example) a closed cycle running around one of the loops.

The example presented is that of the $\mathfrak{f}_1$ leading singularity. The diagram for this is shown in figure C.3. This has an integrand and C-matrix given by

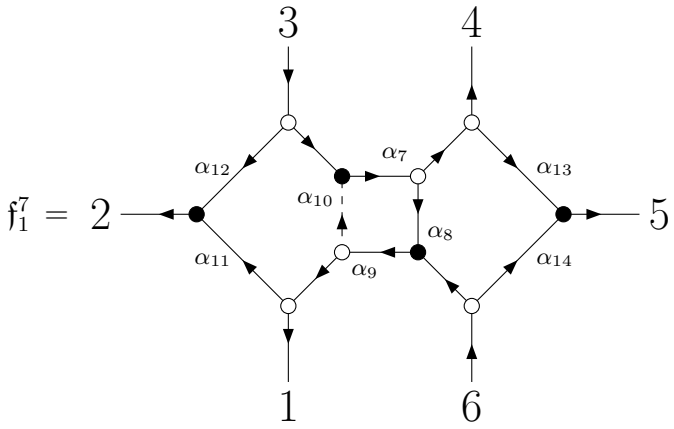

Figure C.3: Diagram for 2-loop $\mathfrak{f}_1^7$ MHV leading singularity

$$\mathfrak{f}_1^7 = \int \prod_{i=7}^{14} \frac{d\alpha_i}{\alpha_i^2} \frac{1}{\alpha_7\alpha_9} \frac{\Delta\alpha_7\alpha_{10}\alpha_{11}\alpha_{12}\alpha_{13}\alpha_{14}}{\alpha_{11}\alpha_{14}} \langle 23\rangle[23]\langle 56\rangle[56]\langle 36\rangle[12][45]$$
$$\times ([84] + \alpha_{13}[85])\, \mathcal{J}_C^3 \delta^{(4|14)}(C\cdot\widetilde{\lambda})\delta^{(8)}(\lambda\cdot C^{\perp}),$$
$$C = \begin{pmatrix} -\Delta\alpha_7\alpha_8\alpha_9 & -\alpha_{12} - \Delta\alpha_7\alpha_8\alpha_9\alpha_{11} & 1 & -\Delta\alpha_7 & -\Delta\alpha_7\alpha_{13} & 0 \\ -\Delta\alpha_9 & -\Delta\alpha_9\alpha_{11} & 0 & -\Delta\alpha_7\alpha_9\alpha_{10} & -\alpha_{14} - \Delta\alpha_7\alpha_9\alpha_{10}\alpha_{13} & 1 \end{pmatrix}, \tag{C.2.1}$$

with $\mathcal{J}_C = \Delta^{-1} = (1 - \alpha_7\alpha_8\alpha_9\alpha_{10})$. The square brackets involving $\widetilde{\lambda}_8$ are expanded using $\widetilde{\lambda}_8 = \widetilde{\lambda}_6 - \alpha_{14}\widetilde{\lambda}_5$ along with

$$\begin{aligned} \alpha_{13} &= \frac{(56)}{(46)}, \\ \alpha_{14} &= \frac{(45)}{(46)}, \end{aligned} \tag{C.2.2}$$

such that after performing all the integrals we will be left with the invariant $(k_4 + k_5 + k_6)^2$. The Jacobian for conversion to a Grassmannian integral is given by

$$\frac{d^{2\times 6}C}{\mathrm{GL}(2)} = \Delta^6\alpha_7^3\alpha_9^3. \tag{C.2.3}$$

We can use

$$\Delta^9\alpha_7^6\alpha_8\alpha_9^6\alpha_{10}\alpha_{11}^2\alpha_{12}\alpha_{13}\alpha_{14}^2 = \mathrm{PT}(6)\langle 23\rangle\langle 56\rangle\langle 14\rangle \tag{C.2.4}$$

to convert the remainder of the integrand into a GL(2) invariant form and after

integration we find

$$\mathfrak{f}_1^7 = \delta^{(4|14)}\langle 36\rangle \frac{[12][23][45][56](k_4+k_5+k_6)^2}{\mathrm{PT}(6)\langle 14\rangle\langle 36\rangle}. \tag{C.2.5}$$

Appendix D

AdS Spinor Helicity Identities

This appendix will review a number of useful formulae for working with AdS spinor helicity and identities that may be derived from those given in section 2.3.1. In section D.1 we then show how to specifically apply these identities to simplify the W_s^B term in equation (4.2.14).

We start with the spinor expressions for dot products of polarisation vectors with each other and with momenta. Using the polarisations in equation (2.3.13) and the bispinor form of the boundary momentum in equation (2.3.10), we obtain the following useful formulas for inner products

$$\begin{aligned} 2\mathbf{k}_a \cdot \epsilon_b^+ &= \frac{\langle a\bar{b}\rangle\langle \bar{b}\bar{a}\rangle}{ik_b}, \qquad 2\mathbf{k}_a \cdot \epsilon_b^- = \frac{\langle ab\rangle\langle \bar{a}b\rangle}{ik_b}, \\ 2\epsilon_a^+ \cdot \epsilon_b^+ &= -\frac{\langle \bar{a}\bar{b}\rangle^2}{k_a k_b}, \qquad 2\epsilon_a^- \cdot \epsilon_b^- = -\frac{\langle ab\rangle^2}{k_a k_b}, \\ 2\epsilon_a^- \cdot \epsilon_b^+ &= -\frac{\langle a\bar{b}\rangle^2}{k_a k_b}. \end{aligned} \tag{D.0.1}$$

These are used as the starting point for converting all the helicity amplitudes in section 4.2.3 into spinor form.

To derive spinor identies, we start from momentum conservation in equation (2.3.12)

and contract with various other spinors. At three points, this reduces to

$$\begin{aligned} \lambda_1^\alpha \bar{\lambda}_1^\beta + \lambda_2^\alpha \bar{\lambda}_2^\beta + \lambda_3^\alpha \bar{\lambda}_3^\beta &= iE\epsilon^{\alpha\beta}, \\ k_1 + k_2 + k_3 &= E, \\ \boldsymbol{k}_1 + \boldsymbol{k}_2 + \boldsymbol{k}_3 &= 0. \end{aligned} \tag{D.0.2}$$

To start, one identity can be derived from the 4-momentum dot product by expanding it in terms of 3-momenta and the radial components, then using momentum conservation

$$\begin{aligned} \langle bc\rangle\langle \bar{b}\bar{c}\rangle &= 2k_b^\mu k_{c\mu} = (\mathbf{k}_b + \mathbf{k}_c)^2 + (ik_b + ik_c)^2, \\ &= k_a^2 - (k_b + k_c)^2 = E(k_a - k_b - k_c). \end{aligned} \tag{D.0.3}$$

Other identities can be obtained by contracting the top line of equation (D.0.2) with various spinors:

$$\begin{aligned} \langle bc\rangle\langle \bar{b}\bar{c}\rangle &= E(k_a - k_b - k_c), \\ \langle ab\rangle\langle \bar{b}\bar{c}\rangle &= iE\langle a\bar{c}\rangle, \\ \langle ab\rangle\langle \bar{b}c\rangle &= i\langle ac\rangle(k_a + k_b - k_c), \\ \langle a\bar{b}\rangle\langle b\bar{c}\rangle &= i\langle \bar{a}\bar{c}\rangle(k_c - k_a - k_b), \\ \langle a\bar{b}\rangle\langle b\bar{c}\rangle &= i\langle a\bar{c}\rangle(k_a + k_c - k_b), \end{aligned} \tag{D.0.4}$$

for distinct particle labels a, b, c.

We can carry out the same process at four points where there are a few extra possibilities as we have more freedom to contract with different momenta:

$$\begin{aligned} \langle ab\rangle\langle \bar{a}\bar{b}\rangle - \langle cd\rangle\langle \bar{c}\bar{d}\rangle &= E(k_c + k_d - k_a - k_b), \\ \langle ab\rangle\langle \bar{b}\bar{d}\rangle + \langle ac\rangle\langle \bar{c}\bar{d}\rangle &= iE\langle a\bar{d}\rangle, \\ \langle ab\rangle\langle \bar{b}d\rangle + \langle ac\rangle\langle \bar{c}d\rangle &= i\langle ad\rangle(k_a + k_b + k_c - k_d), \\ \langle \bar{a}\bar{b}\rangle\langle b\bar{d}\rangle + \langle \bar{a}\bar{c}\rangle\langle c\bar{d}\rangle &= i\langle \bar{a}\bar{d}\rangle(k_d - k_a - k_b - k_c), \\ \langle a\bar{b}\rangle\langle b\bar{d}\rangle + \langle a\bar{c}\rangle\langle c\bar{d}\rangle &= i\langle a\bar{d}\rangle(k_a + k_d - k_b - k_c), \\ \langle ab\rangle\langle \bar{a}\bar{b}\rangle + \langle ac\rangle\langle \bar{a}\bar{c}\rangle + \langle ad\rangle\langle \bar{a}\bar{d}\rangle &= -2Ek_a, \end{aligned} \tag{D.0.5}$$

where a, b, c, d are distinct particle labels.

Some of these identities imply additional useful relations. For example, consider the following structures:

$$\begin{aligned} A &= \langle 1\bar{2}\rangle\langle \bar{1}\bar{3}\rangle\langle \bar{4}\bar{1}\rangle + \langle 2\bar{1}\rangle\langle \bar{2}\bar{4}\rangle\langle \bar{3}\bar{2}\rangle, \\ B &= \langle 3\bar{4}\rangle\langle \bar{1}\bar{3}\rangle\langle \bar{3}\bar{2}\rangle + \langle 4\bar{3}\rangle\langle \bar{2}\bar{4}\rangle\langle \bar{4}\bar{1}\rangle. \end{aligned} \tag{D.0.6}$$

Using momentum conservation to expand the mixed brackets we then find

$$\begin{aligned} A = \frac{1}{iE}\Big(&\langle 13\rangle\langle \bar{3}\bar{2}\rangle\langle \bar{1}\bar{3}\rangle\langle \bar{4}\bar{1}\rangle + \langle 14\rangle\langle \bar{4}\bar{2}\rangle\langle \bar{1}\bar{3}\rangle\langle \bar{4}\bar{1}\rangle \\ &+ \langle 23\rangle\langle \bar{3}\bar{1}\rangle\langle \bar{2}\bar{4}\rangle\langle \bar{3}\bar{2}\rangle + \langle 24\rangle\langle \bar{4}\bar{1}\rangle\langle \bar{2}\bar{4}\rangle\langle \bar{3}\bar{2}\rangle\Big) = B, \end{aligned} \tag{D.0.7}$$

where the second equality is obtained by rearranging the terms and applying momentum conservation again. In fact, these types of identities appear naturally when evaluating Witten diagrams, as we demonstrate in the next subsection. Noting that a 4-momentum $\lambda\bar{\lambda}$ is invariant under the little group transformation $\left(\lambda, \bar{\lambda}\right) \to \left(\alpha\lambda, \alpha^{-1}\bar{\lambda}\right)$, we see that that the above structures transform in the same way as an all-plus amplitude and will therefore be useful for simplifying that amplitude. It turns out that there are analogous identities for all helicities. The four cases are given by

$$\begin{aligned} \langle b\bar{a}\rangle\langle \bar{b}\bar{d}\rangle\langle \bar{b}\bar{c}\rangle + \langle a\bar{b}\rangle\langle \bar{a}\bar{c}\rangle\langle \bar{a}\bar{d}\rangle &= \langle c\bar{d}\rangle\langle \bar{a}\bar{c}\rangle\langle \bar{b}\bar{c}\rangle + \langle d\bar{c}\rangle\langle \bar{b}\bar{d}\rangle\langle \bar{a}\bar{d}\rangle, \\ \langle ba\rangle\langle \bar{b}\bar{d}\rangle\langle \bar{b}\bar{c}\rangle + \langle \bar{a}\bar{b}\rangle\langle a\bar{c}\rangle\langle a\bar{d}\rangle &= \langle c\bar{d}\rangle\langle a\bar{c}\rangle\langle \bar{b}\bar{c}\rangle + \langle d\bar{c}\rangle\langle \bar{b}\bar{d}\rangle\langle a\bar{d}\rangle, \\ \langle ba\rangle\langle \bar{b}\bar{d}\rangle\langle \bar{b}c\rangle + \langle \bar{a}\bar{b}\rangle\langle ac\rangle\langle a\bar{d}\rangle &= \langle \bar{c}\bar{d}\rangle\langle ac\rangle\langle \bar{b}c\rangle + \langle dc\rangle\langle \bar{b}\bar{d}\rangle\langle a\bar{d}\rangle, \\ \langle \bar{b}a\rangle\langle b\bar{d}\rangle\langle b\bar{c}\rangle + \langle \bar{a}b\rangle\langle a\bar{c}\rangle\langle a\bar{d}\rangle &= \langle c\bar{d}\rangle\langle a\bar{c}\rangle\langle b\bar{c}\rangle + \langle d\bar{c}\rangle\langle b\bar{d}\rangle\langle a\bar{d}\rangle, \end{aligned} \tag{D.0.8}$$

where the four lines are all-plus, single-minus, alternating MHV and split MHV, respectively. The other cases can be obtained by conjugation. These identities are all consequences of momentum conservation and the Schouten identity, but proving them is slightly different for each helicity configuration. The identities in (D.0.8) can also be related to each other in different factorisation channels. For example, in

the all-plus case we have

$$\langle 4\bar{1}\rangle\langle\bar{2}\bar{4}\rangle\langle\bar{3}\bar{4}\rangle + \langle 1\bar{4}\rangle\langle\bar{1}\bar{3}\rangle\langle\bar{1}\bar{2}\rangle = \langle 1\bar{2}\rangle\langle\bar{1}\bar{3}\rangle\langle\bar{1}\bar{4}\rangle + \langle 2\bar{1}\rangle\langle\bar{2}\bar{4}\rangle\langle\bar{2}\bar{3}\rangle - E^2\langle\bar{1}\bar{3}\rangle\langle\bar{2}\bar{4}\rangle\langle\bar{1}\bar{2}\rangle\langle\bar{3}\bar{4}\rangle, \tag{D.0.9}$$

which relates the s- and t-channel.

D.1 Simplifying Witten Diagrams

In this subsection, we will explain how to simplify the term W_s^B in equation (4.2.14) when written in terms of spinors, which is crucial for obtaining concise formulae for AdS_4 amplitudes. For concreteness, we will focus on the case $-+++$, since a similar strategy can be applied to other helicity configurations. Writing (4.2.14) in spinor notation gives

$$\begin{aligned} W_s^{B,-+++} = \frac{1}{8k_1k_2k_3k_4}\frac{1}{Es}\Big(&\langle 1\bar{2}\rangle^2\Big(\langle 4\bar{3}\rangle\langle\bar{3}\bar{4}\rangle(\langle 1\bar{4}\rangle\langle\bar{1}\bar{4}\rangle - \langle 2\bar{4}\rangle\langle\bar{2}\bar{4}\rangle) \\ &\quad + \langle 3\bar{4}\rangle\langle\bar{3}\bar{4}\rangle(\langle 1\bar{3}\rangle\langle\bar{1}\bar{3}\rangle - \langle 2\bar{3}\rangle\langle\bar{2}\bar{3}\rangle)\Big) \\ &+ \langle\bar{3}\bar{4}\rangle^2\Big(\langle 21\rangle\langle 1\bar{2}\rangle(\langle 3\bar{2}\rangle\langle\bar{3}\bar{2}\rangle + \langle 4\bar{2}\rangle\langle\bar{2}\bar{4}\rangle) \\ &\quad + \langle 1\bar{2}\rangle\langle\bar{1}\bar{2}\rangle(\langle 13\rangle\langle 1\bar{3}\rangle + \langle 41\rangle\langle 1\bar{4}\rangle)\Big) \\ &+ 2\langle\bar{2}\bar{4}\rangle^2\langle 12\rangle\langle 1\bar{2}\rangle\langle 4\bar{3}\rangle\langle\bar{3}\bar{4}\rangle + 2\langle\bar{2}\bar{3}\rangle^2\langle 12\rangle\langle 1\bar{2}\rangle\langle 3\bar{4}\rangle\langle\bar{3}\bar{4}\rangle \\ &- 2\langle 1\bar{3}\rangle^2\langle 1\bar{2}\rangle\langle\bar{1}\bar{2}\rangle\langle 3\bar{4}\rangle\langle\bar{3}\bar{4}\rangle - 2\langle 1\bar{4}\rangle^2\langle 1\bar{2}\rangle\langle\bar{1}\bar{2}\rangle\langle 4\bar{3}\rangle\langle\bar{3}\bar{4}\rangle\Big). \end{aligned} \tag{D.1.1}$$

Note that there are 4 terms with a factor of 2, and 8 terms without. These pair up in such a way that we can apply the Schouten a total of 8 times. Each of these gives a factor of k_i. For example, from the first line we have

$$\begin{aligned} \langle 1\bar{2}\rangle\langle\bar{3}\bar{4}\rangle\langle 1\bar{4}\rangle\langle 4\bar{3}\rangle\Big(\langle 1\bar{4}\rangle\langle\bar{2}\bar{1}\rangle + \langle 1\bar{2}\rangle\langle\bar{1}\bar{4}\rangle\Big) &= -2ik_1\langle 1\bar{2}\rangle\langle\bar{3}\bar{4}\rangle\langle 1\bar{4}\rangle\langle 4\bar{3}\rangle\langle\bar{2}\bar{4}\rangle, \\ \langle 1\bar{2}\rangle\langle\bar{3}\bar{4}\rangle\langle\bar{2}\bar{4}\rangle\langle 4\bar{3}\rangle\Big(\langle 21\rangle\langle\bar{4}\bar{2}\rangle + \langle 2\bar{4}\rangle\langle\bar{2}1\rangle\Big) &= 2ik_2\langle 1\bar{2}\rangle\langle\bar{3}\bar{4}\rangle\langle\bar{2}\bar{4}\rangle\langle 4\bar{3}\rangle\langle 1\bar{4}\rangle, \end{aligned} \tag{D.1.2}$$

where we have added pieces from the last four terms and used the Schouten identity. We note that there is a factor of $\langle 1\bar{2}\rangle\langle\bar{3}\bar{4}\rangle$ common to all terms. In addition, while

there still seem to be a lot of unpromising terms, factoring out the k_i gives

$$\begin{aligned} W_s^{B,-+++} = \frac{2i}{8k_1k_2k_3k_4}\frac{1}{Es}\Big((k_3+k_4)\Big(\langle\bar{1}\bar{2}\rangle\langle 1\bar{3}\rangle\langle 1\bar{4}\rangle + \langle 12\rangle\langle\bar{2}\bar{4}\rangle\langle\bar{3}\bar{2}\rangle\Big), \\ + (k_2-k_1)\Big(\langle 4\bar{3}\rangle\langle 1\bar{4}\rangle\langle\bar{2}\bar{4}\rangle + \langle 3\bar{4}\rangle\langle\bar{2}\bar{3}\rangle\langle 1\bar{3}\rangle\Big)\Big). \end{aligned} \tag{D.1.3}$$

We can then use the second line from (D.0.8) to get

$$W_s^{B,-+++} = \frac{i\langle 1\bar{2}\rangle\langle\bar{3}\bar{4}\rangle}{4k_1k_2k_3k_4}\frac{E-2k_1}{Es}\Big(\langle\bar{1}\bar{2}\rangle\langle 1\bar{3}\rangle\langle 1\bar{4}\rangle + \langle 12\rangle\langle\bar{2}\bar{4}\rangle\langle\bar{3}\bar{2}\rangle\Big). \tag{D.1.4}$$

Similar steps can be applied for any helicity configuration, and the final result will be proportional to $E - 2\sum_{i\in -} k_i$. For completeness, we list the all-plus and MHV cases. Others can be obtained by relabelling or conjugation:

$$\begin{aligned} W_s^{B,++++} &= \frac{i\langle\bar{1}\bar{2}\rangle\langle\bar{3}\bar{4}\rangle}{4k_1k_2k_3k_4}\frac{1}{s}\Big(\langle 2\bar{1}\rangle\langle\bar{2}\bar{4}\rangle\langle\bar{3}\bar{2}\rangle + \langle 1\bar{2}\rangle\langle\bar{1}\bar{3}\rangle\langle\bar{4}\bar{1}\rangle\Big), \\ W_s^{B,-+-+} &= \frac{i\langle 1\bar{2}\rangle\langle 3\bar{4}\rangle}{4k_1k_2k_3k_4}\frac{E-2k_1-2k_3}{Es}\Big(\langle 21\rangle\langle\bar{2}\bar{4}\rangle\langle 3\bar{2}\rangle + \langle\bar{1}\bar{2}\rangle\langle 31\rangle\langle 1\bar{4}\rangle\Big), \\ W_s^{B,--++} &= \frac{i\langle 12\rangle\langle\bar{3}\bar{4}\rangle}{4k_1k_2k_3k_4}\frac{E-2k_1-2k_2}{Es}\Big(\langle 1\bar{2}\rangle\langle 2\bar{4}\rangle\langle 2\bar{3}\rangle + \langle 2\bar{1}\rangle\langle 1\bar{3}\rangle\langle 1\bar{4}\rangle\Big). \end{aligned} \tag{D.1.5}$$

Appendix E

4pt Special Galileon Wavefunction Coefficient

In this appendix we include some more details about the 4pt wavefunction coefficient for the special Galileon that appears in chapters 5 and 6. We start with the explicit expression in $d = 3$ that was used to obtain the soft limit for a minimally coupled scalar ($\Delta = 3$) in (5.3.64). We then look at the wavefunction coefficient for general d and include some useful identities for obtaining the integrands in section 6.2.1 along with the integrands resulting from the $\hat{s}_{ab}^3$ operator.

E.1 Wavefunction Coefficient for minimally coupled scalars

The simplest way to get an expression for the special Galileon is from the cubic product of operators $\hat{s}_{12}^2 \hat{s}_{34}$ summed over cyclic permutations of (234). The action of these operators was given in equation (5.3.7). A more symmetric expression can be found by first summing over the exchange $(12) \leftrightarrow (34)$ or equivalently summing $(\hat{s}_{12} + \hat{s}_{34})\, \hat{s}_{12}\hat{s}_{34}$ over the three cyclic permutations. These expressions are obviously equivalent via the conformal Ward identities but at the level of integrands they are

only equal up to integration-by-parts identities (and the dropping of corresponding surface terms). The final integrated expressions will be related by boundary momentum conservation. We therefore schematically use $\hat{s} \equiv \hat{s}_{12} \equiv \hat{s}_{34}$, $\hat{t} \equiv \hat{s}_{14} \equiv \hat{s}_{23}$ and $\hat{s} \equiv \hat{s}_{13} \equiv \hat{s}_{24}$ to represent this combination of operators in a compact way.

For minimally coupled scalars we find that

$$
\begin{aligned}
(\hat{s}^3+\hat{t}^3+\hat{u}^3)\mathcal{C}_4^{\Delta=3} = \frac{360}{E^7}&k_1k_2k_3k_4k_1^\mu k_{2,\mu}k_3^\nu k_{4,\nu}\,(k_1^\sigma k_{2,\sigma}+k_3^\sigma k_{4,\sigma})\\
&\times\left(1+\frac{E}{6}\sum_{a=1}^{4}\frac{1}{k_a}+\frac{E^2}{30k_1k_2k_3k_4}\sum_{a<b}k_ak_b\right)\\
&+\frac{60}{E^6}k_1k_2k_3k_4\left((k_3+k_4)(k_1^\mu k_{2,\mu})^2+(k_1+k_2)(k_3^\mu k_{4,\mu})^2\right)\\
&+\frac{24}{E^5}\Bigg(10k_1k_2k_3k_4k_1^\mu k_{2,\mu}k_3^\nu k_{4,\nu}\\
&\quad+\frac{1}{2}\sum_{a<b}k_ak_b\Big(2k_1k_2k_3k_4\,(k_1^\mu k_{2,\mu}+k_3^\mu k_{4,\mu}-k_1k_2-k_3k_4)\\
&\qquad-2k_3^2k_4^2k_1^\mu k_{2,\mu}-2k_1^2k_2^2k_3^\mu k_{4,\mu}\\
&\qquad+2(k_1k_2+k_3k_4)k_1^\mu k_{2,\mu}k_3^\nu k_{4,\nu}\\
&\qquad+k_3k_4(k_1^\mu k_{2,\mu})^2+k_1k_2(k_3^\mu k_{4,\mu})^2\Big)\\
&\quad+\left(1+\sum_{a\neq b}\frac{k_a}{k_b}\right)k_1k_2k_3k_4\boldsymbol{k}_1\cdot\boldsymbol{k}_2\boldsymbol{k}_3\cdot\boldsymbol{k}_4\\
&\quad-(k_1^2k_2^2+k_3^2k_4^2)\boldsymbol{k}_1\cdot\boldsymbol{k}_2\boldsymbol{k}_3\cdot\boldsymbol{k}_4\\
&\quad+k_3^2k_4^2\boldsymbol{k}_1\cdot\boldsymbol{k}_2\left(-k_1^2-k_2^2+2(k_1k_2+k_3k_4)\right)\\
&\quad+k_1^2k_2^2\boldsymbol{k}_3\cdot\boldsymbol{k}_4\left(-k_3^2-k_4^2+2(k_1k_2+k_3k_4)\right)\\
&\quad-\frac{1}{2}\left(4k_1^2k_2^2k_3^2k_4^2+k_1^2k_2^2+(\boldsymbol{k}_3\cdot\boldsymbol{k}_4)^2+(\boldsymbol{k}_1\cdot\boldsymbol{k}_2)^2\right)\Bigg)\\
&+\frac{6}{E^4}\Bigg(\left(k_1k_2k_3k_4\sum_{a=1}^{4}\frac{1}{k_a}+\sum_{a\neq b}k_ak_b^2\right)\boldsymbol{k}_1\cdot\boldsymbol{k}_2\boldsymbol{k}_3\cdot\boldsymbol{k}_4\\
&\quad-2k_3^2k_4^2(k_3+k_4)\boldsymbol{k}_1\cdot\boldsymbol{k}_2-2k_1^2k_2^2(k_1+k_2)\boldsymbol{k}_3\cdot\boldsymbol{k}_4\Bigg)\\
&+\frac{2}{E^3}\Bigg(2\boldsymbol{k}_1\cdot\boldsymbol{k}_2\boldsymbol{k}_3\cdot\boldsymbol{k}_4(\boldsymbol{k}_1\cdot\boldsymbol{k}_2+\boldsymbol{k}_3\cdot\boldsymbol{k}_4)-\sum_{a<b}k_ak_b\boldsymbol{k}_1\cdot\boldsymbol{k}_2\boldsymbol{k}_3\cdot\boldsymbol{k}_4\\
&\quad+2k_3^2k_4^2\boldsymbol{k}_1\cdot\boldsymbol{k}_2+2k_1^2k_2^2\boldsymbol{k}_3\cdot\boldsymbol{k}_4\Bigg)\\
&+\frac{4}{E}\boldsymbol{k}_1\cdot\boldsymbol{k}_2\boldsymbol{k}_3\cdot\boldsymbol{k}_4+\text{cyc}(234),
\end{aligned}
\tag{E.1.1}
$$

where $k_a^\mu k_{b,\mu}=\boldsymbol{k}_a\cdot\boldsymbol{k}_b-k_ak_b$. This expression mixes different types of dot products in order to obtain a more compact form. This appears to be a generic feature of

minimally coupled scalar wavefunction coefficients.

E.2 4-point sGal Soft Limit

We now look at how to instead obtain an expression for an integrand with general d and Δ. For the purposes of taking soft limits it is better to use the conformal Ward identities to write the wavefunction coefficient as a sum of cubes of operators as in equation (6.2.14). The downside is that the action of the conformal generators is more complicated to work out.

To evaluate the $\hat{s}^3_{ab}$ terms in (6.2.14) we use the definitions in (2.1.15) along with their action on bulk-to-boundary propagators from equation 5.1.4

$$\begin{aligned} D\mathcal{K}_\nu &= \eta\tfrac{\partial}{\partial\eta}\mathcal{K}_\nu, \qquad P^i\mathcal{K}_\nu = k^i\mathcal{K}_\nu, \\ K_i\mathcal{K}_\nu &= \eta^2 k_i\mathcal{K}_\nu, \qquad M_{ij}\mathcal{K}_\nu = 0. \end{aligned} \tag{E.2.1}$$

To evaluate the action of $\hat{s}^3_{ab}$ we also need

$$\begin{aligned} K_i(k_a\phi) &= \eta^2 k_i k_a\phi - 2\eta\delta_{ai}\dot{\phi}, \\ K_i\dot{\phi} &= k_i(\eta^2\dot{\phi} + 2\eta\phi), \\ K_i(k_a k_b\phi) &= \eta^2 k_i k_a k_b\phi - 2(\delta_{ia}k_b + \delta_{ib}k_a)(\phi + \eta\dot{\phi}) + 2k_i\delta_{ab}\phi, \\ K_i\ddot{\phi} &= k_i(\eta^2\ddot{\phi} + 4\eta\dot{\phi} + 2\phi), \\ D\dot{\phi} &= \eta\ddot{\phi} + \dot{\phi}, \\ M_{ab}\left(\boldsymbol{k}_a\cdot\boldsymbol{k}_b f(k_a,k_b)\right) &= 2(d-1)\boldsymbol{k}_a\cdot\boldsymbol{k}_b f(k_a,k_b), \\ M_{ab}\left((\boldsymbol{k}_a\cdot\boldsymbol{k}_b)^2 f(k_a,k_b)\right) &= 4\left(d(\boldsymbol{k}_a\cdot\boldsymbol{k}_b)^2 - k_a^2k_b^2\right) f(k_a,k_b), \end{aligned} \tag{E.2.2}$$

where $f(k_a,k_b)$ is some function depending only on the magnitudes of the momenta. These operations were implemented in Mathematica in the form of replacement rules (this enables the integrands to be evaluated much faster than if it were evaluating them as derivatives) in [4].

The action of the cubic operator is then given by

$$\begin{aligned}\hat{s}^3_{12}\phi_1\phi_2 = \eta^6\Bigg[&(\boldsymbol{k}_1\cdot\boldsymbol{k}_2)^3\phi_1\phi_2 + 3(\boldsymbol{k}_1\cdot\boldsymbol{k}_2)^2\dot{\phi}_1\dot{\phi}_2 + 3(\boldsymbol{k}_1\cdot\boldsymbol{k}_2)\ddot{\phi}_1\ddot{\phi}_2 + \dddot{\phi}_1\dddot{\phi}_2\\
&+\frac{3}{\eta}\Big(2(\boldsymbol{k}_1\cdot\boldsymbol{k}_2)^2(\dot{\phi}_1\phi_2+\phi_1\dot{\phi}_2)\\
&\quad+(\boldsymbol{k}_1\cdot\boldsymbol{k}_2)\left(-k_1^2\phi_1\dot{\phi}_2 - k_2^2\dot{\phi}_1\phi_2 + 3(\ddot{\phi}_1\dot{\phi}_2+\dot{\phi}_1\ddot{\phi}_2)\right)\\
&\quad-k_1^2\dot{\phi}_1\ddot{\phi}_2 - k_2^2\ddot{\phi}_1\dot{\phi}_2 + \dddot{\phi}_1\ddot{\phi}_2 + \ddot{\phi}_1\dddot{\phi}_2\Big)\\
&+\frac{1}{\eta^2}\Big((10-3d)(\boldsymbol{k}_1\cdot\boldsymbol{k}_2)^2\phi_1\phi_2\\
&\quad+2(\boldsymbol{k}_1\cdot\boldsymbol{k}_2)\Big(2(\ddot{\phi}_1\phi_2+\phi_1\ddot{\phi}_2)+(29-3d)\dot{\phi}_1\dot{\phi}_2-(k_1^2+k_2^2)\phi_1\phi_2\Big)\\
&\quad+2k_1^2k_2^2\phi_1\phi_2\\
&\quad-k_1^2(5\dot{\phi}_1\dot{\phi}_2+4\phi_1\ddot{\phi}_2)-k_2^2(5\dot{\phi}_1\dot{\phi}_2+4\ddot{\phi}_1\phi_2)+\dddot{\phi}_1\dot{\phi}_2+\dot{\phi}_1\dddot{\phi}_2\Big)\\
&+\frac{1}{\eta^3}\Big(4(3-d)\boldsymbol{k}_1\cdot\boldsymbol{k}_2(\dot{\phi}_1\phi_2+\phi_1\dot{\phi}_2)+(d-6)k_1^2\phi_1\dot{\phi}_2\\
&\quad+(d-6)k_2^2\dot{\phi}_1\phi_2+3(\ddot{\phi}_1\dot{\phi}_2+\dot{\phi}_1\ddot{\phi}_2)\Big)\\
&+\frac{1}{\eta^4}\left((d-2)^2\boldsymbol{k}_1\cdot\boldsymbol{k}_2\phi_1\phi_2+\dot{\phi}_1\dot{\phi}_2\right)\Bigg].\end{aligned} \tag{E.2.3}$$

We can then compute the soft limit

$$\begin{aligned}\lim_{\boldsymbol{k}_1\to 0}\hat{s}^3_{12}\phi_1\phi_2 =\eta^6\Bigg(&\dddot{\phi}_1\dddot{\phi}_2+\frac{3}{\eta}\left(-k_2^2\ddot{\phi}_1\dot{\phi}_2+\dddot{\phi}_1\ddot{\phi}_2+\ddot{\phi}_1\dddot{\phi}_2\right),\\
&+\frac{1}{\eta^2}\left(-k_2^2(5\dot{\phi}_1\dot{\phi}_2+4\ddot{\phi}_1\phi_1)+\dddot{\phi}_1\dot{\phi}_2+9\ddot{\phi}_1\ddot{\phi}_2+\dot{\phi}_1\dddot{\phi}_2)\right),\\
&+\frac{1}{\eta^3}\left((d-6)k_2^2\dot{\phi}_1\dot{\phi}_2+3(\ddot{\phi}_1\dot{\phi}_2+\dot{\phi}_1\ddot{\phi}_2)\right)+\frac{1}{\eta^4}\dot{\phi}_1\dot{\phi}_2\Bigg)+\mathcal{O}(k_1).\end{aligned} \tag{E.2.4}$$

To unambiguously fix all the curvature corrections as was done in section 6.2.1 also requires the subleading soft limit. This is omitted here as the full expansion is quite lengthy.

Appendix F

Soft limit of 6pt DBI in dS

This Appendix, provides more details about the calculation in section 6.3.2. In particular, it presents an algorithm for systematically applying equivalence relations to express the 6-point tree-level wavefunction coefficient in terms of linearly independent terms. This allows all the couplings to be fixed from enhanced soft limits, implemented in Mathematica in order to obtain the results in chapter 6.
The equivalence relations that can be applied to the wavefunction coefficients are

- conformal Ward identities in terms of the $\hat{s}_{ab}$ operators,
- boundary momentum conservation,
- equations of motion for the bulk-to-boundary wavefunctions,
- integration by parts identities/ addition of a total derivative to the integrand.

Note that any boundary contributions that may come from integration by parts are neglected since they have delta function support when Fourier transformed to position space. Although the relations implied by conformal Ward identities can also be obtained from a combination of the other three equivalence relations, in practice use all four are used in such a way as to remove the need for guesswork. In particular, momentum conservation, equations of motion, and integration by parts relations are applied in a particular order such that the latter can be constructed systematically.

After fixing Δ from the enhanced soft limit at four points, it is sufficient to work to leading order in the soft momentum in order to fix the 6-point couplings. The procedure for fixing these couplings is as follows:

1. Write the soft limit of an exchange diagram as a contact diagram by cancelling numerator and denominator in this limit (see (6.3.12)).

2. Sum all diagrams over permutations to obtain the wavefunction coefficient. The wavefunction coefficient is now of the form $f(\hat{s}_{ab})\mathcal{C}_6$, where f is a polynomial up to cubic order in the $\hat{s}_{ab}$.

3. Apply the conformal Ward identities to eliminate one leg and one $\hat{s}_{ab}$, mimicking the use of momentum conservation needed to demonstrate enhanced limits of amplitudes in flat space. We choose to eliminate leg n and $\hat{s}_{n-2\,n-1}$ using $\hat{s}_{an} = -\sum_{b=1}^{n-1} s_{ab}$ and $\left(\sum_{a=1}^{n-1}\mathcal{D}_a\right)^2 = \hat{s}_{nn}$. At each stage we can also apply $\hat{s}_{aa} \sim -m^2$. Note that this will remove any derivatives acting on the field ϕ_n. It will not however remove all occurrences of $\boldsymbol{k}_{n-2}\cdot\boldsymbol{k}_{n-1}$ in the integrand since they can also appear from the successive action of $\hat{s}_{a\,n-2}\hat{s}_{a\,n-1}$, for example. This means that we can still apply boundary momentum conservation to eliminate quantities that are not independent.

4. Use (6.2.2) to finish taking the soft limit and use the propagator equation of motion to remove factors of k_a^2.

5. Use boundary momentum conservation to remove $\boldsymbol{k}_{n-2}\cdot\boldsymbol{k}_{n-1}$. This will re-introduce the magnitudes k_a^2 (including k_n) so we again apply equations of motion such that the integrand contains only functions not linked by equations of motion.

6. The equations of motion will introduce derivatives of ϕ_n so use integration by parts to remove $\ddot{\phi}_n$ and then $\dot{\phi}_n$. This step can be done systematically by identifying terms of the form $\int d\eta\, g(\eta, \boldsymbol{k}_a, \partial_\eta^l\phi_{b\neq n})\partial_\eta^m\phi_n$ for some function g and deriving the appropriate total derivative which contains it.

7. The wavefunction coefficient can now be seen to vanish for specific choices of the coefficients A, B, C in (6.3.7).

Finally, it is interesting to note that operators which are quadratic or cubic in leg 1 can be written as combinations of operators that are at most linear in leg 1, up to $\mathcal{O}(k_1)$. It is this property for example that leads to equation (6.3.12). It can also be used to write

$$\begin{aligned}\hat{s}_{12}^3\mathcal{C}_6^{\Delta=d+1} &= \Big((d^2+d+1)\hat{s}_{12}+d(d+1)\Big)\,\mathcal{C}_6^{\Delta=d+1}+\mathcal{O}(k_1^2),\\ \hat{s}_{12}\hat{s}_{13}\hat{s}_{23}\mathcal{C}_6^{\Delta=d+1} &= \Big(\hat{s}_{23}^2+\hat{s}_{13}\hat{s}_{23}-(d+1)\hat{s}_{12}+d\hat{s}_{23}\Big)\,\mathcal{C}_6^{\Delta=d+1}+\mathcal{O}(k_1^2).\end{aligned} \tag{F.0.1}$$

This is a non-exhaustive list. In principal, these properties could be used to solve for the unknown coefficients without needing to consider the full integrand.

F.1 Matching 6-point Wavefunctions

This section shows that the wavefunction coefficient obtained from the Lagrangian in (6.3.15) gives the same wavefunction coefficient as the one obtained from enhanced soft limits. Applying the free equation of motion to rewrite the $(\nabla\phi)^2\phi^4$ as a ϕ^6 interaction gives

$$\begin{aligned}\frac{\mathcal{L}_6^{\rm DBI}}{\sqrt{|g|}} = &-\frac{1}{2}(\nabla\phi)^2+\frac{d+1}{2}\phi^2-\frac{1}{8}(\nabla\phi)^4\\ &-\frac{1}{4}(d+3)(\nabla\phi)^2\phi^2+\frac{3(d+1)(d+3)}{4!}\phi^4-\frac{3}{48}(\nabla\phi)^6\\ &-\frac{3(d+5)}{16}(\nabla\phi)^4\phi^2+\frac{6(d+1)(d+3)(d+5)}{6!}\phi^6.\end{aligned} \tag{F.1.1}$$

This gives the following contribution from 6-point contact Witten diagrams:

$$\begin{aligned}\Psi_{6,\,\rm cont}^{\rm DBI} = \Big[&3\left(\hat{s}_{12}\hat{s}_{34}\hat{s}_{56}+\text{perms}\right)-(5+d)\left(\hat{s}_{12}\hat{s}_{34}+\text{perms}\right)\\ &+6(1+d)(3+d)(5+d)\Big]\mathcal{C}_6^{\Delta=d+1},\end{aligned} \tag{F.1.2}$$

where the terms are summed over all inequivalent permutations. The contribution from exchange diagrams is given by

$$\begin{aligned}\Psi^{\text{DBI}}_{6,\,\text{exch}} = \frac{1}{(\mathcal{D}_1+\mathcal{D}_2+\mathcal{D}_3)^2+m^2}\Big[\Big(&\hat{s}_{12}\hat{s}_{3L}+\text{Cyc.}[123]-3(1+d)(3+d)\\ &-(d+3)\left(\hat{s}_{12}+\hat{s}_{23}+\hat{s}_{31}+\mathcal{D}_L\cdot(\mathcal{D}_1+\mathcal{D}_2+\mathcal{D}_3)\right)\Big)\\ &\times(123)\leftrightarrow(456)\Big]\mathcal{C}_6^{\Delta=d+1}+\text{perms.}\end{aligned} \tag{F.1.3}$$

Next the conformal Ward identity $-\mathcal{D}_L=\mathcal{D}_1+\mathcal{D}_2+\mathcal{D}_3$ can be used at the vertex to express the terms quadratic in boundary conformal generators terms as an inverse propagator plus a constant

$$\begin{aligned}\Psi^{\text{DBI}}_{6,\,\text{exch}} = \frac{1}{(\mathcal{D}_1+\mathcal{D}_2+\mathcal{D}_3)^2+m^2}\Big[\Big(&\hat{s}_{12}\hat{s}_{3L}+\text{Cyc.}[123]-3(1+d)(3+d)\\ &-(d+3)\left(\frac{1}{2}\left((\mathcal{D}_1+\mathcal{D}_2+\mathcal{D}_3)^2+m^2\right)+2(d+1)\right)\Big)\\ &\times(123)\leftrightarrow(456)\Big]\mathcal{C}_6^{\Delta=d+1}+\text{perms},\end{aligned} \tag{F.1.4}$$

where $\mathcal{D}_a^2\sim -m^2$ has been used to simplify the constant. This can be identified as the exchange diagram from (6.3.10) plus a new contact contribution

$$\Psi^{\text{DBI}}_{6,\,\text{exch}} = \frac{\Psi_L\Psi_R}{(\mathcal{D}_1+\mathcal{D}_2+\mathcal{D}_3)+m^2}\mathcal{C}_6^{\Delta=d+1}+\tilde{\Psi}^{DBI}_{6,\,\text{cont}}, \tag{F.1.5}$$

where

$$\begin{aligned}\tilde{\Psi}^{\text{DBI}}_{6,\,\text{cont}} = \Big[\frac{1}{2}(d+3)(\Psi_L+\Psi_R)+\frac{1}{4}(d+3)^2\left((\mathcal{D}_1+\mathcal{D}_2+\mathcal{D}_3)^2+m^2\right)\Big]\mathcal{C}_6^{\Delta=d+1}\\ +\text{perms}.\end{aligned} \tag{F.1.6}$$

The new contact contribution is now considered in detail, summing over the 10 factorisation channels and comparing to the form in (F.1.2). To do this, the quadratic term needs to be expressed as a sum of terms each with 4 distinct labels. This can be accomplished using the conformal Ward identities to write $\mathcal{D}_L=\mathcal{D}_4+\mathcal{D}_5+\mathcal{D}_6$ to get

$$\Psi_L=\hat{s}_{12}(\hat{s}_{34}+\hat{s}_{35}+\hat{s}_{36})+\text{Cyc.}[123]-(1+d)(3+d), \tag{F.1.7}$$

and analogously for Ψ_R. The quadratic term from $\Psi_L + \Psi_R$ will contain 18 terms so the sum over 10 channels will give a permutation-invariant sum of 180 terms. Since there are 45 unique $\hat{s}_{ab}\hat{s}_{cd}$, this gives us a symmetry factor of 4. A similar analysis of the linear terms from $(\mathcal{D}_1 + \mathcal{D}_2 + \mathcal{D}_3)^2$ gives a symmetry factor of 4 as well. The new contact contribution can therefore be expressed as

$$\begin{aligned}\tilde{\Psi}^{\text{DBI}}_{6,\,\text{cont}} = \Big[&2(d+3)(\hat{s}_{12}\hat{s}_{34} + \text{perms}) + (d+3)^2(\hat{s}_{12} + \text{perms}) \\ &- 5(d+1)(d+3)^2\Big]\mathcal{C}_6^{\Delta=d+1}.\end{aligned} \tag{F.1.8}$$

Noting that $(\hat{s}_{12} + \text{perms}) = 3m^2 = -3(d+1)$, this becomes

$$\tilde{\Psi}^{\text{DBI}}_{6,\,\text{cont}} = \Big[2(d+3)(\hat{s}_{12}\hat{s}_{34} + \text{perms}) - 8(d+1)(d+3)^2\Big]\,\mathcal{C}_6^{\Delta=d+1}. \tag{F.1.9}$$

This can be combined with equation (F.1.2) to give

$$\Psi^{\text{DBI}}_{6,\,\text{cont}} = \Big[(d+1)(\hat{s}_{12}\hat{s}_{34} + \text{perms}) + 2(d+1)(9-d^2)\Big]\,\mathcal{C}_6^{\Delta=d+1}, \tag{F.1.10}$$

matching the result obtained from the enhanced soft limit. This wavefunction coefficient therefore also corresponds to the one obtained from (6.3.14).

Bibliography

[1] Connor Armstrong, Joseph A. Farrow and Arthur E. Lipstein. '$\mathcal{N} = 7$ On-shell diagrams and supergravity amplitudes in momentum twistor space'. In: *JHEP* 01 (2021), p. 181.
doi:10.1007/JHEP01(2021)181.
arXiv:2010.11813 [hep-th].

[2] Connor Armstrong, Arthur E. Lipstein and Jiajie Mei. 'Color/kinematics duality in AdS_4'. In: *JHEP* 02 (2021), p. 194.
doi:10.1007/JHEP02(2021)194.
arXiv:2012.02059 [hep-th].

[3] Connor Armstrong, Humberto Gomez, Renann Lipinski Jusinskas, Arthur Lipstein and Jiajie Mei. 'Effective field theories and cosmological scattering equations'. In: *JHEP* 08 (2022), p. 054.
doi:10.1007/JHEP08(2022)054.
arXiv:2204.08931 [hep-th].

[4] Connor Armstrong, Arthur Lipstein and Jiajie Mei. 'Enhanced soft limits in de Sitter space'. In: *JHEP* 12 (2022), p. 064.
doi:10.1007/JHEP12(2022)064.
arXiv:2210.02285 [hep-th].

[5] Stephen J. Parke and T. R. Taylor. 'Gluonic Two Goes to Four'. In: *Nucl. Phys. B* 269 (1986), pp. 410–420.
doi:10.1016/0550-3213(86)90230-0.

[6] Stephen J. Parke and T.R. Taylor. 'An Amplitude for n Gluon Scattering'. In: *Phys. Rev. Lett.* 56 (1986), p. 2459.
doi:10.1103/PhysRevLett.56.2459.

[7] Nima Arkani-Hamed, Jacob L. Bourjaily, Freddy Cachazo, Alexander B. Goncharov, Alexander Postnikov and Jaroslav Trnka. *Grassmannian Geometry of Scattering Amplitudes*. Cambridge University Press, Apr. 2016.
doi:10.1017/CBO9781316091548.
arXiv:1212.5605 [hep-th].

[8] James Drummond, Jack Foster, Ömer Gürdoğan and Chrysostomos Kalousios. 'Tropical fans, scattering equations and amplitudes'. In: *JHEP* 11 (2021), p. 071.
doi:10.1007/JHEP11(2021)071.
arXiv:2002.04624 [hep-th].

[9] Nima Arkani-Hamed, Song He, Giulio Salvatori and Hugh Thomas. 'Causal diamonds, cluster polytopes and scattering amplitudes'. In: *JHEP* 11 (2022), p. 049.
doi:10.1007/JHEP11(2022)049.
arXiv:1912.12948 [hep-th].

[10] Nima Arkani-Hamed, Tzu-Chen Huang and Yu-tin Huang. 'The EFT-Hedron'. In: *JHEP* 05 (2021), p. 259.
doi:10.1007/JHEP05(2021)259.
arXiv:2012.15849 [hep-th].

[11] Nima Arkani-Hamed, Aaron Hillman and Sebastian Mizera. 'Feynman polytopes and the tropical geometry of UV and IR divergences'. In: *Phys. Rev. D* 105.12 (2022), p. 125013.
doi:10.1103/PhysRevD.105.125013.
arXiv:2202.12296 [hep-th].

[12] Nima Arkani-Hamed and Jaroslav Trnka. 'The Amplituhedron'. In: *JHEP* 10 (2014), p. 030.
doi:10.1007/JHEP10(2014)030.
arXiv:1312.2007 [hep-th].

[13] Nima Arkani-Hamed, Hugh Thomas and Jaroslav Trnka. 'Unwinding the Amplituhedron in Binary'. In: *JHEP* 01 (2018), p. 016.
doi:10.1007/JHEP01(2018)016.
arXiv:1704.05069 [hep-th].

[14] Livia Ferro and Tomasz Lukowski. 'Amplituhedra, and Beyond'. In: (July 2020).
arXiv:2007.04342 [hep-th].

[15] Ruth Britto, Freddy Cachazo, Bo Feng and Edward Witten. 'Direct proof of tree-level recursion relation in Yang-Mills theory'. In: *Phys. Rev. Lett.* 94 (2005), p. 181602.
doi:10.1103/PhysRevLett.94.181602.
arXiv:hep-th/0501052.

[16] Nima Arkani-Hamed, Jacob L. Bourjaily, Freddy Cachazo, Simon Caron-Huot and Jaroslav Trnka. 'The All-Loop Integrand For Scattering Amplitudes in Planar N=4 SYM'. In: *JHEP* 01 (2011), p. 041.
doi:10.1007/JHEP01(2011)041.
arXiv:1008.2958 [hep-th].

[17] Rutger H. Boels. 'On BCFW shifts of integrands and integrals'. In: *JHEP* 11 (2010), p. 113.
doi:10.1007/JHEP11(2010)113.
arXiv:1008.3101 [hep-th].

[18] Andrew Hodges. 'Eliminating spurious poles from gauge-theoretic amplitudes'. In: *JHEP* 05 (2013), p. 135.

doi:10.1007/JHEP05(2013)135.

arXiv:0905.1473 [hep-th].

[19] Nima Arkani-Hamed, Jacob L. Bourjaily, Freddy Cachazo, Andrew Hodges and Jaroslav Trnka. 'A Note on Polytopes for Scattering Amplitudes'. In: *JHEP* 04 (2012), p. 081.

doi:10.1007/JHEP04(2012)081.

arXiv:1012.6030 [hep-th].

[20] Arthur E. Lipstein and Lionel Mason. 'From the holomorphic Wilson loop to 'd log' loop-integrands for super-Yang-Mills amplitudes'. In: *JHEP* 05 (2013), p. 106.

doi:10.1007/JHEP05(2013)106.

arXiv:1212.6228 [hep-th].

[21] Arthur E. Lipstein and Lionel Mason. 'From d logs to dilogs the super Yang-Mills MHV amplitude revisited'. In: *JHEP* 01 (2014), p. 169.

doi:10.1007/JHEP01(2014)169.

arXiv:1307.1443 [hep-th].

[22] Paolo Benincasa. 'On-shell diagrammatics and the perturbative structure of planar gauge theories'. In: (Oct. 2015).

arXiv:1510.03642 [hep-th].

[23] Paolo Benincasa and David Gordo. 'On-shell diagrams and the geometry of planar $\mathcal{N} < 4$ SYM theories'. In: *JHEP* 11 (2017), p. 192.

doi:10.1007/JHEP11(2017)192.

arXiv:1609.01923 [hep-th].

[24] Nima Arkani-Hamed, Jacob L. Bourjaily, Freddy Cachazo, Alexander Postnikov and Jaroslav Trnka. 'On-Shell Structures of MHV Amplitudes Beyond the Planar Limit'. In: *JHEP* 06 (2015), p. 179.

doi:10.1007/JHEP06(2015)179.

arXiv:1412.8475 [hep-th].

[25] Sebastian Franco, Daniele Galloni, Brenda Penante and Congkao Wen. 'Non-Planar On-Shell Diagrams'. In: *JHEP* 06 (2015), p. 199. doi:10.1007/JHEP06(2015)199. arXiv:1502.02034 [hep-th].

[26] Jacob L. Bourjaily, Sebastian Franco, Daniele Galloni and Congkao Wen. 'Stratifying On-Shell Cluster Varieties: the Geometry of Non-Planar On-Shell Diagrams'. In: *JHEP* 10 (2016), p. 003. doi:10.1007/JHEP10(2016)003. arXiv:1607.01781 [hep-th].

[27] Andrew Hodges. 'New expressions for gravitational scattering amplitudes'. In: *JHEP* 07 (2013), p. 075. doi:10.1007/JHEP07(2013)075. arXiv:1108.2227 [hep-th].

[28] James Bedford, Andreas Brandhuber, Bill J. Spence and Gabriele Travaglini. 'A Recursion relation for gravity amplitudes'. In: *Nucl. Phys. B* 721 (2005), pp. 98–110. doi:10.1016/j.nuclphysb.2005.016. arXiv:hep-th/0502146.

[29] Freddy Cachazo and Peter Svrcek. 'Tree level recursion relations in general relativity'. In: (Feb. 2005). arXiv:hep-th/0502160.

[30] Paul Heslop and Arthur E. Lipstein. 'On-shell diagrams for $\mathcal{N} = 8$ supergravity amplitudes'. In: *JHEP* 06 (2016), p. 069. doi:10.1007/JHEP06(2016)069. arXiv:1604.03046 [hep-th].

[31] Andrew Hodges. 'A simple formula for gravitational MHV amplitudes'. In: (Apr. 2012). arXiv:1204.1930 [hep-th].

[32] David Skinner. 'Twistor strings for $\mathcal{N} = 8$ supergravity'. In: *JHEP* 04 (2020), p. 047.
doi:10.1007/JHEP04(2020)047.
arXiv:1301.0868 [hep-th].

[33] Yvonne Geyer, Arthur E. Lipstein and Lionel J. Mason. 'Ambitwistor Strings in Four Dimensions'. In: *Phys. Rev. Lett.* 113.8 (2014), p. 081602.
doi:10.1103/PhysRevLett.113.081602.
arXiv:1404.6219 [hep-th].

[34] Jaroslav Trnka. 'Towards the Gravituhedron: New Expressions for NMHV Gravity Amplitudes'. In: *JHEP* 04 (2021), p. 253.
doi:10.1007/JHEP04(2021)253.
arXiv:2012.15780 [hep-th].

[35] Joseph A. Farrow and Arthur E. Lipstein. 'From 4d Ambitwistor Strings to On Shell Diagrams and Back'. In: *JHEP* 07 (2017), p. 114.
doi:10.1007/JHEP07(2017)114.
arXiv:1705.07087 [hep-th].

[36] Joao Penedones. 'Writing CFT correlation functions as AdS scattering amplitudes'. In: *JHEP* 03 (2011), p. 025.
doi:10.1007/JHEP03(2011)025.
arXiv:1011.1485 [hep-th].

[37] Suvrat Raju. 'New Recursion Relations and a Flat Space Limit for AdS/CFT Correlators'. In: *Phys. Rev. D* 85 (2012), p. 126009.
doi:10.1103/PhysRevD.85.126009.
arXiv:1201.6449 [hep-th].

[38] Juan Martin Maldacena. 'The Large N limit of superconformal field theories and supergravity'. In: *Int. J. Theor. Phys.* 38 (1999), pp. 1113–1133.
doi:10.1023/A:1026654312961.
arXiv:hep-th/9711200.

[39] Z. Bern, J.J.M. Carrasco and Henrik Johansson. 'New Relations for Gauge-Theory Amplitudes'. In: *Phys. Rev. D* 78 (2008), p. 085011. doi:10.1103/PhysRevD.78.085011. arXiv:0805.3993 [hep-ph].

[40] H. Kawai, D.C. Lewellen and S.H.H. Tye. 'A Relation Between Tree Amplitudes of Closed and Open Strings'. In: *Nucl. Phys. B* 269 (1986), pp. 1–23. doi:10.1016/0550-3213(86)90362-7.

[41] Freddy Cachazo, Song He and Ellis Ye Yuan. 'Scattering of Massless Particles in Arbitrary Dimensions'. In: *Phys. Rev. Lett.* 113.17 (2014), p. 171601. doi:10.1103/PhysRevLett.113.171601. arXiv:1307.2199 [hep-th].

[42] Zvi Bern, John Joseph M. Carrasco and Henrik Johansson. 'Perturbative Quantum Gravity as a Double Copy of Gauge Theory'. In: *Phys. Rev. Lett.* 105 (2010), p. 061602. doi:10.1103/PhysRevLett.105.061602. arXiv:1004.0476 [hep-th].

[43] John Joseph M. Carrasco and Henrik Johansson. 'Five-Point Amplitudes in N=4 Super-Yang-Mills Theory and N=8 Supergravity'. In: *Phys. Rev. D* 85 (2012), p. 025006. doi:10.1103/PhysRevD.85.025006. arXiv:1106.4711 [hep-th].

[44] Z. Bern, J.J.M. Carrasco, L.J. Dixon, H. Johansson and R. Roiban. 'Simplifying Multiloop Integrands and Ultraviolet Divergences of Gauge Theory and Gravity Amplitudes'. In: *Phys. Rev. D* 85 (2012), p. 105014. doi:10.1103/PhysRevD.85.105014. arXiv:1201.5366 [hep-th].

[45] Dong-pei Zhu. 'Zeros in Scattering Amplitudes and the Structure of Nonabelian Gauge Theories'. In: *Phys. Rev. D* 22 (1980), p. 2266. doi:10.1103/PhysRevD.22.2266.

[46] Suvrat Raju. 'BCFW for Witten Diagrams'. In: *Phys. Rev. Lett.* 106 (2011), p. 091601. doi:10.1103/PhysRevLett.106.091601. arXiv:1011.0780 [hep-th].

[47] Juan M. Maldacena and Guilherme L. Pimentel. 'On graviton non-Gaussianities during inflation'. In: *JHEP* 09 (2011), p. 045. doi:10.1007/JHEP09(2011)045. arXiv:1104.2846 [hep-th].

[48] Suvrat Raju. 'Recursion Relations for AdS/CFT Correlators'. In: *Phys. Rev. D* 83 (2011), p. 126002. doi:10.1103/PhysRevD.83.126002. arXiv:1102.4724 [hep-th].

[49] Suvrat Raju. 'Four Point Functions of the Stress Tensor and Conserved Currents in AdS_4/CFT_3'. In: *Phys. Rev. D* 85 (2012), p. 126008. doi:10.1103/PhysRevD.85.126008. arXiv:1201.6452 [hep-th].

[50] Soner Albayrak and Savan Kharel. 'Towards the higher point holographic momentum space amplitudes'. In: *JHEP* 02 (2019), p. 040. doi:10.1007/JHEP02(2019)040. arXiv:1810.12459 [hep-th].

[51] Soner Albayrak and Savan Kharel. 'Towards the higher point holographic momentum space amplitudes. Part II. Gravitons'. In: *JHEP* 12 (2019), p. 135. doi:10.1007/JHEP12(2019)135. arXiv:1908.01835 [hep-th].

[52] Joseph A. Farrow, Arthur E. Lipstein and Paul McFadden. 'Double copy structure of CFT correlators'. In: *JHEP* 02 (2019), p. 130.
doi:10.1007/JHEP02(2019)130.
arXiv:1812.11129 [hep-th].

[53] Arthur E. Lipstein and Paul McFadden. 'Double copy structure and the flat space limit of conformal correlators in even dimensions'. In: *Phys. Rev. D* 101.12 (2020), p. 125006.
doi:10.1103/PhysRevD.101.125006.
arXiv:1912.10046 [hep-th].

[54] Adam Bzowski, Paul McFadden and Kostas Skenderis. 'Holography for inflation using conformal perturbation theory'. In: *JHEP* 04 (2013), p. 047.
doi:10.1007/JHEP04(2013)047.
arXiv:1211.4550 [hep-th].

[55] Nima Arkani-Hamed and Juan Maldacena. 'Cosmological Collider Physics'. In: (Mar. 2015).
arXiv:1503.08043 [hep-th].

[56] Steven Weinberg. 'Quantum contributions to cosmological correlations'. In: *Phys. Rev. D* 72 (2005), p. 043514.
doi:10.1103/PhysRevD.72.043514.
arXiv:hep-th/0506236.

[57] Juan Martin Maldacena. 'Non-Gaussian features of primordial fluctuations in single field inflationary models'. In: *JHEP* 05 (2003), p. 013.
doi:10.1088/1126-6708/2003/05/013.
arXiv:astro-ph/0210603.

[58] Nima Arkani-Hamed, Paolo Benincasa and Alexander Postnikov. 'Cosmological Polytopes and the Wavefunction of the Universe'. In: (Sept. 2017).
arXiv:1709.02813 [hep-th].

[59] Daniel Baumann, Carlos Duaso Pueyo, Austin Joyce, Hayden Lee and Guilherme L. Pimentel. 'The Cosmological Bootstrap: Spinning Correlators from Symmetries and Factorization'. In: (May 2020). arXiv:2005.04234 [hep-th].

[60] Aaron Hillman and Enrico Pajer. 'A differential representation of cosmological wavefunctions'. In: *JHEP* 04 (2022), p. 012. doi:10.1007/JHEP04(2022)012. arXiv:2112.01619 [hep-th].

[61] Charlotte Sleight. 'A Mellin Space Approach to Cosmological Correlators'. In: *JHEP* 01 (2020), p. 090. doi:10.1007/JHEP01(2020)090. arXiv:1906.12302 [hep-th].

[62] Humberto Gomez, Renann Lipinski Jusinskas and Arthur Lipstein. 'Cosmological Scattering Equations'. In: *Phys. Rev. Lett.* 127.25 (2021), p. 251604. doi:10.1103/PhysRevLett.127.251604. arXiv:2106.11903 [hep-th].

[63] Humberto Gomez, Renann Lipinski Jusinskas and Arthur Lipstein. 'Cosmological scattering equations at tree-level and one-loop'. In: *JHEP* 07 (2022), p. 004. doi:10.1007/JHEP07(2022)004. arXiv:2112.12695 [hep-th].

[64] David B. Fairlie. 'A Coding of Real Null Four-Momenta into World-Sheet Coordinates'. In: *Adv. Math. Phys.* 2009 (2009), p. 284689. doi:10.1155/2009/284689. arXiv:0805.2263 [hep-th].

[65] David J. Gross and Paul F. Mende. 'The high-energy behavior of string scattering amplitudes'. In: *Physics Letters B* 197.1 (1987), pp. 129–134.

https://www.sciencedirect.com/science/article/pii/0370269387903558

doi:https://doi.org/10.1016/0370-2693(87)90355-8.

[66] Freddy Cachazo, Song He and Ellis Ye Yuan. 'Scattering of Massless Particles: Scalars, Gluons and Gravitons'. In: *JHEP* 07 (2014), p. 033.

doi:10.1007/JHEP07(2014)033.

arXiv:1309.0885 [hep-th].

[67] Lionel Mason and David Skinner. 'Ambitwistor strings and the scattering equations'. In: *JHEP* 07 (2014), p. 048.

doi:10.1007/JHEP07(2014)048.

arXiv:1311.2564 [hep-th].

[68] Freddy Cachazo, Song He and Ellis Ye Yuan. 'Scattering Equations and Matrices: From Einstein To Yang-Mills, DBI and NLSM'. In: *JHEP* 07 (2015), p. 149.

doi:10.1007/JHEP07(2015)149.

arXiv:1412.3479 [hep-th].

[69] Eduardo Casali, Yvonne Geyer, Lionel Mason, Ricardo Monteiro and Kai A. Roehrig. 'New Ambitwistor String Theories'. In: *JHEP* 11 (2015), p. 038.

doi:10.1007/JHEP11(2015)038.

arXiv:1506.08771 [hep-th].

[70] Clifford Cheung, Chia-Hsien Shen and Congkao Wen. 'Unifying Relations for Scattering Amplitudes'. In: *JHEP* 02 (2018), p. 095.

doi:10.1007/JHEP02(2018)095.

arXiv:1705.03025 [hep-th].

[71] Lorenz Eberhardt, Shota Komatsu and Sebastian Mizera. 'Scattering equations in AdS: scalar correlators in arbitrary dimensions'. In: *JHEP* 11 (2020), p. 158.

doi:10.1007/JHEP11(2020)158.

arXiv:2007.06574 [hep-th].

[72] Kai Roehrig and David Skinner. 'Ambitwistor strings and the scattering equations on $AdS_3 \times S^3$'. In: *JHEP* 02 (2022), p. 073.

doi:10.1007/JHEP02(2022)073.

arXiv:2007.07234 [hep-th].

[73] Pranav Diwakar, Aidan Herderschee, Radu Roiban and Fei Teng. 'BCJ amplitude relations for Anti-de Sitter boundary correlators in embedding space'. In: *JHEP* 10 (2021), p. 141.

doi:10.1007/JHEP10(2021)141.

arXiv:2106.10822 [hep-th].

[74] Aidan Herderschee, Radu Roiban and Fei Teng. 'On the differential representation and color-kinematics duality of AdS boundary correlators'. In: *JHEP* 05 (2022), p. 026.

doi:10.1007/JHEP05(2022)026.

arXiv:2201.05067 [hep-th].

[75] Aidan Herderschee. 'A New Framework for Higher Loop Witten Diagrams'. In: (Dec. 2021).

arXiv:2112.08226 [hep-th].

[76] Steven Weinberg. 'Infrared photons and gravitons'. In: *Phys. Rev.* 140 (1965), B516–B524.

doi:10.1103/PhysRev.140.B516.

[77] Chris D. White. 'Factorization Properties of Soft Graviton Amplitudes'. In: *JHEP* 05 (2011), p. 060.

doi:10.1007/JHEP05(2011)060.

arXiv:1103.2981 [hep-th].

[78] Freddy Cachazo and Andrew Strominger. 'Evidence for a New Soft Graviton Theorem'. In: (Apr. 2014).
arXiv:1404.4091 [hep-th].

[79] Andrew Strominger. 'On BMS Invariance of Gravitational Scattering'. In: *JHEP* 07 (2014), p. 152.
doi:10.1007/JHEP07(2014)152.
arXiv:1312.2229 [hep-th].

[80] Temple He, Vyacheslav Lysov, Prahar Mitra and Andrew Strominger. 'BMS supertranslations and Weinberg's soft graviton theorem'. In: *JHEP* 05 (2015), p. 151.
doi:10.1007/JHEP05(2015)151.
arXiv:1401.7026 [hep-th].

[81] Laura Donnay, Andrea Puhm and Andrew Strominger. 'Conformally Soft Photons and Gravitons'. In: *JHEP* 01 (2019), p. 184.
doi:10.1007/JHEP01(2019)184.
arXiv:1810.05219 [hep-th].

[82] Murray Gell-Mann and M Levy. 'The axial vector current in beta decay'. In: *Nuovo Cim.* 16 (1960), p. 705.
doi:10.1007/BF02859738.

[83] Steven Weinberg. 'Nonlinear realizations of chiral symmetry'. In: *Phys. Rev.* 166 (1968), pp. 1568–1577.
doi:10.1103/PhysRev.166.1568.

[84] Steven Weinberg. 'Phenomenological Lagrangians'. In: *Physica A* 96.1-2 (1979). Ed. by S. Deser, pp. 327–340.
doi:10.1016/0378-4371(79)90223-1.

[85] Stephen L. Adler. 'Consistency conditions on the strong interactions implied by a partially conserved axial vector current'. In: *Phys. Rev.* 137 (1965),

B1022–B1033.

doi:10.1103/PhysRev.137.B1022.

[86] Nima Arkani-Hamed, Freddy Cachazo and Jared Kaplan. 'What is the Simplest Quantum Field Theory?' In: *JHEP* 09 (2010), p. 016.

doi:10.1007/JHEP09(2010)016.

arXiv:0808.1446 [hep-th].

[87] Clifford Cheung, Karol Kampf, Jiri Novotny and Jaroslav Trnka. 'Effective Field Theories from Soft Limits of Scattering Amplitudes'. In: *Phys. Rev. Lett.* 114.22 (2015), p. 221602.

doi:10.1103/PhysRevLett.114.221602.

arXiv:1412.4095 [hep-th].

[88] Clifford Cheung, Karol Kampf, Jiri Novotny, Chia-Hsien Shen and Jaroslav Trnka. 'A Periodic Table of Effective Field Theories'. In: *JHEP* 02 (2017), p. 020.

doi:10.1007/JHEP02(2017)020.

arXiv:1611.03137 [hep-th].

[89] James Bonifacio, Kurt Hinterbichler, Austin Joyce and Diederik Roest. 'Exceptional scalar theories in de Sitter space'. In: *JHEP* 04 (2022), p. 128.

doi:10.1007/JHEP04(2022)128.

arXiv:2112.12151 [hep-th].

[90] Henriette Elvang and Yu-tin Huang. *Scattering Amplitudes in Gauge Theory and Gravity*. Cambridge University Press, 2015.

doi:10.1017/CBO9781107706620.

[91] Johannes M. Henn and Jan C. Plefka. *Scattering Amplitudes in Gauge Theories*. Vol. 883. Berlin: Springer, 2014.

doi:10.1007/978-3-642-54022-6.

[92] Mark Srednicki. *Quantum Field Theory*. Cambridge University Press, 2007.

doi:10.1017/CBO9780511813917.

[93] L. Ferro. 'Yangian Symmetry in N=4 super Yang-Mills'. In: (July 2011). arXiv:1107.1776 [hep-th].

[94] Slava Rychkov. *EPFL Lectures on Conformal Field Theory in D>= 3 Dimensions*. SpringerBriefs in Physics. Jan. 2016. doi:10.1007/978-3-319-43626-5. arXiv:1601.05000 [hep-th].

[95] Nima Arkani-Hamed, Jacob L. Bourjaily, Freddy Cachazo and Jaroslav Trnka. 'Local Integrals for Planar Scattering Amplitudes'. In: *JHEP* 06 (2012), p. 125. doi:10.1007/JHEP06(2012)125. arXiv:1012.6032 [hep-th].

[96] Clifford Cheung, Karol Kampf, Jiri Novotny, Chia-Hsien Shen and Jaroslav Trnka. 'On-Shell Recursion Relations for Effective Field Theories'. In: *Phys. Rev. Lett.* 116.4 (2016), p. 041601. doi:10.1103/PhysRevLett.116.041601. arXiv:1509.03309 [hep-th].

[97] Marcus Spradlin, Anastasia Volovich and Congkao Wen. 'Three Applications of a Bonus Relation for Gravity Amplitudes'. In: *Phys. Lett. B* 674 (2009), pp. 69–72. doi:10.1016/j.physletb.2009.02.059. arXiv:0812.4767 [hep-th].

[98] Song He, Dhritiman Nandan and Congkao Wen. 'Note on Bonus Relations for N=8 Supergravity Tree Amplitudes'. In: *JHEP* 02 (2011), p. 005. doi:10.1007/JHEP02(2011)005. arXiv:1011.4287 [hep-th].

[99] Soner Albayrak, Chandramouli Chowdhury and Savan Kharel. 'Study of momentum space scalar amplitudes in AdS spacetime'. In: *Phys. Rev. D* 101.12 (2020), p. 124043.

doi:10.1103/PhysRevD.101.124043.

arXiv:2001.06777 [hep-th].

[100] Vijay Balasubramanian, Steven B. Giddings and Albion Lawrence. 'What do CFTs tell us about anti-de Sitter spacetimes?' In: *Journal of High Energy Physics* 1999.03 (June 1999), p. 001.

https://dx.doi.org/10.1088/1126-6708/1999/03/001

doi:10.1088/1126-6708/1999/03/001.

[101] Sachin Jain, Nilay Kundu, Suman Kundu, Abhishek Mehta and Sunil Kumar Sake. 'A CFT interpretation of cosmological correlation functions in $\alpha-$vacua in de-Sitter space'. In: *JHEP* 05 (2023), p. 111.

doi:10.1007/JHEP05(2023)111.

arXiv:2206.08395 [hep-th].

[102] Paul McFadden and Kostas Skenderis. 'Holography for Cosmology'. In: *Phys. Rev. D* 81 (2010), p. 021301.

doi:10.1103/PhysRevD.81.021301.

arXiv:0907.5542 [hep-th].

[103] Paul McFadden and Kostas Skenderis. 'Holographic Non-Gaussianity'. In: *JCAP* 05 (2011), p. 013.

doi:10.1088/1475-7516/2011/05/013.

arXiv:1011.0452 [hep-th].

[104] Zvi Bern, John Joseph Carrasco, Marco Chiodaroli, Henrik Johansson and Radu Roiban. 'The Duality Between Color and Kinematics and its Applications'. In: (Sept. 2019).

arXiv:1909.01358 [hep-th].

[105] Karol Kampf, Jiri Novotny and Jaroslav Trnka. 'Tree-level Amplitudes in the Nonlinear Sigma Model'. In: *JHEP* 05 (2013), p. 032.

doi:10.1007/JHEP05(2013)032.

arXiv:1304.3048 [hep-th].

[106] Kurt Hinterbichler and Austin Joyce. 'Hidden symmetry of the Galileon'. In: *Phys. Rev. D* 92.2 (2015), p. 023503.
doi:10.1103/PhysRevD.92.023503.
arXiv:1501.07600 [hep-th].

[107] Enrico Herrmann and Jaroslav Trnka. 'Gravity On-shell Diagrams'. In: *JHEP* 11 (2016), p. 136.
doi:10.1007/JHEP11(2016)136.
arXiv:1604.03479 [hep-th].

[108] Jin-Yu Liu and En Shih. 'Bonus scaling and BCFW in $\mathcal{N} = 7$ supergravity'. In: *Phys. Lett. B* 740 (2015), pp. 151–157.
doi:10.1016/j.physletb.2014.11.046.
arXiv:1409.1710 [hep-th].

[109] Shailesh Lal and Suvrat Raju. 'The Next-to-Simplest Quantum Field Theories'. In: *Phys. Rev. D* 81 (2010), p. 105002.
doi:10.1103/PhysRevD.81.105002.
arXiv:0910.0930 [hep-th].

[110] Henriette Elvang, Yu-tin Huang and Cheng Peng. 'On-shell superamplitudes in N<4 SYM'. In: *JHEP* 09 (2011), p. 031.
doi:10.1007/JHEP09(2011)031.
arXiv:1102.4843 [hep-th].

[111] Frits A. Berends, W.T. Giele and H. Kuijf. 'On relations between multi - gluon and multigraviton scattering'. In: *Phys. Lett. B* 211 (1988), pp. 91–94.
doi:10.1016/0370-2693(88)90813-1.

[112] Nima Arkani-Hamed, Freddy Cachazo, Clifford Cheung and Jared Kaplan. 'A Duality For The S Matrix'. In: *JHEP* 03 (2010), p. 020.
doi:10.1007/JHEP03(2010)020.
arXiv:0907.5418 [hep-th].

[113] Nima Arkani-Hamed, Jacob Bourjaily, Freddy Cachazo and Jaroslav Trnka. 'Unification of Residues and Grassmannian Dualities'. In: *JHEP* 01 (2011), p. 049.
doi:10.1007/JHEP01(2011)049.
arXiv:0912.4912 [hep-th].

[114] Dhritiman Nandan, Anastasia Volovich and Congkao Wen. 'A Grassmannian Etude in NMHV Minors'. In: *JHEP* 07 (2010), p. 061.
doi:10.1007/JHEP07(2010)061.
arXiv:0912.3705 [hep-th].

[115] J.M. Drummond, M. Spradlin, A. Volovich and C. Wen. 'Tree-Level Amplitudes in N=8 Supergravity'. In: *Phys. Rev. D* 79 (2009), p. 105018.
doi:10.1103/PhysRevD.79.105018.
arXiv:0901.2363 [hep-th].

[116] Paolo Benincasa and Matteo Parisi. 'Positive geometries and differential forms with non-logarithmic singularities. Part I'. In: *JHEP* 08.08 (2020), p. 023.
doi:10.1007/JHEP08(2020)023.
arXiv:2005.03612 [hep-th].

[117] Luis F. Alday and Juan Martin Maldacena. 'Gluon scattering amplitudes at strong coupling'. In: *JHEP* 06 (2007), p. 064.
doi:10.1088/1126-6708/2007/06/064.
arXiv:0705.0303 [hep-th].

[118] Andreas Brandhuber, Paul Heslop and Gabriele Travaglini. 'MHV amplitudes in N=4 super Yang-Mills and Wilson loops'. In: *Nucl. Phys. B* 794 (2008), pp. 231–243.
doi:10.1016/j.nuclphysb.2007.11.002.
arXiv:0707.1153 [hep-th].

[119] J.M. Drummond, J. Henn, G.P. Korchemsky and E. Sokatchev. 'On planar gluon amplitudes/Wilson loops duality'. In: *Nucl. Phys. B* 795 (2008), pp. 52–68.
doi:10.1016/j.nuclphysb.2007.11.007.
arXiv:0709.2368 [hep-th].

[120] L.J. Mason and David Skinner. 'The Complete Planar S-matrix of N=4 SYM as a Wilson Loop in Twistor Space'. In: *JHEP* 12 (2010), p. 018.
doi:10.1007/JHEP12(2010)018.
arXiv:1009.2225 [hep-th].

[121] Simon Caron-Huot. 'Notes on the scattering amplitude / Wilson loop duality'. In: *JHEP* 07 (2011), p. 058.
doi:10.1007/JHEP07(2011)058.
arXiv:1010.1167 [hep-th].

[122] Andreas Brandhuber, Paul Heslop, Adele Nasti, Bill Spence and Gabriele Travaglini. 'Four-point Amplitudes in N=8 Supergravity and Wilson Loops'. In: *Nucl. Phys. B* 807 (2009), pp. 290–314.
doi:10.1016/j.nuclphysb.2008.09.010.
arXiv:0805.2763 [hep-th].

[123] Enrico Herrmann, Cameron Langer, Jaroslav Trnka and Minshan Zheng. 'Positive geometry, local triangulations, and the dual of the Amplituhedron'. In: (Sept. 2020).
arXiv:2009.05607 [hep-th].

[124] Jacob L. Bourjaily, Enrico Herrmann, Cameron Langer, Andrew J. McLeod and Jaroslav Trnka. 'Prescriptive Unitarity for Non-Planar Six-Particle Amplitudes at Two Loops'. In: *JHEP* 12 (2019), p. 073.
doi:10.1007/JHEP12(2019)073.
arXiv:1909.09131 [hep-th].

[125] Taro V. Brown, Umut Oktem and Jaroslav Trnka. 'Poles at infinity in on-shell diagrams'. In: *JHEP* 02 (2023), p. 003.
doi:10.1007/JHEP02(2023)003.
arXiv:2212.06840 [hep-th].

[126] Nathan Berkovits and Edward Witten. 'Conformal supergravity in twistor-string theory'. In: *JHEP* 08 (2004), p. 009.
doi:10.1088/1126-6708/2004/08/009.
arXiv:hep-th/0406051.

[127] Tim Adamo and Lionel Mason. 'Einstein supergravity amplitudes from twistor-string theory'. In: *Class. Quant. Grav.* 29 (2012), p. 145010.
doi:10.1088/0264-9381/29/14/145010.
arXiv:1203.1026 [hep-th].

[128] Louise Dolan and Jay N. Ihry. 'Conformal Supergravity Tree Amplitudes from Open Twistor String Theory'. In: *Nucl. Phys. B* 819 (2009), pp. 375–399.
doi:10.1016/j.nuclphysb.2009.04.003.
arXiv:0811.1341 [hep-th].

[129] Tim Adamo and Lionel Mason. 'Conformal and Einstein gravity from twistor actions'. In: *Class. Quant. Grav.* 31.4 (2014), p. 045014.
doi:10.1088/0264-9381/31/4/045014.
arXiv:1307.5043 [hep-th].

[130] Joseph A. Farrow and Arthur E. Lipstein. 'New Worldsheet Formulae for Conformal Supergravity Amplitudes'. In: *JHEP* 07 (2018), p. 074.
doi:10.1007/JHEP07(2018)074.
arXiv:1805.04504 [hep-th].

[131] Zvi Bern, David Kosower and Julio Parra-Martinez. 'Two-loop n-point anomalous amplitudes in N=4 supergravity'. In: *Proc. Roy. Soc. Lond. A* 476.2235 (2020), p. 20190722.

doi:10.1098/rspa.2019.0722.

arXiv:1905.05151 [hep-th].

[132] Henrik Johansson and Josh Nohle. 'Conformal Gravity from Gauge Theory'. In: (July 2017).

arXiv:1707.02965 [hep-th].

[133] Henrik Johansson, Gustav Mogull and Fei Teng. 'Unraveling conformal gravity amplitudes'. In: *JHEP* 09 (2018), p. 080.

doi:10.1007/JHEP09(2018)080.

arXiv:1806.05124 [hep-th].

[134] Arshia Momeni, Justinas Rumbutis and Andrew J. Tolley. 'Massive Gravity from Double Copy'. In: *JHEP* 12 (2020), p. 030.

doi:10.1007/JHEP12(2020)030.

arXiv:2004.07853 [hep-th].

[135] Laura A. Johnson, Callum R.T. Jones and Shruti Paranjape. 'Constraints on a Massive Double-Copy and Applications to Massive Gravity'. In: (Apr. 2020).

arXiv:2004.12948 [hep-th].

[136] Hong Liu and Arkady A. Tseytlin. 'On four point functions in the CFT / AdS correspondence'. In: *Phys. Rev. D* 59 (1999), p. 086002.

doi:10.1103/PhysRevD.59.086002.

arXiv:hep-th/9807097.

[137] Ricardo Monteiro and Donal O'Connell. 'The Kinematic Algebra From the Self-Dual Sector'. In: *JHEP* 07 (2011), p. 007.

doi:10.1007/JHEP07(2011)007.

arXiv:1105.2565 [hep-th].

[138] Adam Bzowski, Paul McFadden and Kostas Skenderis. 'Implications of conformal invariance in momentum space'. In: *JHEP* 03 (2014), p. 111.

doi:10.1007/JHEP03(2014)111.

arXiv:1304.7760 [hep-th].

[139] James Bonifacio, Harry Goodhew, Austin Joyce, Enrico Pajer and David Stefanyszyn. 'The graviton four-point function in de Sitter space'. In: (Dec. 2022).

arXiv:2212.07370 [hep-th].

[140] Connor Armstrong, Harry Goodhew, Arthur Lipstein and Jiejie Mei. 'Graviton Trispectrum from Gluons'. In: (In preparation).

[141] Adam Bzowski, Paul McFadden and Kostas Skenderis. 'Conformal n-point functions in momentum space'. In: *Phys. Rev. Lett.* 124.13 (2020), p. 131602.

doi:10.1103/PhysRevLett.124.131602.

arXiv:1910.10162 [hep-th].

[142] Luis F. Alday, Connor Behan, Pietro Ferrero and Xinan Zhou. 'Gluon Scattering in AdS from CFT'. In: *JHEP* 06 (2021), p. 020.

doi:10.1007/JHEP06(2021)020.

arXiv:2103.15830 [hep-th].

[143] Shing Yan Li, Yi Wang and Siyi Zhou. 'KLT-Like Behaviour of Inflationary Graviton Correlators'. In: *JCAP* 12 (2018), p. 023.

doi:10.1088/1475-7516/2018/12/023.

arXiv:1806.06242 [hep-th].

[144] A.R. Fazio. 'Cosmological correlators, In–In formalism and double copy'. In: *Mod. Phys. Lett. A* 35.11 (2020), p. 2050076.

doi:10.1142/S0217732320500765.

arXiv:1909.07343 [hep-th].

[145] Yvonne Geyer, Lionel Mason, Ricardo Monteiro and Piotr Tourkine. 'Loop Integrands for Scattering Amplitudes from the Riemann Sphere'. In: *Phys. Rev. Lett.* 115.12 (2015), p. 121603.

doi:10.1103/PhysRevLett.115.121603.

arXiv:1507.00321 [hep-th].

[146] Joseph A. Farrow, Yvonne Geyer, Arthur E. Lipstein, Ricardo Monteiro and Ricardo Stark-Muchão. 'Propagators, BCFW Recursion and New Scattering Equations at One Loop'. In: (July 2020).

arXiv:2007.00623 [hep-th].

[147] Louise Dolan and Peter Goddard. 'Proof of the Formula of Cachazo, He and Yuan for Yang-Mills Tree Amplitudes in Arbitrary Dimension'. In: *JHEP* 05 (2014), p. 010.

doi:10.1007/JHEP05(2014)010.

arXiv:1311.5200 [hep-th].

[148] Idse Heemskerk, Joao Penedones, Joseph Polchinski and James Sully. 'Holography from Conformal Field Theory'. In: *JHEP* 10 (2009), p. 079.

doi:10.1088/1126-6708/2009/10/079.

arXiv:0907.0151 [hep-th].

[149] Paolo Creminelli, Jorge Noreña and Marko Simonović. 'Conformal consistency relations for single-field inflation'. In: *JCAP* 07 (2012), p. 052.

doi:10.1088/1475-7516/2012/07/052.

arXiv:1203.4595 [hep-th].

[150] Kurt Hinterbichler, Lam Hui and Justin Khoury. 'An Infinite Set of Ward Identities for Adiabatic Modes in Cosmology'. In: *JCAP* 01 (2014), p. 039.

doi:10.1088/1475-7516/2014/01/039.

arXiv:1304.5527 [hep-th].

[151] Nilay Kundu, Ashish Shukla and Sandip P. Trivedi. 'Constraints from Conformal Symmetry on the Three Point Scalar Correlator in Inflation'. In: *JHEP* 04 (2015), p. 061.

doi:10.1007/JHEP04(2015)061.

arXiv:1410.2606 [hep-th].

[152] Paolo Creminelli. 'On non-Gaussianities in single-field inflation'. In: *JCAP* 10 (2003), p. 003.
doi:10.1088/1475-7516/2003/10/003.
arXiv:astro-ph/0306122.

[153] Valentin Assassi, Daniel Baumann and Daniel Green. 'On Soft Limits of Inflationary Correlation Functions'. In: *JCAP* 11 (2012), p. 047.
doi:10.1088/1475-7516/2012/11/047.
arXiv:1204.4207 [hep-th].

[154] Nilay Kundu, Ashish Shukla and Sandip P. Trivedi. 'Ward Identities for Scale and Special Conformal Transformations in Inflation'. In: *JHEP* 01 (2016), p. 046.
doi:10.1007/JHEP01(2016)046.
arXiv:1507.06017 [hep-th].

[155] Ashish Shukla, Sandip P. Trivedi and V. Vishal. 'Symmetry constraints in inflation, α-vacua, and the three point function'. In: *JHEP* 12 (2016), p. 102.
doi:10.1007/JHEP12(2016)102.
arXiv:1607.08636 [hep-th].

[156] Noah Bittermann and Austin Joyce. 'Soft limits of the wavefunction in exceptional scalar theories'. In: (Mar. 2022).
arXiv:2203.05576 [hep-th].

[157] Adam Bzowski, Paul McFadden and Kostas Skenderis. 'Scalar 3-point functions in CFT: renormalisation, beta functions and anomalies'. In: *JHEP* 03 (2016), p. 066.
doi:10.1007/JHEP03(2016)066.
arXiv:1510.08442 [hep-th].

[158] Adam Bzowski, Paul McFadden and Kostas Skenderis. 'Renormalised 3-point functions of stress tensors and conserved currents in CFT'. In: *JHEP* 11 (2018), p. 153.

doi:10.1007/JHEP11(2018)153.

arXiv:1711.09105 [hep-th].

[159] Adam Bzowski, Paul McFadden and Kostas Skenderis. 'Renormalised CFT 3-point functions of scalars, currents and stress tensors'. In: *JHEP* 11 (2018), p. 159.

doi:10.1007/JHEP11(2018)159.

arXiv:1805.12100 [hep-th].

[160] Adam Bzowski, Paul McFadden and Kostas Skenderis. 'A handbook of holographic 4-point functions'. In: *JHEP* 12 (2022), p. 039.

doi:10.1007/JHEP12(2022)039.

arXiv:2207.02872 [hep-th].

[161] Paolo Benincasa. 'Cosmological Polytopes and the Wavefuncton of the Universe for Light States'. In: (Sept. 2019).

arXiv:1909.02517 [hep-th].

[162] Christoph Bartsch, Karol Kampf and Jaroslav Trnka. 'Recursion relations for one-loop Goldstone boson amplitudes'. In: *Phys. Rev. D* 106.7 (2022), p. 076008.

doi:10.1103/PhysRevD.106.076008.

arXiv:2206.04694 [hep-th].

[163] Charlotte Sleight and Massimo Taronna. 'Bootstrapping Inflationary Correlators in Mellin Space'. In: *JHEP* 02 (2020), p. 098.

doi:10.1007/JHEP02(2020)098.

arXiv:1907.01143 [hep-th].

[164] Guilherme L. Pimentel. 'Inflationary Consistency Conditions from a Wavefunctional Perspective'. In: *JHEP* 02 (2014), p. 124.

doi:10.1007/JHEP02(2014)124.

arXiv:1309.1793 [hep-th].

[165] Paul McFadden. 'Soft limits in holographic cosmology'. In: *JHEP* 02 (2015), p. 053.
doi:10.1007/JHEP02(2015)053.
arXiv:1412.1874 [hep-th].

[166] Freddy Cachazo, Peter Cha and Sebastian Mizera. 'Extensions of Theories from Soft Limits'. In: *JHEP* 06 (2016), p. 170.
doi:10.1007/JHEP06(2016)170.
arXiv:1604.03893 [hep-th].

[167] Clifford Cheung, Karol Kampf, Jiri Novotny, Chia-Hsien Shen, Jaroslav Trnka and Congkao Wen. 'Vector Effective Field Theories from Soft Limits'. In: *Phys. Rev. Lett.* 120.26 (2018), p. 261602.
doi:10.1103/PhysRevLett.120.261602.
arXiv:1801.01496 [hep-th].

[168] Clifford Cheung, Paolo Creminelli, A. Liam Fitzpatrick, Jared Kaplan and Leonardo Senatore. 'The Effective Field Theory of Inflation'. In: *JHEP* 03 (2008), p. 014.
doi:10.1088/1126-6708/2008/03/014.
arXiv:0709.0293 [hep-th].

[169] Daniel Green and Enrico Pajer. 'On the Symmetries of Cosmological Perturbations'. In: *JCAP* 09 (2020), p. 032.
doi:10.1088/1475-7516/2020/09/032.
arXiv:2004.09587 [hep-th].

[170] Enrico Pajer. 'Building a Boostless Bootstrap for the Bispectrum'. In: *JCAP* 01 (2021), p. 023.
doi:10.1088/1475-7516/2021/01/023.
arXiv:2010.12818 [hep-th].

[171] Tanguy Grall, Sadra Jazayeri and David Stefanyszyn. 'The cosmological phonon: symmetries and amplitudes on sub-horizon scales'. In: *JHEP* 11

(2020), p. 097.

doi:10.1007/JHEP11(2020)097.

arXiv:2005.12937 [hep-th].

[172] Daniel Green, Yiwen Huang and Chia-Hsien Shen. 'Inflationary Adler Conditions'. In: (Aug. 2022).

arXiv:2208.14544 [hep-th].

[173] Yue-Zhou Li. 'Flat-space structure of gluon and graviton in AdS'. In: (Dec. 2022).

arXiv:2212.13195 [hep-th].

[174] Lorenzo Iacobacci, Charlotte Sleight and Massimo Taronna. 'From Celestial Correlators to AdS, and back'. In: (Aug. 2022).

arXiv:2208.01629 [hep-th].

[175] Charlotte Sleight and Massimo Taronna. 'Celestial Holography Revisited'. In: (Jan. 2023).

arXiv:2301.01810 [hep-th].

[176] Panagiotis Katsaroumpas, Bill Spence and Gabriele Travaglini. 'One-loop N=8 supergravity coefficients from N=4 super Yang-Mills'. In: *JHEP* 08 (2009), p. 096.

doi:10.1088/1126-6708/2009/08/096.

arXiv:0906.0521 [hep-th].